Spring 2017

Investigation of hydraulic fracture complexity and the benefits of maximizing or minimizing complexity in unconventional resources

Rashid Sheikh Kassim

Department: Geosciences and Geological and Petroleum Engineering

INVESTIGATION OF HYDRAULIC FRACTURE COMPLEXITY AND THE BENEFITS OF MAXIMIZING OR MINIMIZING COMPLEXITY IN UNCONVENTIONAL RESOURCES

BY

RASHID SHEIKH KASSIM

A DISSERTATION

PRESENTED TO THE FACULTY OF THE GRADUATE SCHOOL OF THE

MISSOURI UNIVERSITY OF SCIENCE AND TECHNOLOGY

IN PARTIAL FULFILLMENT OF THE REQUIREMENTS FOR THE DEGREE

DOCTOR OF PHILOSOPHY

IN

PETROLEUM ENGINEERING

2017

APPROVED BY

SHARI DUNN-NORMAN, ADVISOR

LARRY K. BRITT

RALPH FLORI

KELLY H.LIU

BAOJUN BAI

MINGZHEN WEI

ABSTRACT

This dissertation discusses two separate, yet inter-related studies. The first study was an extension of historical work comparing transversely fractured versus longitudinally fractured horizontal wells in multiphase flow environment. The second study investigated hydraulic fracture complexities and the benefits of maximizing or minimizing complexities in unconventional resources and tight reservoirs.

The main objective of this research was to investigate fracture complexity and its impact on well performance and economics. To achieve that objective, three different integrated completions and reservoir models were built. Two of the three models, a hybrid reservoir model and micro-seismic based SRV (stimulated reservoir volume) model, were built to capture presences of discrete fracture networks (DFN). The results of the DFN-based models were compared to an integrated planar fracture model, which had bi-wing fractures with limited or no fracture complexity. The second objective of this research was to determine reservoir permeability based cut-off criterion that can be used as guide when selecting whether to drill transversely fractured versus longitudinally fractured horizontal wells in multiphase flow environment. The reservoir models built for the multiphase flow would also investigate the effects of stress dependent permeability, adsorption gas and non-Darcy flow effect.

The third objective of this research was to develop a calibrated hydraulic fracture and reservoir model for the Montney shale, particularly for the Upper Montney Formation. This model would help companies select best lateral placement options in the Upper Montney, stage perforation targets and model-based stage spacing

ACKNOWLEDGMENTS

First and foremost, all praise and thanks to Almighty God, for the countless blessings that He has bestowed on me, my family and my fellow human beings. Truly, it was with the help of Almighty God (Allah) that I was able to successfully finish my PhD in petroleum engineering.

I am truly grateful and thankful to my research advisors, Dr. Shari Dunn-Norman and Prof. Larry Britt, for their encouragement, guidance and patience with me during my PhD studies. Additionally, it was an honor to have worked with them, both academically and professionally as a consultant engineer.

Sincere appreciation to Dr. Kelly H Liu, Dr. Ralph Flori, Dr. Baojun Bai and Dr. Mingzhen Wei for accepting to be on my advisory committee and for their invaluable suggestions.

I would like to thank and acknowledge the Chancellor's fellowship and the Bradley fellowship for their generous financial support, which helped me to pursue my PhD studies. I am especially thankful to the support and love of my family (particularly my parents, my son Hamza, my sisters, my brothers and my uncle Bile). I would like to extend special thanks to my friend Abdiaziz Hussen for his continuous support and encouragement.

Finally, I would like to thank all those who have helped me throughout my life from sea to shining sea or anywhere in the universe where they might happened to live. Special thanks to Prof. Larry Britt, who was my co-advisor and had prominent role in my PhD research through his guidance, support and advice. I sincerely hope the record reflects that!

TABLE OF CONTENTS

LIST OF ILLUSTRATIONS

Page

LIST OF TABLES

Page

NOMENCLATURE

Symbol	Description
β	Beta
α	Change in Coupler Angle

1. INTRODUCTION

In this section, an overview of the unconventional resources, research objectives and the scope of the research are be presented.

1.1. BACKGROUND AND OVERVIEWS

Defining what constitutes as unconventional resources requires criteria-based classifications and cut-offs of relevant parameters, though there is no industry-wide accepted formal definition. Some researcher have proposed permeability-based criteria, and stated that any reservoir with permeability of less than 0.1 mD (milli-Darcy) should be classified as an unconventional resource, especially if it is associated with basin-centered accumulations (Meckel and Thomasson, 2008). However, (Cander 2012) presented a paper titled "What Are Unconventional Resources? A Simple Definition Using Viscosity and Permeability", and stated that if only permeability of less than 0.1 mD was used, then coal-bed methane reservoirs/plays such as San Juan Basin and River Basin, which have permeabilities exceeding more than 1.0 mD might not fit the criteria. Figure 1-1 shows one of the vividly and simple to understand classifications of unconventional resources definition criteria that was proposed by (Cander 2012). The method uses viscosity (μ) versus permeability (k) cut-offs.

In general, unconventional resources have low permeability and cannot be economically produced at commercial rates without stimulation. Normally, this requires hydraulic fracturing or some other type of special recovery processes such as acid fracturing or steam injection. (Cander 2012) stated that unconventional resources require technology to increase the ratio of permeability over viscosity (k/μ) in order to achieve

commercial rates. Hydraulic fracturing increases reservoir conductivity (and by extension the permeability of the stimulated reservoir area), and steam flooding decreases reservoir fluid viscosity.

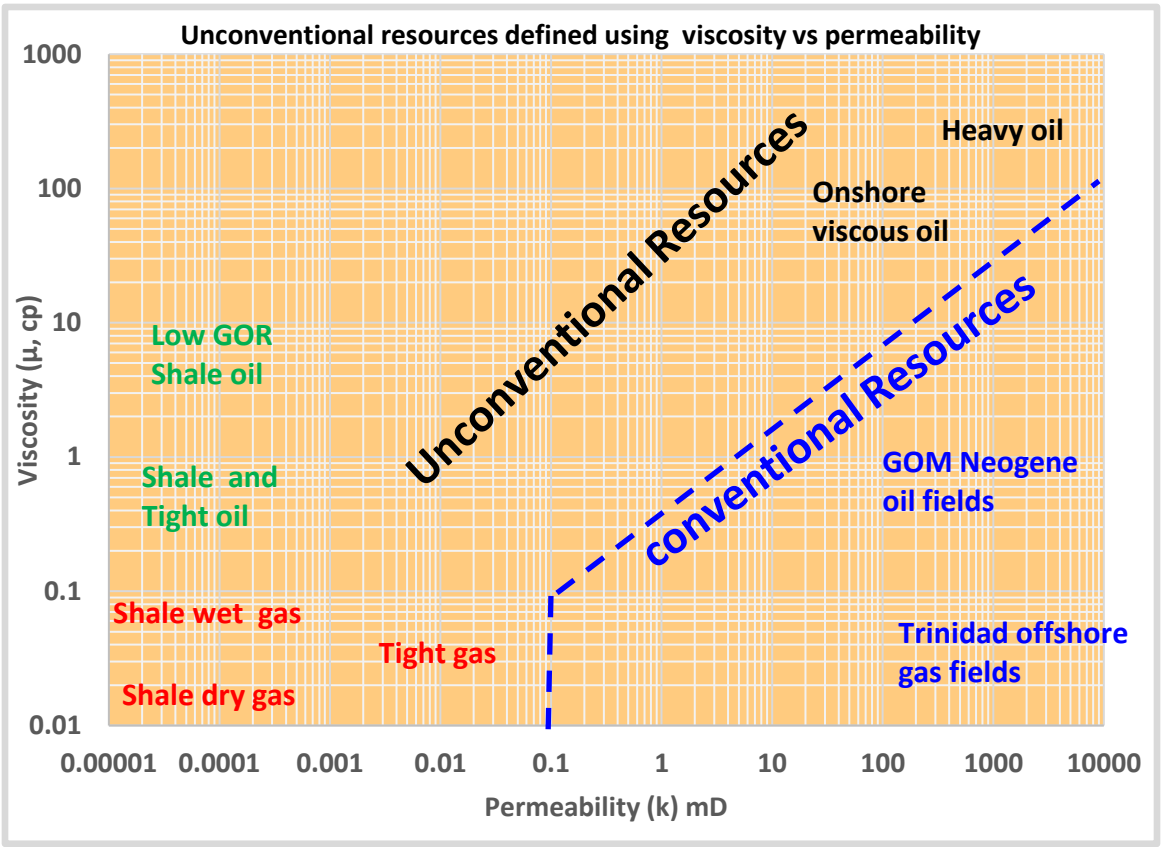

Figure 1-1: Defining unconventional resources based on viscosity (μ) versus permeability (k) (modified from Cander 2012)

Another method of identification and classification of unconventional resources is based on major organic components such as kerogen and thermal maturity and their hydrocarbon generating potential. Shale rocks are one of three sedimentary rocks that are usually found in petroleum systems, while the other two rock types are sandstone and

carbonates. However, unlike other sedimentary rocks in conventional oil and gas, the shale rock (or organic rich shale) is both the source rock and the reservoir in unconventional resources. Dawson (2013) classified shale reservoirs into three groups: (i) Organic-rich black shales that have high TOC (total organic carbon), high-adsorbed gas, low matrix water saturation and mature source rock. (ii) Silt-laminated shales, which have gas stored in silt and shale, low TOC and higher permeability in silt layers. (iii) Highly fractured shales, which have low TOC, low adsorbed gas, and high matrix water saturation.

North America has a series of massive and widely spread unconventional resources such as tight reservoirs, shale gas and shale oil plays. Figure 1-2 shows the extent of these unconventional resources, and their geographic locations. Figure 1-2 also shows the study area of this research, Montney Formation (1) in Canada, which extends from southwestern Alberta to northeast British Columbia, Permian basin (2) and Eagle-Ford formation (3), which are both located in Texas, USA. Similarly, a technical report prepared for the EIA (U.S. Energy Information Administration) by (Kuuskraa et al. 2013) on global shale oil and shale gas estimated that the North American "risked technically recoverable" oil and gas reserves as 69.6 B-bbls (billion barrels) and 2,2279 TCF (trillion cubic feet). Since 2010, the US oil production has increased from 5.5 million (BPD) to over 9.5 million (BPD) and most of the production increase came from unconventional resources (U.S. Energy Information Administration 2016). However, recoverable oil and gas reserves are highly susceptible to technology and commodity prices.

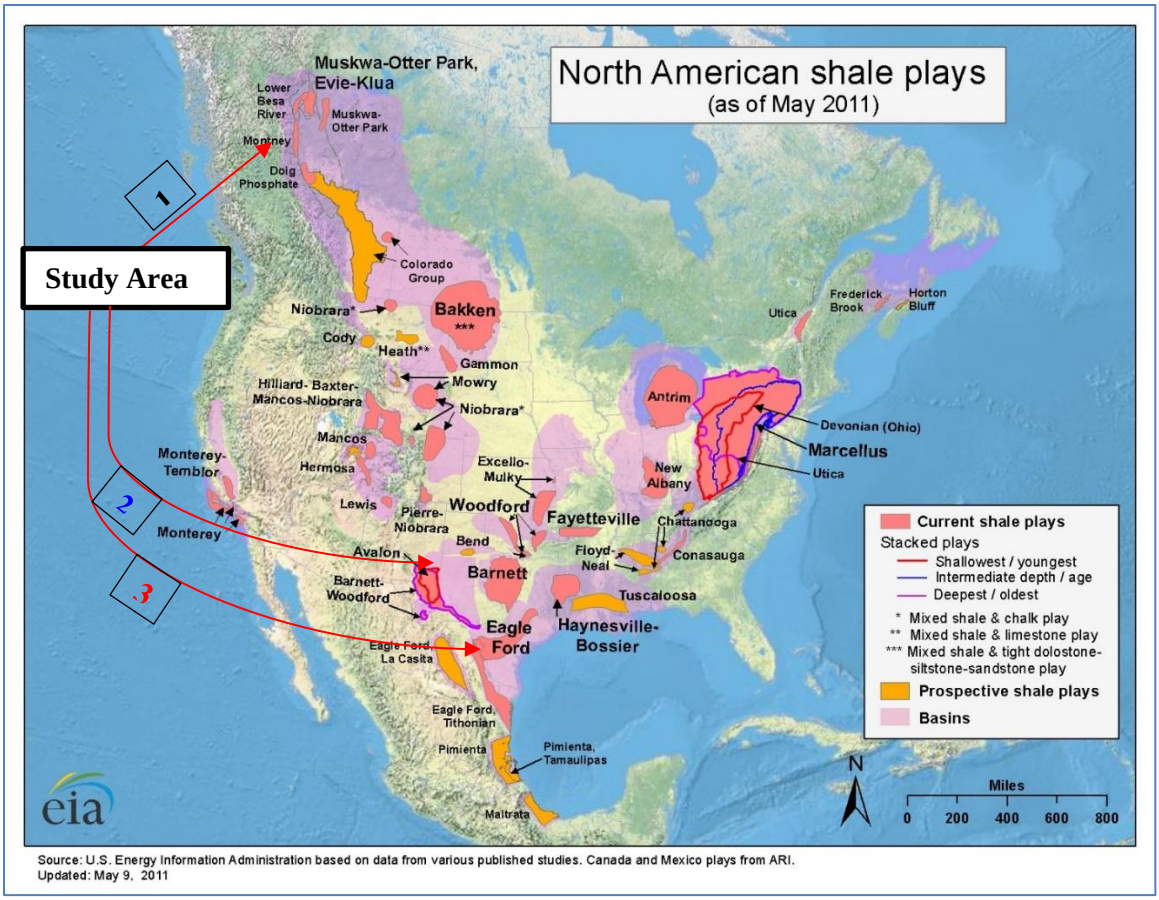

Figure 1-2: North American Shale plays map, and location of the study area (modified from U.S. Energy Information Administration, 2011)

Figure 1-3 shows time series of U.S. tight oil production from selected plays and monthly imported crude oil from different regions of the globe. There is an inverse relationship between oil production from unconventional resources and imported crude oil into the U.S, which means increasing tight oil production has significantly reduced the U.S. dependence on foreign oil. Figure 1-3 also shows that before the advent of tight oil production, the U.S. was importing over 10 million barrels of oil per day, but lately, crude oil imports have declined to as low as 6.6 million per day.

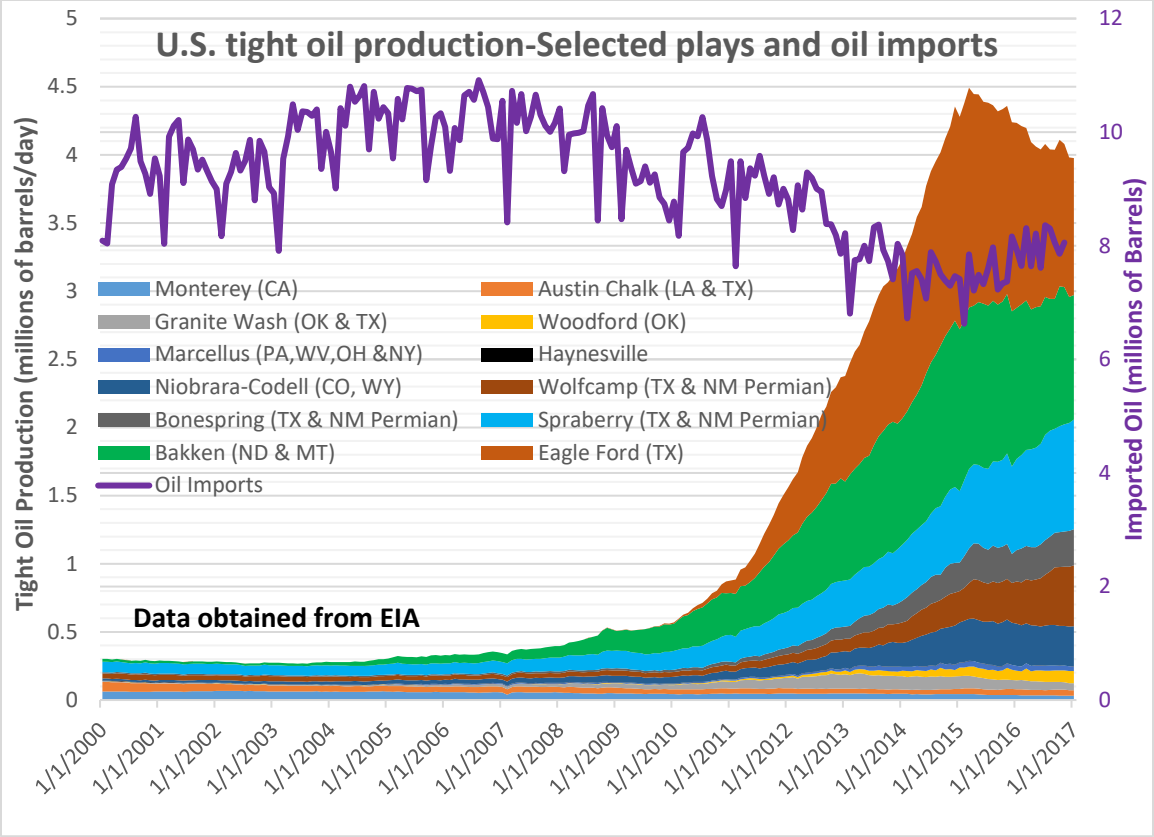

Figure 1-3: U.S tight oil production from selected geological plays

The unconventional natural gas boom started with the success of the Barnett shale, which was discovered in 1981 when the first completion attempt was made (Bowker 2007). However, the real success of the Barnett shale came in 1991 when the Gas Research Institute (GRI) subsidized Mitchel Energy's first successful horizontal well in Fort Worth Basin (Anderson 2013). Figure 1-4 shows U.S. shale gas production from selected plays. Most of the shale gas production before 2009 came from Barnett shale, and there was very little natural gas contribution from unconventional resources in early 2000. However, the impact of the shale gas revolution on energy markets was clearly felt in the U.S. in early 2009 after the financial crisis, which led to precipitous drop in natural gas prices. Figure 1-4

shows that since 2010, there has been massive increases in shale gas production, especially from the Marcellus and Haynesville shales.

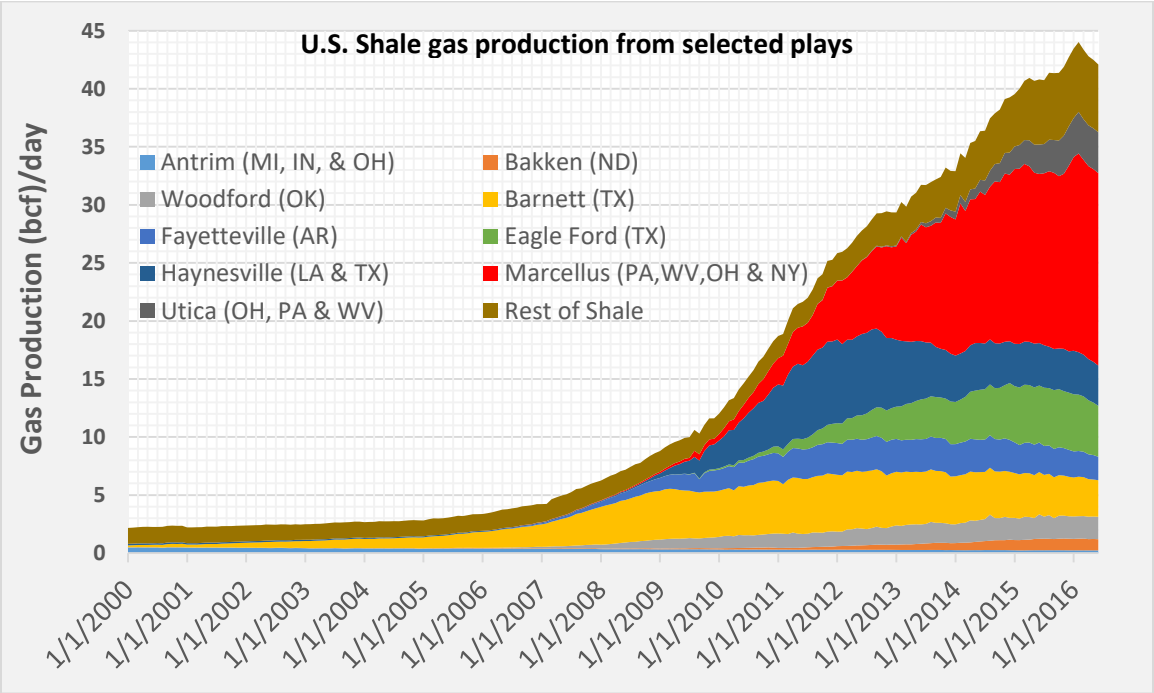

Figure 1-4: U.S Shale gas production from selected plays (data from EIA)

The massive increase of oil and gas production from unconventional resources in the US has led to supply and demand divergence, which resulted in precipitous drop in oil and gas prices. Figure 1-5 shows the US natural gas production and consumption, and prices from 2000 to 2016. Before the advent of unconventional resources, the US was a net importer of LNG (liquefied natural gas). However, because of the exploration and production from the massive unconventional natural gas resources, the US moved from an importer to exporter of LNG, and shipped its first export of LNG produced from the lower 48 states to Portugal on February 24, 2016. Additionally, there are fifteen LNG export

terminals that the US department of energy (DOE) has approved (as of 2016), and some of them are either planned or are at different phases of construction (DOE/FE, 2016).

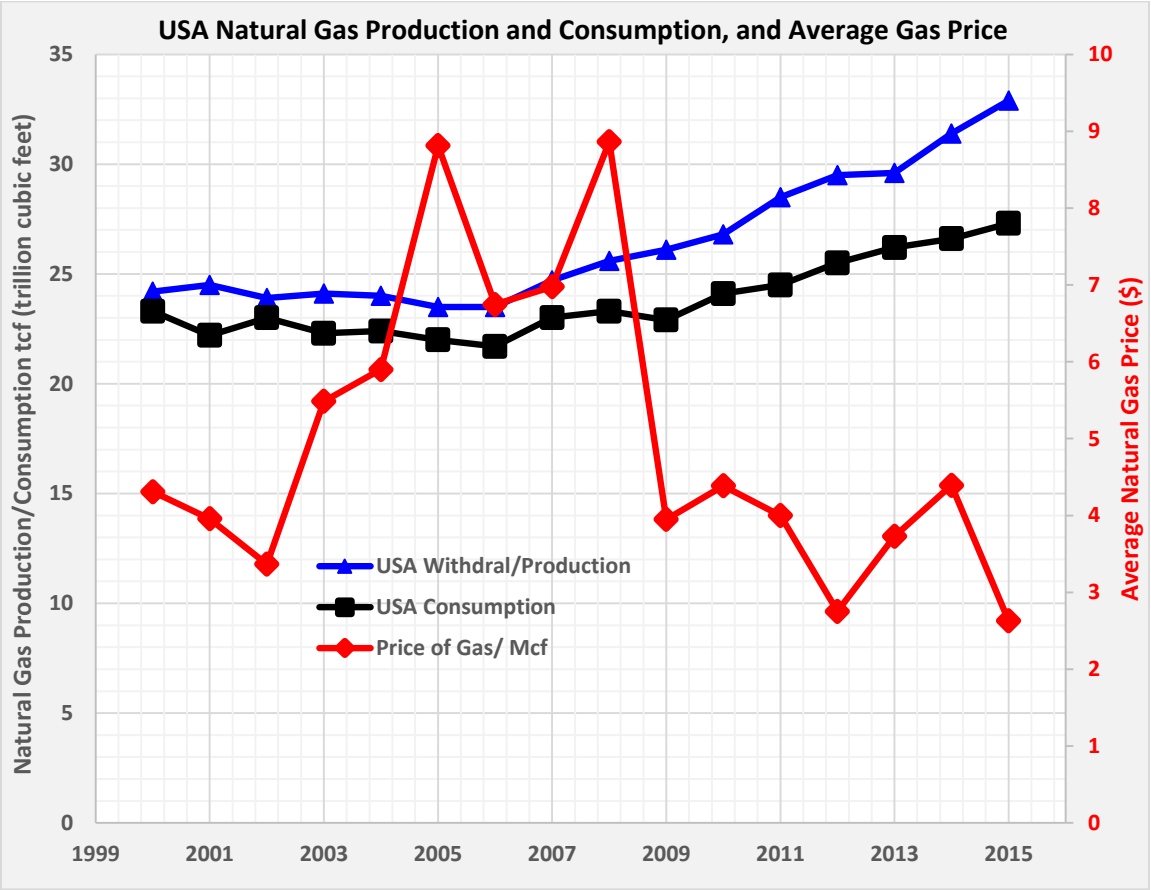

Figure 1-5: USA supply and demand divergence has led to precipitous drop in natural gas price (Data obtained from EIA)

Two technologies, horizontal drilling and hydraulic fracturing have enabled the exploration and development of unconventional resources, which just few decades ago were considered commercially not viable. Since 2008, production from unconventional resources have significantly increased, and currently it accounts for more than half of all

gas production, and an increasing percentage of oil production in the US (U.S. Energy Information Administration, 2015). The transfer of unconventional resources technology and development from North America to the rest of the world is rapidly expanding. For instance, exploration and production of unconventional resources have become critical to China's energy mix (Rassenfoss 2013),(Journal of Petroleum Technology, July 2012); and even Saudi Aramco has massive unconventional resources program (Armaco JT, 2015),(JPT, July 2011). Hence, unconventional resources are increasingly playing a bigger role in the oil and gas markets, and are expected to have a bigger impact on the global energy policy in the long term.

Though geological and technical considerations drive the exploration and productions from unconventional resources, justifying investment requires an acceptable return on investment (ROI). The oil and gas industry is capital intensive and investment projects require long lead-times. The two biggest cost drivers in unconventional resources are (horizontal) drilling and completion. Figure 1-6 shows the breakdown of the average cost for some of the major US onshore Basin/shale plays. The result shows that completions cost, which includes casings/liners, wellhead, pumping units, and hydraulic fracturing, is the biggest and accounts for 63% of the total well cost. Drilling cost, which used to be the biggest cost in conventional oilfields, is now 33%. In some of the shale plays, drilling cost has been declining to as low as a quarter of the total cost (U.S Energy Information Administration, 2016a). Additionally, the percentage of horizontal wells drilled in the US has increased from 24% in 2010 to 77% in 2015 (U.S Energy Information Administration, 2016b).

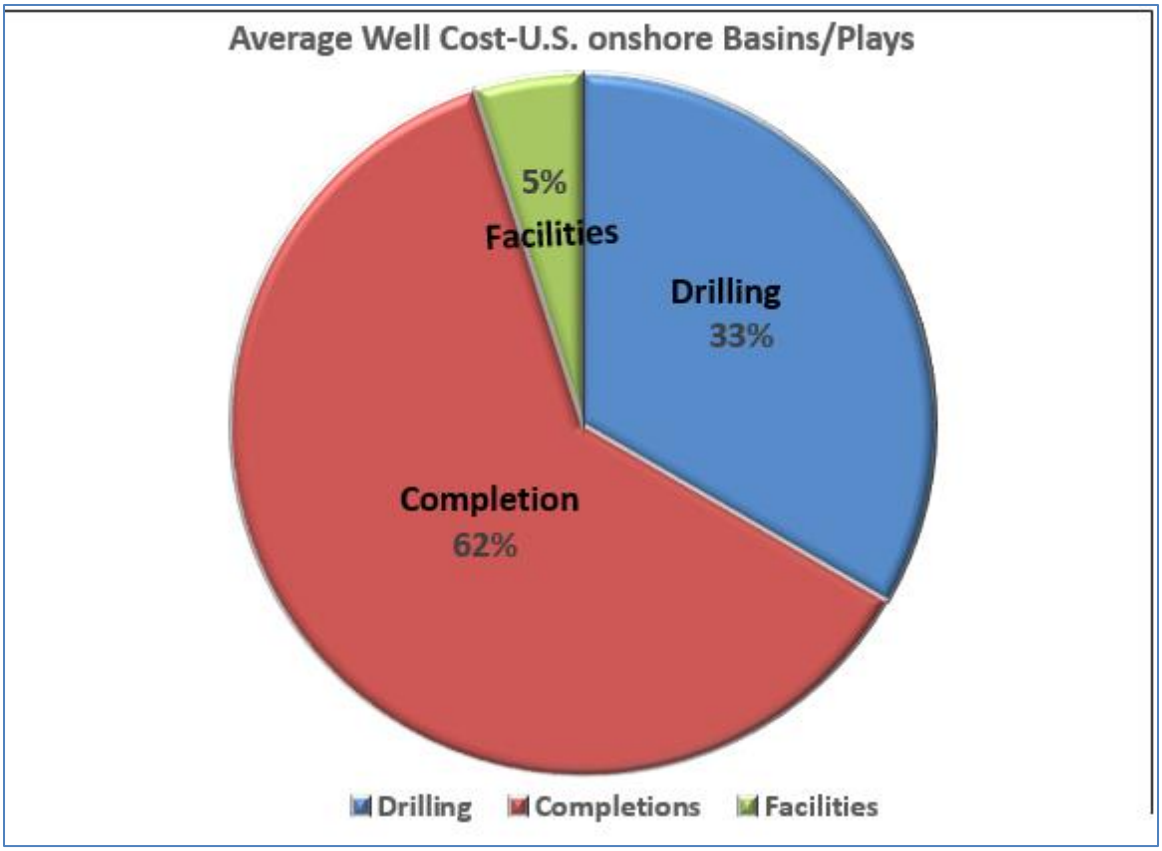

Figure 1-6: Average well cost for some of the major US onshore Basin shale plays (data obtained from (U.S Energy Information Administration 2016a))

1.2. RESEARCH OBJECTIVES

The objective of this research was to study the effect of complexities, in-situ stress anisotropy, direction and azimuth, on the performance of hydraulically fractured horizontal wells. The objective task was accomplished using the following processes:

1. Construct multiphase flow reservoir simulation models to study the performance of transversely fractured versus longitudinally fractured horizontal wells.
2. Develop integrated completions and reservoir models to analyze the impact of fracture network complexities, reservoir characteristics and drainage on production performance

3. Develop methods for optimizing stimulation designs based on hydraulic fracture treatment volumes (proppant mass), number of fracture clusters per stage, and fracture spacing on horizontal wells.

1.3. THE SCOPE AND ASSUMPTIONS OF THE RESEARCH

Some of the assumptions that were made in this research are:

1. Gas adsorption and desorption in organic rich shales were modeling using Langmuir Isotherm and isotherm type 1 is generally considered good fit for modeling methane gas adsorption in porous media
2. The data from Montney Formation used in this research is representative of other shale condensate reservoirs, especially those reservoirs that have similar rock and fluid properties
3. The integrated model does not include exogenous assumptions on the hydraulically fractured wells such as interference from neighboring wells or induced fractures encountering depleted zones or activating faults. It assumes homogenous rock and fluid properties throughout the closed drainage system.
4. The model PVT (pressure, volume, and temperature) analysis assumes the fluid phase behavior can be accurately modeled using EoS (equation of state) from PR (Peng-Robinson, 1978), especially for modeling the two-phase flash calculation.

The scope of the research can broadly be divided into two major sections; the first section investigated the performance comparison of transversely fractured versus longitudinally fractured horizontal wells. Factors such as PVT (pressure, volume and temperature) properties and characteristics were modeled by fitting EoS (equation of state)

and fine-tuned with second EoS after lumping into seven pseudo-components. Impact of stress dependent permeability, adsorption and desorption, and non-Darcy flow effects on productions were modeled.

The second part of the research studied fracture complexities in unconventional resources and optimizations of hydraulically fractured horizontal wells. This was the major part of the PhD research, and had five different tasks. Factors investigated were the use of low quality micro-seismic data to build calibrated stimulation models, effect of fracture complexities, use of curvature data to characterize and evaluate existence of natural fractures, and methodologies for optimizing hydraulic fracture designs. Figure 1-7 shows the scope of the research and the execution plan used to carryout different tasks of the research.

In summary, here are the research objectives that were accomplished with this dissertation:

- Part 1:
  - Determined reservoir permeability based cut-off criterion that can be used when selecting whether to drill transverse vs longitudinal fractured horizontal wells
  - The result of the multiphase flow study can be use as completion and field development guide for horizontal well fracture spacing as a function of reservoir permeability

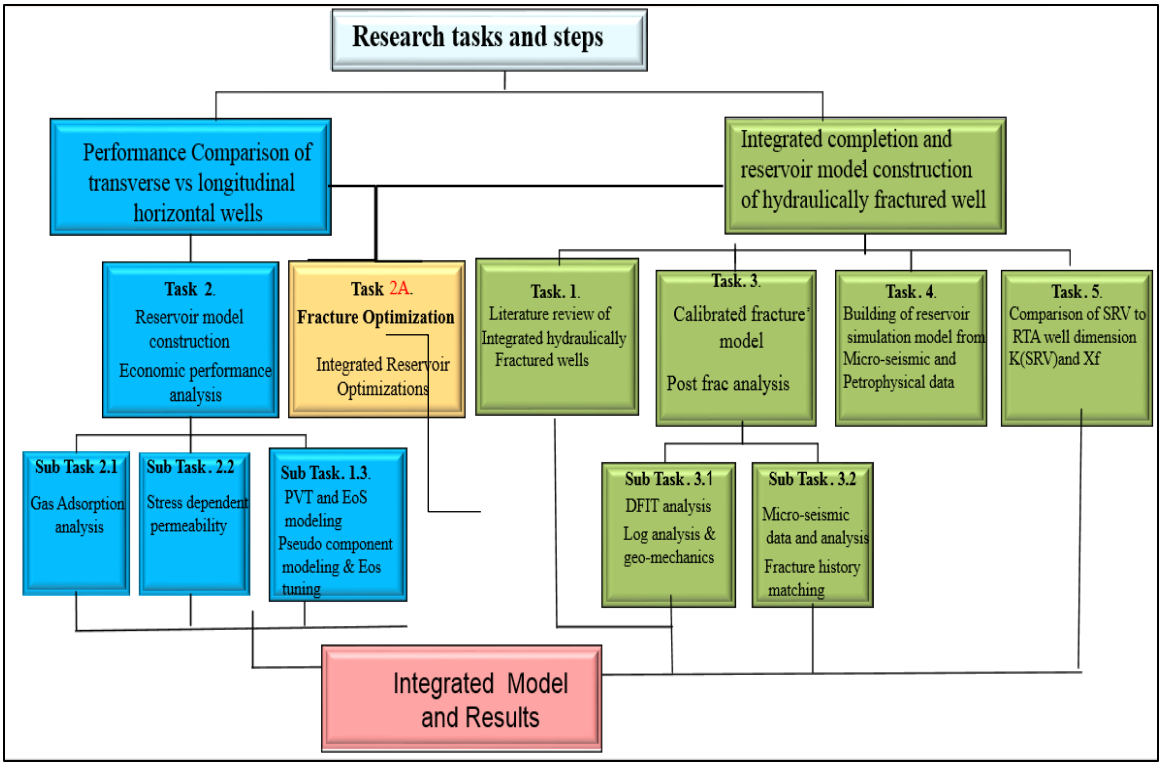

Figure 1-7: Research scope and plan outline

- Part 2:
  - Investigated hydraulic fracture complexities and the benefits of minimizing or maximizing complexity in unconventional resources and tight reservoirs
  - Developed methodology for constructing calibrated fracture model from low quality micro-seismic survey (with location bias and signal-to-noise ratio issues)
  - Developed integrated completion and reservoir models (planar, hybrid DFN and SRV + micro-seismic) using all available data to optimize and forecast well production for different scenarios

- Developed stimulation optimization parameters based on proppant mass, fracture spacing and number of clusters, and developed methods to measure optimization effectiveness.
- Investigated impact of the new optimization trends in hydraulic fracturing such as “big frac” sands per stage (300 M-kg, 400 M-kg), shorter fracture spacing and use of slick-water as fracturing fluid.

2. LITERATURE REVIEW

The contributions of low-permeability reservoirs such as tight sands, and shale gas and shale oil to the overall production has significantly increased, and currently accounts for more than half of all gas production, and an increasing percentage of oil production in the US (U.S. Energy Information Administration, 2015). Two technological innovations, horizontal drilling and hydraulic fracturing, are primarily responsible for the economic viability of these low-permeability reservoirs, which were considered commercially not viable two decades ago (U.S Energy Information Administration 2016a). Though both technological innovations have been in existence since the late 1960s, operational challenges made execution more difficult, especially in the stimulation technology. Issues such as deviation in the wellbore, misalignment of perforations and principal stresses, and weakly consolidated formations made stimulation execution more difficult by requiring higher treatment pressure (and more horse power), which meant higher stimulation cost.

2.1. MULTIPHASE PERFORMANCE COMPARISON OF TRANSVERSELY FRACTURED VERSUS LONGITUDINALLY FRACTURED HORIZONTAL WELLS

Previous studies that compared the performance of transversely fractured horizontal wells versus longitudinal horizontal wells were limited in scope either by the range of reservoir permeability studied or the single-phase flow models that were used in the study. Secondly, none of the previous work undertook extensive integrated completion and reservoir simulation study that modeled multiphase flow in transversely fractured versus longitudinally fractured horizontal wells. Thirdly, most of the previous studies included cost (from one or two oilfields) in their analysis, which might have limited the

applicability of the recommendations since cost is a subjective issue and varies across regions and companies. In this study, discounted recovery (production) and present value (PV) were used for the economic analysis. Fourth, this study incorporated the effect of non-Darcy flow, adsorption gas, relative permeability effect on fluid flow in the fracture, and the impact of stress dependent permeability on fracture conductivity, which were missing in previous studies. In this study, the range of reservoir permeabilities covered from 0.000001 md to 1.0 md.

Research from field and laboratory tests of rock mechanics have shown that hydraulic fractures propagate perpendicular to the minimum horizontal stress (σ_h) in a normal fault environment, creating transverse fractures. This occurs if the perforations are aligned with the preferred fracture plane (PFP), which in this case is the maximum horizontal stress (σ_H). However, the debate has centered on whether transversely fractured horizontal wells or longitudinally fractured horizontal wells are appropriate and "best practice" in a given area and reservoir permeability. This is important since oil and gas companies are simultaneously exploring and producing from both unconventional and conventional resources.

Pearson et al. (1992) presented a paper titled "Results of Stress-Oriented and Aligned Perforating in Fracturing Deviated Wells" based on a study of the Kuparuk River Field, Alaska. Pearson stated that successful perforation alignment significantly reduced the perforation friction losses encountered during hydraulic fracturing, and the lower perforation friction pressure allowed them operationally to execute larger fracture treatments, and to obtain longer fracture half-lengths (x_f).

Valko at al. (1996) studied the performance of hydraulically fractured horizontal wells in high permeability reservoirs and stated that longitudinally fractured horizontal wells deserve further attention and research. Generally, high permeability formations are fractured in a process called “Frac-Packs” where the desired fracture treatment outcome is to develop screen-outs, leading to wider but shorter fractures. Valko compared production rates and cumulative productions for longitudinally fractured horizontal wells versus fractured and non-fractured vertical wells. For economic analysis, Valko used the concept of “discounted revenue,” which takes the “time-value of money” into consideration. This allows easy calculation of net-present value (NPV), discounted return on investment (DROI), and probably the most important parameter, discounted profit-to-investment ratio (DPIR), which R.D. Seba (1987) argued as “the only investment selection criterion you would ever need” in his paper of the same title.

A hydraulic fracturing optimization study titled “Horizontal Well Completion, Stimulation Optimization, and Risk Mitigation” was presented by Britt and Smith (2009). In the study, they developed well performance and economic criteria for drilling longitudinal and transverse horizontal wells, given reservoir objectives and geomechanical limitation. Britt and Smith concluded that “economic optimization studies can be undertaken to align the completion and stimulation plans with the horizontal well objectives,” and highly emphasized the role in-situ stress plays in horizontal well completion and fracture stimulation successes.

Economides et al. (2010) presented detailed evaluation results from transverse, longitudinal and verticals wells for both oil and gas reservoirs. The permeability range of the study was from 0.001 md to 500 md and mostly had similar reservoir and fracture input

data for the fracture design model. Though Economides evaluated large number of fracture designs and produced the results shown in, the models used for the parametric studies lacked multiphase flow capability and may not be suitable for liquids-rich tight sands and shale plays. Table 2-1 gives suitable options for selecting completion design based on reservoir permeability for both oil and gas wells derived from this study versus Economides' study.

Table 2-1: Comparison of results from this study compared to Economides' results

Suitable options for fracturing wells (from this Study) compared to Economides' Study					**Economides' Results**	
Best Option	**Critical Permeability in volatile oil and Condensate reservoirs (API 48)**	**Black oil type reservoirs (API 38)**	**Dry gas reservoirs**	**Comments**	**Oil Well**	**Gas Well**
Longitudinal Fractures	**K > 1.8 md**	**K >2.0md**	**K>0.9 md**	Reservoir fluid composition effects	k > 10 md	k > 5 md
Transverse Fractures	**K < 0.07 md**	**K<0.3 md**	**K<0.05d**	Non-Darcy flow effects transverse at higher permeability	k < 10 md	k < 0.5 md

Liu et al. (2012) focused on moderate permeability gas reservoirs (0.01 md to 5.0 md) in the study of transversely versus longitudinally fractured horizontal wells using unified fracture design (UFD) method introduced by Economides et al. (2002), and included in his analysis non-Darcy flow effect on well productivity. However, Liu

concludes that the optimization of drainage and mechanism of flow are more important than well architecture (i.e. transverse vs longitudinal fracturing). This conclusion seems to minimize the integrated nature of fracture conduits and reservoir drainage in low permeability reservoirs and its impact on flow mechanism.

Yang et al. (2015) conducted one of the most extensive research projects in the performance comparison of transversely versus longitudinally fractured horizontal wells, and presented her findings in a paper titled "The Effect of Well Azimuth or Don't Let Your Landman Plan Your Well Path!" Yang used a single phase numerical simulator, and covered a wider range of permeability reservoirs, from 0.0005 md to 5 md, and modeled both oil and gas reservoirs. In her conclusion, Yang stated that there is a critical permeability in which longitudinally fractured horizontal wells outperforms transversely fractured horizontal wells, and for oil and gas reservoirs the critical permeability was 0.4 and 0.04 md, respectively for open hole completions.

The motivation for conducting this research came out of the realization that all previous studies that looked into the performance comparison of transversely versus longitudinally fractured horizontal wells were limited in scope either by the range of reservoir permeability studied or the single phase-flow models that were used in the study. Secondly, none of the previous work undertook extensive integrated completion and reservoir simulation study that modeled multiphase flow in transversely fractured versus longitudinal fractured horizontal wells. Thirdly, most of the previous studies included cost (from one or two oilfields) in their analysis, which might have limited the applicability of the recommendations since cost is a subjective issue and varies across regions and companies. In this study, discounted recovery (production) and present value (PV) were

used for the economic analysis. Fourth, this study incorporated the effect of non-Darcy flow, adsorption/desorption of gas, relative permeability effect on fluid flow in the fracture, and impact of stress dependent permeability on fracture conductivity, which were not considered in previous studies.

2.2. INTEGRATED COMPLETION AND RESERVOIR MODELING OF HYDRAULICALLY FRACTURED WELLS

The combination of horizontal drilling and multistage hydraulic fracturing of horizontal wells have enabled the exploration and development of unconventional resources, which few decades ago were considered commercially not viable. However, integrating information from drilling, completion, and reservoir to drive operational excellence is now the objective of many producers. This is critically important in low commodity price environment where the focus needs to shift to optimizing completion techniques and improving well recovery. Energy companies are integrating data from different functional groups (using GIS (geographic information systems)) to develop integrated completion, production and reservoir models that are updated and refined as more information becomes available. Use of "Best practice" methods, and continuously researching what works or does not work in a given shale play is now well-documented in the industry. Okouma et al. (2012) presented a paper titled "Play-wide Well Performance Analysis in Montney Siltstone" and stated that developing "consistent workflow for analyzing well performance and predicting future performance of wells" requires assessing and determining practices worth replicating across the Montney play.

Quirk et al. (2010) presented workflow for integrating micro-seismic, fracture modeling and reservoir simulation to study fractured horizontal well in the Cardium tight

oil formation. Quirk stated that the objective of the project was to measure fracture orientations and geometries with micro-seismic survey and to create calibrated fracture model. In the Cardium tight oil formation study, Quirk used pseudo-3D fracture simulator and black oil reservoir simulator. However, in this study, fully-3D fracture simulator and compositional reservoir simulators were used. This is critically important because previous studies (Kassim et al. 2016) have shown that capturing the effect of fluid composition changes in the reservoir simulation greatly improves the model's reliability and ability to forecast.

Integrated modeling of horizontal wells using micro-seismic data and stimulated reservoir volume (SRV) concepts have been widely used in the oil and gas industry (Maxwell et al. 2002), (Fisher et al. 2002). However, both micro-seismic survey and SRV have inherent uncertainties, which can introduce new complexities into the simulation model that may or may not add value to our understanding of the stimulation or the reservoir. (Cipolla and Wallace 2014) presented a detailed evaluation of micro-seismic survey and stimulated reservoir volume (SRV) in a paper titled "Stimulated Reservoir Volume: A Misapplied Concept?" Cipolla stated that "interpretation of micro-seismic data and the calculation of SRV are poorly linked to the actual hydraulic fracture geometry and distribution of fracture conductivity". Cipolla also compared SVR concept to the use of RTA (rate transient analysis) and linear flow analysis techniques to approximate complex fracture networks. RTA and linear flow analysis provide estimate of fracture half-length and enhanced reservoir permeability (K_{SRV}), which give non-unique values and may not be appropriate for completion optimization.

Mayerhofer et al. (2008) presented one of first papers that studied the concept of stimulated reservoir volume (SRV) in a paper titled "What is Stimulated Reservoir Volume (SRV)?" Mayerhofer stated that SRV "does not provide any details about the effectively producing fracture structure or spacing." The author introduced an equation that can be used to calculate total fracture length (L_{tot}) for the entire SRV of a complex hydraulic fracture, and is succinctly shown below.

$$L_{Tot} = \left(\frac{4x_f f_w}{S_f}\right) + 2x_f + F_w \quad \text{... (1)}$$

Where

L_{Tot} = total fracture length, ft

x_f = fracture network half-length, ft.

S_f = fracture spacing, ft.

f_w = fracture width (in the x, y, z) plane in feet.

The fracture modeling was done using commercial software (Stimplan, MFRAC) that modeled fracture propagation versus time and treatment pressure. These models simultaneously compute conservation of mass, momentum and continuity equation. Elasticity (and plasticity), material balance, fluid flow and width opening equations are combined to predict fracture geometry. Rock (E,ν (Young's modulus and Poisson's ratio)) and fluid mechanics (μ,v (viscosity and velocity)) control fracture propagation and geometry. However, the most important equation for fracture propagation is material balance because V_i (volume) is the injected volume into the reservoir/well, and V_L (volume) is lost to the formation, which is considered wasted energy and does not contribute to fracture creations.

$$V_i = q_i t_p \quad \text{... (2)}$$

Where

t_p = pumping time and q_i= injection rate.

The fracture volume (V_f) created is given by

$$V_f = h_f(\bar{\dot{w}}_f * 2x_f) = \eta V_i \quad \text{... (3)}$$

Where

h_f = fracture height,

$\bar{\dot{w}}_f$ = average fracture width,

η = fluid efficiency and

x_f = fracture half-length.

The 1D fluid loss (V_L) was developed by Carter and is considered a material balance equation for fluid treatment entering one-wing of the fracture. Carter's equation is given by

$$\frac{q_i}{2} = 2\int_0^t \frac{C_L}{\sqrt{t-\tau}}\left(\frac{dA}{dt}\right) + (w + 2S_P)\frac{dA}{dt} + A\frac{dw}{dt} \quad \text{... (4)}$$

where

q_i = fluid injection rate, (bbls/min)

C_L = total fluid leak-off, [ft./min$^{1/2}$]

$\left(\frac{dA}{dt}\right)$ = rate of fracture area change with time, (ft^2/min)

w = fracture width, ft

S_P = spurt loss, [gal/100 ft^2]

$\frac{dw}{dt}$ = rant of fracture width change with time, (ft.min)

$\sqrt{t-\tau}$ = start time (t) minus (τ) the injection time when fluid leak-off starts to until fracture closes.

The right-hand side of equation (4) is made up of 3 parts; the fracture growth (fracture volume), volume losses (spurt losses and leak-off rates) and losses due to width (w) changes. Nolte (Nolte 1986) formulated the leak-off co-efficient (C_L) formula in a series of papers, and is given below in concise form

$$V_L \cong 6C_L h_h x_f \sqrt{t_p} + 4x_f h_f S_p \quad \text{... (5)}$$

Where

S_p= spurt loss (gal/100 ft^2), and the fracture half-length can be calculated by re-arranging above equations to equation (6);

$$x_f = \frac{q_i t_p}{\left(6C_L h_h \sqrt{t_p} + 4h_f S_p + 2\dot{\bar{w}}_f h_f\right)} \quad \text{... (6)}$$

However, the most important equation in hydraulic fracture is the net pressure equation, which is BHIP (bottom-hole injection pressure) minus the total pressure losses due to friction (ΔP_{tot}) and σ_h (minimum horizontal stress)

$$P_{Net} = BHIP - \sigma_h - \Delta P_{tot} \quad \text{... (7)}$$

$$\Delta P_{tot} = \Delta P_{tbg} + \Delta P_{perfs} + \Delta P_{tort} + \Delta P_{perf\_misalign} + \Delta P_{Ball\ seat} \quad \text{... (8)}$$

$$P_{net} = \left[\frac{\acute{E}^3}{h_f^4}(\mu q_i L) + P_{tip}^4\right]^{1/4} \quad \text{... (9)}$$

Where;

ΔP_{tot} = total pressure drop, psi or kPa,

$\acute{E}^3$ = plane strain modulus (E/ (1-ν^2))

ΔP_{perfs} = friction pressure through perforations, P_{tip} = pressure due to fracture effects

ΔP_{tubing} = pressure in the flowline and tubing/casings

$\Delta P_{tortuosity}$ = tortuosity (fracture turning) pressure drop

$\Delta P_{perf\_misalign}$ = friction pressure due to perforation misalignment

$\Delta P_{Ball\ seat}$ = friction pressure due to the ball seat.

B.R. Meyer (1989) presented a paper titled "Three-Dimensional Hydraulic Fracturing Simulation on Personal Computers: Theory and Comparison Studies", which formulated detailed governing equations for hydraulic fracture propagation. Meyer, who later founded MFRAC, showed coupled rock and fluid mechanics equations that govern fracture propagation. Meyer stated that the paper improves Carter and Nolte's equations by accounting for the effects of fluid rheology (which was captured in the conservation of momentum).

Multiphase flow modeling in reservoir simulation consists of conservation laws (mass, momentum and energy), equation of state and Darcy's law. (Khalid and Antonin 1979) wrote one of the earliest reservoir simulation books, and presented detailed workflow on multiphase flow simulation. The generalized multiphase flow equation is

$$\nabla.[\lambda_\alpha(\nabla P_\alpha - \gamma_\alpha \nabla z)] = \frac{\partial}{\partial t}\left[\frac{\emptyset S_\alpha}{B_\alpha}\right] + q_\alpha \quad \text{... (10)}$$

Where;

α = fluid phase (oil or water), λ = mobility ratio

∇ =gradient and

(∇.) = divergent

S, ∅, P = saturation, porosity and pressure respectively.

$\gamma_a = \rho_\alpha \left(\frac{g}{g_c}\right)$ parameter for fluid density multiplied by unit conversion.

Lopez et al. (2014) presented a paper titled "Coupled Fluid Flow/Geomechanics Simulator for Modeling Multiphase Flow and Geomechanical Processes" where he provided methodology for coupling fluid flow and geomechanics. The multiphase equations for oil and water are;

$$\nabla.\left(\frac{KK_\alpha}{B_\alpha \mu_\alpha}\nabla P_\alpha\right) = \frac{\emptyset S_\alpha}{B_\alpha}\left[\left(C_{bc} - C_r(1+\emptyset)\right)\frac{dP_\alpha}{dt} - \left(C_{bc} - C_r\right)\frac{d}{dt}\left(\frac{\varepsilon_v}{C_{bc}}\right)\right] + \frac{\emptyset}{B_\alpha}\frac{dS_\alpha}{dt} + \emptyset S_\alpha \frac{d}{dt}\left(\frac{1}{B_\alpha}\right) + \widetilde{q_\alpha} \quad \text{...(11)}$$

Where

α = fluid phase (oil or water),

C_{bc} & C_r = bulk and rock compressibilities,

ε_v = volumetric strain

2.2.1. Fracture Complexities and Benefits of Optimizing it. Companies that were exploring unconventional natural gas reservoirs in tight sands pioneered the use of micro-seismic survey to monitor and image hydraulic fracture geometries. In most cases, geophones in offset wells recorded small "magnitude events" caused by either shear or tensile deformation. This mostly created planar fractures in tight sands, and micro-seismic

survey was used to estimate fracture geometry and dimensions. However, shale reservoirs often have pre-existing natural fractures, which interact with the induced fractures, creating complex branching network of fractures that expand in different directions. Hence, there was a need for developing complex fracture models that capture fracture geometries observed during micro-seismic mapping of hydraulic fractures in shale oil and gas reservoirs.

Previous researches have shown that most hydraulic fracturing operations create bi-wing fractures because they require less energy to propagate (Warpinski et al. 1997), (Warpinski et al. 1999). Secondly, hydraulic fracture monitoring using micros-seismic mapping have confirmed the existence of mostly bi-wing fractures (Wolhart et al. 2006). However, there are boundary conditions that can force the activation of discrete fractures in multiple directions that require less energy than bi-wing fractures (Meyer and Bazan 2011). Though micro-seismic mapping provides a lot of valuable information about fracture dimensions and geometry, the debate has been what micro-seismic events, source parameters and uncertainties, and workflow to use for building complex fracture models.

The interaction between induced fractures and natural fracture or even interactions between discrete fractures can cause fluid loss and mechanical interference, limiting fracture propagation. However, the question is whether fracture complexity is beneficial to well performance or it's something to be avoided because there is benefit in minimizing fracture complexity in unconventional resources, especially in shale oil and shale gas reservoirs. Warpinski et al. (2008) conducted one of the earliest research on fracture complexity and presented in a paper tilled "Stimulating Unconventional Reservoirs: Maximizing Network Growth While Optimizing Fracture Conductivity" where the authors

stated “ultra-low shale permeability reservoirs require an interconnected fracture network of moderate conductivity with relatively small spacing to obtain reasonable recovery factors.” Figure 2-1 shows schematic diagrams of different types of fracture complexities postulated by (Warpinski et al. 2008), which was divided into four groups.

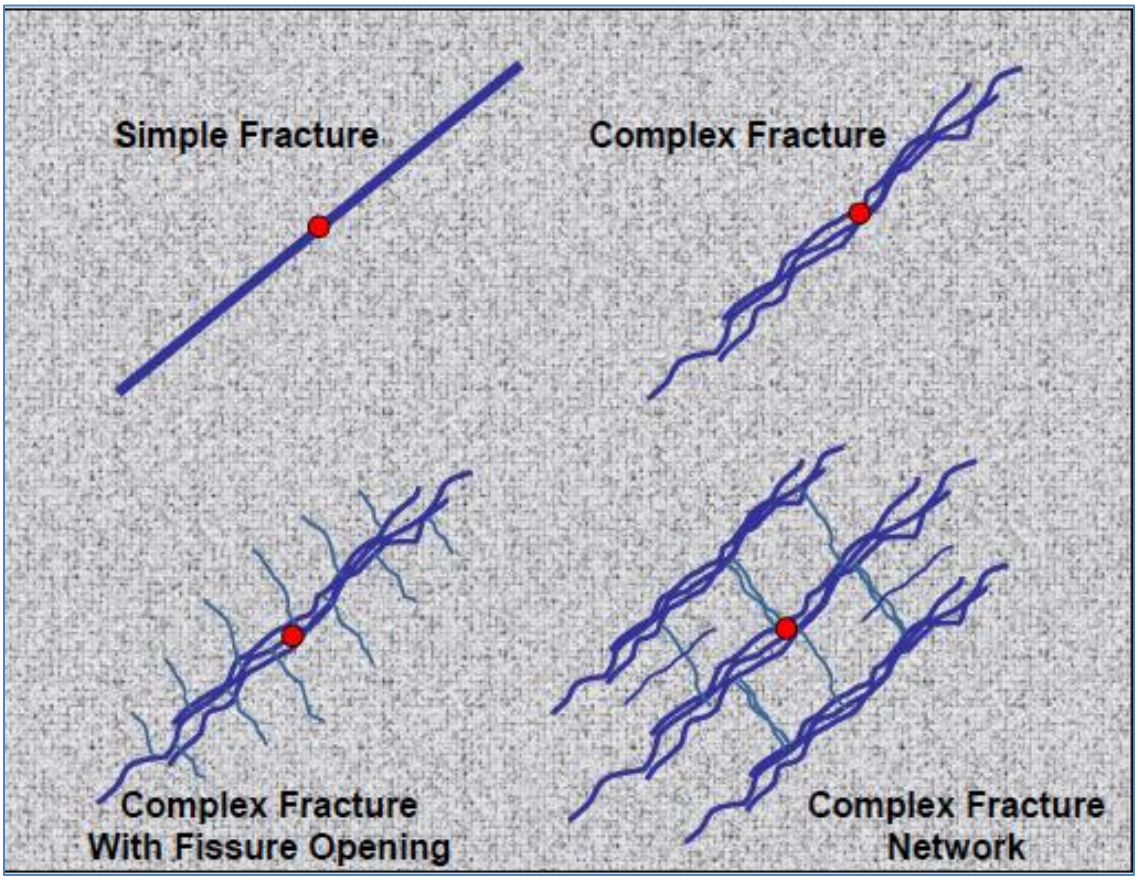

Figure 2-1: Fracture growth and complexities for different scenarios (SPE 119890)

The question is how does fracture growth and complexities for different scenarios account for proppant transportation during fracture treatment, and after fracture closure both in the induced fractures and discrete fracture networks? Previous research in mine-

backs and coalbed methane reservoirs have shown the presence of fracture complexity in geologically heterogeneous environments (Branagan et al. 1996), (Fast et al. 1994).

In fractured reservoirs, there would be interactions between induced hydraulic fractures and natural fissures, and the degree of interaction and distribution of proppant mass during stimulation treatment depends on natural fracture density, spacing and in-situ stress environment.

The distribution and probability of discrete fracture networks greatly influences the success of stimulation design and well productivity. Therefore, fracture designs should be tailored to well performance objectives and whether to target or avoid fracture complexity. Cipolla et al. (2010) presented fracture design guidelines for situation where fracture complexity is anticipated during hydraulic fracture treatment. Factors such as the type of fracture treatment fluid to use, reservoir permeability and micro-seismic mapping data should be defined, analyzed and consulted.

Cipolla et al. (2010) presented three different cases of proppant mass distribution in complex fracture networks and then used reservoir simulations to model well performance for each case. Figure 2-2 shows the three cases modeled; evenly distributed (case 1) proppant mass between the induced hydraulic fracture and natural fractures. In case 1, the result showed that proppant concentration was inadequate and less than 10% of the area was propped, which made the created fracture behave more like un-propped fracture. In case 2, most of the proppant stayed within induced hydraulic fracture, making it infinitely conductive. The authors stated that when the induced fracture behaves infinitely conductive, the network fracture conductivity required decrease by a factor of 10. The third

proppant distribution scenario is probably the most difficult to achieve and model because the proppant settles in “pillars” at specific sites within the discrete fracture network.

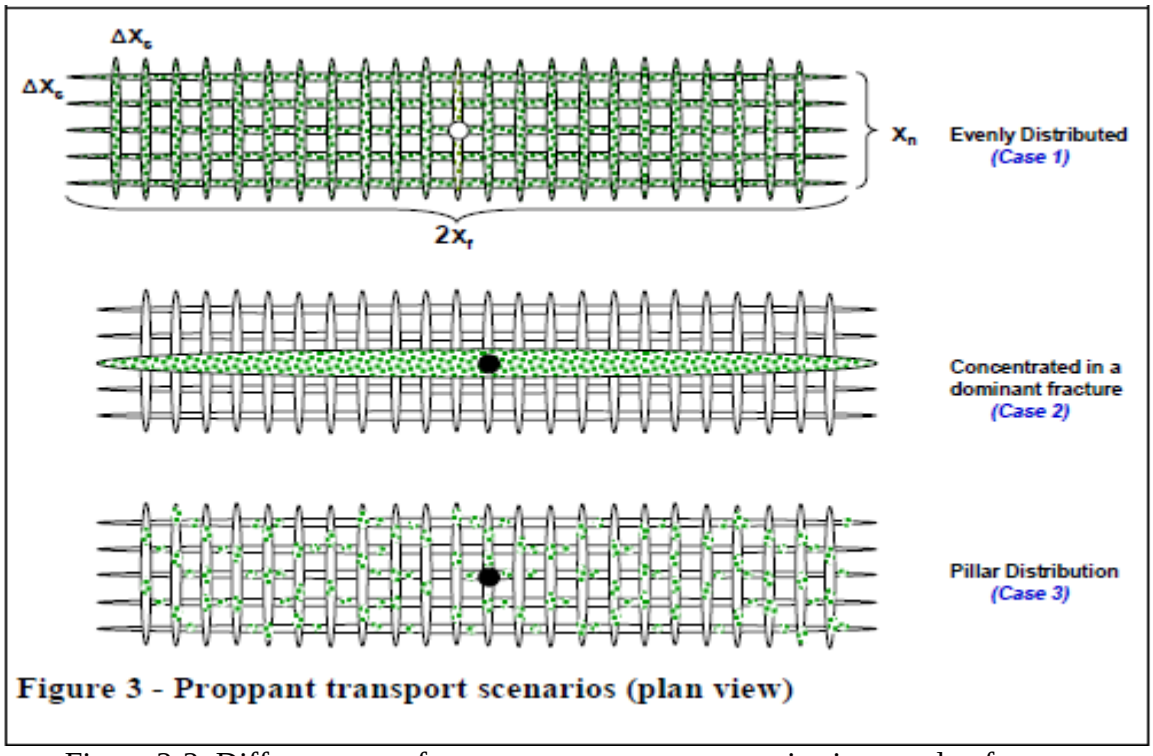

Figure 2-2: Different cases for proppant transport scenarios in complex fracture networks-plain view (SPE 115769)

Unconventional gas reservoirs such the Marcellus gas shale play have shown the existence of fracture networks, which are mostly observed in rock outcrops and confirmed by micro-seismic mapping. Figure 2-3 shows joint sets (J_1 and J_2), which are two regional joint sets found in the Marcellus gas shale of North-Eastern United States. Figure 2-3 also shows that the two joint sets are orthogonal to each other and form unevenly spaced fracture networks. Engelder et al. (2009) who is a leading authority on Marcellus gas shale play

stated that the presence of the two regional joint sets "enhance production from Middle and Upper Devonian gas shales of the Appalachian Basin." The authors stated that joint (J_1) is parallel to the maximum horizontal stress (S_{Hmax}), and fracture stimulations in vertical wells intersect and drain only joint (J_2), making fracture stimulations in horizontal wells the preferred method to intersect and drain both joint sets (J_1 and J_2).

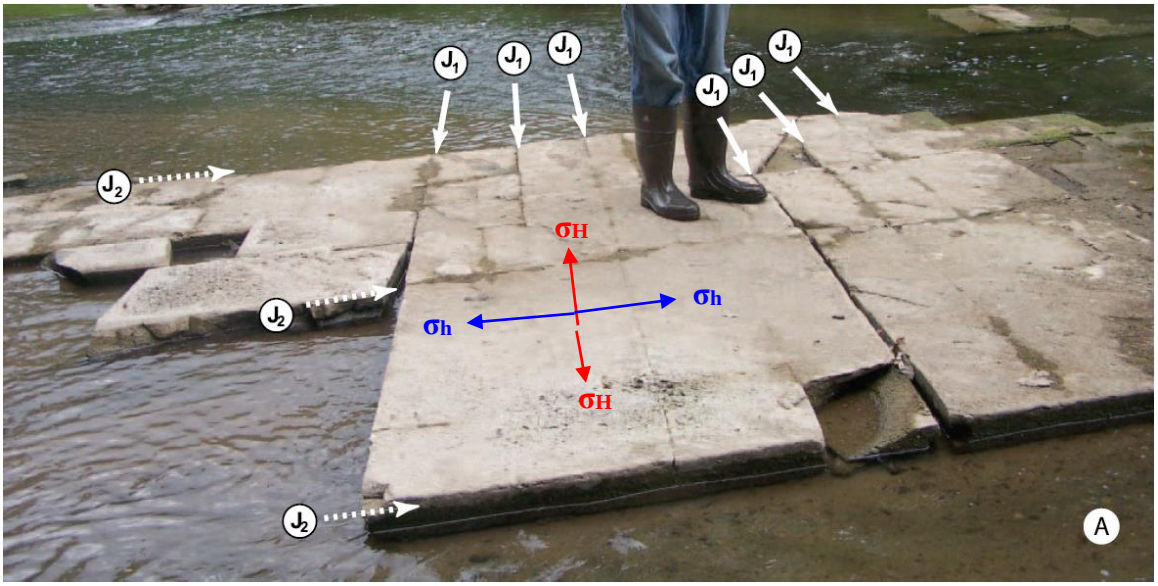

Figure 2-3: Crosscutting J1 and J2 joints in the Marcellus black shale exposed in Oatka Creek, Le Roy, New York. View is to the east-northeast (obtained from Engelder et al. 2009)

Most of the wells in the ultra-low permeability reservoirs are horizontally drilled in the direction of the minimum horizontal stress (S_{Hmin}), and are stimulated to create transverse fractures (Denney 2013), (Hulsey et al. 2010). Figure 2-4 illustrates multiple well pads design showing micro-seismic mapping, the two geological joints in the Marcellus shale play (J_1 and J_2), and the interaction between the induced hydraulic fractures

and natural fissures. The wells were drilled in the direction of the minimum horizontal stress, which created transverse fractures that are parallel to (J_1 joints). However, the (J_2) joints are at an angle to the induced fractures, creating network of discrete fractures that interact and crosscut multiple times with each induced fractures. Figure 2-4 also shows number of faults, which are parallel to (J_1 joints), and got activated (in the case of well B) during the hydraulic fracture treatment.

There is an increasing degree of skepticism about the desirability of fracture complexity in ultra-low permeability reservoirs because natural fissures compete with the induced hydraulic fractures. Hence, natural fractures either limit hydraulic fracture growth or interact with the hydraulic fractures causing increased fluid loss, which reduces stimulation efficiency. Secondly, most of the benefits cited from fracture complexities are based on two arguments; first, is the perceived increase in production that is attributed to horizontal wells that target natural fractures. Evidence of natural fractures are either from cores or image logs. The second often cited evidence of fracture complexity benefits is that of the Barnett Shale, which previous research have shown to have natural fractures (Fisher et al. 2002), but most shale plays do not have petrophysical properties similar to that of the Barnett shale (Rickman et al. 2008).

Multiple studies that compare production performance of wells with and without facture complexity have shown that planar fractured wells had better productivity and EUR. Cipolla and Wallace (2014) conducted one of the most extensive study that compared gas recovery for planar fractures versus two DFN (discrete fracture network) models; one DFN model had 50-feet natural fracture spacing and the other DFN model had 75-feet.

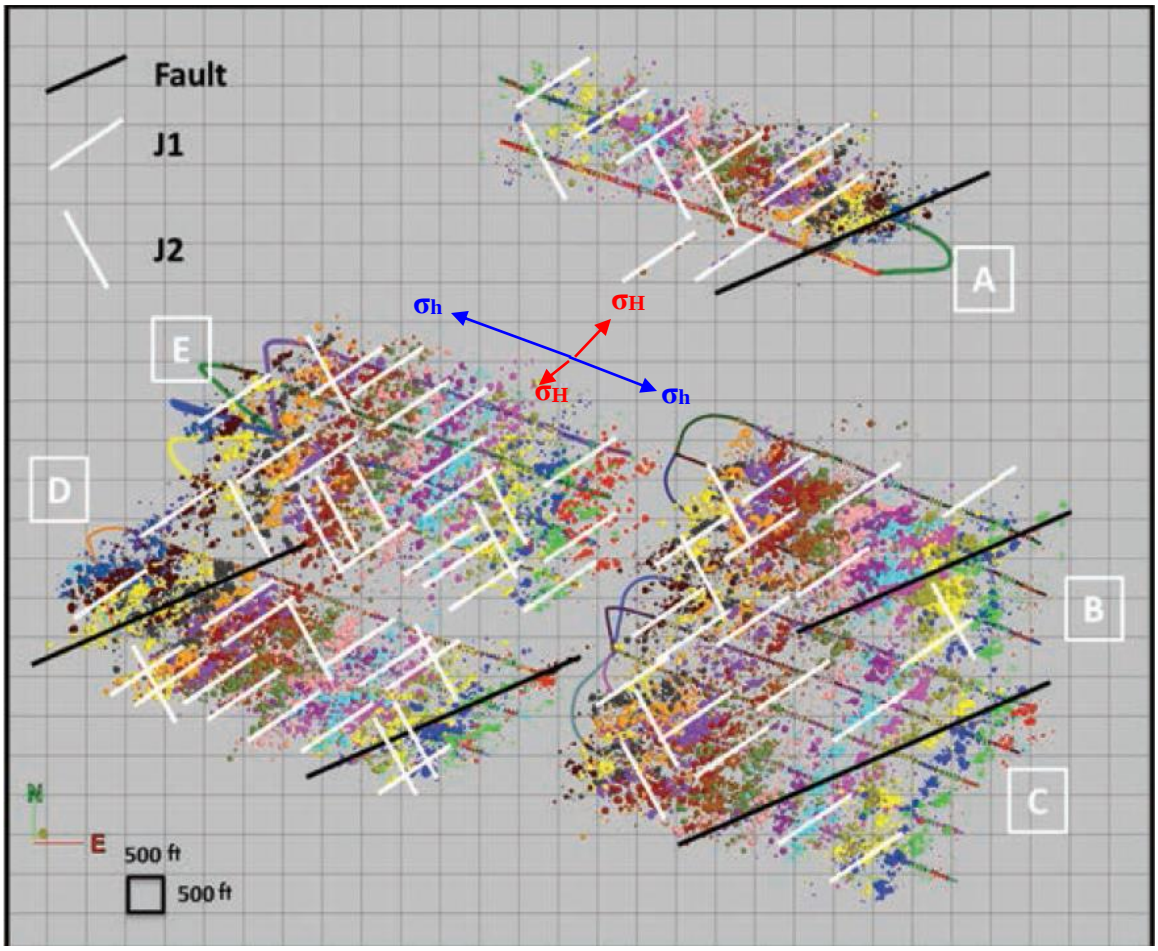

Figure 2-4: Multiple well pads showing micro-seismic events, two sets of joints (J_1 and J_2) and interactions of induced hydraulic fractures and natural fractures (modified from Denney 2013)

Figure 2-5 shows the result from Cipolla and Wallace's (2014) study, which shows that the planar fracture model outperformed the two other models that had discrete fracture networks.

In this dissertation, natural fracture location, density and orientation were determined from two sources; micro-seismic mapping and curvature data from 3D seismic. Secondly, natural fracture spacing or presence of discrete fracture network were

determined from micro-seismic events' distribution and orientation versus in-situ stresses and lateral direction of the horizontal wells.

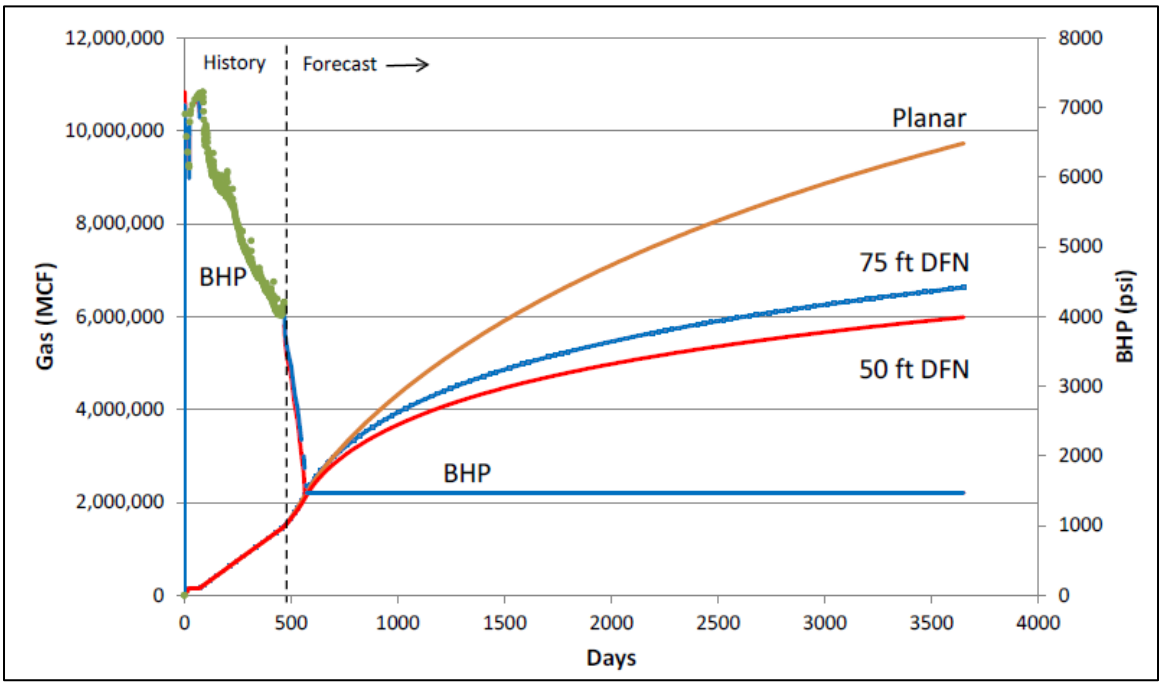

Figure 2-5: Comparison of planar fracture model versus DFN (discrete fracture network) models (from SPE 168596)

2.2.2. Hydraulic Fracture Optimization. Stimulation design and optimizations have always been critical to the exploration and production of unconventional resources. There are many reasons for optimizing well completions, especially hydraulic fracturing. Some of the major reasons are reducing cost, improving efficiency, accelerating and enhancing the development of unconventional resources. Secondly, there have been multiple proposals and workflows for optimizing stimulations, which were developed based on multiple, and sometimes conflicting sets of parameters. However, since

optimization is a sequential process and each subsequent decision limits the number of options available, stimulation optimization can broadly be grouped into three major categories; optimizations based on completion type, fracture treatment design and volumes, and fracture diagnostics.

Stimulation optimizations based on well completion type requires identifying key parameters that might have the biggest impact on well performance. Parameters such as casing design (open-hole versus cased-hole), rock mechanics (in-situ stress magnitude and direction), well placement (which effects number of fracture stages and clusters per stage) and completion equipment needed. Britt and Smith (2009a) presented an optimization study that showed the importance of lateral length, fracture spacing, number of stages, fracture half-length, and casing design (open-hole versus cased hole) to production performance. The authors emphasized the importance of reservoir geomechanics and concluded, "Stimulation optimization should be aligned with objectives" such as improving well productivity, economics and EUR.

Hydraulic fracture optimizations based on "fracture treatment design and volumes" have been the focus of a lot of research lately. Impact of parameters such as proppant mass per stage, treatment fluid type, and "zipper fracture design", which has improved efficiency and reduced the impact of stress shadowing during stimulation, have greatly enhanced well productivity. Saldungaray and Palisch (2012) proposed hydraulic fracturing optimization for horizontal wells based four parameters; fracture conductivity, well placement and lateral length, fracture spacing, and completion hardware.

The success of any hydraulic fracture optimization study depends on the quality and integration of the data deployed for the optimization exercise. Fracture diagnostics is

a major area of study, and new technologies for measuring fracture dimensions and geometry are becoming critical to well performance and optimization. Factors such as lateral length or stage efficiency (showing which parts of the lateral or which stages are contributing to production), perforation efficiency, proppant coverage, fracture conductivity and half-length can be estimated using fracture diagnostic tools. For instance, chemical tracers and downhole pressure gauges are near-wellbore fracture diagnostic tools. However, some of the new fracture diagnostic tools are being used for hydraulic fracture optimizations are DTS (distributed temperature sensing), DAS (distributed acoustic sensing), and downhole and surface micro-seismic mapping.

3. MODELING MULTIPHASE PERFORMANCE COMPARISON OF TRANSVERSE VERSUS LONGITUDINAL HORIZONTAL WELLS

The study of multiphase flow and performance comparison of multiple fractured transverse horizontal wells versus longitudinally fractured horizontal wells in tight sands and unconventional reservoirs with stress dependent permeability was conducted using three different reservoir simulations models that were built for each of the reservoir fluid type studied. The first reservoir simulation models were for dry gas reservoirs (in contact with water) that produced only gas and water. The second reservoir simulation models were built for black oil model type reservoirs (under-saturated), which honored accurate reservoir fluid properties for Permian Basin oil and had general rock properties. The third reservoir simulation models were built for saturated reservoirs and used compositional reservoir simulations. The compositional model honored the reservoir fluid properties of Eagle-Ford oil, and used representative rock and fluid properties.

Figure 3-1 shows the processes and steps used to build the multiphase flow reservoir simulation models for the three reservoir fluid types studied; dry gas, black oil and compositional reservoir models. For the black oil and compositional models, steps such as fluid sampling, PVT analysis and EOS (equation of state) modeling, and generation of pseudo-components were included. The impact of stress dependent permeability was incorporated into all three reservoir fluid types using two different methods of calculating effect of stress dependent permeability on induced hydraulic fractures. However, the effect of gas adsorption was included only in the dry gas reservoir modeling using the Langmuir Isotherm.

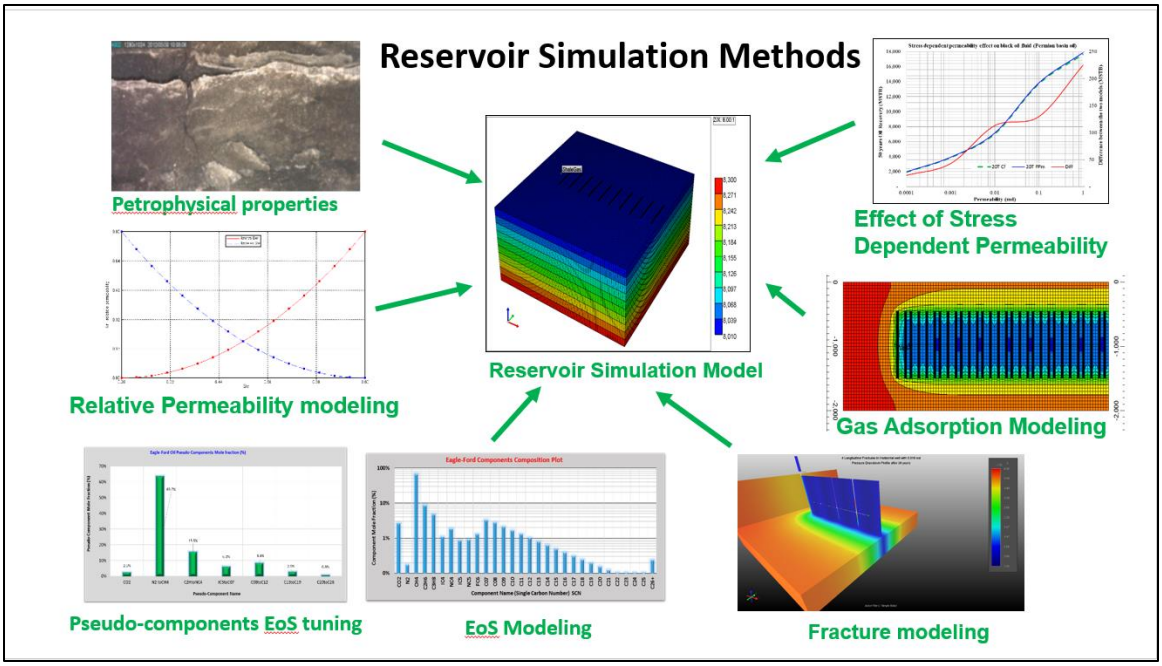

Figure 3-1: Multiphase flow reservoir modeling processes and steps

Additionally, Table 3-1 shows an example of the 72 static reservoir simulation models built and run for the dry gas reservoir. The table shows the range of reservoir permeabilities studied, the number of fractures in each reservoir simulation run, the fracture dimensions (x_f, k_f, w_f), and whether the well was transversely fractured or longitudinally fractured horizontal well. Table 3-1 also shows the range of reservoir permeabilities studied was from 0.00001 mD to 10.0 mD, which covers wide range of unconventional reservoirs and mid-range conventional reservoirs. Secondly, the hydraulic fractures were assumed to be propped and had fracture conductivity of 50 mD-ft. Secondly, even though only two longitudinal fractures were finally modeled and compared to transverse fractures in this study, the results of two, three and four longitudinal fractured horizontal wells behaved similarly.

Table 3-1: Example of the 72 Static reservoir models built for one of the 3 reservoir types

Cases Run	Permeability	Lateral	Xf	K_fW_f	Number of Transverse Fractures in each Case							Longitudinal Fractures	
	k (md)	Length (ft)	(ft)	(md-ft)	4	6	8	10	20	30	40	2L	4L
Case 1	0.000001	4,000	500	50	✓	✓	✓	✓	✓	✓	✓	☑	☑
Case 2	0.00001	4,000	500	50	✓	✓	✓	✓	✓	✓	✓	☑	☑
Case 3	0.0001	4,000	500	50	✓	✓	✓	✓	✓	✓	✓	☑	☑
Case 4	0.001	4,000	500	50	✓	✓	✓	✓	✓	✓	✓	☑	☑
Case 5	0.01	4,000	500	50	✓	✓	✓	✓	✓	✓	✓	☑	☑
Case 6	0.10	4,000	500	50	✓	✓	✓	✓	✓	✓	✓	☑	☑
Case 7	1.0	4,000	500	50	✓	✓	✓	✓	✓	✓	✓	☑	☑
Case 8	10	4,000	500	50	✓	✓	✓	✓	✓	✓	✓	☑	☑

3.1. WELL ECONOMICS AND PERFORMANCE ANALYSIS

Two methods of economic analysis, discounted recovery (DR) and present value (PV), were used in this study. In general, capital budgeting and asset valuations require two steps; first, estimate production or expected cash flow from the project, and then evaluate the riskiness of the projected production and cash-flow to determine the appropriate interest rate to use. The interest rate used in the study was 10% per annum.

Discounted recovery (DR), which is cumulative recovery discounted at an annual interest rate, was used to compare the economic performance of each horizontal well type.

$$DR = \sum_{i=1}^{n} \frac{N_i}{(1+r)^i} \quad \ldots (12)$$

Where;

$DR =$ Discounted recovery in (bbls or Mscf)

$N_i =$ Cumulative production (bbls or Mscf) in time, i

$r =$ interest rate (%), and n = number of years

The present value (PV) is the expected future cash-flow coming from the oil and gas production discounted at an annual rate, and can be calculated by multiplying DR (discounted recovery) by the price of oil or gas as shown below by equation 12.

$$PV = (P_O) * \sum_{i=1}^{n} \frac{N_i}{(1+r)^i} \quad ...(13)$$

Where;

P_O = price of oil or gas per unit of measure (e.g. barrels or Mcf)

P_O parameter in the present value (PV) calculation formula was set to one in this study. It is similar to the discount factor tables used in finance. Hence, to calculate the PV in any price or currency, you just multiple equation (13) by the price oil or gas.

3.2. PRINCIPAL STRESSES AND FRACTURE ORIENTATION

In a normal fault stress environment, the vertical stress ($\boldsymbol{\sigma_V}$) is principal stress one, the maximum horizontal stress ($\boldsymbol{\sigma_H}$) is principal stress two, and the minimum horizontal stress ($\boldsymbol{\sigma_h}$) is least principal stress. Figure 3-2 below shows a horizontal well with 10 transverse fracture, where the well was drilled in the direction of the minimum horizontal stress ($\boldsymbol{\sigma_h}$) and Figure 3-3 shows a horizontal well with 4 longitudinal fractures, where the well was drilled in the direction of the maximum horizontal stress ($\boldsymbol{\sigma_H}$).

In rock mechanics, there are three methods of determining in-situ stresses; field tests such as mini-frac and step-rate tests, laboratory tests such uniaxial and tri-axial tests, and stress calculations from rock elastic properties using well logs i.e. Young's modulus (E) and Poisson's Ratio (ν). However, it is not easy to determine the intermediate principal

stress, which in a normal fault environment, would be maximum horizontal stress (σ_H) because it is greatly impacted by tectonic plate stresses.

While this study compared the performance of transversely fractured to longitudinally fractured horizontal wells, the author(s) understands that there is a well-documented uncertainty in the direction and azimuth of the longitudinal fracture configuration once it exits the perforations. The direction of propagation is dictated by the intermediate and far-field in-situ stresses.

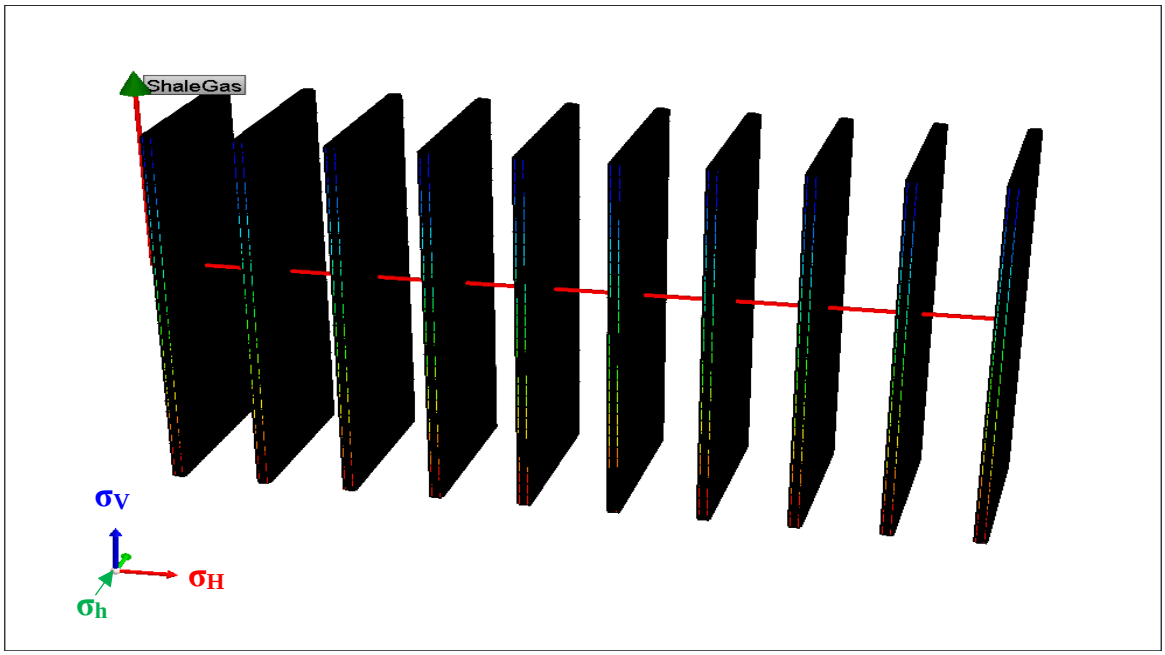

Figure 3-2: A horizontal well with 10 transverse fractures and 500 ft. of fracture half-length

In one of the earlier studies, (Hallam and Last, 1991) presented an experimental result, which showed that deviation of more 10^0 (degrees) from the azimuth of preferred

fracture plane would always create transverse fractures as the fracture propagates away from the wellbore. Similarly, (Economides et al. 2010) stated that “unless the wellbore azimuth is very tightly controlled, transverse fractures are the most likely scenario.” Similarly, (Economides et al. 2010) stated that hydraulic fractures whether longitudinal or transverse have other benefits such sand control, connection of layered or laminated formations by vertical penetrations and mitigation of turbulent flow effect in high permeability reservoirs.

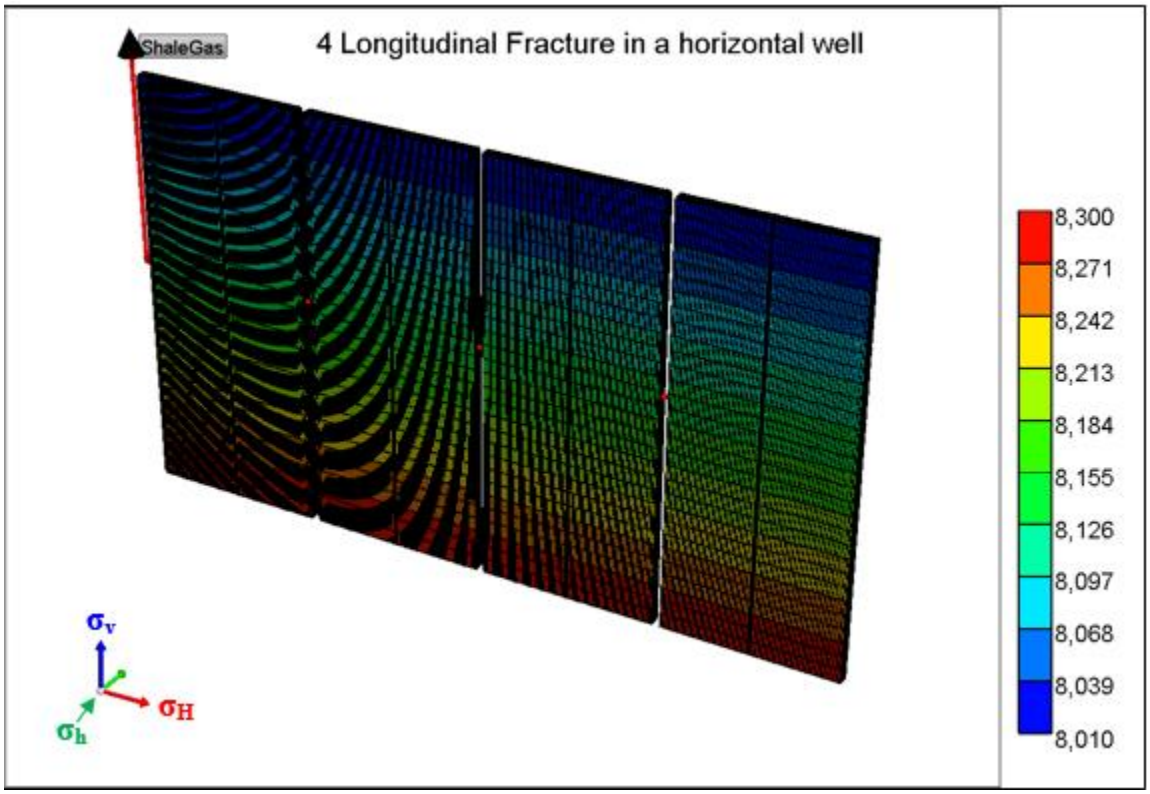

Figure 3-3: Horizontal well with 4 longitudinal fractures and 500 ft. of fracture half-length

3.3. STATIC RESERVOIR MODEL DESCRIPTION

A static 3D reservoir simulation model was built for the study that incorporated in-situ reservoir fluid and rock properties. Table 3-2 shows reservoir and well-input data used in the simulations. Similarly, Table 3-2 also presents the approaches used to calculate PVT correlations such as the Z-factor or oil and gas viscosities, which were critical to the reservoir simulation process.

Table 3-2: Reservoir input Parameters used in the Simulation Models

Static 3D Reservoir Simulator input Data				PVT input Data			Well Data			
Drainage	A	640	Acres	Permeability anisotrpy	K_H/K_V	10	Well type	Horizontal		
Top of Payzone	D_t	8000	ft	Gas FVF	F_g	Through Z factor	Radius	r_w 5.5	inches	
Bottom of Payzone	D_b	8300	ft	Oil viscoty	μ_O	Peng-Robinson EoS	Lateral Length	L 4000	ft	
Net pay	h	300	ft	Gas Z factor	Z_g	Peng-Robinson EoS	Fracture half-Lenth	X_f 500	ft	
Reservoir Pressure	Pi	4000	psi	Gas Viscosity	ϕ	Peng-Robinson EoS	Fracture Width	W_f 0.12	inches	
Porosity	ϕ	0.05		Water Saturation	S_I	0.25	Fracture Orientation	or Longitudinal		
Permeability	k	0.000001-to-10.0	md	Reservoir Temperature	T	250 ^{0}F				
Rock compressibility	C_r	1.45E-06	1/psia	Gas Adsorption	ADS	Langmuir Isotherm				
Fracture compressibility	C_f	Equations and tables		Non-Darcy Flow	FoP	Forchheimer Equation				

Figure 3-4 shows the 3D gridding scheme of the static reservoir simulation models, which was used in all of the simulation models. The static reservoir models had 10 layers each, used different methods of initializations such gravity depth equilibrium and vertical block centered to calculate pressure, saturation and relative permeability changes. Additionally, to model hydraulically fractured wells, the study incorporated Local Grid Refinement (LGR) to closely match the grid-block size to actual fracture width (w_f).

Secondly, the top layer of Figure 3-4 shows location of the well (ShaleGas) in the reservoir simulation model and an example of a model with ten transverse hydraulic fractures.

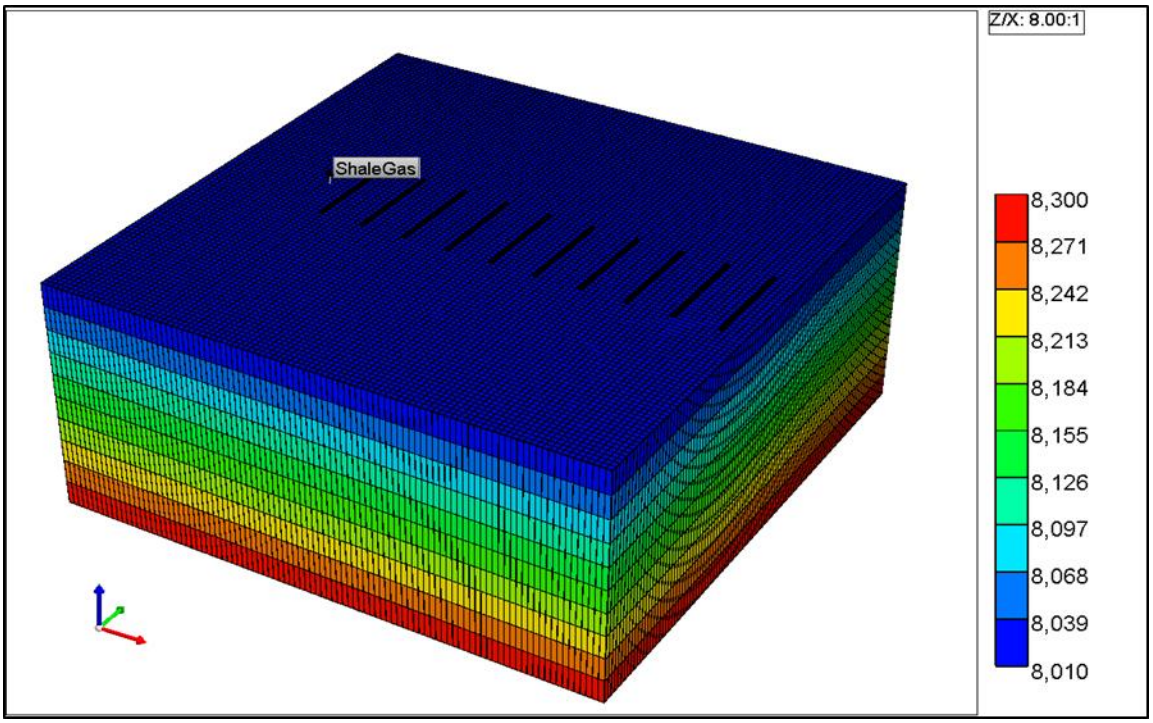

Figure 3-4: Example of the 3D gridding scheme used for building the static reservoir simulation model

3.4. PVT AND EQUATION OF STATE (EOS) MODELING.

Reservoir simulation studies require good PVT data, and the use of "best practices," especially when acquiring reservoir fluid samples or carrying out laboratory PVT analysis. This is especially important for oil reservoirs since both the reservoir fluid composition and the properties vary from one oilfield to another or in the same reservoir. Figure 3-5 shows Eagle-Ford oil molar composition of each molecule.

Similarly, Figure 3-6 shows Eagle-Ford oil pseudo-components that were generated after lumping the 26 components into seven pseudo-components. In general, because of complexities, unknown chemical structures of heavy components (C_{30+}), and long computer run-times, it is considered "best practice" to lump components that have close physical and chemical properties. The main reason for deploying pseudo-components was that it was not feasible to run reservoir simulation models with 30 components.

The pseudo-components were fine-tuned with second equation of state (EoS) to preserve components and phase properties. Additionally, the second equation of state (EoS) was needed to make sure that the 2-phase envelope has not shifted during the lumping process, and to conserve phase behaviors such as saturation pressure and fluid viscosity after the lumping scheme. The pseudo-components were then imported into the compositional reservoir simulator, and used in the simulation models (modified from Whitson and Sunjerga 2012).

Eagle-Ford oil composition was primarily made of lighter hydrocarbon components, as shown in Figure 3-5 and Figure 3-6, and the percentage of C1 (Methane) to C2 (Ethane) was 71.8% of the overall mole fraction. Secondly, the initial reservoir pressure (P_i) was 4,000 psi, as shown in Table 3-2, but the saturation pressure (bubble point, P_b) obtained from the flash calculation of Eagle-Ford oil was 4,220 psi. This meant that the reservoir was saturated (below bubble point pressure), and all the three phases (oil, gas and water) existed at reservoir conditions from the start. That is why a compositional reservoir simulator was used in the Eagle-Ford oil modeling. Secondly, Figure 3-6 shows the lumped pseudo-components of the Eagle-Ford oil, and highlights that the C8+ mole fracture was less than 12%, indicating very light oil properties. Additionally, there were

changes in fluid composition, reservoir pressure and reservoir temperature during modeling.

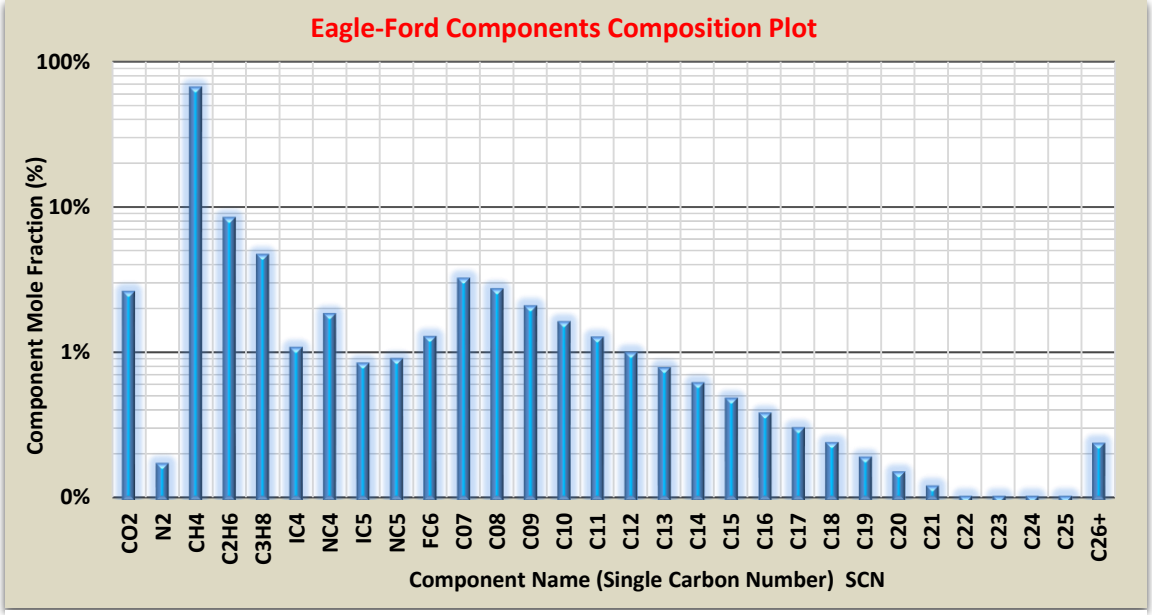

Figure 3-5: Eagle-Ford Oil Composition and Mole Fraction of SCN distribution (%)

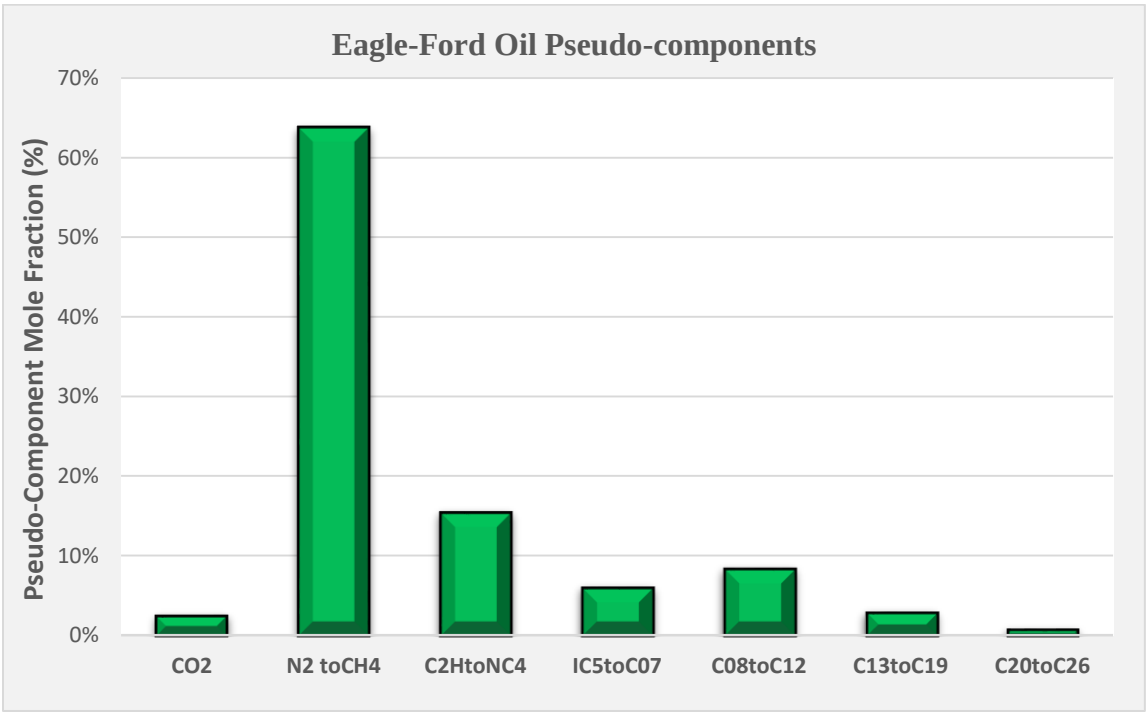

Figure 3-6: Eagle-Ford Pseudo-Components generated after lumping

The PVT analysis was carried out using cubic equations-of-state (EoS) to match saturation pressure, and to predict reservoir fluid properties of un-lumped oil composition (single carbon number SCN) components shown in Figure 3-5 (i.e. C1-to-C26+). Similarly, the pseudo-components were fine-tuned with another (2^{nd}) EoS (equation-of-State) after the components were lumped into seven pseudo-components based on the relative closeness of the physical and chemical properties of the components. Figure 3-6 shows the result of lumped oil composition (for Eagle-Ford oil). The EOS used in the study was the 1978 Peng-Robinson cubic equation shown below.

$$P = \frac{RT}{v-b} + \frac{a}{v(v+b)+b(v-b)} \quad \text{... (14)}$$

Or in terms of Z-factor

$$Z^3 - (1-B)Z^2 + (A - 3B^2 - 2B)Z - (AB - B^2 - B^3) \quad \text{...(15)}$$

Where;

P = Pressure, psia

R = gas constant, $\frac{ft^3 * psia}{R^0 * lb-mole}$

T= temperature in Rankine, R^0

$a = attraction\ parameter$

$v = specific\ volume, ft/mole$

$b = repulsion\ parameter$

$Z_C = critical\ compressibility\ factor\ and\ for\ Peng - Robinson\ EoS,$

$Z_C = 0.3074$

The two EOS constants, attraction and repulsion parameters (a & b), are defined at the critical points, and are function of P_C (critical pressure) and T_C (critical temperature) as expressed in equations 16 and 17 (for more details see (Whiston and Brulé 2000)):

$$b(T_C) = \Omega_b \frac{RT_C}{P_C} = 0.07780 \frac{RT_C}{P_C} \quad ...(16)$$

$$a(T_C) = \Omega_a \frac{R^2 T_C^2}{P_C} = 0.45724 \frac{R^2 T_C^2}{P_C} \quad ...(17)$$

However, when calculating points outside the critical point, the value of $b(T_C)$ does not change in the flash envelope, but the value of $a(T)$ changes and need to be re-calculated using equation 18 and 19.

$$a(T) = b(T_C) * \alpha(T_r, \omega) \quad ...(18)$$

$$\alpha(T_r, \omega) = 1 + (0.3796 + 1.485\omega - 0.1644\omega^2 + 0.01667\omega^3)(1 - T_r^{0.5}) \quad .. (19)$$

Where;

ω = acentric factor,

T_r = reduced temperature

The acentric factor is a thermodynamic property and is almost zero for spherical molecules, but is defined for pure components just like T_C and P_C. Secondly, the reduced temperatures and pressures greatly affect compressibility (Z-factor), especially for gases. Different gases behave similarly at the same reduced temperature and pressure.

For mixtures, the mixing rules formula was used to calculate binary interaction parameters (BIPs) as shown by equations 20, 21 and 22.

$$b = \sum_i^n y_i b_i \quad ...(20)$$

$$a(T) = \sum_{i}^{n}\sum_{j}^{n}[y_i y_j a(T)_{ij}] \quad ...(21)$$

$$a(T)_{ij} = \left(1 - \delta_{ij}\right)\left[a(T)_i a(T)_j\right] \quad ...(22)$$

Where

$\delta_{ij} =$ binary interaction coefficients and is assumed to be independent of pressure and temperature.

The EOS was fine-tuned through regression analysis by adjusting P_C (critical pressure), T_C (critical temperature), and the interaction coefficients (ω), especially for the large and heavy molecules such as C25 and C26+. These large and heavy molecules' physical properties and real chemical structure are unknown. Hence, it is "best practice" in reservoir simulations to adjust the properties of components with most uncertainty during fluid sampling and PVT analysis.

3.5. MODELING GAS ADSORPTION, STRESS DEPENDENT PERMEABILITY AND NON-DARCY FLOW

Two of the key geochemical properties used for assessing the potential of shale gas reservoirs are the total organic carbon (TOC), and gas volume and capacity. In shale gas reservoirs, the total gas in place (GIP) is made of gas adsorbed on the surface of the kerogen, and gas stored in the primary and secondary porosity. In this study, Langmuir isotherm (LI) was used to model gas adsorption and desorption. The isotherm (LI) requires two parameters; Langmuir volume (V_L), which is the maximum adsorbed gas, and Langmuir pressure (P_L), which is the pressure at half the Langmuir volume (V_L). For

methane (CH4), V_L = 0.10 (gmole/lb.) = 165 (SCF/ton), and P_L = 550 psi was used, which were obtained from Langmuir isotherm for gases presented by (Lane 1995). The moles of adsorbed gas per unit mass rock (gmole/lb.) were calculated using equations 23 for single component, and equation 24 for multi-component adsorption.

$$\nu_i = \left(\frac{V_L P}{P_L + P}\right) \quad ...(23)$$

$$\nu_i = \nu_{i,max}\left(\frac{{y_{i,g}}^{P}/_{P_{L,i}}}{1+\sum_i\left({y_{j,g}}^{P}/_{P_{L,j}}\right)}\right) \quad ...(24)$$

Where;

ν_i = moles of adsorbed gas per unit mass rock (gmole/lb.)

P = reservoir pressure, psi

$y_{i,g}$ = mole fraction of component (i) adsorbed in the gas phase

Models that describe pressure dependency of permeability, and porosity are generally very similar because of the good correlations between porosity and permeability i.e. the Kozeny equation. Secondly, most of the models either use an exponential relationship or power-law relationship. Evan et al. (1997) presented an exponential relationship for stress-dependent permeability, which he stated as the "best fit" equation to his experimental data and is given below.

$$K = K_o \exp(-\gamma P_e) \quad ...(25)$$

Where;

K = permeability at effective stress, P_e,

K_O = sample permeability when P_e = 0,

γ = curve fitting parameter.

Shi and Wang (1986) research paper suggested that stress-dependent permeability is best estimated by a power-law equations like;

$$K = K_O \left(\frac{P_e}{P_O}\right)^{-p} \quad ...(26)$$

Where

p = is a material constant.

In this study, stress dependent permeability and porosity were calculated in two methods; the first method was using equation 27 below;

$$\phi = \phi_0 \left[1 + C_f (P - P_0)\right] \quad ...(27)$$

Where

ϕ_0 = original porosity,

P_0 = original pressure, psi

C_f = formation compressibility.

To use equation 27, two types of rock formation were defined in the reservoir simulator; rock type 1 for the matrix rock, and rock type 2 for the fracture. The second method used to calculate stress dependent permeability (SDP) was the use of pressure dependent permeability tables, which uses dimensionless multipliers (m) for both porosity and permeability. The SDP arrays were generated using equation,

$$K(P) = K_m + m[exp(-\alpha(P_c - P)] \quad ...(28)$$

Where;

α = material dependent parameter that can be determined from laboratory tests,

K_m = minimum permeability, mD.

In hydraulically fractured wells, especially in shale gas, there are multiple flow regimes that can occur within the stimulated reservoir volume (SRV). For shale gas, there is Darcy flow and diffusion in the matrix, and Darcy flow and non-Darcy flow, in the fractures. In this study, all 3-flow regimes were incorporated into the models. The non-Darcy flow effect was modeled using Forchheimer Flow equation.

$$\nabla P = \frac{\mu}{K} v + \beta \rho \quad ...(29)$$

$$\frac{1}{K_{ap}} = \frac{\nabla P}{\mu v} = \frac{1}{k} + \beta \frac{\rho v}{\mu} \quad ...(30)$$

Where;

P = pressure, psi,

v = superficial velocity, ft/s,

β = beta factor and is experimentally determined from the slope of Forchheimer graph, which is a plot of the inverse of apparent permeability ($1/K_{ap}$) versus a pseudo-Reynolds number (ρv/μ).

However, because β is a property of the porous media, numerous empirical correlation have been proposed, but in this study (Evans and Civan,1994) beta (β) correlation was used, which is given below.

$$\beta_f = \frac{1.485 * 10^9}{K^{1.021}} \quad \text{...(31)}$$

4. MODLING INTEGRATED COMPLETION AND RESERVOIR SIMULATIONS OF HYDRAULICALLY FRACTURED WELLS

Usually, multidisciplinary teams made up of earth scientist (geologist and geophysicist) and engineers (completions, production and reservoir engineers) are involved in the construction of integrated models that capture the complexities of horizontal wells in unconventional resources. Companies are producing from multi-layered reservoirs that have different lithology, petro-physical and geomechanical properties, but still require multi-stage hydraulic fracturing. Additionally, some of the hydraulically fractured horizontal wells are underperforming despite multiple attempts to identify optimization opportunities. Hence, the need for multidisciplinary based integrated completions and reservoir modeling.

In this study, we developed an integrated methodology that utilizes all available data to improve well stimulation and productivity. The objective was to present a new methodology for selecting lateral well placement, completion strategy and determination of stimulated reservoir volume (SRV) by integrating available data such as curvature data from 3D seismic, micro-seismic, geo-mechanical data, well logs, fracability index, mini-frac test, step-rate test, DFIT analysis, core data, and post-fracture treatment data to optimize well productivity, hydrocarbon recovery and well economics.

The process of developing the hybrid model involved integrating the completions design with compositional reservoir simulator using a two-step process; first, the hydraulic fracture design was calibrated using only the micro-seismic data from the stages that were closest to the geophone/receiver (avoiding location bias or signal-noise ratio issues) in order to develop a reliable fracture geometry model. The calibrated fracture model was then used for history matching and re-modeling of all the fracture stages, in each of the

wells in the study. Fracture geometry and dimensions for each stage was obtained from the calibrated fracture models.

Secondly, compositional reservoir simulators were built using reservoir geology, PVT data, production data and well deviations. Fracture dimensions obtained from the calibrated fracture model were then transferred into the reservoir simulator. Finally, curvature data obtained from 3D seismic was used to predict the location, density and direction of secondary fissures within the well drainage area, and were then incorporated into the compositional reservoir simulator.

The integrated completions and reservoir modeling was conducted using well data from Montney formation. The Montney formation is one of the most commercially attractive unconventional resources in North America. The integrated completion and reservoir simulation models had eleven steps; five in the construction of the calibrated fracture model, and six in the compositional reservoir simulation modeling. Figure 4-1 shows the steps and process used to construct the integrated completion and reservoir simulation models.

Figure 4-1 shows that each of the eleven steps was an iterative process and required multiple refinements before the two major models, the completion model and reservoir model, were integrated. Secondly, most of the major parts of the reservoir simulation modeling are explained in chapter five, which deals with the performance of transversely fractured versus longitudinally fractured horizontal wells in multiphase flow environment. Some of the additions steps like natural fracture modeling are explained in the integrated reservoir simulation chapter.

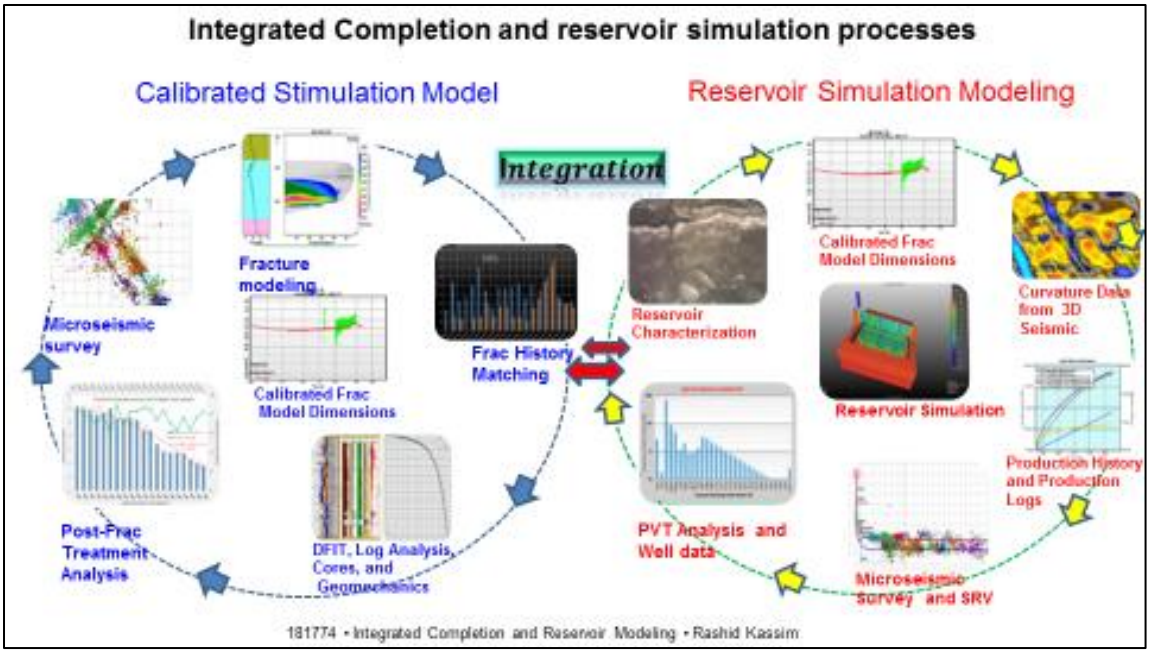

Figure 4-1: Diagram showing the eleven steps used in the construction of the integrated completion and reservoir simulation process

4.1. BUILDING CALIBRATED FULLY3D HYDRAULIC FRACTURE MODELS AND HISTORY MATCHING

Stimulation techniques and fluid systems used in the Montney play vary widely across regions and companies. (Al-alwani et al. 2015) presented a paper on completion trends in the Montney Formation using data mining and statistical analysis. The paper compared completion methods (open-hole vs cased-hole), stimulation fluids (water-based, binary fluids (CO2-N2), oil-based), stimulation design (treatment volume and proppant mass), and well recovery (initial production and recovery per stage). The authors concluded that cased-hole completed wells performed better than open-hole, and oil-based fracturing fluids yielded higher fracture fluid recovery than water-based fluids

Reynolds et al. 2014 presented a paper titled “A Comparison of the Effectiveness of Various Fracture Fluid Systems Used in Multistage Fractured Horizontal Wells:

Montney Formation, Unconventional Gas", where they compared the effectiveness of different types of fracturing fluids in terms of well productivity and recovery. The authors concluded that foam-based fracturing fluids provide better well performance than water-frac's. However, the wells in this study were stimulated with water-frac treatments.

Reynolds et al. (2014) presented a paper titled "A Comparison of the Effectiveness of Various Fracture Fluid Systems Used in Multistage Fractured Horizontal Wells: Montney Formation, Unconventional Gas", where they compared the effectiveness of different types of fracturing fluids in terms of well productivity and recovery. The authors concluded that foam-based fracturing fluids provide better well performance than water-frack. However, the wells in this study were stimulated with water-frack.

Building the calibrated fracture model required five steps in a sequential and iterative process (shown by Figure 4-2); DFIT (diagnostic fracture injection test) analysis, geomechanical and logs analysis, post-fracture treatment analysis, micro-seismic data interpretation and quality control, and hydraulic fracture history matching and remodeling of all fracture stages with the calibrated fracture model. However, two steps, the fracture modeling and fracture history matching took most of the time, and we critical to the determination of the fracture dimensions.

The proceeding sections would explain in detail each of the five steps shown in Figure 4-2, and would chronological provide the importance of each step to the process of building the calibrated fracture model.

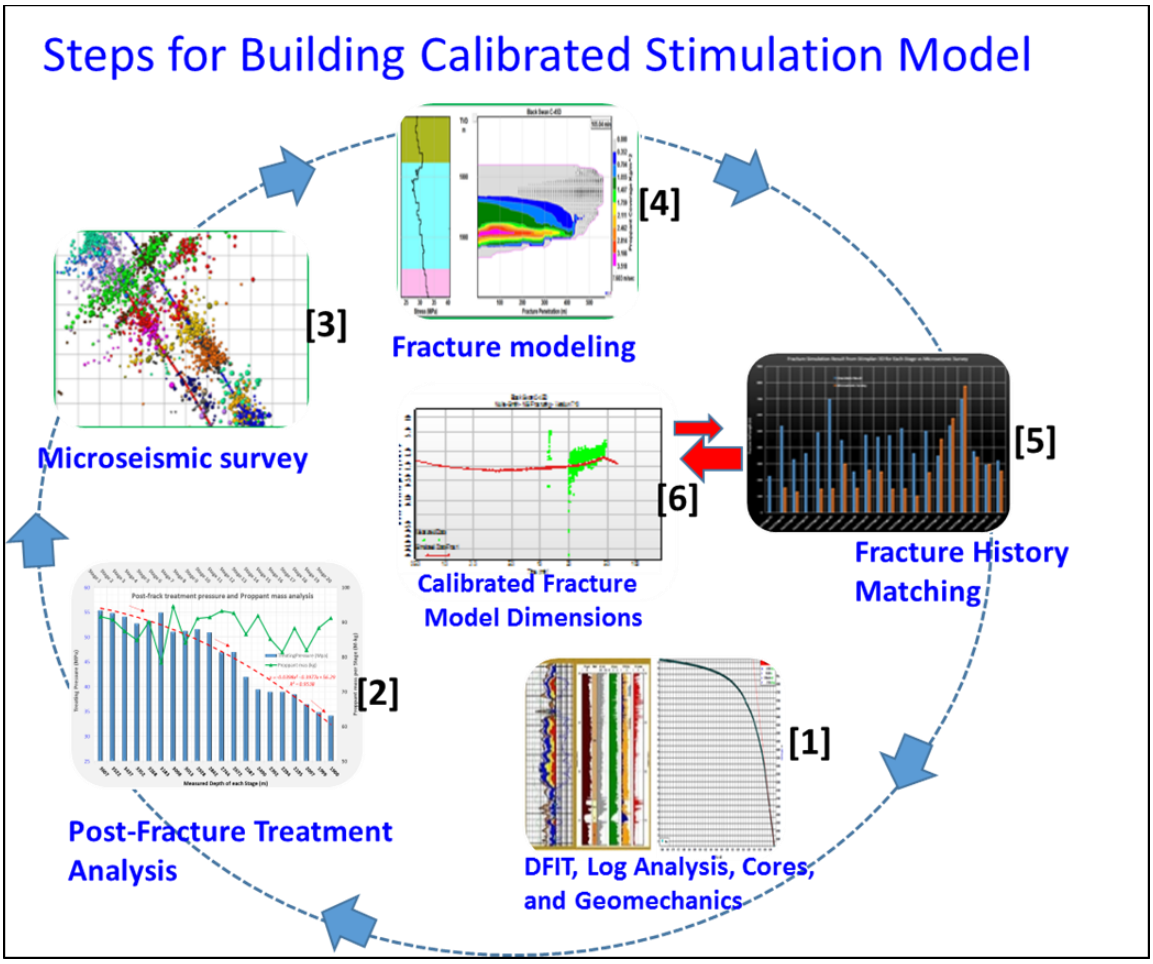

Figure 4-2: Steps for building calibrated fracture models, and method for re-modeling all fracture stages

4.1.1. Diagnostic Fracture Injection Test (DFIT) Analysis. Diagnostic fracture injection tests (DFIT) provide valuable information that are critical to the stimulation design and the understandings of the reservoir properties. DFIT tests such as injection/fall-off test and after-closure analysis (ACA) were analyzed and interpreted in this study. Information such as reservoir pressure (Pi), permeability (k) and reservoir characteristics were obtained from the DFIT test. Figure 4-3 shows an example of the DFIT analysis and interpretation. The plot provides reservoir pressure (Pi), instantaneous shut-in pressure (ISIP), and fracture efficiency. Figure 4-3 also shows that the leak-off

type observed was pressure-dependent leak-off, and shows characteristic “hump” above the normal leak-off line. Pressure dependent leak-off indicates the presence of natural fractures in the reservoir and can effect fracture propagation and efficiency. Further analysis of the DFIT tests yielded reservoir permeability ranges of 0.00015 mD to 0.00018 mD for the wells in the study.

The minimum horizontal stress (σ_{Hmin}) is equal to the closure pressure (P_c) in most cases ($P_c \sim \sigma_{Hmin}$), and Figure 4-3 shows (P_c) = 3,941 psi, and efficiency is 87%. The net pressure (P_{net}), which is the difference between the injection pressure (Pi) and closure pressure, is one of the most important parameter in hydraulic fracture. There are different formulas for calculating (P_{net});

$$P_{net} = BHIP - \Delta P_{loss} - P_c \quad \text{...(32)}$$

$$P_{net} = P_f - P_c \quad \text{...(33)}$$

Where

BHIP = bottom-hole injection pressure, psi

ΔP_{loss} = frictional pressure losses, psi

P_f = pressure in fracture, psi

P_c = closure pressure, psi

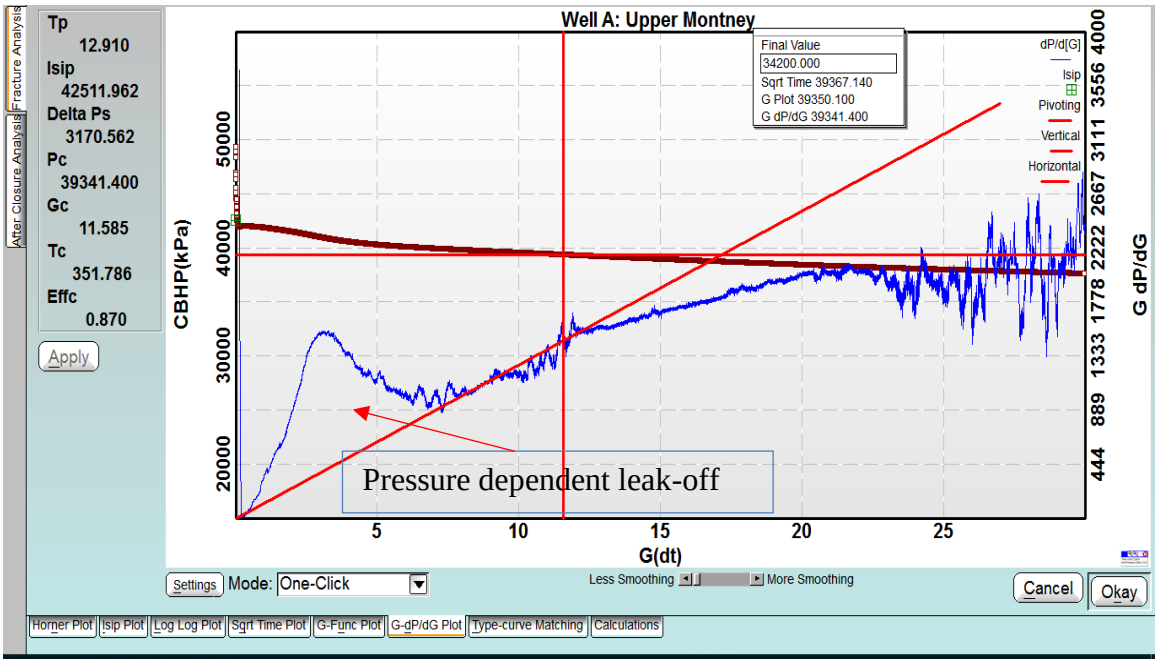

Figure 4-3: G-dP/dG plot showing reservoir properties and leak-off type for one of the wells in Montney.

4.1.2. Logs and Geo-mechanical Analysis. Well logs and geomechanical analysis were done for all the wells in the study. The in-situ stress (minimum horizontal stress) was first calculated from the logs (bulk density, shear and compressional sonic waves), and then corrected using reservoir pressure (pi) obtained from the DFIT test, and core data. Similar steps were used to calculate dynamic Young's modulus (E_d) and Poisson's ratio (ν). The static Young's modulus (E_s) was calculated from the dynamic Young's modulus (E_d) using correlations developed by Britt Rock Mechanics Laboratory that were presented by (Britt and Schoeffler 2009) in a paper titled "The Geomechanics Of A Shale Play: What Makes A Shale Prospective!" Lastly, the static Young's modulus obtained from the core test (tri-axial test) was then used to calibrate the log-derived geomechanical model, especially for the zones of interest.

Figure 4-4 shows an example of the well logs and geomechanical analysis that was conducted in this study. The figure shows well trajectory, location of some of the fracture stages and geomechanical properties (E, ν, σ). The Brittleness Index, which measures the brittleness of the rock shows that the Upper Montney is more brittle than the Lower Montney. The Brittleness Index was calculated using equations 34, 35, and 36 after Rickman and Mullin et al

$$E_n = \left(\frac{E_s - E_{min}}{E_{s\_max} - E_{s\_min}}\right) \quad ...(34)$$

$$\nu_n = \left(\frac{\nu_{max} - \nu}{\nu_{max} - \nu_{min}}\right) \quad ...(35)$$

$$\text{Brittleness } Index = \left(\frac{E_n + \nu_n}{2}\right) \quad ...(36)$$

Where;

E_n = normalized static Young's modulus

ν_n = normalized Poisson's ratio,

E_{s_max}, E_{s_min} = are maximum and minimum static Young's modulus

$\nu_{max}\ and\ \nu_{min}$ = are the maximum and minimum Poisson's ratio.

The fracability index was also calculated using Lame's constants (λ and μ), which are called Lame's first constant (λ) and Lame's second constant (μ), the shear modulus. Both Lame's constant were derived the shear and compressional velocities obtained from the dipole sonic logs.

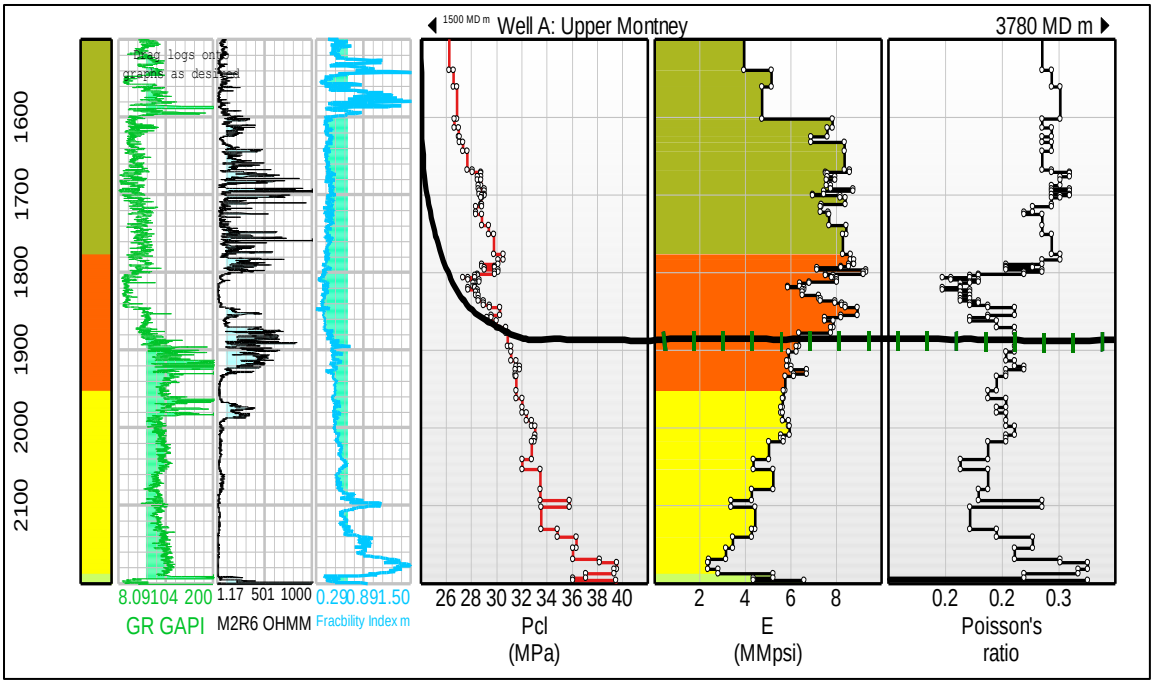

Figure 4-4: Logs and Geomechanics of upper Montney well showing location of frack stages and fracability index

4.1.3. Post-Fracture Treatment Analysis. The post-fracture analysis included statistical analysis of the final Pnet pressure for each stage, ISIP (instantaneous shut-in pressure) per stage, BHP (bottom-hole) WHP changes for each stage, treatment volume per stage, average treatment rate per stage, and proppant mass per stage for each of the wells in the study Figure 4-5 shows treating pressure versus measured depth of each stage, and proppant mass per stage. The plot shows that the surface pump pressure required at the toe of the horizontal well to hydraulically fracture (stages 1, 2, 3 etc.) was considerably higher than the treating pressure required at the heel of the horizontal well. The higher treating pressure seen at the toe was primarily due to frictional pressure losses, and the total friction pressure is given by

$$\Delta P_{tot} = \Delta P_{tubing} + \Delta P_{perfs} + \Delta P_{tort} + \Delta P_{perf\_misalign} + \Delta P_{Ball\ seat} \quad ...(37)$$

where;

ΔP_{tot} = total pressure drop, psi or kPa

ΔP_{tubing} = pressure losses in the flowline and tubing/casings

ΔP_{perfs} = friction pressure through perforations

$\Delta P_{tortuosity}$ = tortuosity (fracture turning) pressure drop

$\Delta P_{perf\_misalign}$ = friction pressure due to perforation misalignment

$\Delta P_{Ball\ seat}$ = friction pressure due to the ball seats.

For hydraulic fracture optimization purposes, friction reducers should be used to allow pumping maximum desired rate during fracturing. The wells in this study had lower pumping rate and higher treating pressure at the toe stages most likely due to increased frictional pressure losses along the lateral length of the horizontal well. Similarly, proppant mass per stage should be tailored to maximize well performance given well operation constraints such as maximum allowable surface pressure, horse power and fracturing materials.

The proppant mass per stage was fairly constant throughout the hydraulic fracture treatment, and was not tailored to maximize the available horse-power at every given stages. Secondly, the polynomial equation fitted to the data shows that the treatment pressure was inversely correlated to the lateral length of the horizontal well. Hence, of the biggest frictional pressure loss came from the first term of equation 37, the pressure losses in the flowline and tubing. The difference between the treatment pressure for stage 1 (at the toe) and stage 20 was 19 MPa (as shown by Figure 4-5)

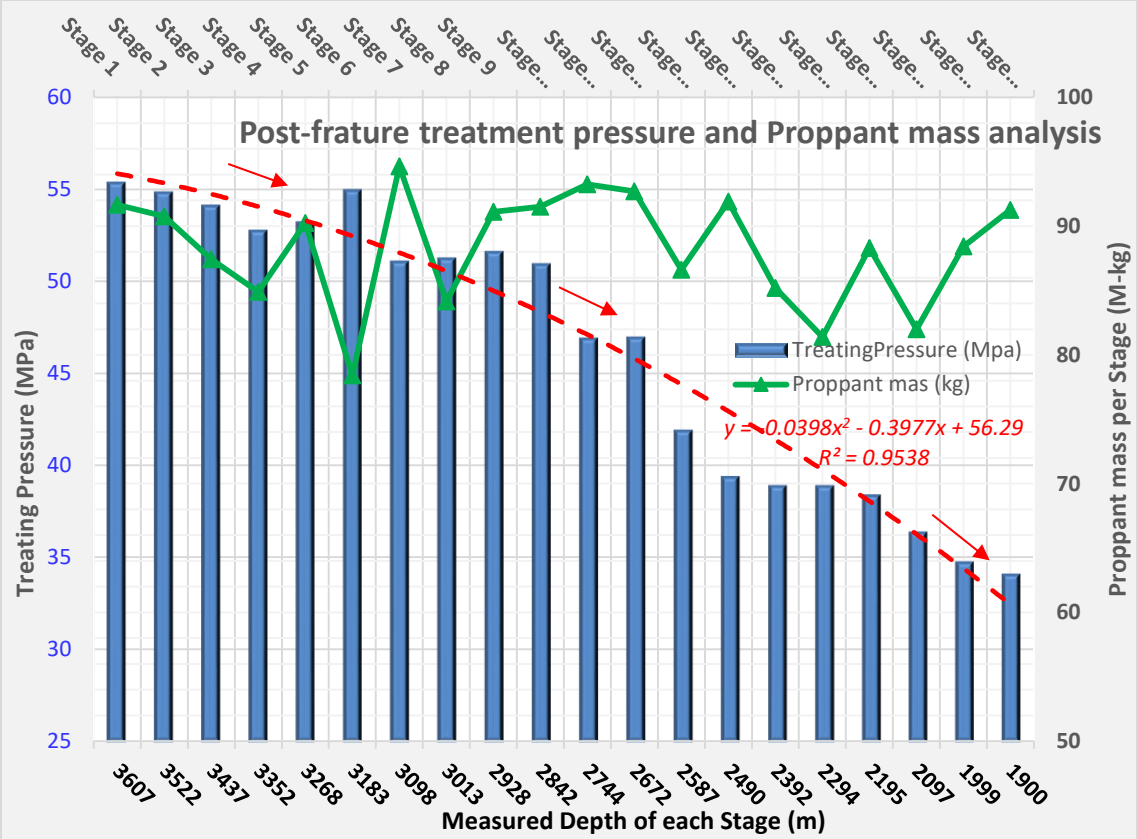

Figure 4-5: Post-fracture treatment pressure as function of measure depth of each stage, and proppant mass per stage

4.1.4. Micros-Seismic Data Analysis and Quality Control. Micro-seismic monitoring and mapping have been used to understand hydraulic fracture dimensions and geometry. Recently, advances in micro-seismic mapping have also provided valuable information for optimizing completions, modeling stimulated reservoir volume (SRV) and managing field development. Cipolla et al. (2012) presented a paper titled "Engineering Guide to the Application of Micro-seismic Interpretation", which provided a workflow on the use of micro-seismic mapping and highlighted the consequences of misapplication of micro-seismic survey. Cipolla stated that good micro-seismic interpretation can provide six primary geometrical observations (fracture length (x_f), fracture height (h_f), fracture

azimuth, fracture complexity, fracture location and signs of anomalous behavior such as fault activation) and estimated stimulated reservoir volume (SRV).

The micro-seismic events had very weak signals and most of the events recorded are in the range of -3.0 to -2.0 on the Richter scale. Secondly, micro-seismic events must be greater than the noise observed at the wellsite so that an acceptable signal-to-noise ratio can be achieved during the micro-seismic monitoring. This is critically important because micro-seismic events of smaller magnitude are not detected by the micro-seismic geophones a few meters away from the receiver. Figure 4-6 shows the number of micro-seismic events recorded versus the micro-seismic moment magnitude for one of the wells used in the study (well A). The result shows that the distribution of the micro-seismic events was skewed to the left, suggesting that there were many more smaller events recorded than larger ones. Zimmer (2011) analyzed uncertainties in micro-seismic event location for some of the major shale plays in Canada (e.g. Montney and Cardium Formation) and stated micro-seismic mapping shows that the Montney Formation has mostly planar fractures. Zimmer (2011) proposed an equation for calculating the number of events (N) versus the magnitude (M), and is given below.

$$\log\big(N(M)\big) = a - b\ (M) \qquad \text{...(38)}$$

Where;

N = number of micro-seismic events

M = micro-seismic moment magnitude

a = constant number, usually one

b = obtained iteratively or by fitting an exponential equation into the data using “best fit or goal seek”

In this study, qualitative and quantitative analysis was used to determine the number of hydraulic fractures in a given well that interact with natural fissures using micro-seismic mapping, DFIT (diagnostic fracture injection test) and curvature data from 3D seismic.

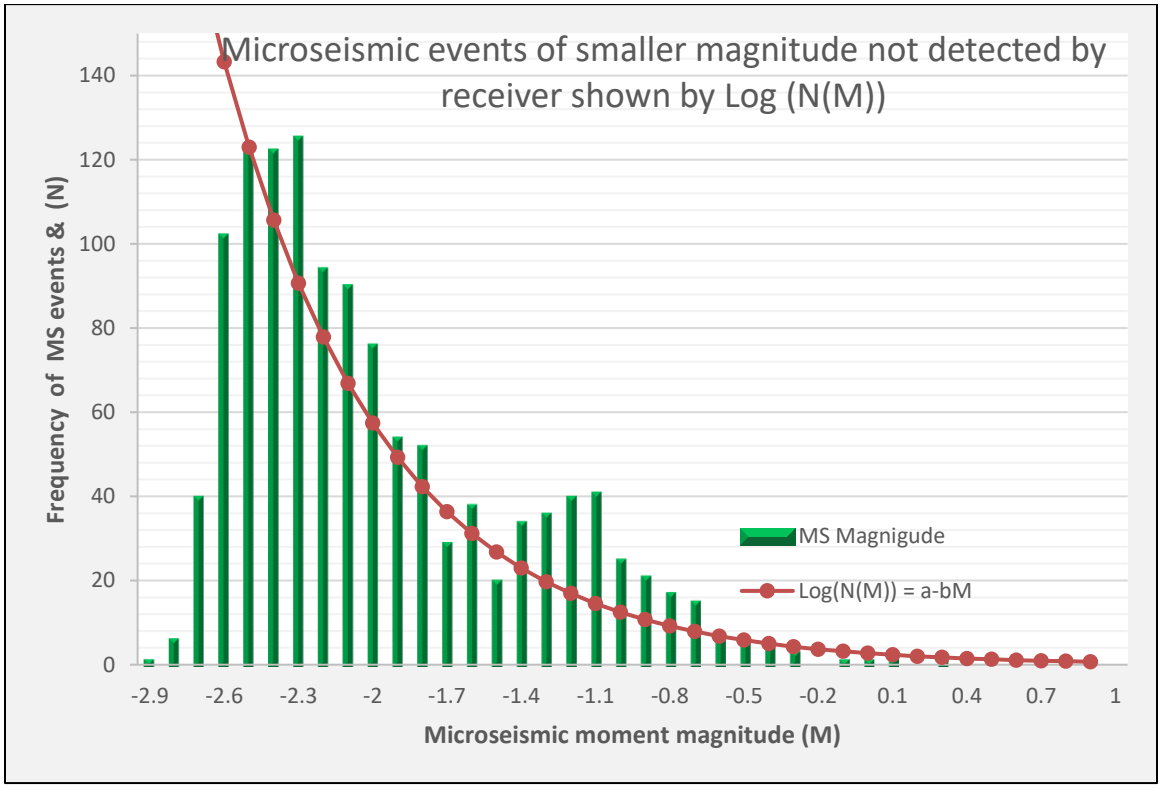

Figure 4-6: Frequency of micro-seismic events versus MS moment magnitude for upper Montney wells

In this study, a new method was developed for interpreting and using micro-seismic survey data that have both location bias (uncertainty in the location of micro-seismic events) and signal-to-noise ratio (SNR). Previous studies (Zimmer 2011) have shown that

the recording of micro-seismic events that have very low magnitudes moments (less -3.0) are under-represented because of limited viewing distance and signal weakness. Figure 4-7 shows micro-seismic mapping of a horizontal well with 20 stages. The result indicates that stages at the toe of the horizontal well had few or no micro-seismic events recorded (even though the treatment volume per stage was constant/similar for all stages as shown by Figure 4-5). Similarly, Figure 4-8 shows micro-seismic mapping for another well that had 16 fracture stages.

There are three important points to highlight; first, both micro-seismic mapping in Figure 4-7 and Figure 4-8 show that there were a lot more micro-seismic events recorded for the stages near the heel of the horizontal wells (i.e. from stages 16 to 20 for well A) though the treatment volume per stage was fairly constant. Secondly, the micro-seismic mapping of both wells A and B show the development of complex fractures and the overlapping of recorded micro-seismic events in some of the fracture stages. For instance, fracture stage 16 of well A and B show that complex fracture networks were created during hydraulic fracturing. Additionally, fracture stage 16 in well B (shown by Figure 4-8) might have activated a fault line or pre-existing fissures (highlighted in yellow circle in Figure 4-7). Thirdly, in well B, fracture stages 1 and 2 had no recorded micro-seismic events. Hence, fracture dimensions for the stages at the toe of the horizontal well could not be determined from micro-seismic mapping.

Generally, it's "best practice" to use two micro-seismic monitoring wells (to limit the impact of location bias and signal-to-noise ratio), but because of cost or production interruption or lack of nearby wells, operators often use one observation well to monitor and record micro-seismic data. Each of the wells in this study had only one micro-seismic

monitoring well (and not 2) for observation and micro-seismic mapping. The monitoring wells were in Lower Montney while the wells used in the study were in the Upper Montney Formation. The micro-seismic receivers were placed at the heels of the monitoring wells (see Figure 4-9 and Figure 4-10).

The methodology developed in this study was to incorporate quality control (QC) in the use of micro-seismic survey data and to use only micro-seismic events that had good micro-seismic magnitude and moments. Using QC (quality control) analysis, only fracture stages that were close to the micro-seismic geophones/receivers and had enough micro-seismic events were used for history matching and fracture model calibration. As a result, micro-seismic survey for stages 16-to-20 were used from well A, and fracture stages (7, 14, 15, and 16) were used in well B for history matching and building the calibrated fracture model.

The fracture model was history matched to the fracture dimensions obtained from the micro-seismic mappings for each of the fracture stages selected (5 stages for well A and 4 stages for well B) by adjusting two parameters; leak-off coefficient (C_L) and stress differences ($\Delta\sigma$). However, in some cases, the Young's modulus (E_s) was adjusted to obtain good history match.

Figure 4-7 shows that the hydraulic fractures created were transverse fracture, which means the horizontal well was drilled in the direction of the minimum horizontal stress. Secondly, the micro-seismic mapping of well A (see Figure 4-7) shows that micro-seismic events from different stages overlapped, indicating that some of the hydraulic fractures might have interacted with each other or with natural fissures. For instance,

micro-seismic events for stage 19 overlapped with stage 20, on one side, and stages 18 & 17, on the other side.

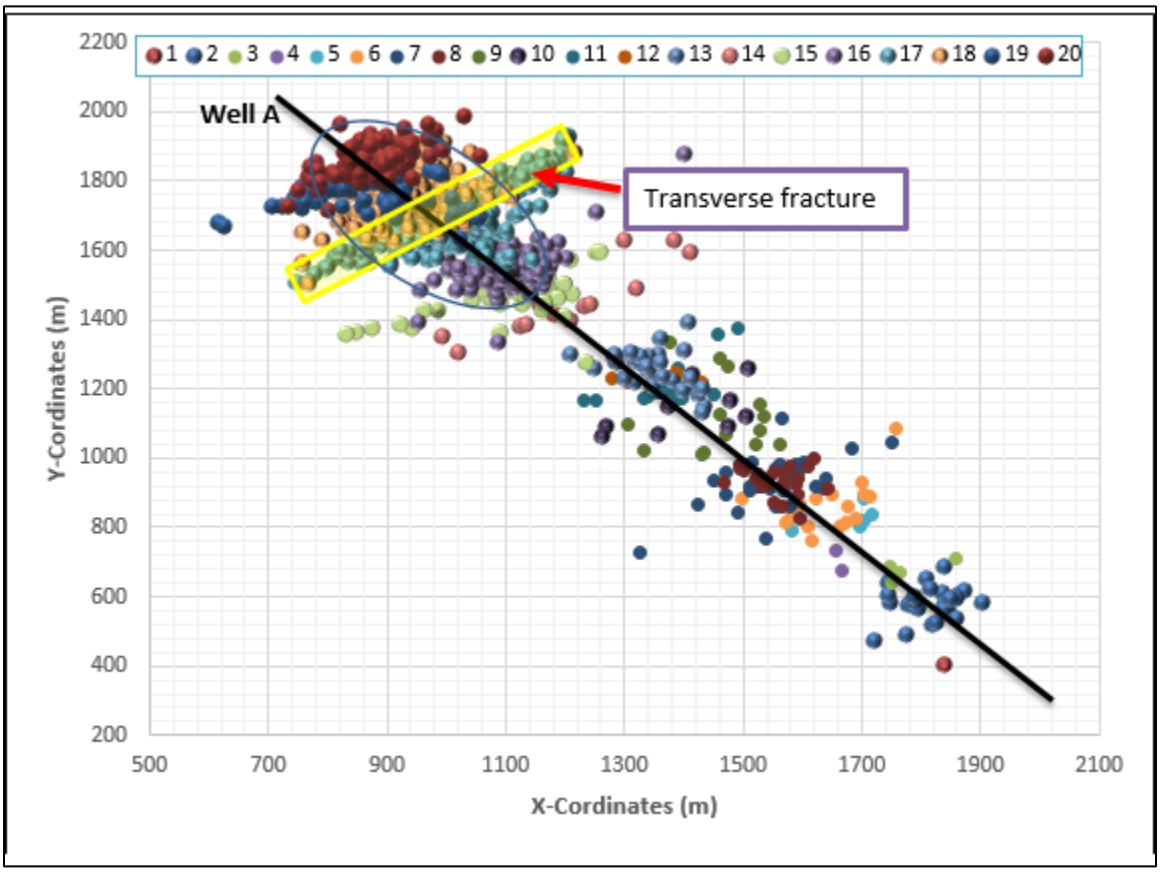

Figure 4-7: Micro-seismic mapping of a horizontal well with 20 stages showing transverse fractures (xy-plane)

The value of micro-seismic monitoring to hydraulic fracture executions, and identifications of problems "real-time" such as partial leak of the well casings/liners or perforation of wrong location, were on display in the case of well B, shown by Figure 4-8. During the "real-time" monitoring of the hydraulic fracture treatment, the micro-seismic mapping revealed valuable information. First, the micro-seismic survey provided "real-

time view" of fracture dimensions and geometry as the stimulation progressed. For instance, parameters such as fracture orientation and type (transverse), fracture half-lengths, and fracture height. Secondly, "real-time" monitoring of the job showed where complex fractures or anomalies like faults might be encountered. For instance, micro-seismic events for stage 16 indicated fault activation.

"Real-time" diagnosing of well integrity-related issues with micro-seismic mapping during hydraulic fracturing provides reliable information. For instance, during the treatment of stage six (see Figure 4-8), abnormal surface pressures were detected, but there was no-way to definitively diagnose the source or even location of the problem. The stimulation treatment crew moved on to the next stage, which was stages seven, but the abnormal surface pressures were still showing up, and micro-seismic events were detected at the heel of the horizontal well. The crew convened to discuss why the micro-seismic events were being recorded near the heel of the horizontal well and what actions to take to remedy the situation. They were wondering whether the micro-seismic geophones malfunctioned or there was partial leak of the casing or liner. Finally, they decided to remove the twelve geophones, which were 30 meters apart, and replaced them with new ones (see the 3D diagram shown by Figure 4-10). However, once the stimulation treatment was restarted, the same well integrity issues were encountered. Looking at the location of the micro-seismic events for stage 7 and the strength of the signals, the crew realized there was a liner leak and then they stopped the well treatment.

The wells were completed with cemented liner/sliding sleeve, and because of the micro-seismic data, which provided reliable information about the source and location of

the problem, the well was salvaged. A remedial workover to repair of the leaking liner was done and the well was safely stimulated and put on production.

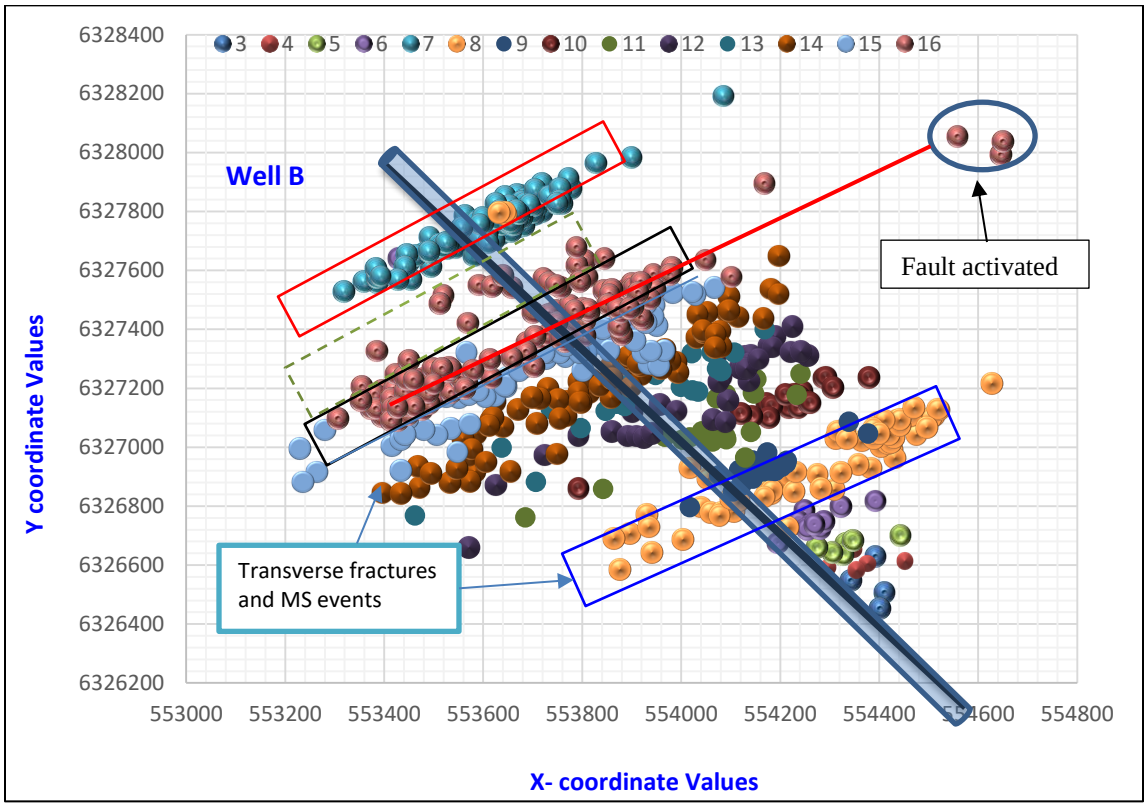

Figure 4-8: Micro-seismic mapping of a horizontal Well B with 16 stages showing transverse fractures and micro-seismic events

Figure 4-9 shows geological layering of the Montney Formation (Upper and Lower Montney) and the Doig Formation, which is above the Montney. The figure also shows depth view of well B micro-seismic survey and lateral location of each stage, the location of monitoring well and the depth and location of micro-seismic receivers.

Figure 4-9 highlights two important points; first, in the Upper Montney Formation, there was no fracture height (H_f) growth, and most of the fractures were constrained within the pay-zone. Secondly, there were no micro-seismic data at the toe of the lateral (highlighted in blue circle) because the stages at the toe were very far from the location of the geophones.

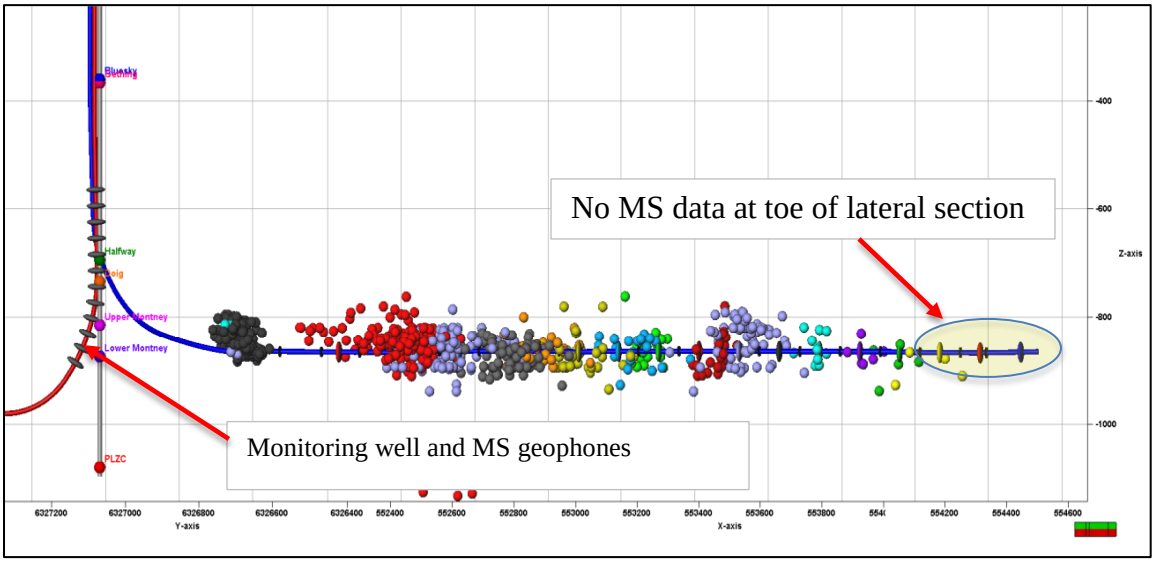

Figure 4-9: Micro-seismic survey per stage, location of monitoring well and geophones. MS data and fracture model both show no height growth in Upper Montney wells

Figure 4-10 shows 3D diagram of the monitoring well, the location of the twelve geophones and the distance of each stage to the micro-seismic receiver. The stages at the toe of the horizontal were 2,000 meters away from the micro-seismic geophones. Figure 4-10 also highlights why two monitoring wells are preferred in micro-seismic mapping of hydraulic fracturing because it improves signal to noise ratio and location uncertainty issues.

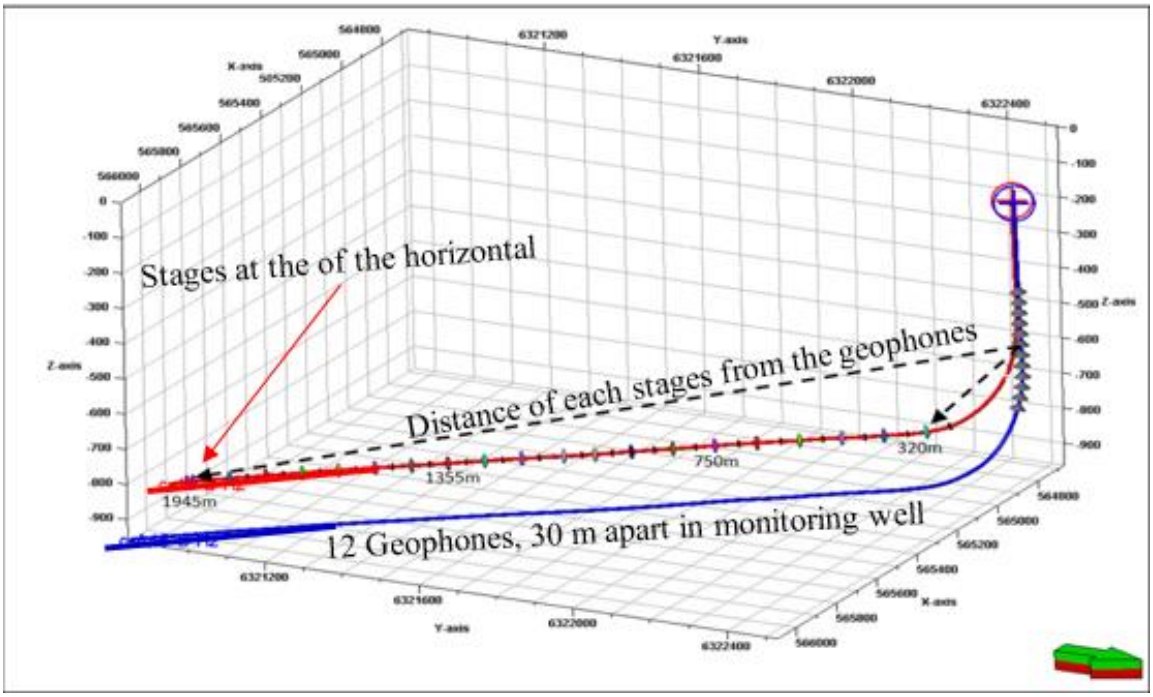

Figure 4-10: Diagram of the monitoring well, location of MS geophones and distance of fractures to the micro-seismic receivers

Figure 4-11 shows the fracture dimensions (fracture half-length, fracture height and number of micro-seismic events) obtained from the micro-seismic mapping for well A. The figure also shows the fracture stages from the micro-seismic survey that were used for history matching (highlighted in blue circle). Secondly, no fracture dimensions were obtained from the micro-seismic survey for stages 1 and 4 (shown by Figure 4-11) because those stages were too far from the micro-seismic geophones/receivers and the signal was too weak.

Additionally, the analysis of the micro-seismic data indicated that the fracture dimensions for stage 17 (Well A) showed anomalous signs. For instance, stage 17 fracture half-length (671 m) was 35% longer than the next longest one (stage 16), and 95% longer than the average fracture half-length (350 m) for well A. Most likely, fracture stage 17

activated a pre-existing fault or long natural fissures. This assessment is consistent with the curvature data from the area. Hence, stage 17 of well A was not used for the model calibration, and the calibrated fracture model could not accurately match its micro-seismic survey fracture dimensions.

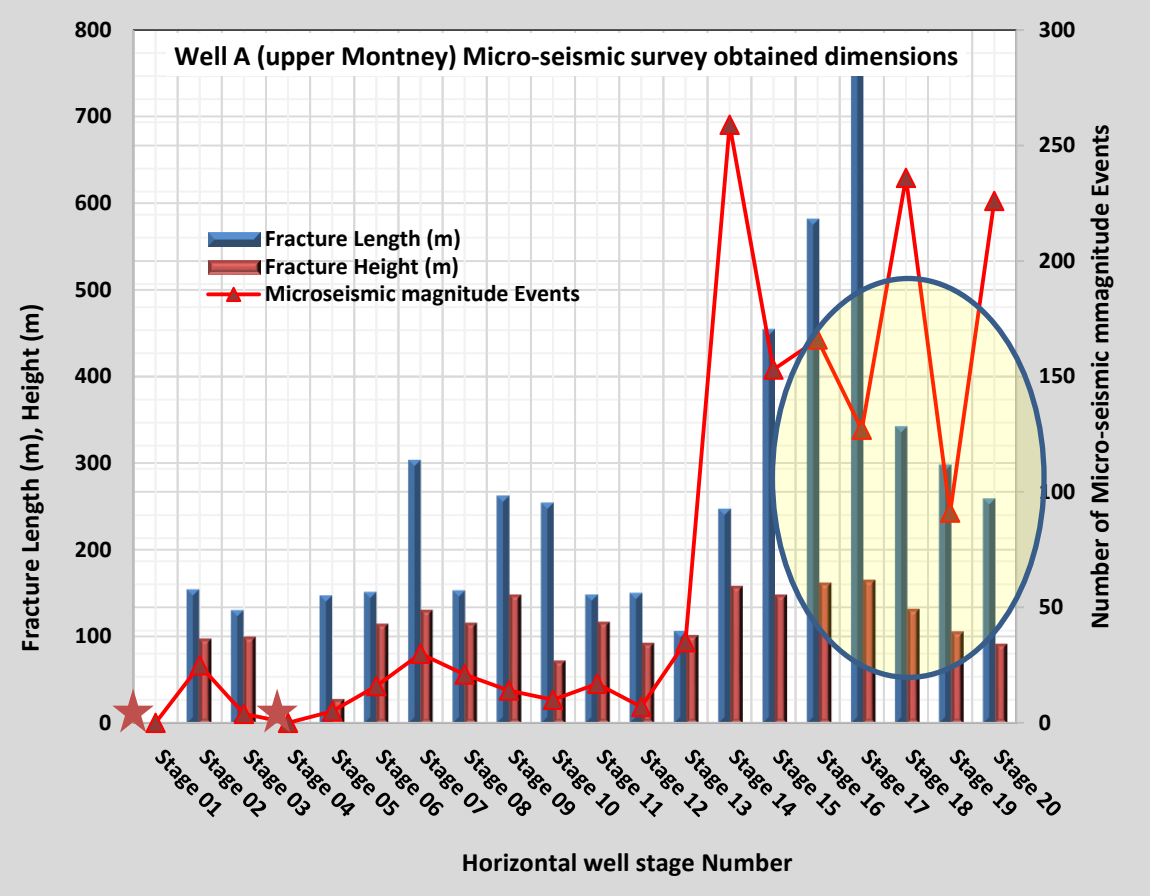

Figure 4-11: Well A fracture dimensions (x_f, H_f and MS events) obtained from micro-seismic mapping, and the 5 stages used for fracture model history matching (highlighted in yellow circle)

4.1.5. Fracture History Matching to Micro-Seismic Data. The calibrated fractured model built and history matched to the micro-seismic survey of the selected stages was used to re-design and re-model all fracture stages for each of the wells in the study. For instance, for well A (shown by Figure 4-11), only the fracture stages highlighted in yellow circle were used for history matching and fracture model calibration. The rest of the stages (1-to-14) were re-modeled using the calibrated fracture model and post-fracture treatment data (fluid volume, proppant mass and treatment pressure, etc.) The process used is similar to post-frac analysis that is often used for determining fracture dimensions and estimating well productivity. However, the difference in in this study was that once the calibrated fracture model was built, only the stress differences ($\Delta\sigma$) were adjusted to match the final net pressure of each stage during the re-modeled process. While this was a unique method of doing post-fracture analysis and building of calibrated fracture model, the result was very impressive and provided representative fracture dimensions and geometry.

4.2. BUILDING FRACTURE MODEL OPTIMIZATION

The current low price environments have made optimization and cost-control efficiency the two major themes in the oil and gas industry. To reduce cost, oil and gas companies have slashed capital spending and delayed or canceled mega exploration and production (E&P) projects. Optimization, on the other hand, covers all phases, levels of company operations, and requires one to “start with end in mind” because the task of field development is a sequential process. Each subsequent decision limits the number of options available for optimization. For instance, the drilling decision affects well placement, casing type and size, and lateral length. Similarly, the completion method deployed effects the

type of completions (open-hole vs cemented), number of fracture clusters per stage, number of stages, treatment volumes and number of wells per pad.

Additionally, the most critical part in stimulation optimization is the quality of the data available and the tools deployed for optimizations. While understanding the reservoir geology and geomechanical properties are critical to hydraulic fracturing, the method of fracture diagnostic technology used can greatly affect the success of any optimization strategy. (Barree et al., 2002) presented a paper titled "A Practical Guide to Hydraulic Fracture Diagnostic Technologies" and stated that fracture diagnostics can be divided into two major groups; indirect diagnostics (numerical fracture modeling, DFIT analysis and production data analysis) and direct diagnostics. The direct diagnostics was further subdivided into near-wellbore (radioactive tracers, temperature and production logs) and far-field diagnostics (such as micro-seismic mapping and tiltmeters). In this study, information from both indirect and direct diagnostics tools were used to develop robust optimization models

Most well optimization activities are cross-functional involving earth scientist, production, completion and reservoir engineers because the task requires an integrated modeling approach. However, most of the time, the completion and reservoir simulation parts are integrated to forecast well productivity and estimated ultimate recovery (EUR).

(Juell and Whitson 2013) presented a paper titled "Optimized Well Modeling of Liquid-Rich Shale Reservoirs", which articulated a modeling strategy that can be used for history matching and optimizing well designs in liquids-rich shale wells found in Montney, Eagle Ford and Bakken. The paper used black-oil reservoir simulators, and a separate optimization software (Petrostreamz 2013).

(Crosby et al. 2016) used inorganic and organic elemental data from drill cuttings and advanced mud-gas analysis at the wellsite coupled with LWD (logging while drilling) gamma ray spectroscopy to optimize completion operations and designs. In a paper titled "Optimized Completions Design With Integrated LWD and Well Site Geochemistry for Petro-physical Analysis and Enhanced Well Placement", the authors stated that this method allowed them to enhance well placement and landing point identification by providing a comprehensive near real-time chemo-stratigraphic interpretation.

Woo et al. (2011) presented a paper titled "Fracture Stimulation Optimization in Horizontal Cardium Completions", which provided optimization process that was deployed to increase production and net present value (NPV) by incorporating reservoir modeling, fracture spacing optimization and the use of solids-free viscoelastic fracturing fluid.

(Ely et al. 2014) presented a paper titled "Slick Water Fracturing and Small Proppant- The future of stimulation or a slippery slope", where the author stated that the vast majority of fracturing fluids are either water (aka. slick-water) with friction reducers or a combination of linear gel and or crosslinked gel that quickly degraded to water once in the formation. The authors attribute to the success of the slick water fracturing fluids to the different geometry created combined with the use of much large volumes. However, probably one of the main reasons for the success and dominance of slick water as a preferred fracturing fluid in the oil and gas industry is because of well economics. Slick water fracturing fluid is cheaper, less damaging to the formation and environmentally friendly because it requires less chemicals.

4.2.1. Optimization Parameter Sensitivities. The stimulation optimization and sensitivity of optimization parameters was done per fracture stage. Figure 4-12 shows diagram of horizontal well with one fracture stage, five clusters and zonal isolations. The completion method highlighted is called the "plug and perforation", and is one of the flexible completions methods that can be deployed by either coil-tubing or regular tubing strings in cased-hole wells.

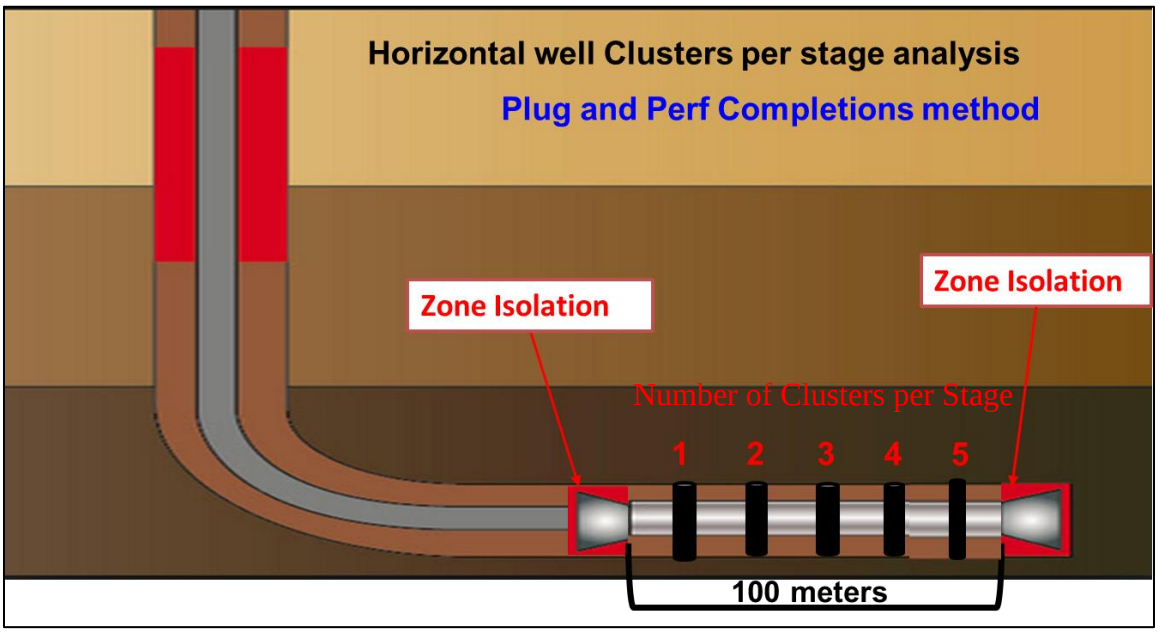

Figure 4-12: Horizontal well picture showing number of clusters per stage, zonal isolations and fracture spacing (modified from drillingformulas.com)

Optimization and cost control have become two key performance indicators of the oil and gas industry. However, hydraulic fracture optimization requires identification of key sets of parameters to study so that the impact of each variable on well performance,

recovery and economics can be measured. (Britt and Smith 2009b) presented a paper titled "Horizontal Well Completion, Stimulation Optimization, and Risk Mitigation", where the authors focused on key elements of well completions and stimulation that are applicable to horizontal wells. The optimization variables studied by (Britt and Smith 2009b) were lateral length, number of fractures, fracture half-length and fracture conductivity.

In this optimization study, there were three sets of parameters; proppant mass (from 50 M-kg-to-150 M-kg) per stage, number of fracture clusters (from 1 cluster-to-5 clusters) per stage, and fracture stage spacing (from 98m to 20m) per cluster stage. The final part of the optimization was to study the impact of each set of parameters on well productivity, reserves and economics using compositional reservoir simulators. Figure 4-13 shows the fracture model optimization workflow and steps used in the study. The first step was to use the calibrated fracture model built from previous steps (shown by Figure 4-2).

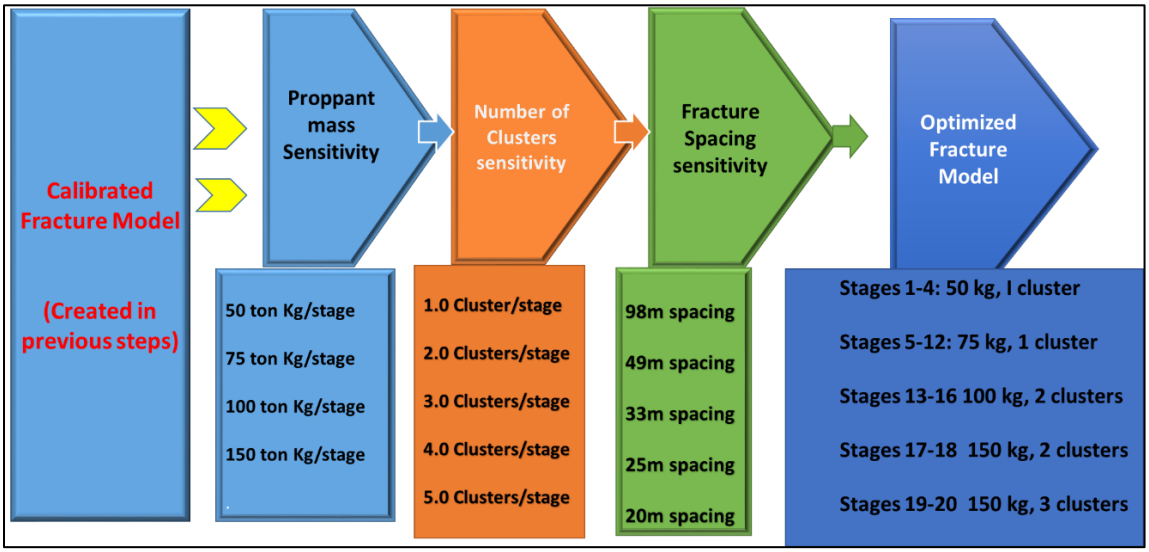

Figure 4-13: Optimization and sensitivity analysis of proppant mass, number of clusters, fracture spacing and development of the optimized model

4.2.2. Hydraulic Fracture Optimization Trends. Currently, different oil and gas companies are experimenting with three hydraulic fracturing optimization trends, and are testing them at different regional shale plays. The first optimization trend is drilling long horizontal wells, sometime referred to as "extended reach laterals." The second optimization trend is decreasing fracture spacing either by increasing the number of stages or number of clusters per stage in horizontal wells. Eclipse Resources completed the longest horizontal well ever drilled in onshore U.S. The horizontal well was named "Purple Hayes", had total measured depth of 27,048 feet, lateral length of 18,500 feet and 124 stages (Eclipse-Resources Investor Presentation August 2016). The company reduced fracture spacing to 150 feet and had the optimization objective of maximizing lateral length.

The third optimization trend is the use of massive amounts of frac sands per stage, and one of the optimization metrics that companies are using to analyze is "pounds of sand per lateral foot" (lb. /ft.) of the horizontal well. Chesapeake Energy completed a horizontal well in Haynesville shale that had 9,764 feet of lateral and pumped 50.185 million pounds of sand (Carroll and Wethe 2017). This well had 5,000 "pounds of sand per lateral foot" (lb. /ft.), and to improve well productivity substantially, the authors stated, "More proppant, more stages and longer laterals is the way to go."

Figure 4-14 shows hydraulically fractured horizontal wells and frac sand use in some of the major U.S. shale plays. In each of the three major shale plays analyzed; Bakken, Eagle-Ford and Permian basin, the amount of proppant in terms of "pounds of sand per lateral foot" (lb. /ft.) have doubled from 2012 to 2016.

In this study, two optimization metrics that were investigated were impacts of the use of massive amount of frac sands per stage (i.e. 400,000 M-kg), and the use of increased number of fracture stages or clusters per stage in horizontal wells.

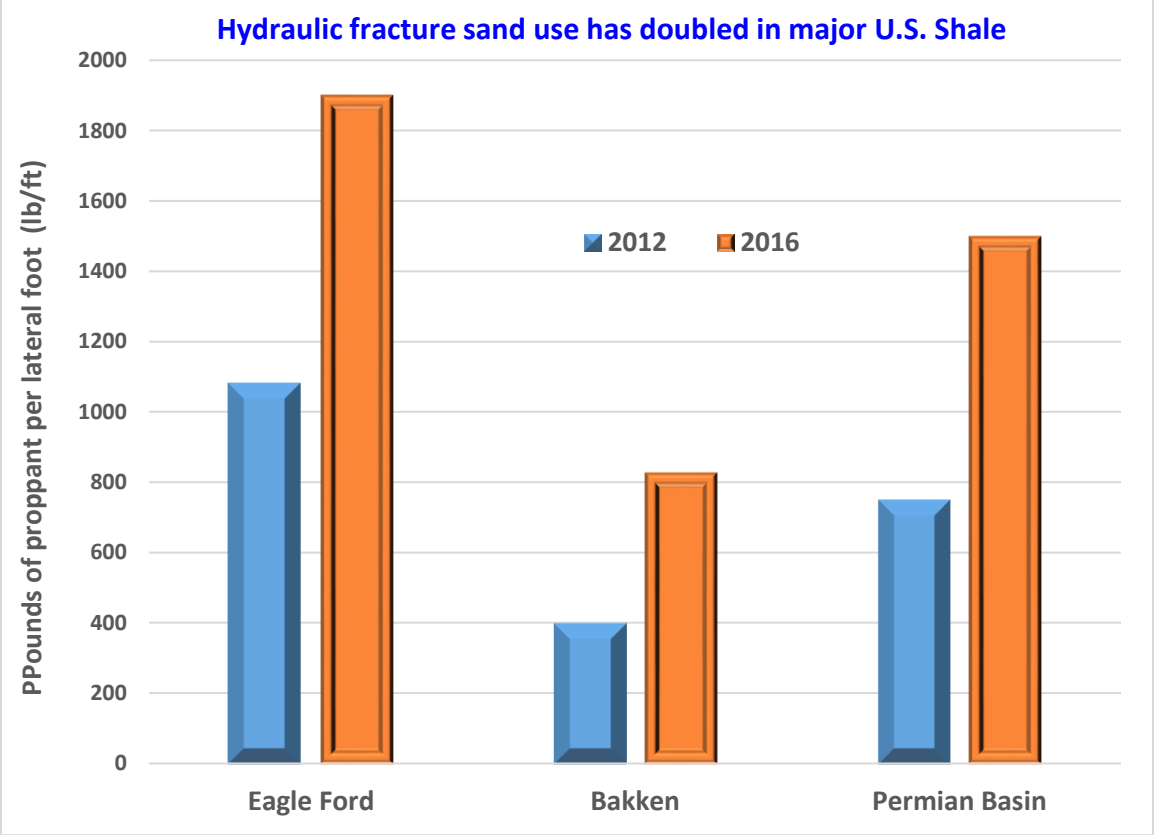

Figure 4-14: Hydraulic fracture sand use has double in most major U.S. Shale plays (modified from (Carroll and Wethe 2017))

Table 4-1 shows the layout of the optimization process, which was analyzed by increasing frac sands per stage from 200,000 kg to 400,000 kg. Similarly, the fracture spacing was reduced from 33 meters to 13 meters per stage. The number of clusters per stage was also increased from three clusters per stage to eight clusters per stage. Secondly,

the optimization study used only water-frac, which is now the dominant fracturing fluids used in most North American shale plays. Thirdly, since water-fracs are not good sand carrying fluids, the slurry and pad volumes were linearly correlated to the proppant mass per stage, and normalized to each well's post-fracture treatment data. For example, in well A, the average slurry volume and proppant mass per stage was about 580 m^3, and 93,000 kg, respectively. Additionally, the calibrated fracture model constructed from previous step was used, eliminating the likelihood of premature screen-outs, which might skew the optimization results.

Table 4-1: Optimization parameters of "big Frac sands" and fracture spacing per stage

Fracture Spacing (m)	Number of Clusters per Stage	Frac Sand per Stage (kg)	Stage Slurry Volume (m_3)
33	3 Clusters	200,000	1180
25	4 Clusters	200,000	1180
20	5 Clusters	200,000	1180
17	6 Clusters	200,000	1180
14	7 Clusters	200,000	1180
13	8 Clusters	200,000	1180
33	3 Clusters	300,000	1770
25	4 Clusters	300,000	1770
20	5 Clusters	300,000	1770
17	6 Clusters	300,000	1770
14	7 Clusters	300,000	1770
13	8 Clusters	300,000	1770
33	3 Clusters	400,000	2655
25	4 Clusters	400,000	2655
20	5 Clusters	400,000	2655
17	6 Clusters	400,000	2655
14	7 Clusters	400,000	2655
13	8 Clusters	400,000	2655

4.3. BUILDING INTEGRATED RESERVOIR SIMULATION MODELS FOR HYDRAULICALLY FRACTURED WELLS

The integrated reservoir modeling was conducted using well data from the Montney formation. The Montney Formation is one of the most prolific and commercially attractive unconventional resources in North America. Figure 4-15 shows the Montney Formation, which is part of Western Canadian Sedimentary Basin. The Montney play has conventional, over-pressured gas and an over-pressured liquids rich fairway. Figure 4-15 also shows a detailed map of the area of study and location of the wells. The wells used in the study are in the northeast British Colombia's liquids-rich area (Aitken Creek) of the Montney play.

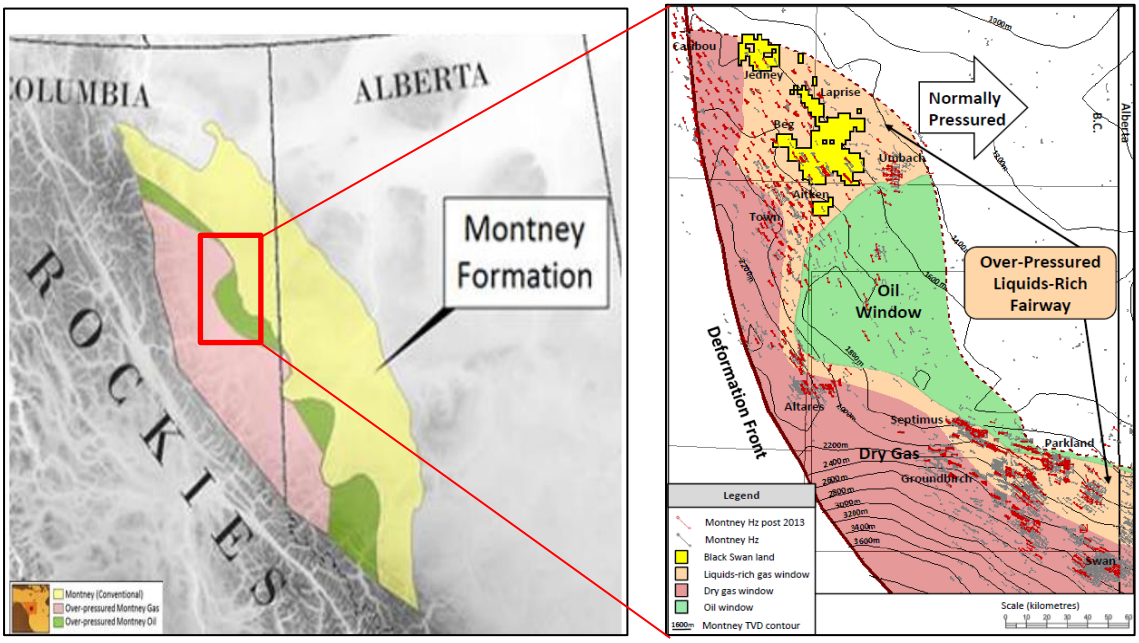

Figure 4-15: Detailed map showing location of the wells in the study (modified from Geoexpro.com and Black Swan Energy)

Most of the liquids-rich shale plays in North America contain condensate fluid types, which makes it very difficult to obtain representative fluid sample for reservoir simulations. Quirk et al. (2010) presented a workflow for integrating micro-seismic, fracture modeling and reservoir simulation to study fractured horizontal wells in the Cardium tight oil formation, which is part of the Western Canadian Sedimentary Basin. Quirk stated that the objective of the project was to measure fracture orientations and geometries with micro-seismic survey and to create a calibrated fracture model. In the Cardium tight oil formation study, Quirk used a pseudo-3D fracture simulator and a black oil reservoir simulator. However, in this study, a fully-3D fracture simulator and compositional reservoir simulators were used. This is critically important because previous studies (Kassim et al. 2016b) have shown that capturing the effect of fluid composition changes in the reservoir simulation greatly improves the model's reliability and forecasting.

The reservoir simulation process and steps used in building the integrated completions and reservoir models are given by Figure 4-1. Similarly, Table 4-2 gives reservoir and fluid properties used in the construction of the reservoir simulation models.

The process of building the reservoir simulation model involved six different steps; first, the micro-seismic data was imported into the model and used to configure drainage area and stimulated reservoir volume (SRV). The second step was the addition of reservoir characterization into the model. Reservoir model permeability and permeability anisotropy, porosity distribution in each reservoir layer and rock properties were incorporated into the model. The third step was incorporating fracture dimensions from the calibrated fracture model into the reservoir simulation model. This step was guided by the

locations of the micro-seismic events recorded for each fracture stage. For accuracy and precision purpose, each hydraulic fracture dimensions incorporated into the reservoir model must overlay the recorded micro-seismic events for each well in the study.The fourth step was addition of fluid properties such as relative permeability, saturation, and composition of each hydrocarbon phase (oil and gas).

Table 4-2: Integrated reservoir Simulation model data used in the simulations

Reservoir data				**Well Data**			
Depth to top of formation	1,800	m		Well type	Horizontal		
Reservoir thickness	100	m		Radius	r_w	0.13	m
Initial reservoir pressure	3,750	psi		Lateral Length	L	2,000	m
Reservoir temperature	78	C		Avg Fracture half-Length	X_f	350	m
Porosity	0.05			Fracture Width	W_f	0.02	m
Permeability	0.00018	md		Fracture Orientation	Transverse		
Initial water saturation	0.25			Number of fractures	n_f	20 & 16	
Rock compressibility	1.00E-06	psi-1		Well Head pressure	WHP	290	psi
Fracture compressibility	1.85E-04	psi-1		Separator pressure	S_p	260	psi
Relative permeability exponent	2			Separator temperature	T_S	18	c

4.3.1. Building the SRV Based Model from Micro-seismic Data. The stimulated reservoir volume (SRV) was determined from the micro-seismic mapping for each of the wells in the study. The micro-seismic data provided the spatial coordinates (x,

y and z) of each micro-seismic events, moment magnitude, time, stage number and P/S ratio. These parameters were used estimated the boundary of the stimulated area, drainage volume and fracture dimensions for each fracture stage and stimulated reservoir volume (SRV). Figure 4-16 shows 3D reservoir simulation model that was built from the micro-seismic data and the geophysical reservoir properties. The 3D reservoir model shows micro-seismic mapping for each fracture stage and the vertical distribution of porosity. Figure 4-16 also shows that the fracture stages at the toe of the horizontal well had little or no micro-seismic mapping data.

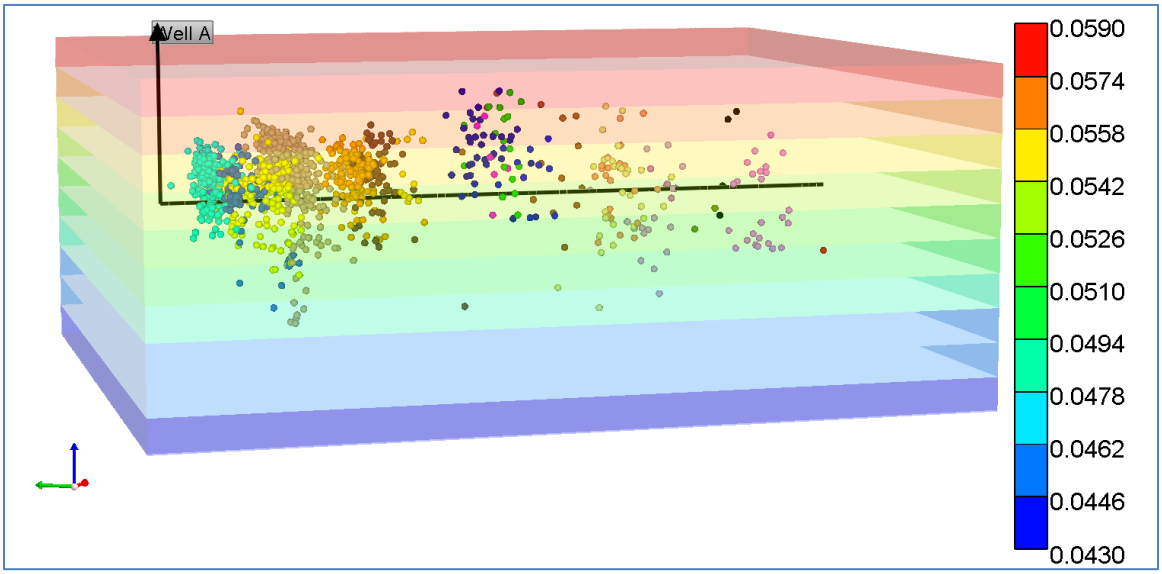

Figure 4-16: 3D reservoir simulation model showing micro-seismic mapping for each stage and vertical distribution of porosity

The Compositional reservoir simulation model built had ten layers as shown by Figure 4-16. The 3D reservoir model was constructed to accurately capture the isotropic distribution of rock and fluid properties such as permeability, porosity, micro-seismic

mapping, and fluid composition. Specifically, the 3D reservoir model captured three important aspects of the study;

- The vertical distribution of porosity, permeability and oil compositions determined from the PVT analysis. Figure 4-16 shows the model built for the SRV (stimulated reservoir volume) from micro-seismic.
- The hydraulic fracture dimensions and geometry determined from the micro-seismic and calibrated fracture model.
- The effect of secondary permeability and porosity from complex fracture, especially discrete fracture network (DFN) system on well performance.

Figure 4-17 shows micro-seismic volume for each stage of the hydraulic fracturing, and estimated stimulated volume for each stages where there was enough micro-seismic events.

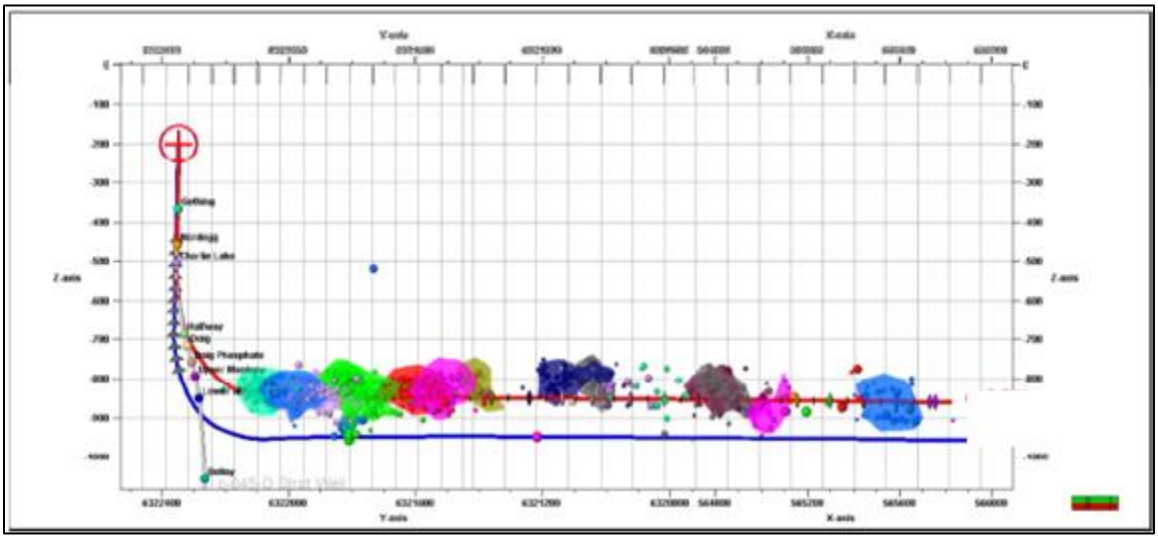

Figure 4-17: Depth view of Well B showing micro-seismic volume of each stage, and stimulated volume.

Some of the stages had little or no micro-seismic events recorded during the hydraulic fracture treatment. Hence, their stimulated volume could not be determined from the micro-seismic mapping data. One of the shortcomings of low quality micro-seismic data (which has either location bias or signal to noise ratio issues) is that any stimulated reservoir volume (SRV) calculated from would under-estimated the effectiveness of the hydraulic facture treatment.

4.3.2. Reservoir Characterization. Reservoir characterization is critical to the understanding of the reservoir and development of oilfield. Reservoir characterization requires geophysical property analysis, seismic interpretation and volumetric analysis. However, to understand reservoir heterogeneity and fluid flow, which are need for reservoir characterization, the distribution of porosity and permeability are critically important. In this study, reservoir characterization was modeled by building a representative reservoir model that captured the vertical distribution of rock and fluid properties.

Figure 4-18 shows the Upper Montney porosity distribution, and the porosity of the wells used in the study (marked with red star). The figure shows that the Upper Montney Formation has very low matrix porosity. Secondly, the porosity values ranged from high of 0.083 to low of 0.033 in the data analyzed as shown by Figure 4-18.

The porosity data was obtained from well logs, core data and regional Upper Montney porosity distribution data. The porosity range of the wells used in the study were 0.05 to 0.053 mD.

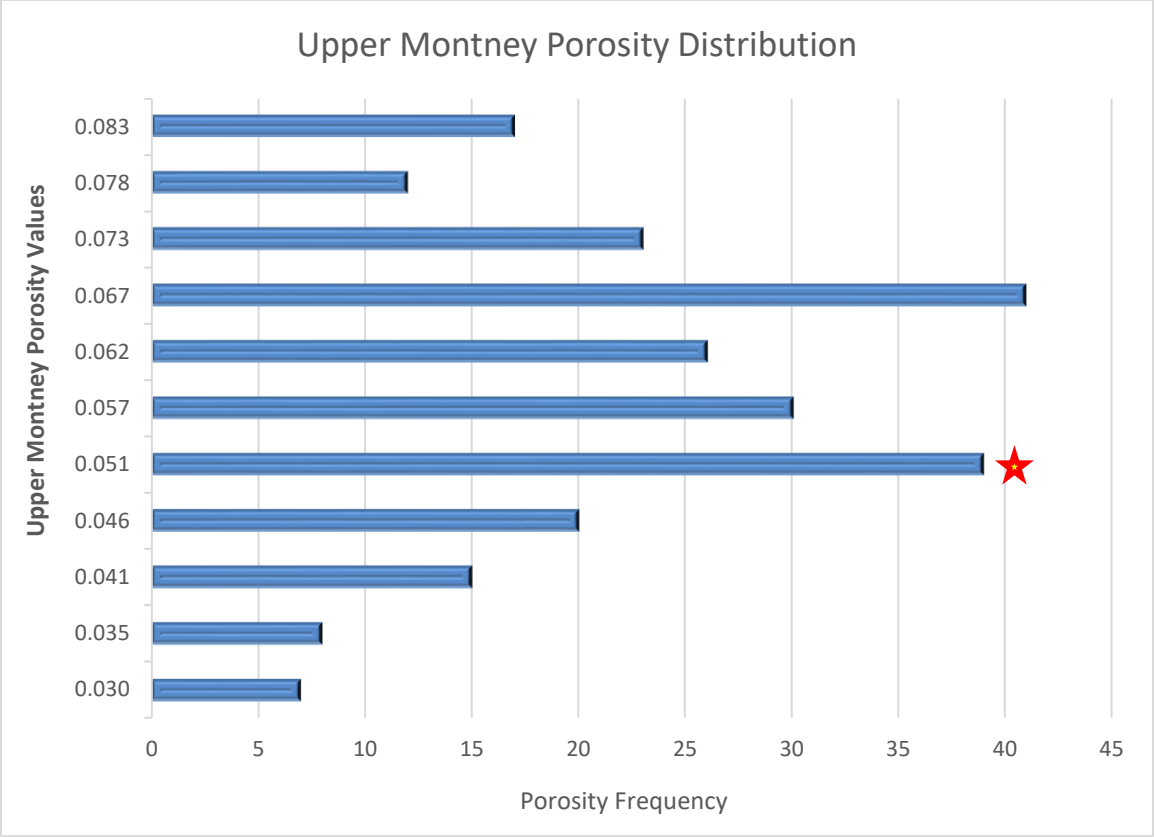

Figure 4-18: Diagram showing Upper Montney Formation porosity distribution, and porosity of the wells used in the study (red star)

Gaussian probability distribution analysis of the Upper Montney porosity showed bell-curved-shaped plot, which meant that the data had symmetry and was not highly skewed. Figure 4-19 shows the probability distribution of the porosity and mean value of the data.

Additional statistical analysis of the data's skewness and kurtosis revealed that the Upper Montney porosity data was a little bit positively skewed and had low kurtosis, but lacked outliers. Secondly, Figure 4-19 also shows that the mean of the porosity distribution was 0.06 (highlighted by the red dashed line), and the data was not heavy-tailed or light-tailed compared to normal distribution.

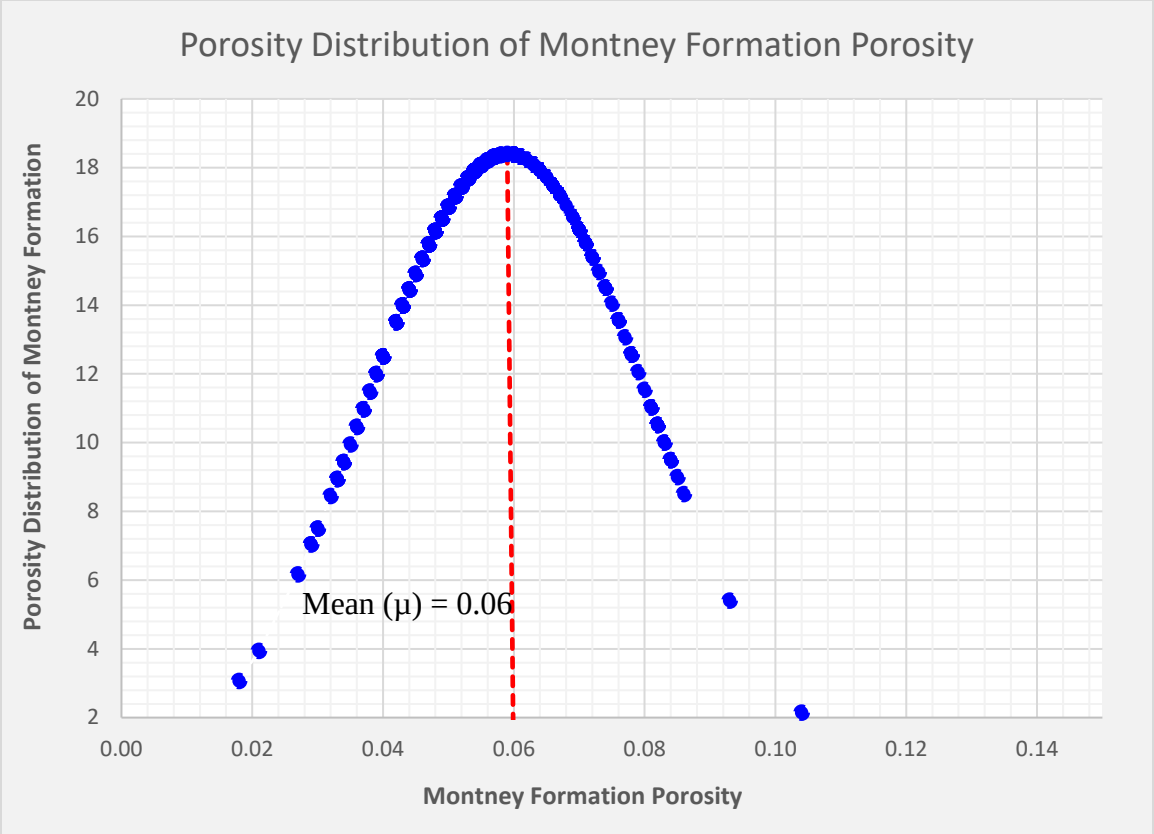

Figure 4-19: Gaussian distribution of Montney Formation porosity, and mean porosity (red line)

One of the biggest problems facing companies exploring and producing from unconventional resources is the difficult of characterizing poor quality reservoirs that might have dual fluid transport and storage mechanism. In addition, some of the shale plays have thin multi-layered target zones or complex rock mineralogy. The Montney Formation consist of inter-bedded siltstone and shale, and is characterized by non-uniform spatial distribution of reservoir properties (Derder 2013). However, the Upper Montney Formation is spatially massive and has thick net-pay.

Figure 4-20 show the Upper Montney Formation pay-zone thickness distribution, and net-pay of the wells used in the study (red star). The average net-pay obtained from

the Montney data was 83 meters. However, at the tail-end of the distribution, the thickness of the Upper Montney becomes massive and approaches 300 meters.

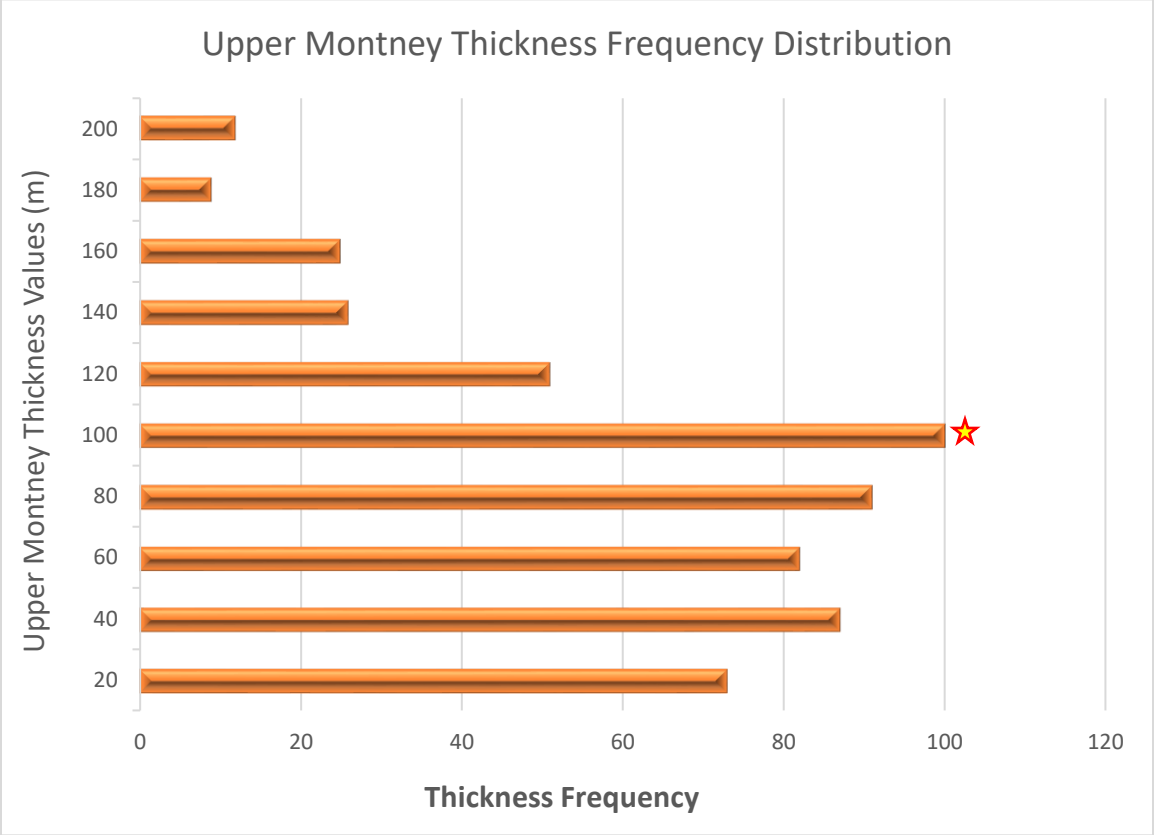

Figure 4-20: Upper Montney Formation pay-zone thickness distribution, and net-pay of the wells used in the study (red star)

The results of Figure 4-20 highlight two important findings; first, the smallest net-pay in the Upper Montney Formation is about twenty meters (65 feet), which is suitable for horizontal well drilling and placement. Secondly, the mode of the net-pay distribution in Upper Montney Formation was about 100 meters, which means that the Upper Montney

is spatially thick formation. Additionally, most the Upper Montney net-pay distribution is between 40 meters and 100 meters as shown by Figure 4-20.

Figure 4-21 shows statistical analysis of the Upper Montney Formation net-pay, and the data indicates that the thickness distribution was positively skewed with a value of 2.06. Additionally, analysis of the Upper Montney data's kurtosis showed it had a value of 7.20, which means the thickness distribution was light-tailed relative to a normal distribution.

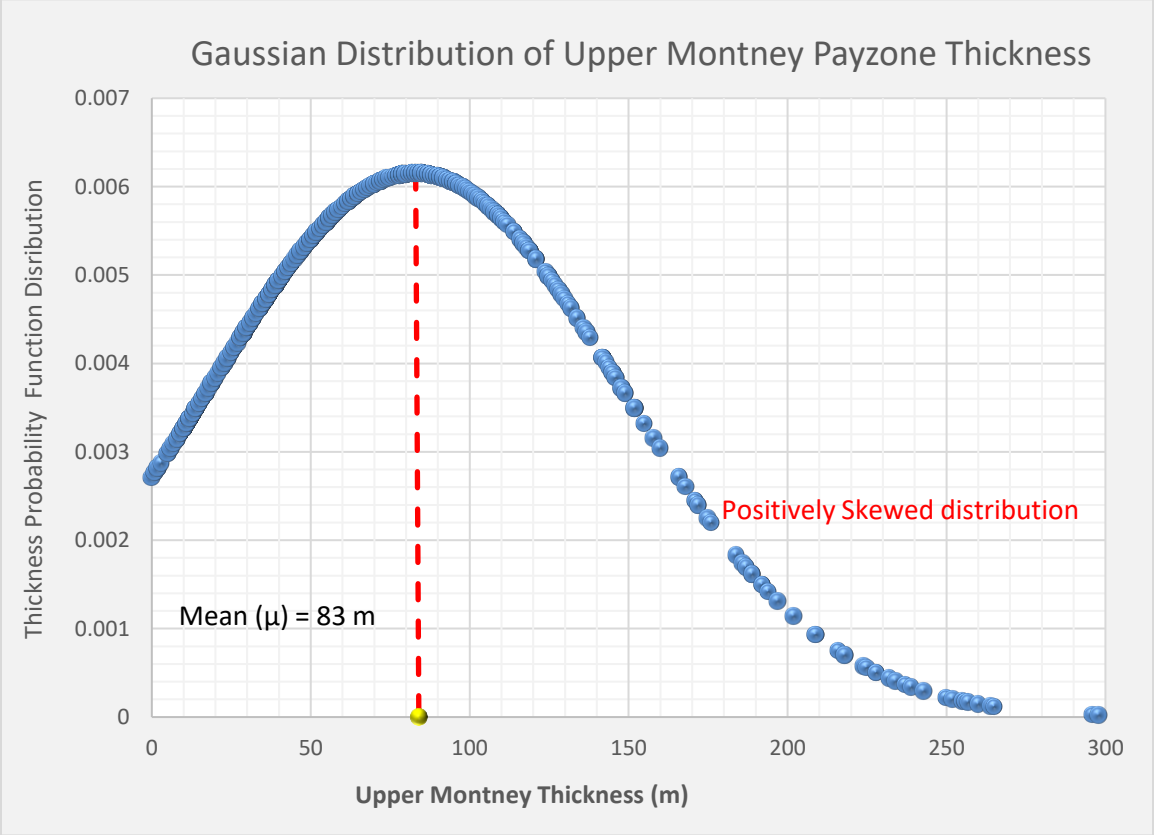

Figure 4-21: Gaussian distribution of Upper Montney thickness and mean net-pay (red line)

Further reservoir characterization using well logs, especially gamma rays, resistivity, dipole sonic logs and bulk density were carried out to assess reservoir properties and their distribution in the Upper Montney Formation.

4.3.3. Importing Calibrated Fracture Model Dimensions into the Planar Reservoir Model. The fracture dimension obtained from the calibrated hydraulic fracture model were imported into the compositional reservoir simulator. Secondly, the effect of non-Darcy flow and stress dependent permeability was added to the model using the steps outline in section 3.5 of this dissertation, using equations 27 and 28. Figure 4-22 shows planar reservoir model with the fracture dimension, drainage area and SRV (stimulated reservoir volume) from the calibrated hydraulic fracture model. Additionally, Figure 4-22 shows three layers of LRG (locally refined grid-blocks) for the fracture stages, two LRGs for the SRV and one LRG for the well drainage area. The reason such highly multi-layered grid refinement was used to model hydraulically fractured well was to closely match the grid-block size to the actual fracture width (w_f). This is critically important because modeling non-Darcy flow effects in hydraulically fractured wells require representative fracture width (w_f), which is implicitly a function of the Forchhiemer formula through the beta factor (β).

Figure 4-22 also shows that two hydraulic fracture stages had very long fracture half-lengths, which presented two challenges; first, the uneven distribution of fracture half-lengths can lead to communication and interference with nearby wells, impacting well productivity. Secondly, having few stages with long fractures can increase the uncertainty of the stimulated area or the well boundary, making oilfield development and planning difficult.

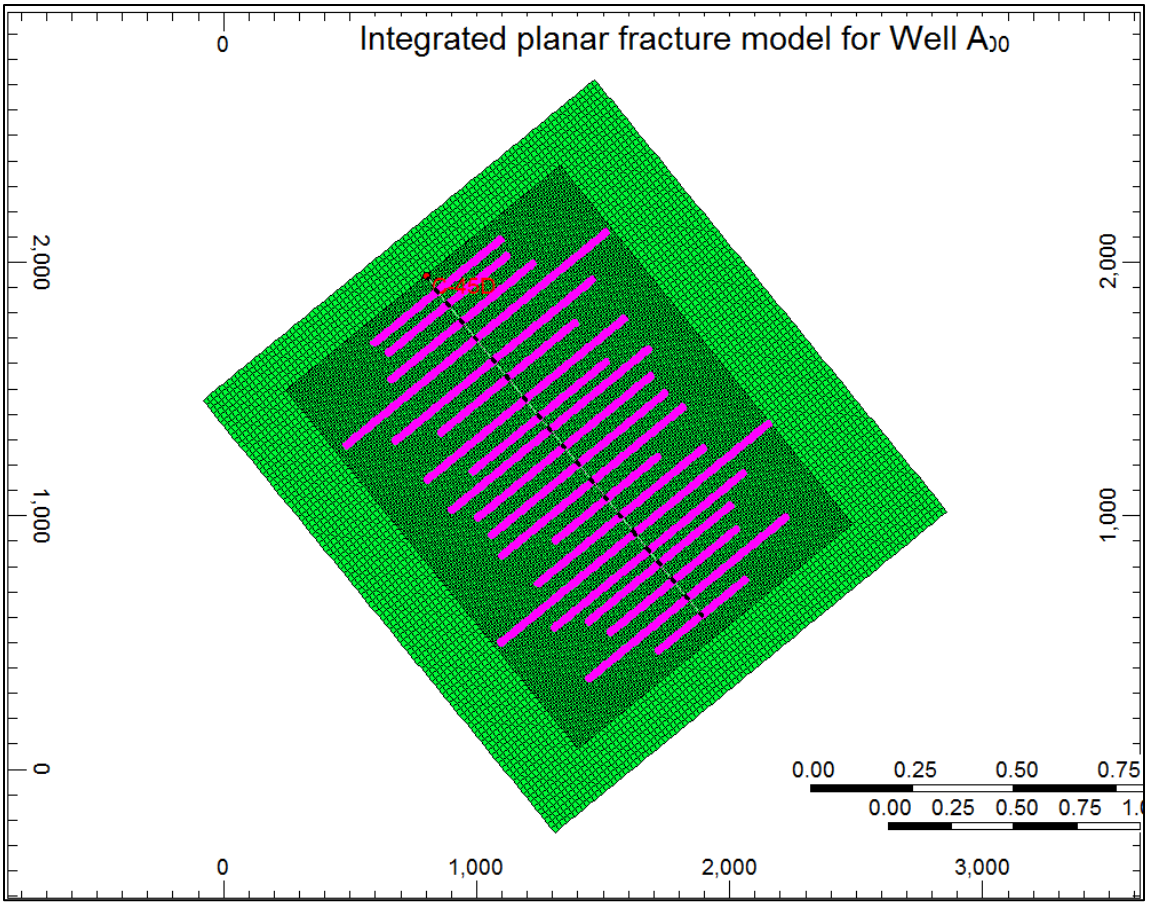

Figure 4-22: Reservoir model showing fracture stages and micro-seismic survey derived drainage area and SRV

4.3.4. PVT Analysis, EOS Modeling and Well Data. The fourth step in the construction of the reservoir simulation model was the addition of reservoir fluid properties and PVT analysis. Gas condensate reservoirs require thorough PVT analysis because it's very difficult to obtain representative fluid samples. Laboratory techniques such as recombination and analysis of well-stream production (PVT data) or the use of gas Chromatography analysis with constant composition expansion (CCE) test are some of the methods lab technicians use. In this study, the gas and liquid samples were recombined in

representative mole ratio to obtain gas condensate composition at the well-stream. The formula for recombining to well-stream composition is given by

$$z_i = F_g y_i + (1 - F_g) x_i \quad \text{...(39)}$$

$$\mathrm{F_g} = \frac{1}{1 + \left[133{,}300 \left({}^{\gamma}/_{\mathrm{M}} \right)_{\mathrm{o}} / \mathrm{R_s} \right]} \quad \text{...(40)}$$

Where

z_i = mole composition of component (i) in the well-stream

x_i = mole fraction of component (i) in the liquid phase

y_i = mole fraction of component (i) in the gas phase

F_g = gas gravity factor

$\mathrm{R_s}$ = solution gas oil ration (scf/bbl)

γ = oil density, and $\mathrm{M_o}$ = oil molecular weight

More details about the procedures for conducting thorough PVT analysis can be found in a paper presented from the work of this dissertation by (Kassim et al. 2016b) or the book referenced by this study written by (Whiston and Brulé 2000).

4.3.5. Modeling Fracture Complexities Using Curvature Data from 3D Seismic. The micro-seismic mapping data showed the presence of complex fractures in

some of the hydraulically fractured stages in Montney Formation. For instance, Figure 4-7 and Figure 4-8 showed that fracture stage 16 in both wells (A and B) indicated the existence of complex fractures in some of the stages. Curvature data from 3D seismic can be used to qualitatively estimate fracture density, spacing and orientation.

Klein et al. (2008) presented a paper titled "3D Curvature attributes: a new approach for seismic interpretation" where he stated that curvature attributes respond to bends and breaks in the seismic reflector and are not affected by changes in amplitude caused by variations in the fluid and lithology. There are different methods of computing curvature data such as divergence formulation (Donias et al. 1998) and fractional derivatives (Chopra and Marfurt 2007) which is given as

$$F_\alpha\left(\frac{\partial \mu}{\partial x}\right) = -i(k_x)^\alpha F(\mu) \quad \text{...(41)}$$

Where

F = Fourier transform, and α = fractional real number (ranges between 1 and 0)

μ = an inline or crossline component of reflector dip

k_x = curvature volume at spatial location x

Core samples obtained from shale plays (Marcellus and Barnett) have shown the presence of natural fractures in shale plays. Similarly, rock outcrops have revealed the presence of cemented fractures (Engelder et al. 2009), and DFIT (diagnostic fracture injection tests) have shown pressure dependent leak-offs, which indicate the presence of natural fracture in the injected zone. Other fracture diagnostic tools such micro-seismic

mapping and curvature data from 3D seismic can reveal locations, density and direction of natural fractures.

Figure 4-23 shows micro-seismic events recorded during hydraulic fracture treatment for well A. the micro-seismic mapping provided three important information that were used in the construction of the integrated completions and reservoir simulation models. First, the micro-seismic data in Figure 4-23 shows the presence of natural fractures, which are either orthogonal or parallel to the wellbore and induced hydraulic fracture.

Secondly, there were discrete network of fractures, with fracture spacing of 20 by 15 meters, which got activated during stimulation treatment. Thirdly, the micro-seismic mapping helps to understand stress directions in the Montney Formation.

The porosity and permeability of the secondary fractures were calculated from data obtained from the micro-seismic data (which was the secondary fracture spacing), and DFIT test, where the permeability of the matrix was obtained, but assumed to equal to the effective secondary fracture permeability. The formula used in the calculated are given below. For Secondary Fracture Porosity ($\emptyset_S$):

$$\emptyset_S = n_f \left(\frac{w_f}{f_S}\right) = \left(\frac{V_{f[i,j,k]}}{V_{GV}}\right) \quad \text{...(42)}$$

Where;

$\emptyset_S$ = Secondary fracture porosity, fraction or percentage

n_f = number of secondary fracture in single grid block

w_f = fracture width, ft.

f_S = secondary fracture spacing, ft.

$V_{f[i,j,k]}$ = spatial volume of secondary fractures in [I, j, k) direction in single grid block

$V_{f[i,j,k]}$ = total volume of single grid-block, which is (i*j*k) values.

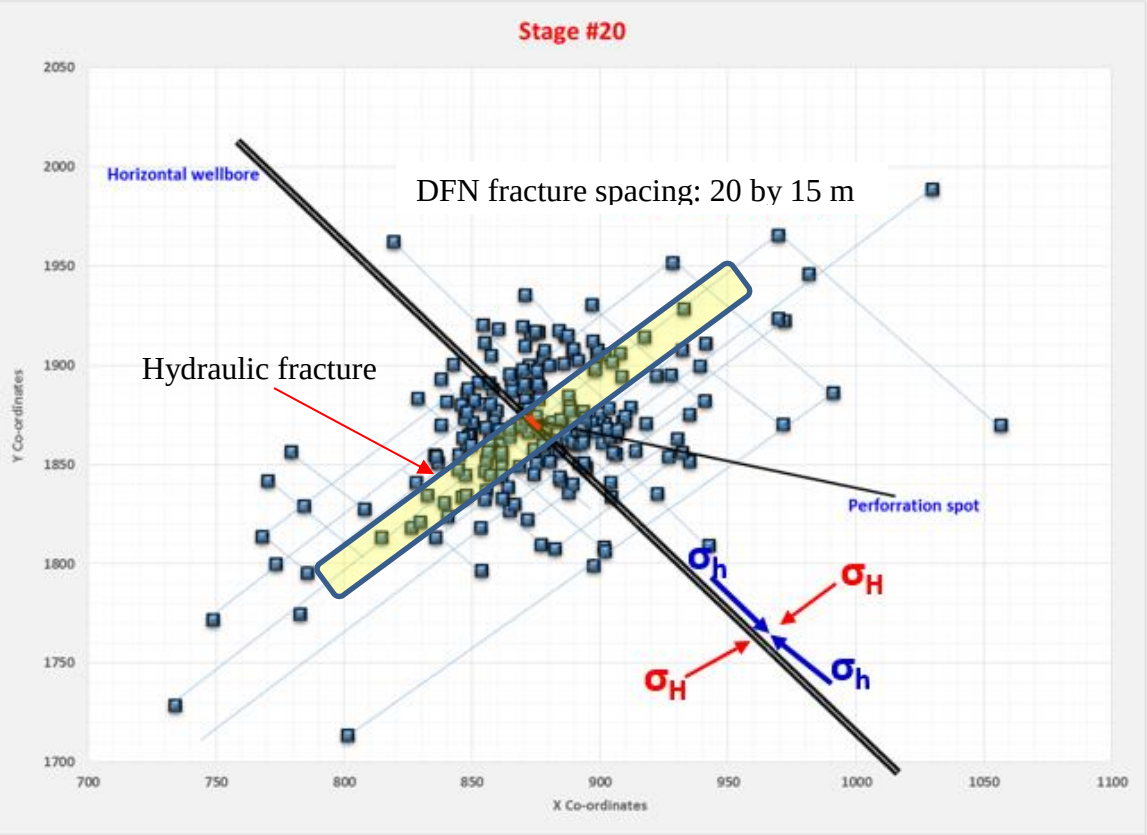

Figure 4-23: Diagram showing micro-seismic events recorded for stage 20 during stimulation treatment and presence of natural fractures

For the secondary fracture permeability calculations, the equation used is given below.

$$k_{frac} = \left(\frac{C_f * n_f}{G_W}\right) \quad ...(43)$$

Where;

k_{frac} = secondary fracture permeability, mD

C_f = secondary fracture conductivity, mD-ft, which is $\left(k_f * w_f\right)$

n_f = number of fractures in a single grid block of the reservoir model

G_W = Grid width from the reservoir model

For instance, the secondary fracture permeability in z-direction was calculated using the plane (x,y) fracture spacing obtained from the micro-seismic data. In this study, since the composition reservoir simulation model was divided into ten layers in order to capture vertical distribution of petro-physical and fluid properties, the secondary fracture spacing was assumed to be equal to the reservoir layering in the z-direction. Hence, there was no need to input fracture spacing for the z-direction (even it could be estimated from the micro-seismic mapping). However, the secondary fracture permeability in the z-direction was calculated using the following formula.

$$k_z = k_f w_f \left(\frac{1}{S_{f(x)}} + \frac{1}{S_{f(y)}}\right) \quad ...(44)$$

Where;

$S_{f(x)}$ = fracture spacing in the x-direction, meters

$S_{f(y)}$ = fracture spacing in the y-direction, meters

The fracture complexity model was based on the probability distribution of natural fractures that were derived from curvature data obtained from 3D seismic. Figure 4-24

shows curvature map highlighting the locations, density and direction of natural fissures. Micro-seismic events from the induced hydraulic factures were also overlaid on top of the curvature data, showing locations where induced fractures interacted with the natural fissures. Figure 4-24, which is the curvature map for well A, shows that there were at least seven hydraulic fracture stages that interacted with natural fractures during the stimulation treatment. Secondly, the orientation of natural fractures were either orthogonal or parallel to the induced hydraulic fractures, and a network of discrete fractures.

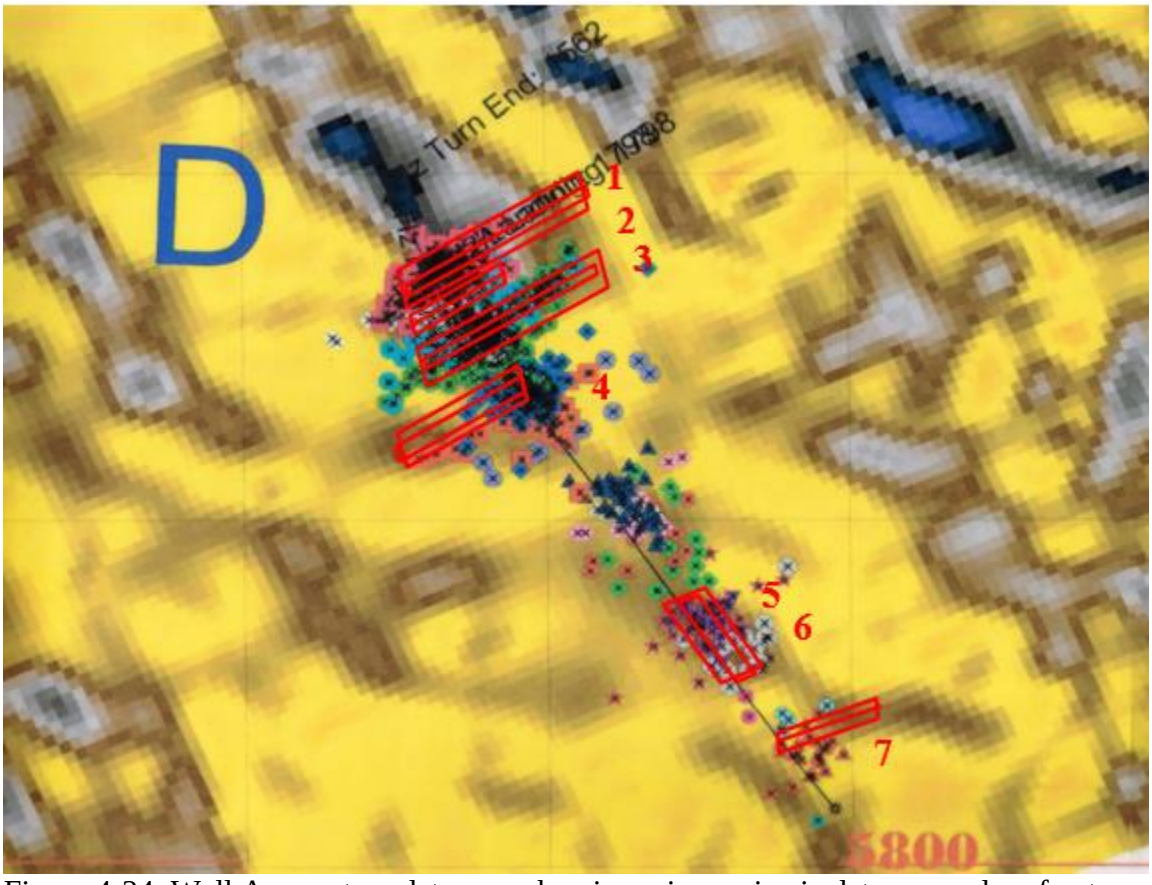

Figure 4-24: Well A curvature data map showing micro-seismic data, secondary fractures density and location (highlighted in red interactions between induced and natural fissures)

The fracture complexity for well B was also determined using curvature data from 3D seismic. Figure 4-25 shows curvature data map from 3D seismic for Well B, and shows location of natural fracture (highlighted in red). The darker gray area in the curvature map indicate presence of natural fissures, and their density and direction. The figure also shows micro-seismic survey (showing location of hydraulic fracture stages and direction) and relative interaction of induced fractures and natural fissures.

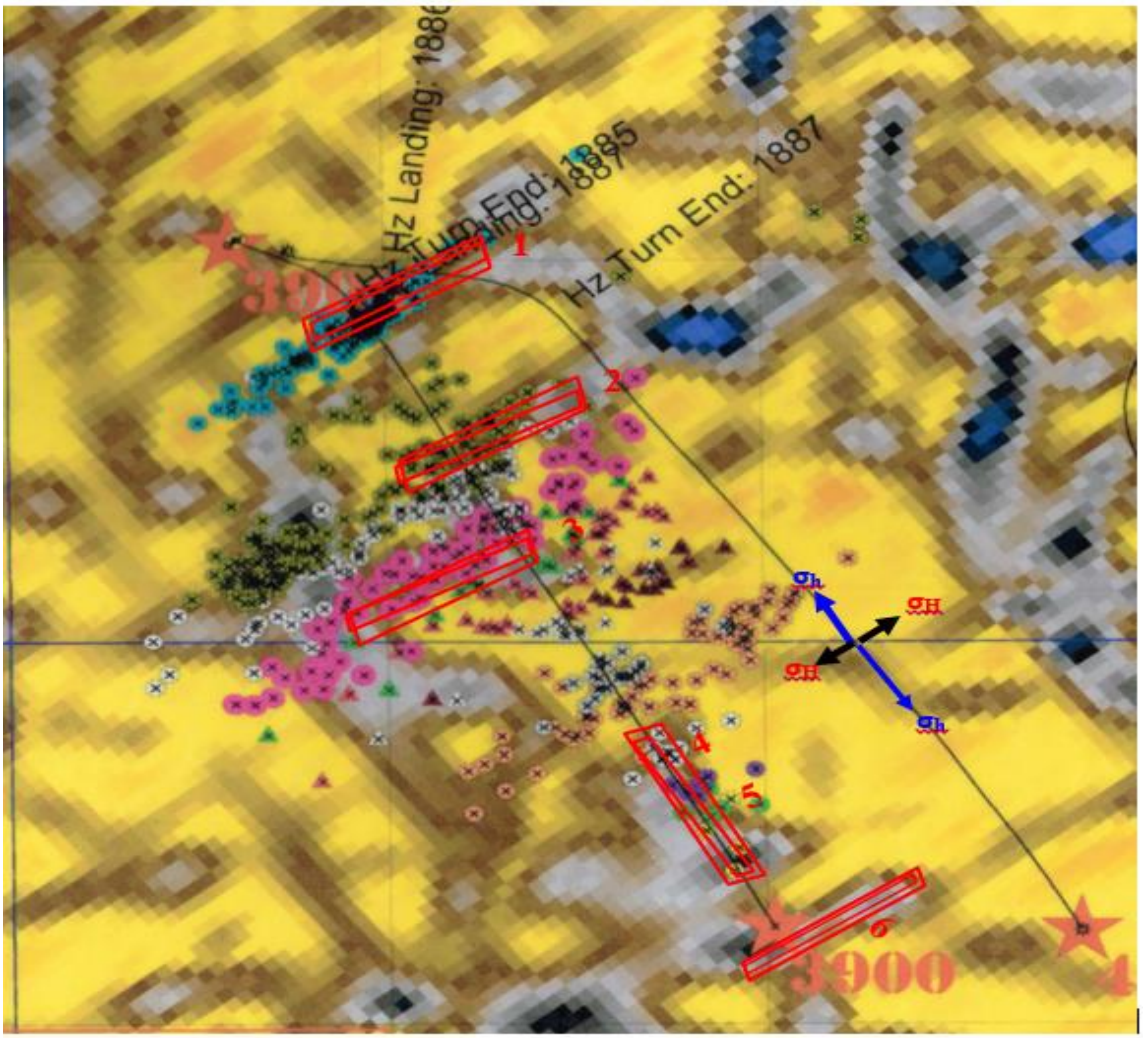

Figure 4-25: Well B curvature data map showing secondary fracture density, direction and location

4.3.6. Sensitivity Analysis, History Matching and Uncertainty Analysis.

Sensitivity analysis was carried out for reservoir properties (ϕ, k), fracture properties ($k_f w_f$, x_f), and fluid properties (C1, CO_2, N_2 etc.) that greatly affect the reservoir simulation models. Secondly, the objective functions (OF) was defined as the target parameters that were to be history matched, which in this study were cumulative gas, oil and water productions, and wellhead and bottom-hole pressures (i.e. well production history). The sensitivity analysis was started with twenty parameters, but after few parametric simulations to test which parameters have the greatest impact on the objective functions (OF), 10 parameters were selected for sensitivity analysis and the results were compared to target (production history) values.

Figure 4-26 shows an example of sensitivity analysis obtained from "simulated data." The result of the sensitivity analysis (SA) from the wells used in the study were considered propriety and confidential data by the company. Hence, the sensitivity analysis (SA) results would not be shown or included in this dissertation. Additionally, Figure 4-26 shows tornado chart generated from the sensitivity analysis (SA) using the "Linear Model Effect Estimates" method. The values displayed in each bar of the tornado chart are the predicted response change that would occur when the value of the parameter changes from the smallest to the highest of the data range specified. For instance, in Figure 4-26, if the fracture half-length (250, 500) is increased from 250 meters to 500 meters, the objective functions (OF), which was gas production history, increases by $2.7*10^7$ cubic meters (m^3).

Figure 4-26 also shows parameter interactions effect, which were calculated using "quadratic model"-a polynomial regression method. For instance, the non-linear quadratic

effect of porosity * porosity shows that it's relatively important to the model and its objective function.

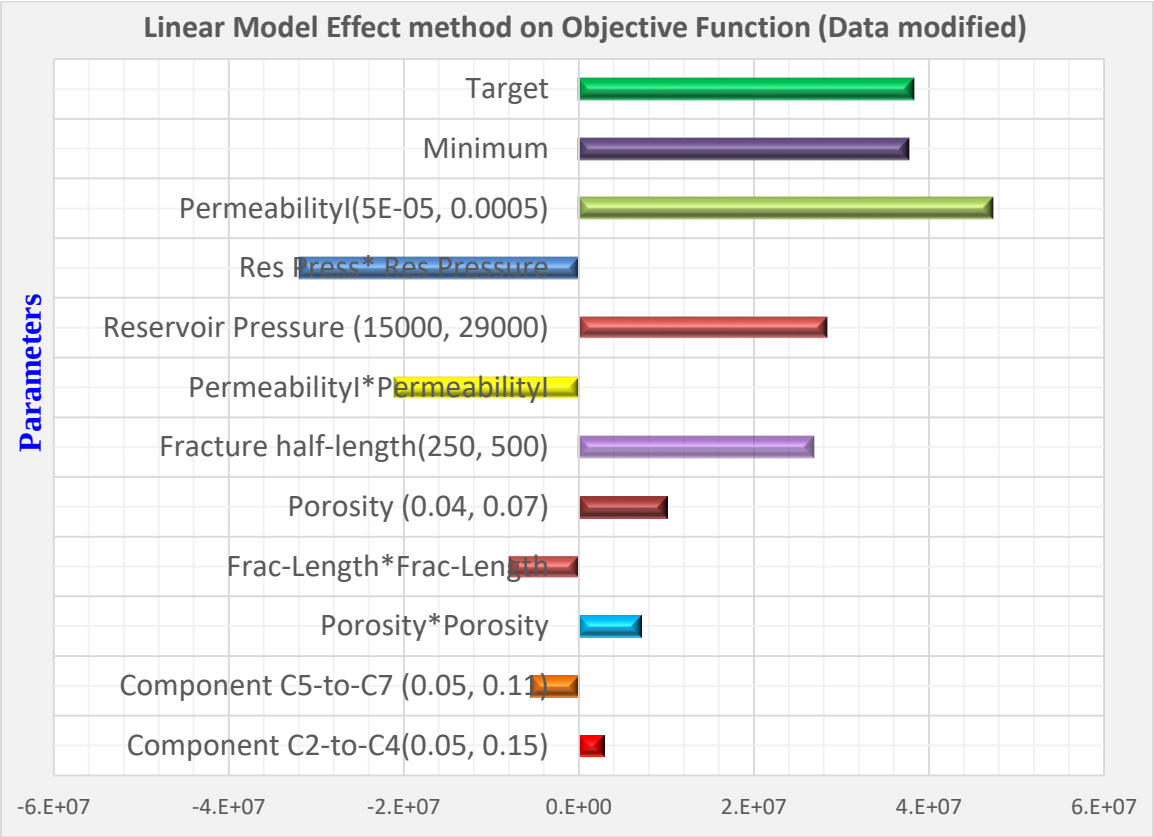

Figure 4-26: Effect of each parameter change on the objective function (simulated data and not real data from the wells in used in the study)

Polynomial regression methods such as "Linear Model Effect Estimates" and "Quadratic Model Effect Estimates" were used to minimize the residual error in the sensitivity analysis SA) and history matching (HM). When there are multiple parameters and multiple objective function (OF), to minimize error between the simulation results and measured data, it is recommended to set up normalization scale for calculating the error. In

this study, global history match error normalization method was used. The calculation method used was the "weighted average", where each objective function was assigned a weight based on its significance and effect on the production history. Equation for global history match error was (obtained from CMG's CMOST)

$$Q_{global} = \frac{1}{\sum_{i=1}^{NW} W_i}\left(\sum_{i=1}^{NW} W_i Q_i\right) \quad ...(45)$$

Where;

Q_{global} = the global objective function (such as cumulative gas production)

Q_i = objective function for well (i)

Q_i = number of wells in the study

W_i = weight of Q_i in the calculation for Q_{global}

Figure 4-27 shows sample of the sensitivity analysis (SA) and history matching results for global history match error that was calculated using the equation given above. The result of Figure 4-27 shows the global error kept on declining as the number of experimental runs increased, eventually approaching low teens.

To reduce the global error in both the sensitivity analysis and history matching, the number of parameters were reduced, removing variables that had below 95% significance level. For example, the history match error for the wellhead pressures was less 7% for well A as shown by Figure 6-24. Additionally, more experimental runs probably would have provided better "optimal solution", but that would have require more computing power and time.

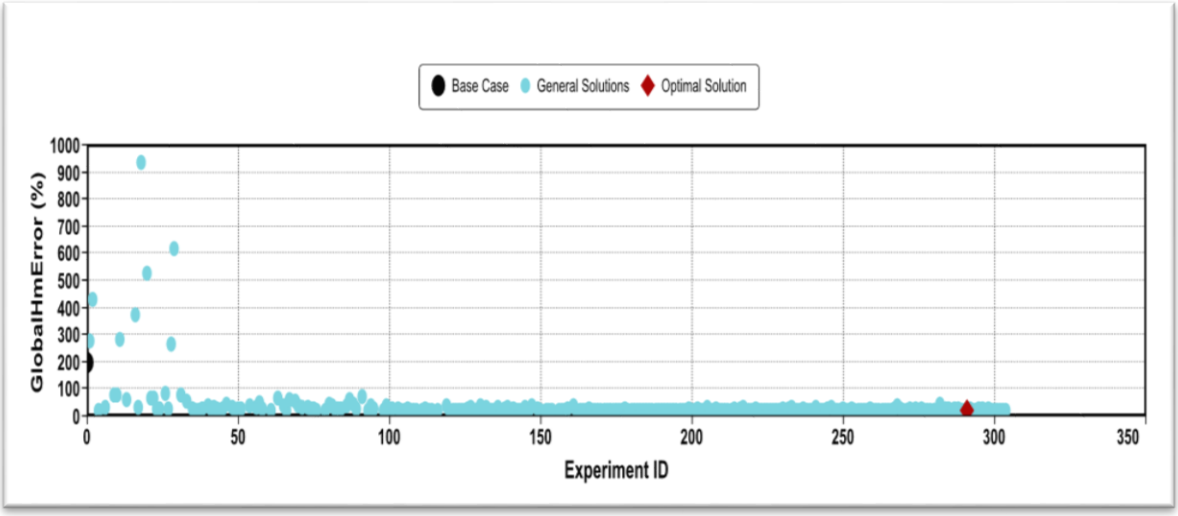

Figure 4-27: History matching and sensitivity analysis models convergence and global error

4.4. RATE TRANSIENT ANALYSIS (RTA) DERIVED K_{SRV} & X_F VERSUS RESERVOIR SIMULATION MODELING

The fifth and final task was to compare the results from the stimulated reservoir volume (SVR) to the rate-transient analysis (RT) derived permeability (K_{SRV}), which is usually called average permeability of stimulated well. Decline curve analysis (DC) and rate transient analysis (RTA) have been historically used for well performance analysis. Fetkovich formulated type-curves that cover the whole production life of the well. He combined transient analysis with boundary dominated flow by solving the transient flow analytically (with the assumption of constant pressure), and then combined them to empirically derived decline curves from Arps.

Ye et al. (2013) presented a paper titled “Beyond Linear Analysis in an Unconventional Oil Reservoir” where the author stated that RTA can be used to evaluate completion and reservoir qualities. Though RTA can be used to determine fracture half-length (x_f) and stimulated reservoir permeability (K_{SRV}), the problem is the non-uniqueness

of the solutions. For a given fracture half-length (xf) and t_{EL} (time to the end of linear flow), many solutions are possible for (K_{SRV}). The plot of $\left({P_i - P_{wf}}/{q}\right)\ vs\ \sqrt{t_{sup}}$, which is the pressure difference divided by production rate versus super-position time gives a straight line slope. Here are the equations used for the RTA analysis (Chu et al. 2015) ;

$$x_f = \left(\frac{4.972 B_o \sqrt{t_{EL}}}{m_{CRL} h \emptyset c_t}\right) \quad ...(46)$$

$$K_{SRV} = (79.01 Y_E^2)\left(\frac{\emptyset \mu c_t}{t_{El}}\right) \quad ...(47)$$

Where

x_f = average fracture half-length, and t_{EL} = time to end of linear flow

$h, \emptyset, c_t$ = fracture height, porosity and total compressibility.

K_{SRV} = average permeability of stimulated reservoir

m_{CRL} = slope of constant rate line (straight)

Y_E = fracture half-length of the isolated SRV associated with each stage

Figure 4-28 shows schematics of linear flow analysis and the plot used to determine the time-to-the end of linear flow (t_{el}). The RTA provided the average fracture half-length and permeability of the stimulated reservoir volume. The dashed red lines indicate the trajectory of boundary dominated curve (BDC) that would be observed if the well has reached of the end-of linear flow period. If the production data fits on the PDC line, then the RTA analysis can be used to estimate the stimulated reservoir area, fracture half-length and average permeability of the stimulated reservoir.

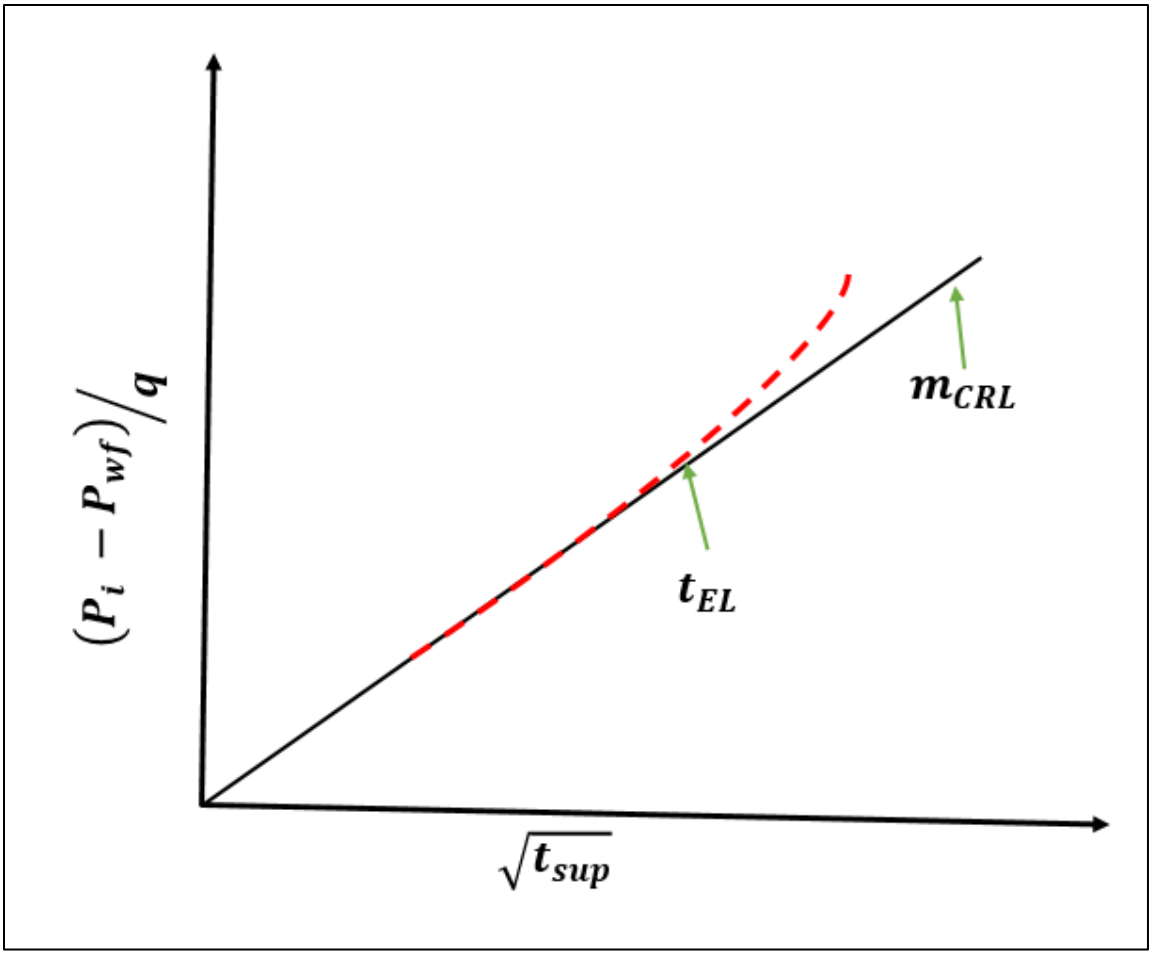

Figure 4-28: Linear flow analysis diagram showing t_{EL} and M_{CRL} modified from (Chu et al. 2015)

The production data may not fit the straight line (m_{CRL}) if it has noise or there are some outliers caused by either cyclical shut-ins or bad measurements. In such cases, the "best practice" is to clean the data before doing any RTA analysis.

5. RESULTS FROM MULTIPHASE PERFORMANCE OF TRANSVERSE VERSUS LONGITUDINAL HORIZONTAL WELLS

The results from each section and task of the research are given below. First, for the multiphase flow performance comparison of transversely fractured horizontal wells versus longitudinally fractured horizontal wells, all the fractures were assumed to be bi-wing planar fractures, and the reservoir had no natural fractures. The reservoir simulation models built for the study had 56 cases of transversely fractured horizontal wells, and 16 cases of longitudinal fractured horizontal wells for each of the three reservoir fluid types studied. In total, there were 168 transverse cases and 48 longitudinal cases just for the base case study of multiphase flow. Additionally, 56 more cases were run to investigate effects of gas adsorption and stress dependent permeability. Hence, this study required a lot of computing power and manpower resources to successfully complete it.

5.1. RESULTS FROM MULITPHASE FLOW -DRY GAS RESERVOIR

The result from the dry gas reservoir modeling was a 2-phase (gas-water) simulation. Figure 5-1 shows comparison of the estimated ultimate recovery (EUR) from the dry gas reservoir simulation for transversely fractured horizontal wells versus longitudinal fractured horizontal wells. Additionally, Figure 5-1 also shows the result of a horizontal well with 42 transverse fractures (42T-SP) that was modeled in previous studies with a single phase numeral simulator by (Yang et al. 2014).

Analysis of the result from the dry gas reservoir shown in Figure 5-1 illustrate three interesting findings; first, comparison of the gas recovery from the single phase simulator (42T-SP) versus the result of 40T (a horizontal well with 40 transverse fractures) from this study were exactly the same, as shown in the graph. Secondly, at permeabilities higher than

1.0 mD, all the transverse horizontal wells (with fractures from 4 to 40), and longitudinally fractured horizontal wells had similar well performance. The number of fracture stages, and well orientation or azimuth didn't make a difference in terms of well productivity or recovery. Thirdly, at lower permeability, longitudinally fractured horizontal wells performed worst among all the horizontal wells studied. This means longitudinally fractured wells are not suitable for low and ultra-low permeability unconventional resources.

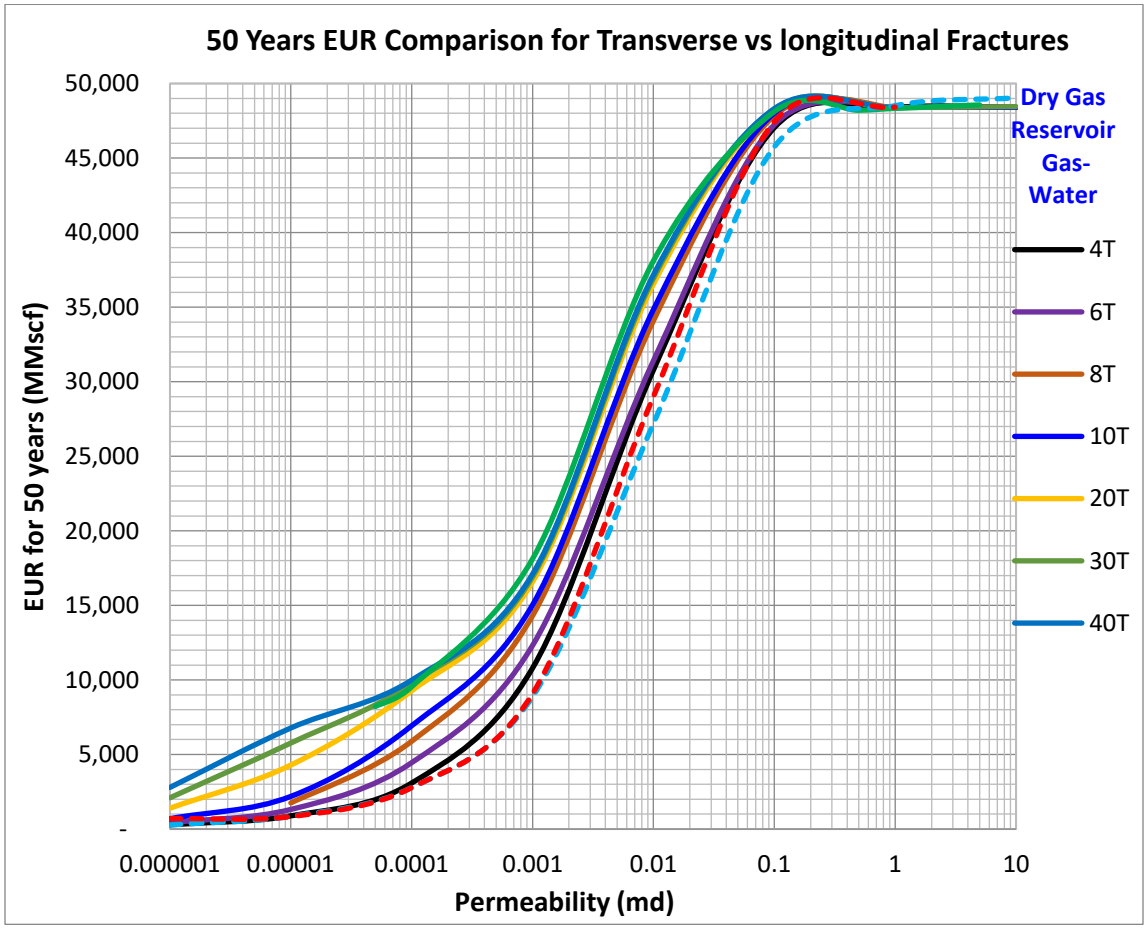

Figure 5-1: Dry Gas Reservoir recovery plot result obtained from the 2-phase (gas-Water) reservoir simulation

Figure 5-2 shows the cumulative gas recovery from transversely fractured and longitudinally fractured horizontal wells in reservoir with permeability of 0.0001 mD. The wells were seven cases of horizontal wells with transverse fractures from 4 (or 4T in the graph) to 40 fractures, and two cases of wells with longitudinal fractures (2L and 4L). The result shows that there was clear separation of the plots in Figure 5-2 which highlights the importance of having more transverse fractures in low permeability gas reservoirs.

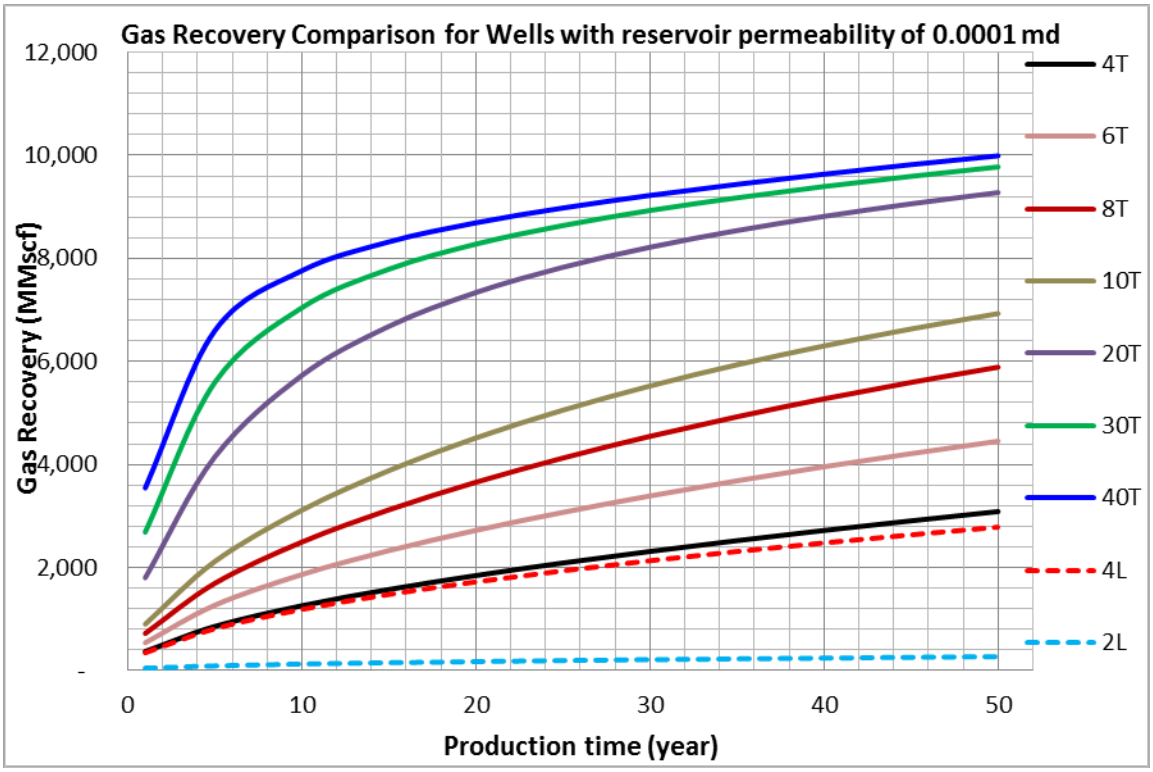

Figure 5-2: Gas recovery comparison for wells with 0.0001 md, but different number of transverse (10T, 30T) and longitudinal (2L & 4L) fractures

Figure 5-2 also shows that there was very sharp increase in cumulative production during the earlier years (10 years or less) for transversely fractured horizontal wells with

30 and 40 fractures, accelerating recovery. Hence, most of the gas recovery happened within the first 10 years. In fact, the 40T (40 transverse fractured) well produced 78% of its cumulative recovery within the first 10 years of production, while the 30T well produced 72%.

Figure 5-3 shows cumulative gas production from transversely and longitudinally fractured horizontals wells with reservoir permeability of 0.1 mD, and different number of fractures. The result shows that for gas reservoirs with permeability of 0.1 mD, when the number of fractures increase, especially for transversely fracture horizontal wells, a point of diminishing return was reached. For instance, the 50 year cumulative gas production was the same for a well with 10T (10 transverse fractures) and one with 40T (40 transverse fractures).

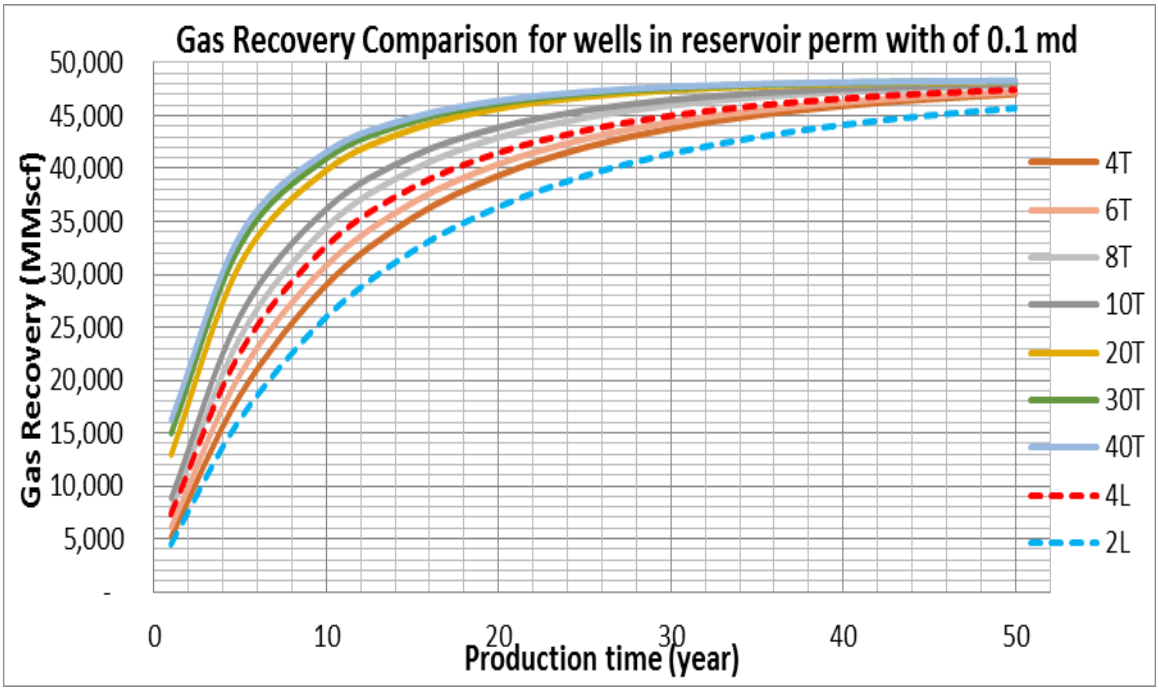

Figure 5-3: Gas recovery comparison for wells with 0.1 md, but different number of Transverse (4T, 10T) and longitudinal (2L & 4L) fractures

5.1.1. Critical Permeability: Longitudinal vs Transverse Fractures in Gas Reservoirs.

Previous studies that investigated the critical permeability at which longitudinal fractures outperform transverse fractures were limited either because of the use of single phase numerical models or the range of reservoir permeability covered. Therefore, this is the first time that a multiphase flow reservoir simulator was used to determine the critical permeability at which longitudinally fractured wells outperforms transversely fractured horizontal wells. Figure 5-4 shows the critical permeability at which longitudinally fractured horizontal wells outperform transversely fractured horizontal wells in dry gas reservoirs.

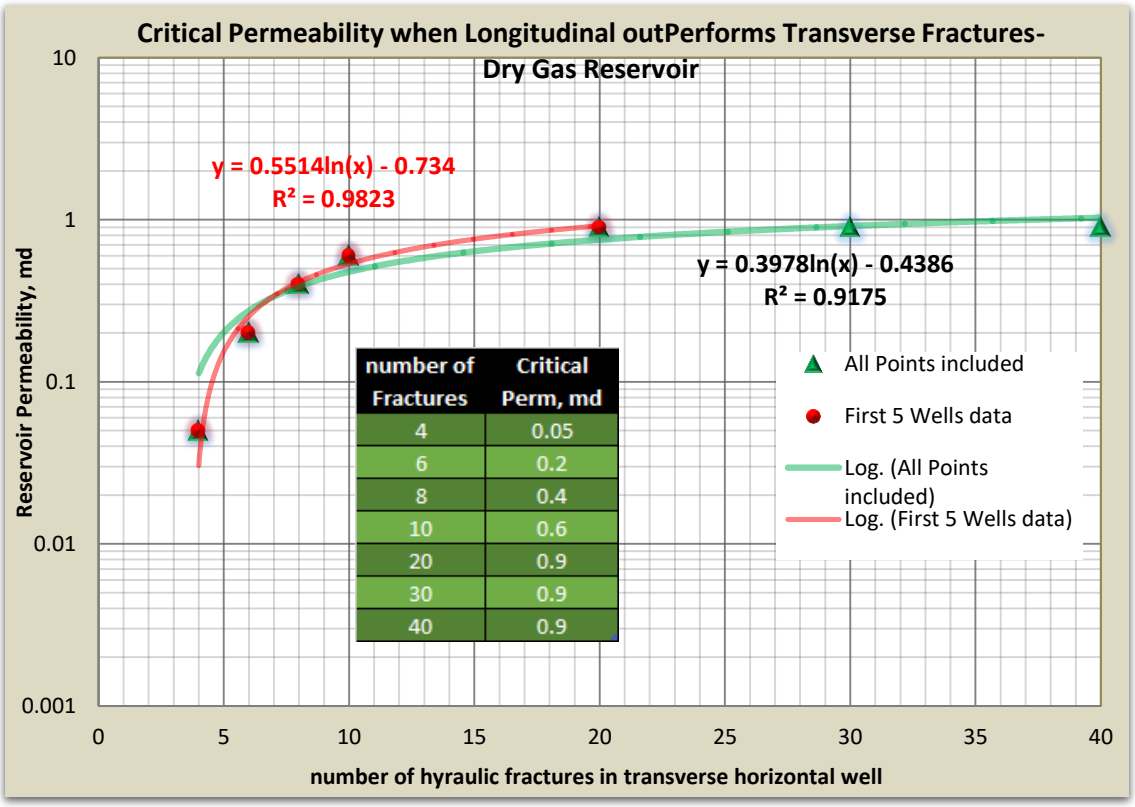

Figure 5-4: Critical permeability when longitudinally fractured outperforms transversely fractured horizontal well in gas reservoirs

5.1.2. Effect of Adsorption Gas on Well Productivity and Reserves. Gas-adsorption on solid surfaces are classified based on the type of isotherm. Brunauer et al (Brunauer et al. 1938) presented research that identified five different types of isotherms, i.e. type 1 to type 5. Langmuir isotherm type 1 shown by equation 23, which is a function of Langmuir volume (V_L) and Langmuir pressure (P_L), and is generally considered good fit for modeling methane gas adsorption and desorption in porous media. Coalbed Methane (CBM), which has free gas and adsorbed gas just like shale gas, was modeled using Langmuir isotherm by (Bumb and McKee 1988) in a study which demonstrated that the process of gas desorption in Coalbed Methane (CBM) and Devonian shale obeys Langmuir isotherm, especially type 1.

Therefore, in this study, Langmuir isotherm was used to study the effect of gas adsorption/desorption on well productivity, reserves and well economics by comparing gas recovery results of reservoir simulation models with Langmuir isotherm versus those without it.

Figure 5-5 compares the result of two simulation cases; one with adsorption and one without adsorption for a transverse horizontal well with 10 fractures. The analysis was done in terms of discounted recovery (at an annual interest rate of 10% and calculated using *equations* 12 & 13) and cumulative gas production. The result shows that there was 19% difference in EUR between the two cases, which can make a big difference in well economics and reserve bookings. Additionally, the result also shows that the differences between the two plots was getting bigger with time, which means that contribution from adsorption gas mostly occurs in the later years of well production when the reservoir pressure has been depleted. However, when discounted recovery method was used to

compare the results of the simulation case with gas adsorption to that of without adsorption, two new finds were discovered. First, most of the economically viable contributions from adsorbed gas occurred in earlier years of production, from year 2 to year 25, maximizing early well production.

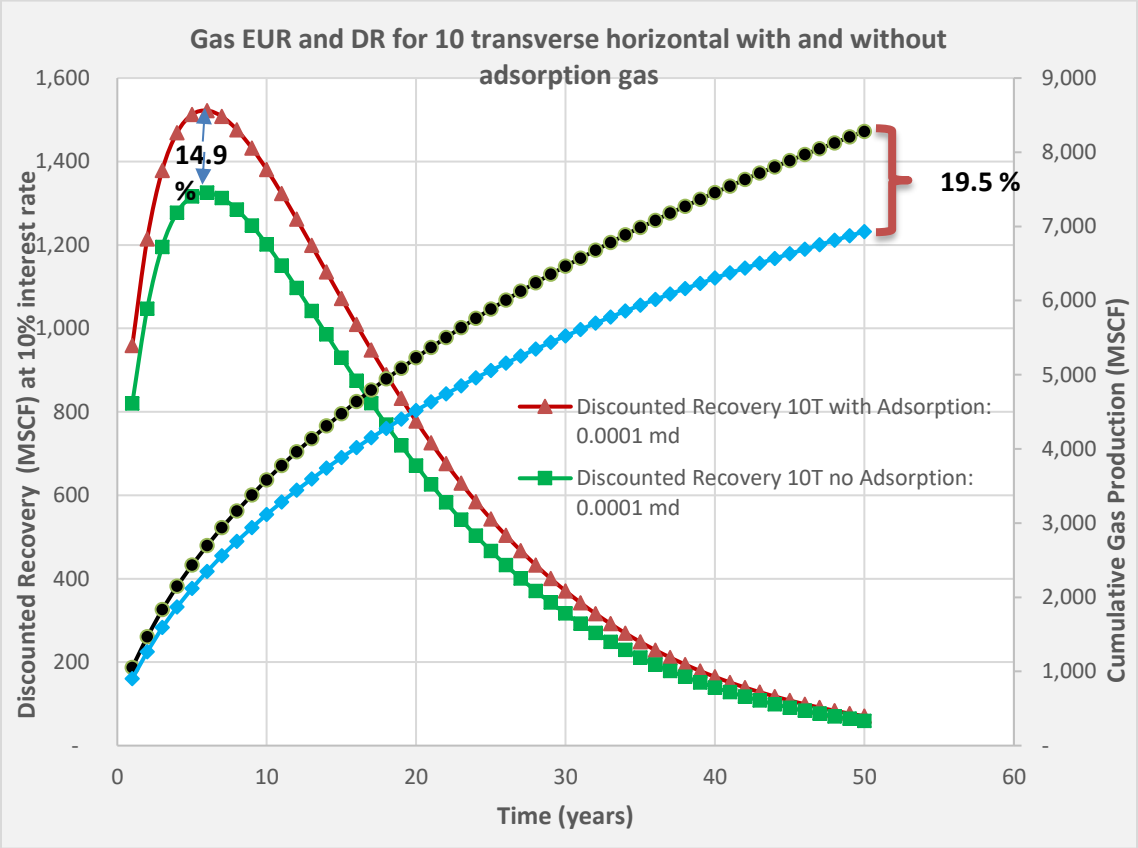

Figure 5-5: Discounted recover and Cumulative gas production with and without adsorption for a transverse horizontal well with 10 fractures in a reservoir permeability of 0.0001 md

Though higher percentage of adsorbed gas contribution occurred in the later years of well production, the economic benefit of the adsorbed gas was diminished by “time

value of money." Secondly, when economic analysis was applied to the results of the two simulation cases, the difference between the case with adsorption and the case without adsorption gas was found to be 14.9%, which is less than the 19.5% obtained from the gas EUR method. Thirdly, the difference between the two simulation cases peaked at year 6, and gradually declined until the end of well production life. These findings suggest that contribution from adsorption gas start earlier than thought in well's production life, and reach peak contribution in the middle years, but decline gradually in the later years. Hence, the benefits of adsorbed gas and its impact on well performance whether in terms of gas EUR (19.5%) or discounted recovery (DR) (14.9%) are significant

Figure 5-6 shows three cases that compares the cumulative gas production of transversely fractured horizontal wells with and without adsorption. The graph compares the result of transverse horizontal wells with 4 fracture, 10 fractures, and 20 fractures. The result highlights three important findings; first, adsorption/desorption requires pressure drawdown and contribution from adsorbed gas would only occur when pressure depletion reaches the Langmuir pressure (P_L).

Secondly, at higher reservoir permeability, adsorbed gas contribution to the well cumulative production was massive and behaved more like Coalbed Methane (CBM) where the major flow regime is gas diffusion. Thirdly, the result also shows the effect of the number of fractures on the contribution of adsorbed gas, especially in mid-range permeabilities (from 0.005 md to 0.9 md). Additionally, other factors like reservoir rock density, and Langmuir parameters (Langmuir pressure (P_L) and Langmuir volume (V_L)) effected contributions from adsorbed gas.

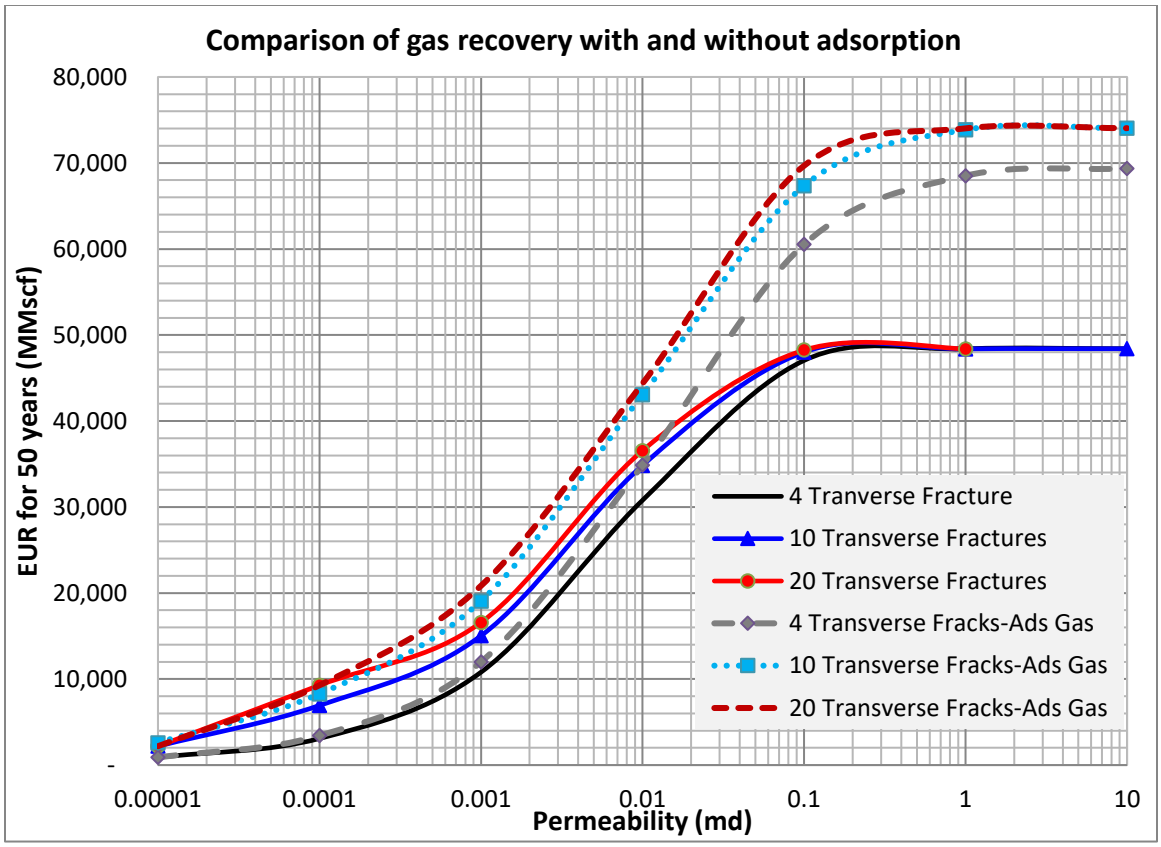

Figure 5-6: Comparison of gas recovery with and without adsorption for transversely fractured horizontal wells

5.2. RESULTS FROM MULITPHASE FLOW-BLACK OIL MODEL

The reservoir fluid used in the black oil model was Permian Basin oil. Table 5-1 shows some of the PVT properties of the Permian basin oil that was used in the multiphase flow simulation study. There were two reasons why a black oil reservoir simulation model was selected and why Permian basin oil was appropriate to use in the study of multiphase flow. First, as Table 5-1 shows, the Permian basin oil's saturation pressure was 2,000 psi while initial reservoir pressure used in the study was 4,000 psi. Hence, at reservoir conditions, there was no-free gas, and only two fluid phases exited; oil and water, which black oil reservoir simulator can fairly model without significant errors. Secondly, test

models were run to compare the results of a black oil model versus a compositional model using the Permian basin oil, and the result showed that there was very little difference in recovery (of oil and gas). Thus, it did not warrant the time and the computing power needed to run compositional simulator.

Table 5-1: Permian Basin oil used in the Multiphase flow modeling

Permian Basin Oil for Black oil Modeling		
Reservoir Temp	**215**	**F**
Bubble Pressure	2000	psi
Solution GOR	576	SCF/STB
API Gravity	38	
Depth	8300	ft.
Initial Pressure	4000	psi
Initial S_w	0.25	

Figure 5-7 shows cumulative production from the black oil reservoir simulator. The result compares oil recovery for transversely fractured horizontal wells versus longitudinally fractured horizontal wells across permeability ranges of 10 Nano-Darcy to 10 mili-Darcy [0.00001 mD-to -10.0 mD]. There were seven transversely fractured horizontal well cases (4, 6, 8,10,20,30 and 40) and two longitudinally fractured horizontal well cases (with 2 and 4 fractures). The results show that at low reservoir permeabilities, longitudinally fractured horizontal wells performed poorer among all cases studied. In fact, a transverse horizontal well with only four fractures in a 4,000 feet lateral length performed better than a longitudinal horizontal well with 4 fractures. However, at higher reservoir permeabilities, longitudinal fractures outperformed transverse fractures. The results in

Figure 5-7 shows that longitudinally fractured horizontal well with only 2 fractures had higher cumulative oil production than a transversely fractured horizontal well with 40 fractures at reservoir permeability of 2.0 md. This is a very important finding because stimulation cost is one of the biggest expenses, and more fracture stages can result greater expenses. Therefore, at higher permeabilities, the optimum well completion method is to drill longitudinally fractured horizontal wells.

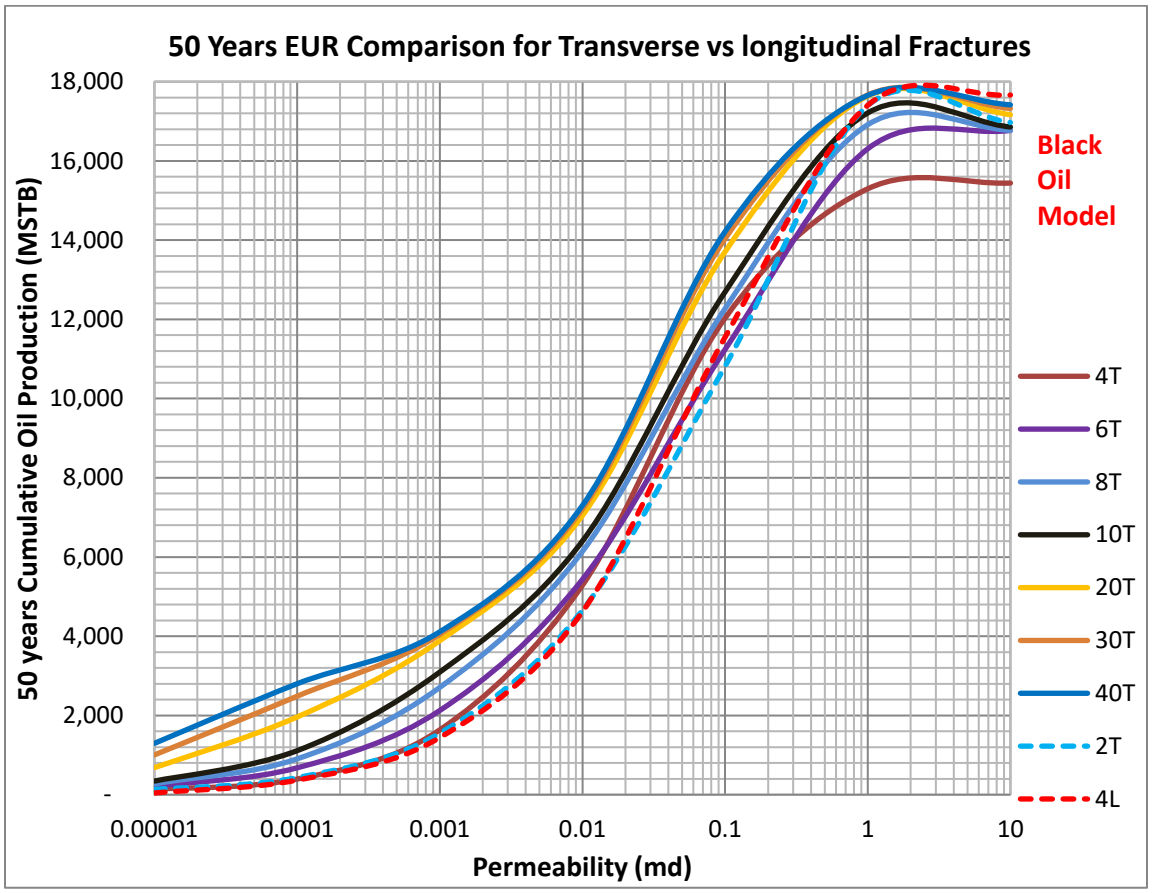

Figure 5-7: Oil EUR for Transversely fractured vs longitudinally fracture horizontal wells

The result in Figure 5-8 below compares oil recovery for transversely fractured versus longitudinally fractured horizontal wells at reservoir permeability of 0.0001 md. There were seven cases of transverse wells with fractures from (4, 6, 8, 10, 20, 30, & 40) and two cases of longitudinal (2L & 4L). The result shows that in low permeability reservoirs, the number of fractures and horizontal well orientation are critical to well performance. The two lowest performing wells were horizontal wells that were longitudinally fractured, which means at reservoir permeability of 0.0001 md, longitudinal wells are not good option.

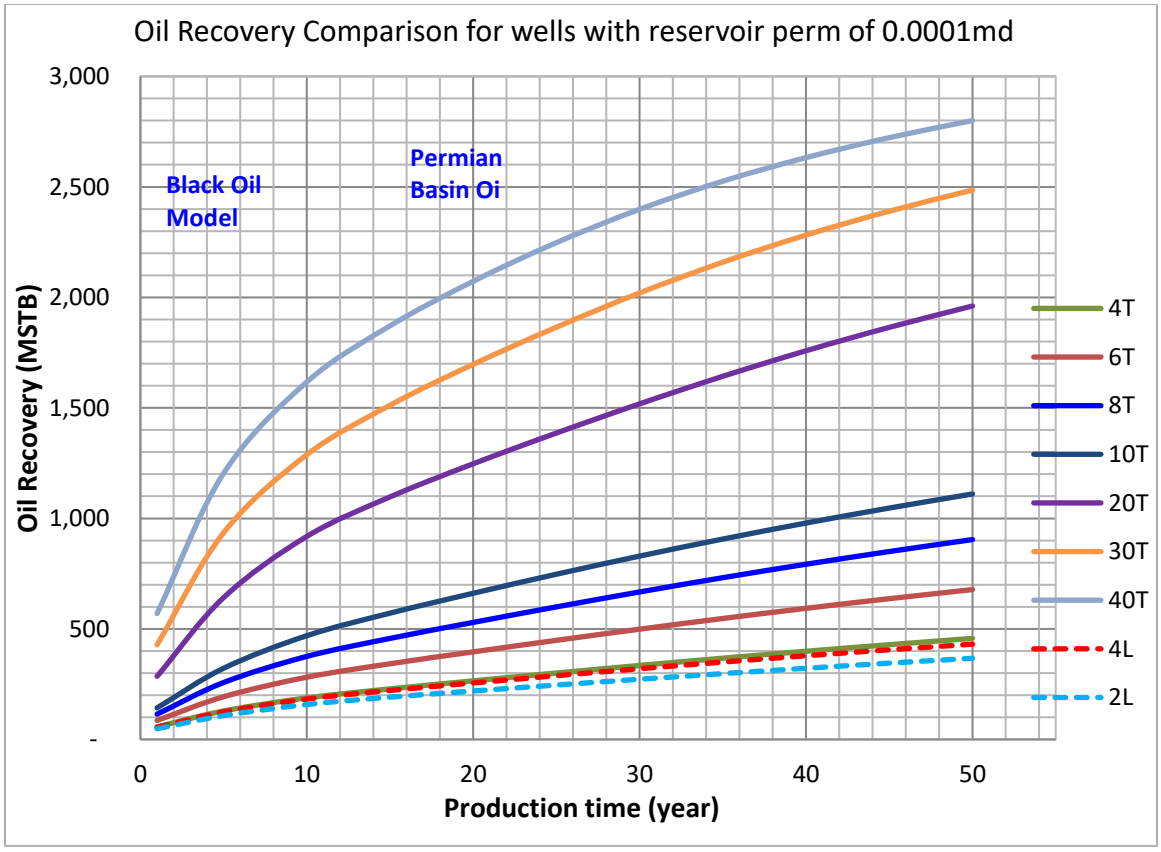

Figure 5-8: Oil recovery comparison at reservoir permeability of 0.0001 md for transverse wells vs longitudinal wells

5.2.1. Oil EUR as Function of Fracture Spacing and Reservoir Permeability for Permian Basin Oil.

Figure 5-9 shows 3D plot of oil recovery as function of two critically important parameters to any hydraulically stimulated horizontal wells; reservoir permeability and hydraulic fracture/stage spacing. The result shows that at low permeability (0.00001 md to 0.01md), reducing fracture stage spacing in transversely fractured horizontal wells would greatly improve oil recovery.

Secondly, at higher reservoir permeabilities (greater than 1.0 md), the benefit of placing more hydraulic fractures in horizontal wells greatly diminishes and there was very little difference between 700 ft fracture stage spacing and 100 ft fracture stage spacing in terms of oil well recovery. Thirdly, the result of Figure 5-9 can be used as guide for hydraulic fracture planning and designing. Additionally, Figure 5-9 can be used for determining the number of fracture stages required in a transverse horizontal well at different ranges of reservoir permeability. However, partial geo-mechanics effects was included in the study through the use of stress dependent permeability, and rock, fluid and thermal compressibility. Hence, the result might not be applicable to highly sensitive reservoirs with geomechanical conditions such as compaction and subsidence.

Thirdly, the finding of Figure 5-9 highlight why oil and gas companies are putting more hydraulic fracture stages or are increasing the number of clusters per stage in horizontal wells, especially in low or ultra-low permeability shale reservoirs. For instance, when the fracture spacing distance was reduced from 1000 feet to 100 feet, the cumulative gas production increased by 10 fold from 287 MMSCF (million cubic feet) to 2,888 MMSCF.

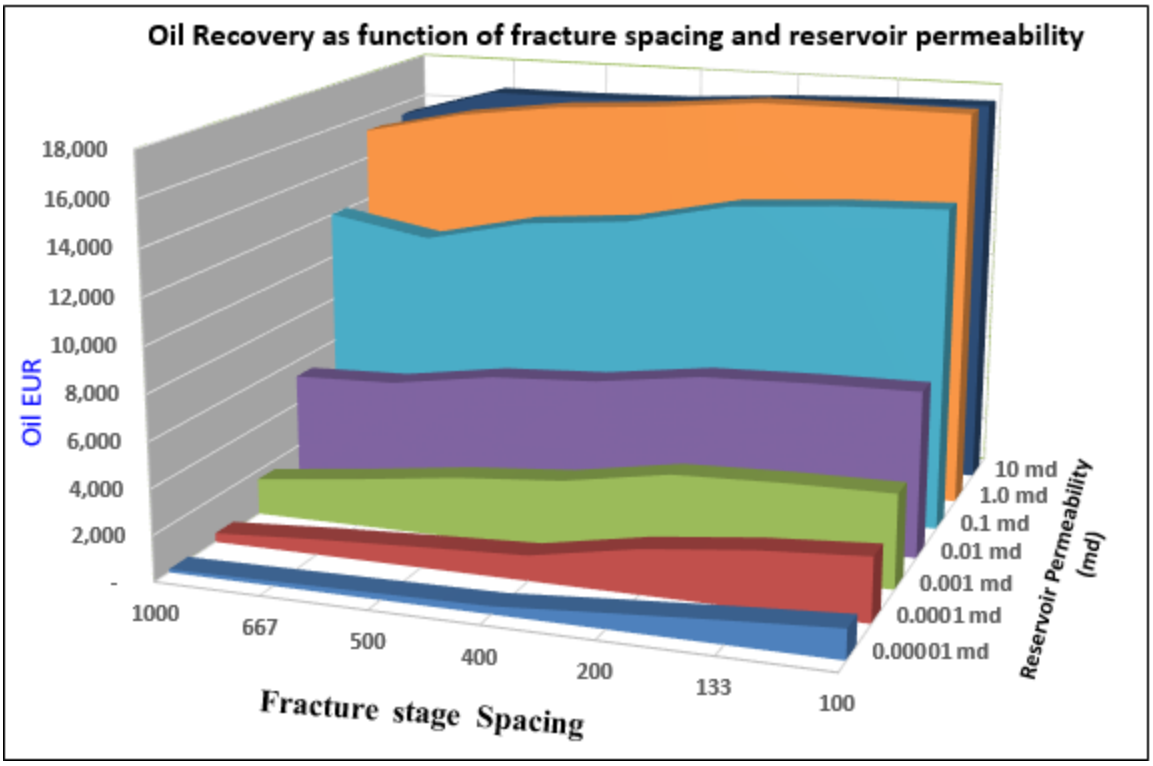

Figure 5-9: Oil EUR as function of fracture spacing (ft.) and reservoir permeability (md)

5.2.2. Critical Permeability of Transverse Versus Longitudinal Fractures in Black Oil Reservoirs.

Critical permeability in multiphase flow has not been well researched, and often people would state a range of permeabilities such as above 10.0 md or 20.0 md for longitudinal fractures, though no one has definitively investigated what the critical permeability cut-off is, especially for oil reservoirs in multiphase environment. Figure 5-10 shows the critical permeability at which longitudinally fractured horizontal wells outperforms transversely fractured horizontal wells. Similarly, the plot also shows two regression lines that were fitted on the data. The first regression line used 5 data points (4, 6, 8, 10 & 20 fractures) and had R-squared of 99%, but drops to 93% when all the data points were included in regression analysis. The critical permeability was 2.0 mD for the 20, 30 and 40 fractures as shown by Figure 5-10.

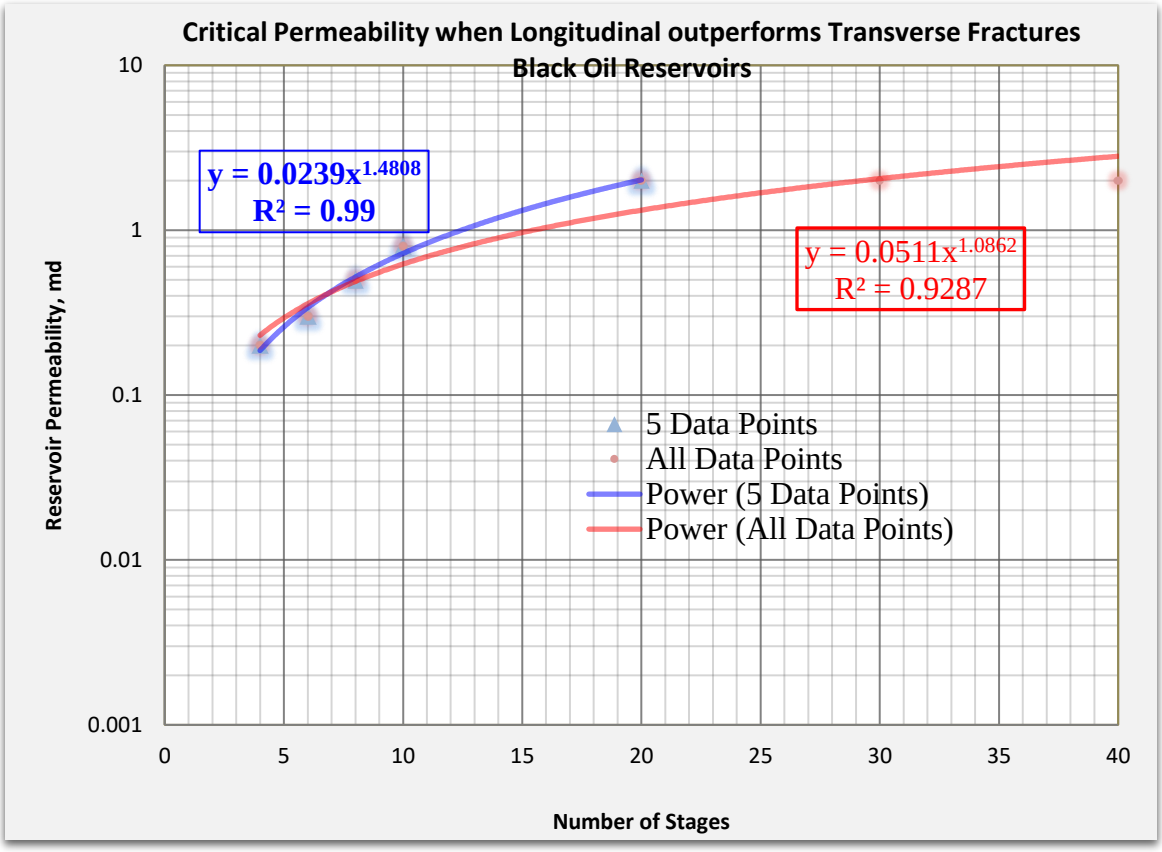

Figure 5-10: Critical permeability at which longitudinal fractures outperform transverse fractures obtained using Black oil model reservoir simulation using Permian basin oil and fluid properties.

The critical permeability was determined to be 2.0 md for black oil type reservoirs that have reservoir fluid properties similar to that of the Permian basin oil. Results in Figure 5-10 shows that after 2.0 mD, the critical permeability at which longitudinally fractured horizontal well outperforms transversely fractured horizontal well, is independent of the number of fractures. Hence, any reservoir with permeability of 2.0 mD or better should be considered only for longitudinal fractured horizontal wells.

5.3. RESULTS FROM MULITPHASE FLOW-COMPOSITIONAL MODEL

The compositional reservoir simulation models had reservoir fluid properties from Eagle-Ford oil that were given by Figure 3-5, Figure 3-6, and Table 5-2. The reservoir models had representative geological model of Eagle-Ford formation. The study used compositional reservoir simulator because the reservoir was saturated (below bubble point pressure, P_b), and all the 3-phases (oil, gas and water) existed at in-situ reservoir conditions as shown by Table 5-2. In the study, the reservoir pressure was 4,000 psi at a reference depth of 8,000 ft. Secondly, the study investigated the effect of reservoir oil composition on the performance of transversely fractured versus longitudinally fractured horizontal wells in tight sands and unconventional reservoirs with stress dependent permeability.

Table 5-2: Eagle-Ford Oil properties for composition modeling

Eagle-Ford Oil for Composition modeling		
Reservoir Temperature	**250**	**F**
Bubble Pressure	4220	psi
Solution GOR	3636	SCF/STB
API Gravity	48	
Depth	8300	ft
Initial Pressure	4000	psi
Initial Sw	0.25	
Gas SG	0.7	
OGR (Oil-Gas Ratio)	275	STB/MMscf

Figure 5-11 shows comparison of oil recovery versus reservoir permeability for transversely fractured versus longitudinal fractured horizontal wells using Eagle-Ford oil fluid properties in a compositional reservoir simulator. The results show three significant findings; first, less oil but more gas was recovered (using the Eagle-Ford oil) compared to the black oil model type reservoir, which used Permian oil fluid properties. In fact, only 3.0 MMbbls of oil were recovered in Eagle-Ford oil compositional modeling compared to the 17 MMbbls of cumulative oil in the Permian Basin oil case. Secondly, longitudinally fractured horizontal wells outperformed transversely fractured horizontal wells at moderate and high permeability ranges, and that the reservoir fluid composition affected the critical permeability. Thirdly, Figure 5-11 displayed unique recovery phenomena that was not seen in previous studies. There was a mirror-image reflection of all the curves at reservoir permeability of 0.05 md. Horizontal wells with more fractures (40, 30, 20 etc.) had better recovery at lower permeability, less than 0.05 md, but had poor recovery at permeability higher than 0.05 md.

There are two theories that might explain the result and the unique shape Figure 5-11. First, convergent non-Darcy flow in transversely fractured wells with high rate or in moderate to high permeability reservoirs can reduce well productivity. This possibly explains why the transverse horizontal well with 40 fractures had the worst recovery. Secondly, the development of segregating gas caps, especially in gas condensate reservoirs, where gas flows preferentially to oil was compounded by the presence of higher number of induced transverse hydraulic fractures (40, 30, 20 etc.). Other factors such as higher vertical permeability, and the difference in mobility ratio ($k_{rg}\mu_o/k_{ro}\mu_w$) between the two phases flowing in the porous media might explain this unique phenomenon in Figure 5-11.

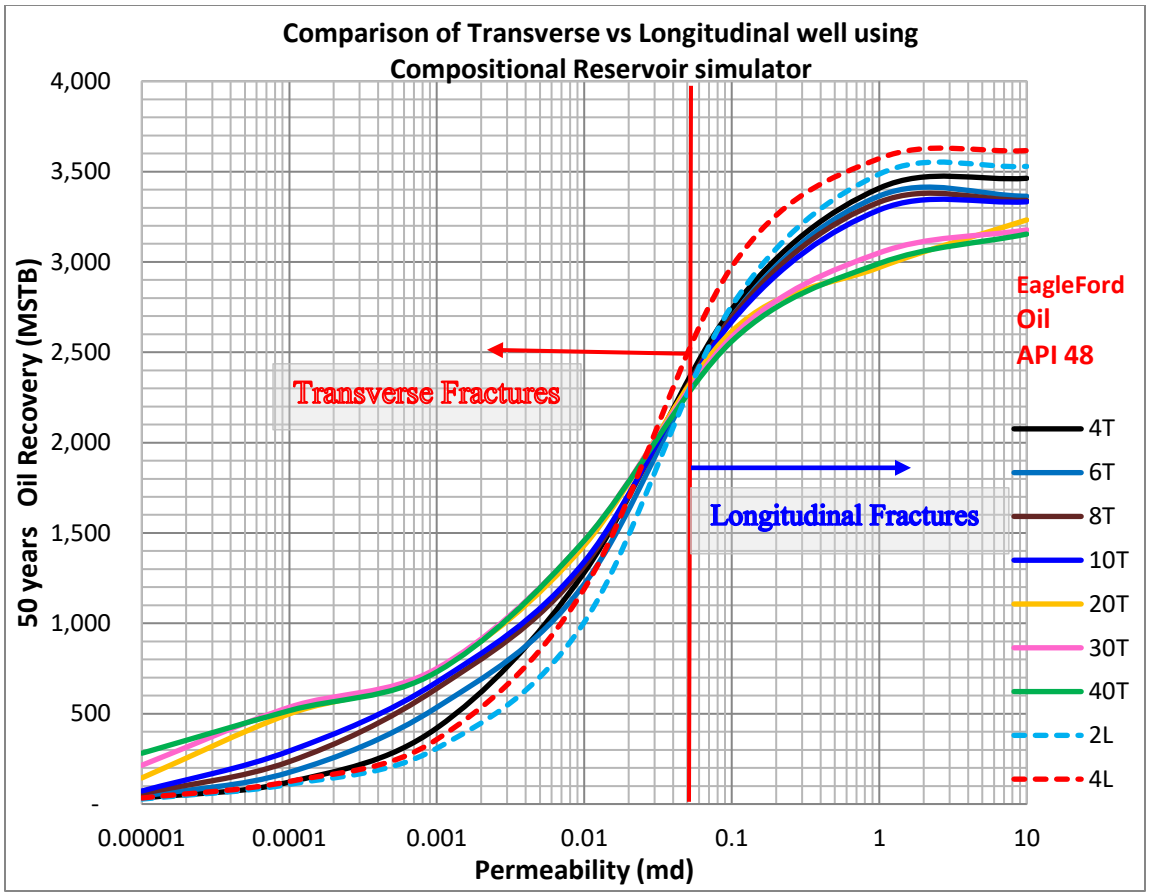

Figure 5-11: Oil recovery vs reservoir permeability of transversely fractured and longitudinally fractured horizontal wells. Notice the mirror-image reflection at reservoir permeability of 0.05 md

The economic analysis of the Eagle-Ford oil type simulation was done using cumulative oil and BOE (barrel of equivalent). Figure 5-12 shows the result of discounted recovery (DR) versus reservoir permeability for transversely fractured vs longitudinally fractured horizontal wells. The result is slightly different from that of Figure 5-11, which used only oil EUR. At permeability above 1.8 md, both longitudinally fractured horizontal wells (2L & 4L) outperformed transversely fractured horizontal wells. Additionally, there was no mirror-image inversion of curves at 0.05 md as we saw in Figure 5-11. However,

because of the price differences between oil and gas, the use of BOE might not be appropriate for using solely as an economic analysis tool.

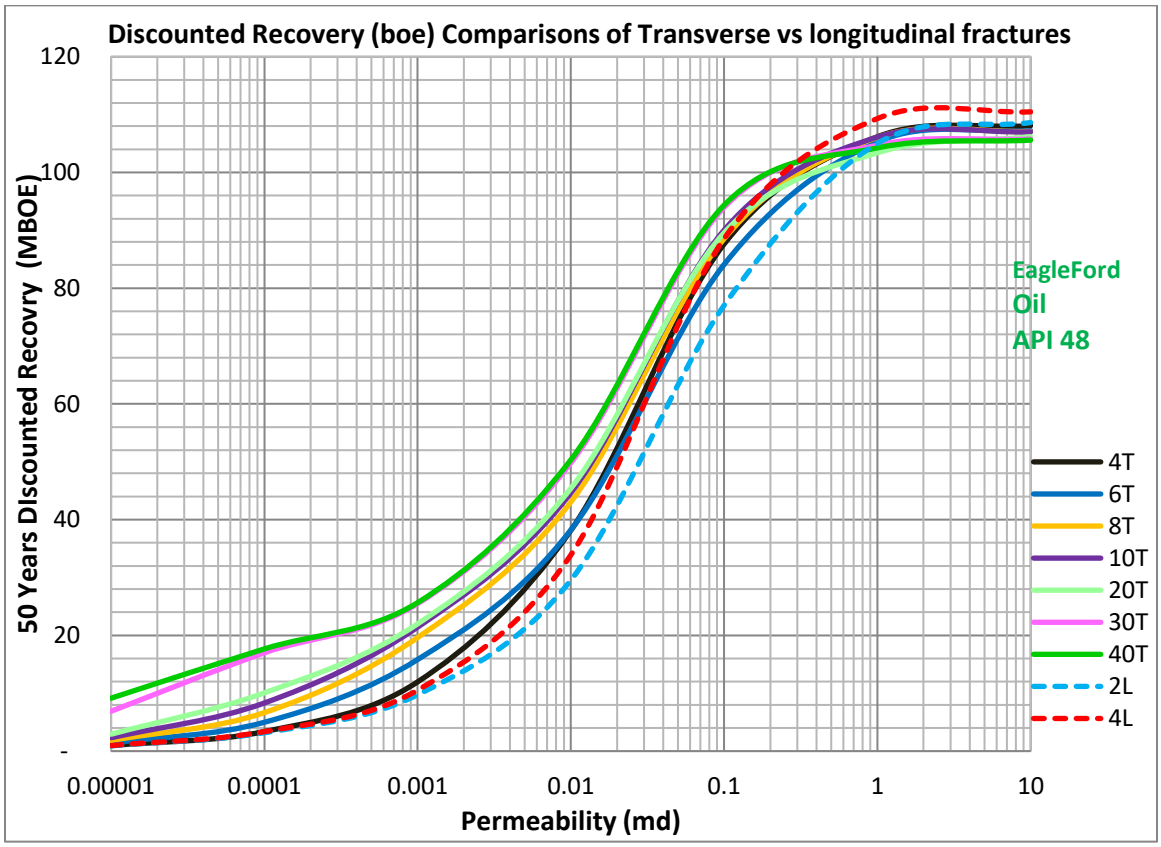

Figure 5-12: Discounted recovery (barrel of oil equivalent (boe)) versus permeability for transversely fractured and longitudinally fractured horizontal wells

5.3.1. Oil Recovery as Function of Fracture Spacing and Permeability: Eagle-Ford Oil. Figure 5-13 summarizes the finding of previous results from (Figure 5-11 and Figure 5-12) and shows that the result of cumulative oil recovery versus hydraulic fracture spacing in a range of reservoir permeabilities (from 0.00001 md to 10.0 md). Similar graphs were shown for the dry gas reservoir and black oil type reservoir models. However, the

result of Figure 5-13 shows that for reservoir permeability greater than 1.0 md, placing more hydraulic fractures in horizontal wells actually reduces oil recovery, especially in gas condensate reservoirs like the Eagle-Ford Formation.

Figure 5-13 can also be used as a guide when designing stimulations for reservoirs with light oils (volatile oil, condensate gas and wet gas reservoirs) that have similar reservoir fluid properties to that of Eagle-Ford oil. The result of the compositional simulation (using Eagle-Ford oil) showed that most of the cumulative oil was produced in the earlier years of the wells' life. However, the cumulative gas production kept on increasing throughout the wells' life.

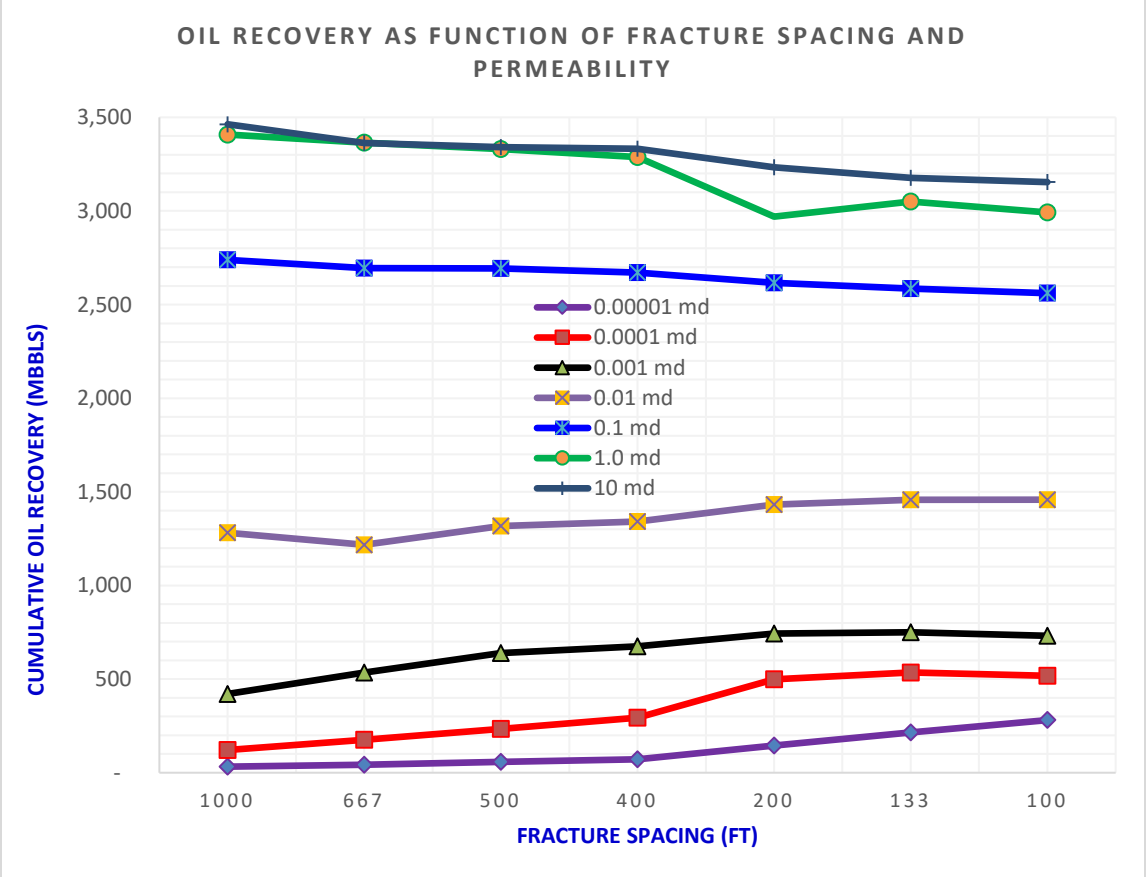

Figure 5-13: Oil recovery as function of hydraulic fracture spacing and permeability (Eagle-Ford oil)

5.3.2. Critical Permeability of Transverse Versus Longitudinal Fractures in Compositional Reservoirs.

The determination of the critical permeability when longitudinally fractured horizontal wells outperform transversely fractured horizontal wells in a condensate reservoirs similar to the Eagle-Ford Formation was done using compositional reservoir simulator, and Table 5-3 shows the results obtained. The result was determined using two methods; oil recovery (EUR) and discounted recovery (DR). The DR was calculated using equations 12 and 13, and in terms of barrel of oil equivalent (BOE). Secondly, Figure 5-14 shows the result of the critical permeability obtained from the two methods.

Table 5-3: Critical Permeability determinations from Eagle-Ford Oil

Critical Permeability in Condensate reservoir			
Oil (EUR)		DR (BOE) barrel of oil equivalent	
Number of transverse fractures	Critical Permeability (md)	Number of transverse fractures	Critical Permeability (md)
4	0.13	4	1.8
6	0.09	6	1.6
8	0.08	8	1.4
10	0.07	10	1
20	0.06	20	0.9
30	0.06	30	0.8
40	0.05	40	0.7

The results shown by Table 5-3 and Figure 5-14 indicate two unique findings. First, in condensate reservoirs, placing more hydraulic fractures in transversely fractured horizontal wells after critical permeability, is negatively correlated to both oil recovery (EUR) and discounted recovery (DR), which were 0.13 md and 1.8 md respectively.

Secondly, depending on the objective and "key performance indicators" of the operator, whether it's maximizing liquids recovery (oil) or maximizing overall production (in terms of boe), the critical permeability used in the decision criteria can differ.

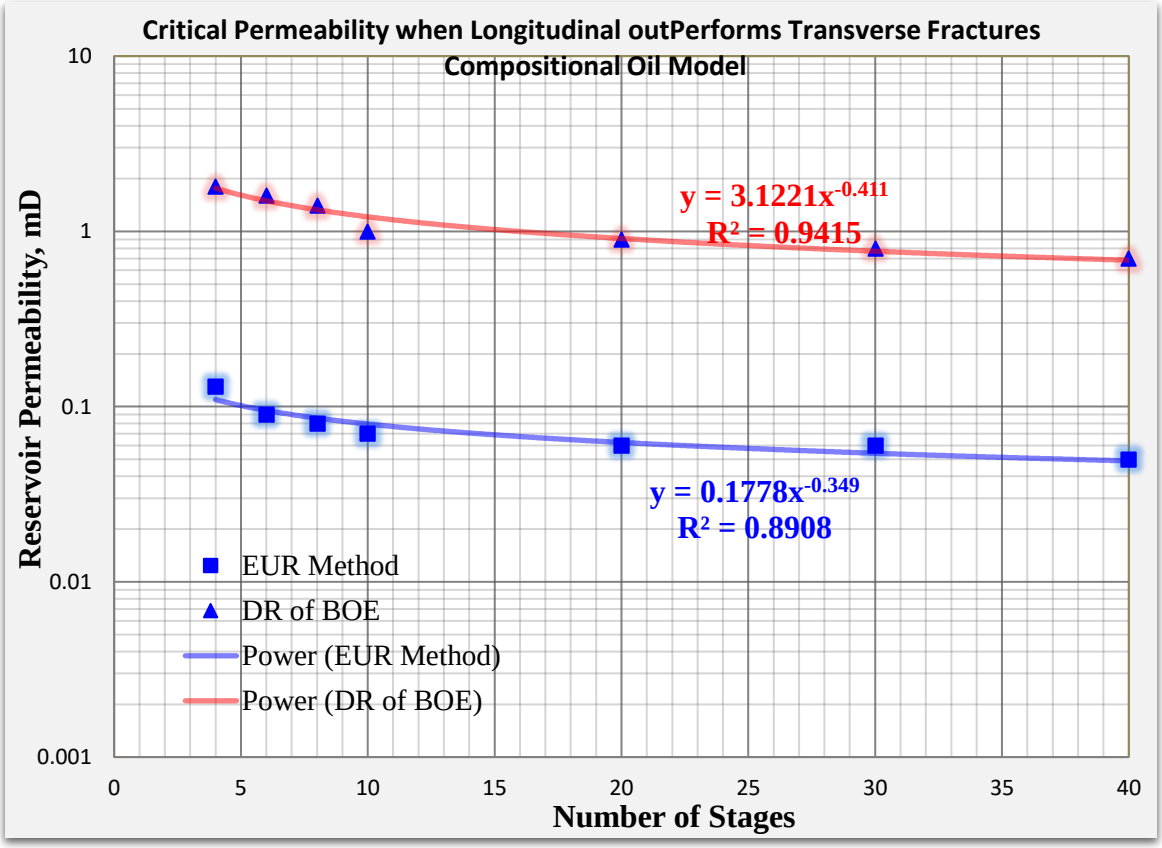

Figure 5-14: Critical permeability at which longitudinal fractures outperform transverse fractures obtained using compositional oil reservoir simulation using Eagle-Ford oil and fluid properties.

Figure 5-14 also shows that the critical permeability behaves differently for gas condensate reservoirs (Eagle-Ford oil with API of 48) than that of black oil type reservoirs (Permian basin oi with API of 38) or dry gas reservoir –all used in this study. The two

regression equations were good fit for both methods used in the analysis. However, the oil EUR and DR regression equations show power-law relationship, which means diminishing returns with increasing number of hydraulic fractures.

5.4. STRESS DEPENDEND PERMEABILITY RESULTS

The effect of stress dependent permeability on well economics, productivity and reserves were investigated for the three reservoir fluid types studied using two methods; porosity and permeability multipliers (m) shown by equation 28, and total compressibility equation shown by equation 27.

Table 5-4 and Figure 5-15 show summarizes the effect of stress dependent permeability on well performance. The table below provides the result of the stress dependent permeability effect on induced fractures for the three reservoir fluid types studied

Table 5-4: Effect of stress dependent permeability on EUR

Reservoir Type	**Number of fracture in Horizontal well and permeability range**	**Change in EUR when (SDP) Stress dependent Permeability modeling was added (equations 15 & 16)**
Dry gas Reservoir	10 Transverse fractures [0.0001 md-to 10 md]	0.0%
Black Oil (AP38) (Permian basin oil)	20 Transverse fractures [0.0001 md-to 10 md]	-1.20%
Condensate Reservoir (API48) (Eagle-Ford oil)	10 Transverse fractures [0.0001 md-to 10 md]	-0.02%

The study investigated the effects of stress dependent permeability (SDP) on induced fractures in dry gas reservoirs, black oil type reservoirs and condensate reservoirs. First, stress dependent permeability(SDP) had no effect on gas EUR in the dry gas reservoir. The SDP results from both equations (using equations 27 and 28) showed no effect on dry gas reservoirs. Previous studies showed that gas can flow in very small cracks, and (Britt and Schoeffler 2009) found that gas can flow through un-propped cracks at effective confining stress. Secondly, the fracture conductivity in this study was 50 mD-ft and the true vertical depth (TVD) of the wells modeled was 8,000 ft. Proppants such as (20/40) Ottawa sands usually retain most its conductivity in low confining stress environment. Similarly, there was no stress dependent permeability effect in the condensate reservoir, which used Eagle-Ford oil

The black oil reservoir simulations, which used Permian basin oil properties showed noticeable impact on oil recovery from stress dependent permeability (SDP) effects on induced fractures. Table 5-4 and Figure 5-15 show the results obtained. There was -1.20% decline in both oil recovery and discounted recovery (DR) when stress dependent permeability was incorporated into the models versus without SDP.

Two important findings highlighted by result of Figure 5-15 are that the effect of stress dependent permeability occurred later in the life of the wells. Secondly, reservoir fluid type (gas, condensate or black oil), rock mechanics and reservoir depth can influence the impact of stress dependent permeability on well recovery. The low viscosity reservoir fluid types such as dry gas and gas condensate were not impacted by stress dependent permeability.

The results of the stress dependent permeability given in Figure 5-15 were obtained using equation 27 for the total compressibility method (C_f), and equation 28 for the porosity and permeability multiplier (PPM) method. The difference between the two equations is given the curve tilled "diff", which show two important points. First, the results of Figure 5-15 shows that at low reservoir permeabilities, there was little stress dependent permeability effect. Secondly, at higher reservoir permeabilities, there was salient SDP effect, especially for the porosity and permeability method, which showed an effect of over 200,000 barrel of lost oil.

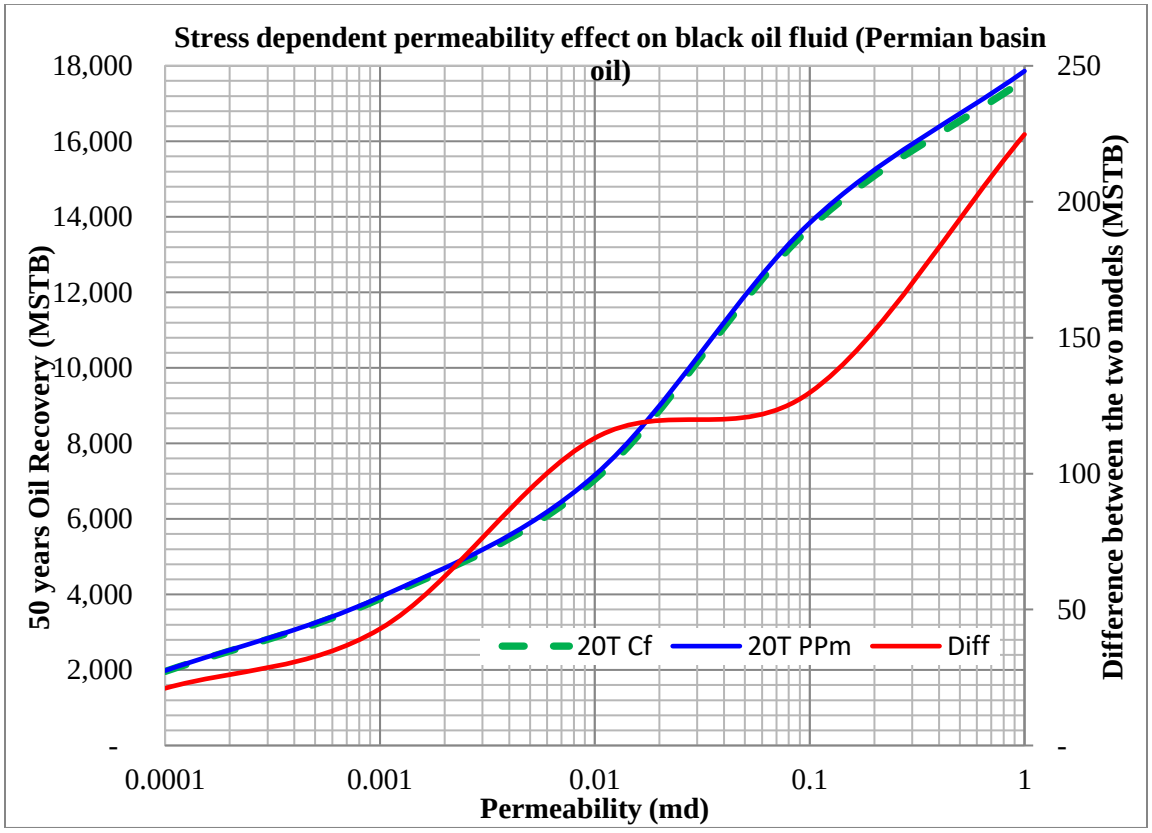

Figure 5-15: Effect of stress dependent permeability on oil recovery from the black oil model simulation using Permian basin oil fluid properties

6. RESULTS AND ANALYSIS FROM INTEGRATED COMPLETION AND RESERVOIR MODELING OF HYDRAULICALLY FRACTURED WELL

The result from the integrated completions and reservoir modeling shows that the hybrid integrated completion and reservoir model can be used for selecting optimum lateral placement to target sweet spots that have secondary fissures and good fracability index to maximize production rates, improve hydrocarbon recovery and enhance well economics. Additionally, this dissertation presented a new hybrid model for determining representative stimulated reservoir volume (SRV), which incorporated discrete fracture network modeling to captures the effects of secondary fissures. The hybrid integrated completions and reservoir model was optimized, and then used for production history matching and forecasting

6.1. CALIBRATED FULLY3D HYDRAULIC FRACTURE MODELS AND HISTORY MATCHED RESULTS

The results from the fracture history matching highlighted two important “best practices” for using micro-seismic mapping and building calibrated fracture models. First, it is critically important for engineers and geoscientist to understand that micro-seismic data can sometime give misleading fracture dimensions, especially if the micro-seismic quality control and interpretations were not properly done. Secondly, in cases where there is low quality micro-seismic data or where one observation well was used, the best practice is to calibrate the facture model only to “the good micro-seismic data” for history matching. Figure 6-1 compares the results obtained from the calibrated fracture model to the micro-seismic survey. The results highlights two unique findings; first, the calibrated fracture model closely matched the results of the micro-seismic survey only for the stages located at the heel of the horizontal well. Secondly, the result shows that the fracture stages at the

toe of the horizontal well, on average, had lower fracture half-length. However, the calibrated fracture model and micro-seismic survey provided vastly different fracture dimensions for 15 out of the 20 stages in well A (see Figure 6-1). For instance, the results for stages 1 and 4 (shown by stars) in Figure 6-1 indicate no fracture dimensions from the micro-seismic mapping even though fracture treatment per stage was relatively constant for all the stages.

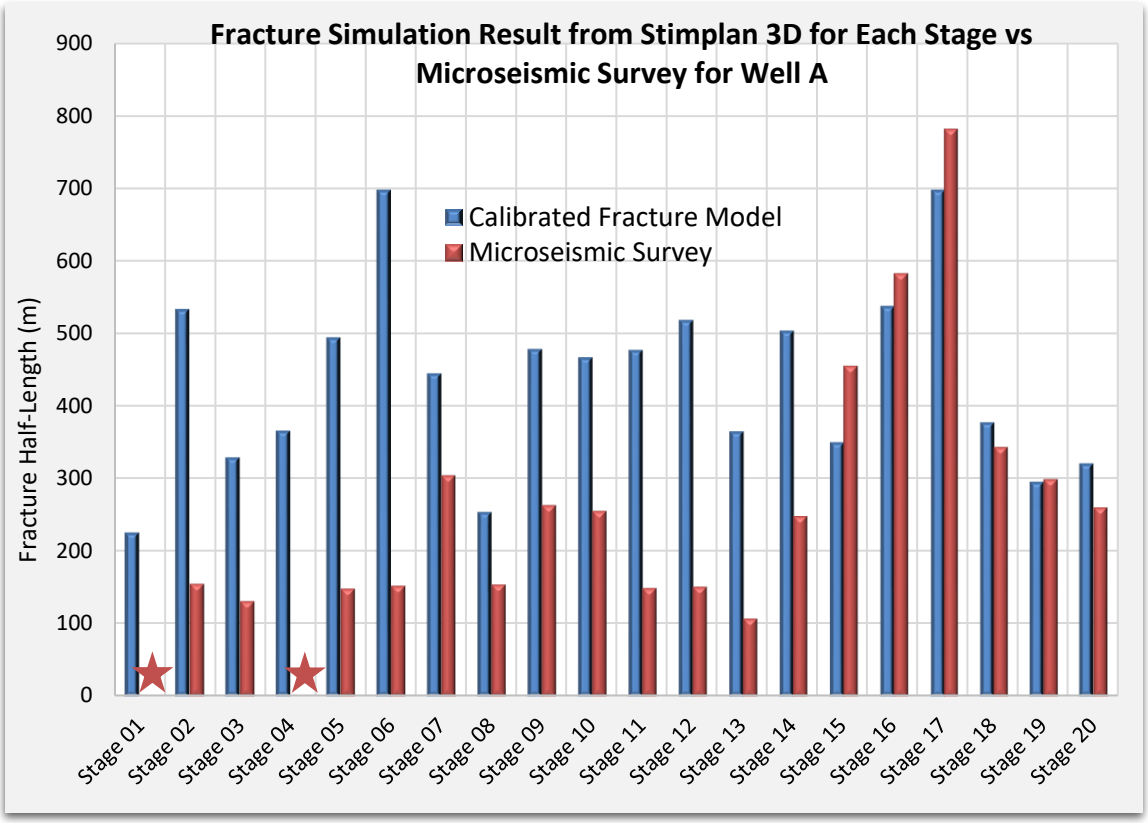

Figure 6-1: Comparison of fracture half-length results from calibrated fracture model versus micro-seismic survey for stage in well A

Figure 6-2 shows the analysis of how the calibrated fracture model faired against the micro-seismic survey based on fracture stage location (the fracture stages were divided

into four sections). The result shows the average fracture half-length (x_f) for each section if the lateral well compared to the micro-seismic data. For instance, the fourth section, which covers stages near the heel of the horizontal well (16-to-20), there was very match between the calibrated fracture and the micro-seismic mapping. However, near the toe of the horizontal well (1-to-4), vastly different fracture dimensions were obtained from calibrated fracture model compared the micro-seismic survey.

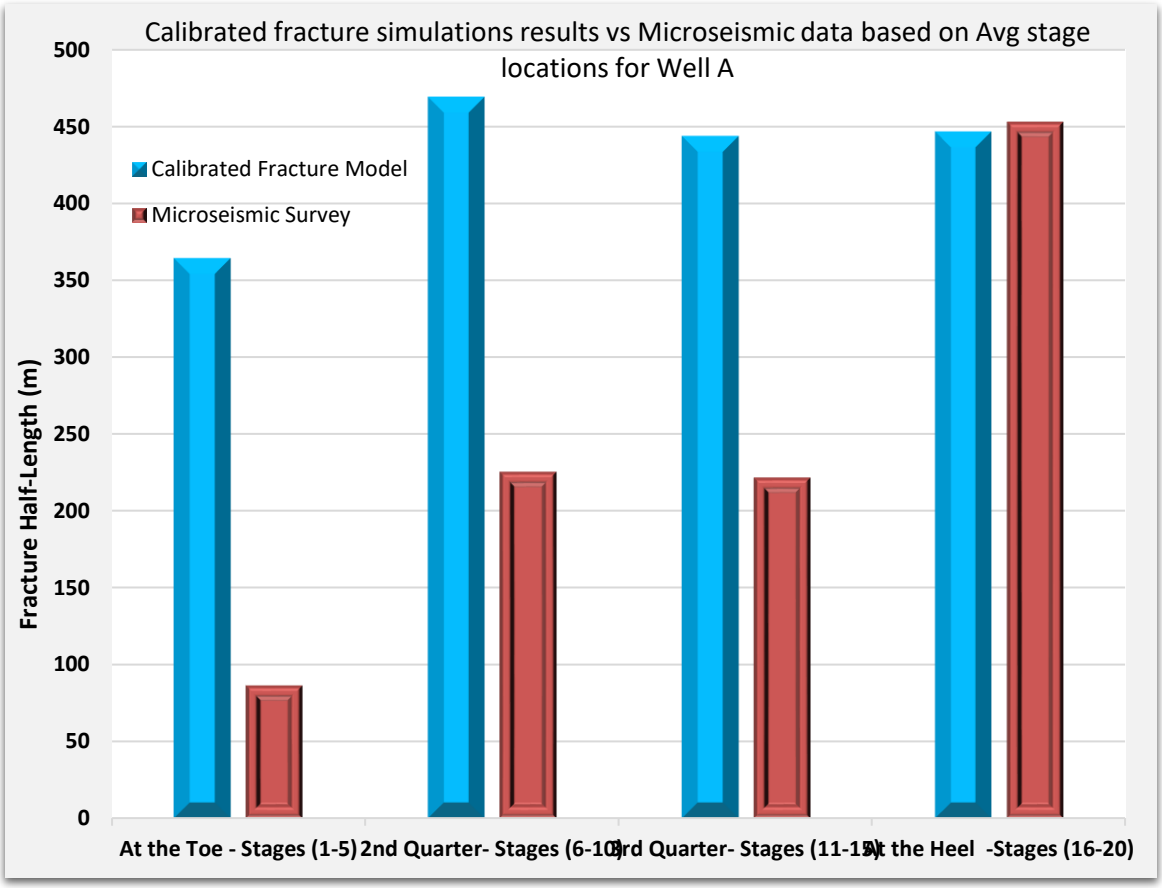

Figure 6-2: Calibrated fracture model accuracy versus micro-seismic survey based on averaged group stage locations of stages for Well A

Similar results were obtained from the calibrated fracture model for well B as shown by Figure 6-3. The results show that the micro-seismic survey data and calibrated fracture model had similar fracture dimensions for the fracture stage treatments that were close to the micro-seismic receiver. However, away from the micro-seismic geophones/receivers, issues such as location uncertainty and signal to-noise ratio (SNR) affected the quality of the micro-seismic mapping and the fracture dimension obtained from it.

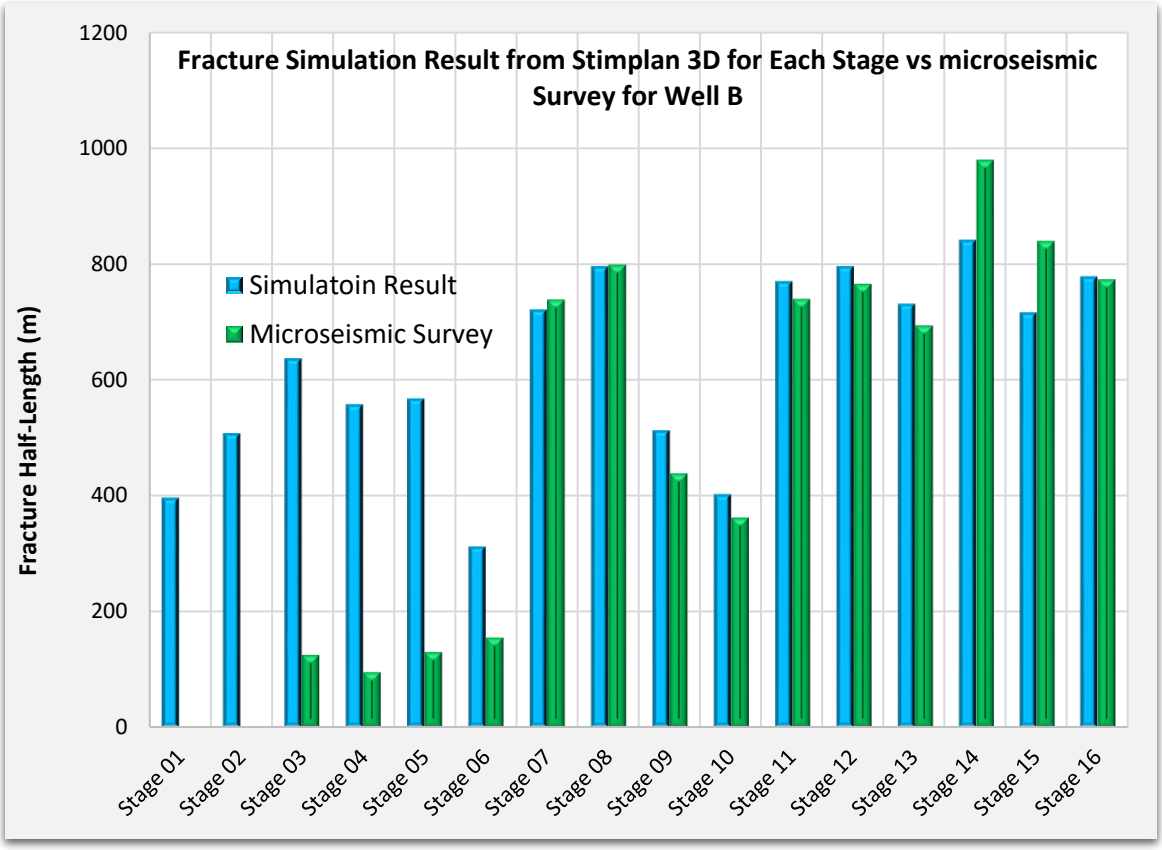

Figure 6-3: Comparison of fracture dimensions for Well B from the Stimplan 3D calibrated model versus micro-seismic survey derived fracture dimensions

The results from fracture history matching for well B, which had liner leak during the hydraulic fracture treatment, were much better than that of well A. Figure 6-4 shows calibrated fracture model accuracy and precision versus the micro-seismic survey based on averaged group stage locations for Well B. The hydraulic fracture half-lengths were longer, on average, for well B compared to well A because of two reasons; first, well B had higher treatment volumes per stage, especially for the stages near the heel, because few stages than designed were finally stimulated.

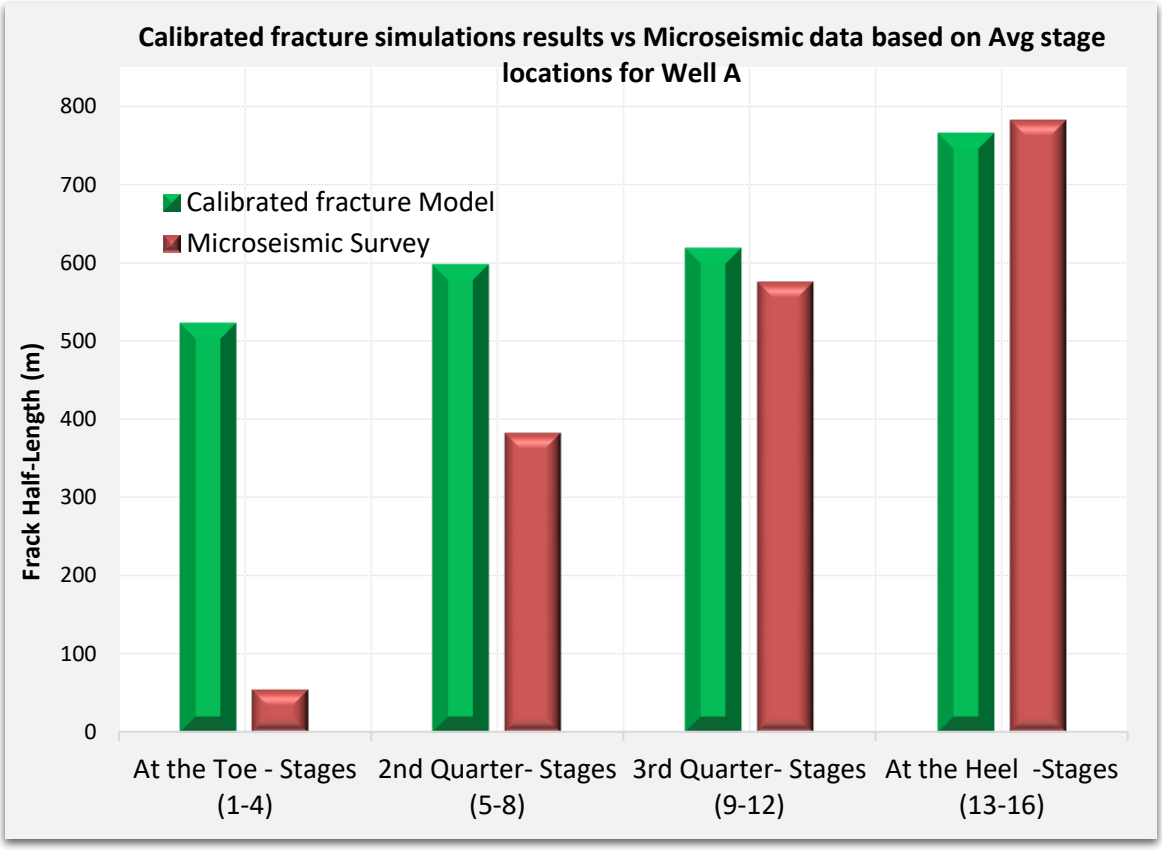

Figure 6-4: Calibrated fracture model accuracy versus micro-seismic survey based on averaged group stage locations of stages for Well B

The well was designed for 20 fracture stages, but because of the liner leak and subsequent workover, only 16 stage were ultimately completed. Secondly, the leak-off co-efficient for well B was less that of well A (0.00035 versus 0.0004 (ft. /(t)$^{0.5}$), which meant less fluid loss and longer fracture growth.

Figure 6-5 shows result of fracture modeling using Stimplan3D, which was the fracture modeling software used in this study. The figure shows stress profile, fracture half-length and proppant coverage for stage 8 of well A.

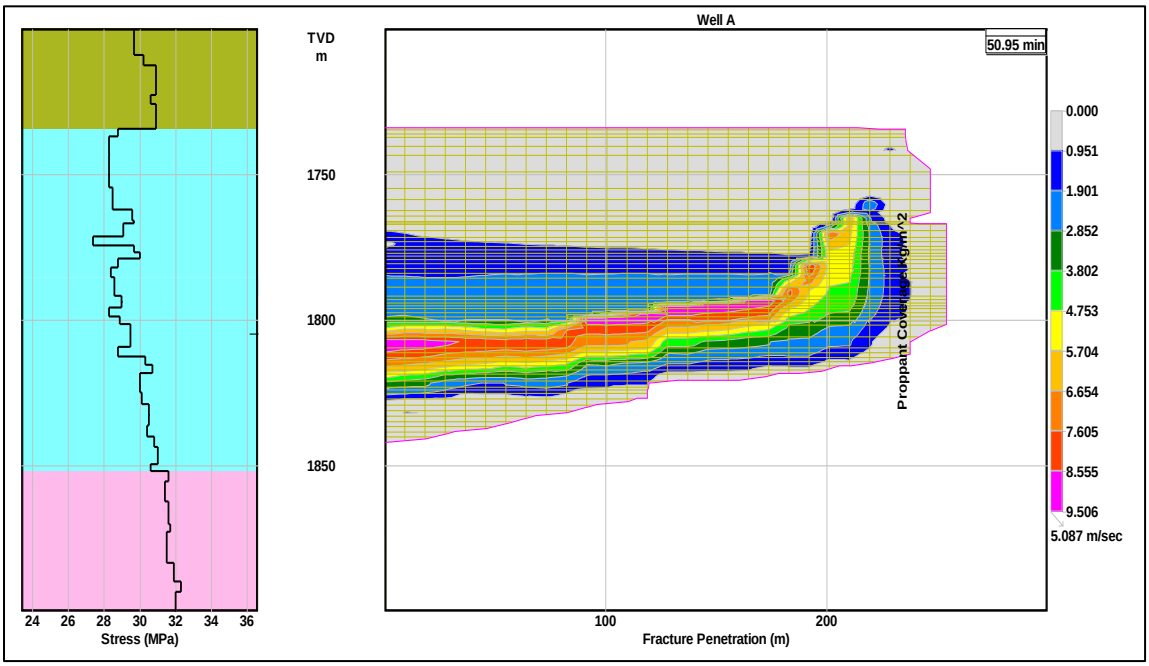

Figure 6-5: Fracture treatment stress profile, length and proppant coverage for stage 8 in Well A

The fracture modeling results for all the wells studied showed two important findings; first, there was no fracture height growth observed in any of the stages and fracture height was contained for the wells in the upper Montney formation. This findings

was also confirmed by the micro-seismic mapping. Secondly, controlling the net treating pressure (Pnet) and staying below the stress differences (Δσ) (between the Doig and upper Montney) resulted in contained fractures.

6.2. FRACTURE MODEL OPTIMZATION RESULTS

The wells used in the study had mostly one fracture cluster per stage, and on average, about 90 ton (kg) of proppant per stage (see Figure 4-5). The first sensitivity analysis was to investigate the impact of either decreasing or increasing the amount of proppant per stage. Figure 6-6 shows the result of changing the amount of proppant mass used per stage in one cluster perforations versus fracture half-length (x_f) created. The results shows that when the proppant mass was increased from (50 ton to 75 ton) kg, the fracture half-length increased, on average, by 28%. However, when the proppant mas was increased from (75 ton to 100 ton) kg, the fracture half-length increased only by 4%, and from (100 ton to 150 ton) kg, there was no change (~1%). Secondly, Figure 6-6 also shows the impact of changes in proppant mass from (50 ton to 150 ton) in kilograms on fracture conductivity. When the proppant mass was increased from (50 ton to 75 ton) kg, the fracture conductivity increased by 33%, from (75 ton to 100 ton) kg, the conductivity increased by 16%, and from (100 ton to 150 ton) kg, the fracture conductivity increased by 40%.

6.2.1. Optimization Parameters and Sensitivity Analysis. The result of Figure 6-6 shows that increasing the amount of proppant mass per stage in a single fracture cluster configuration after 100 ton kilograms adds little value to well performance measured in terms of fracture half-length and stimulated area. In unconventional resources

where the reservoir permeability is very low, the main optimization parameter should be fracture half-length.

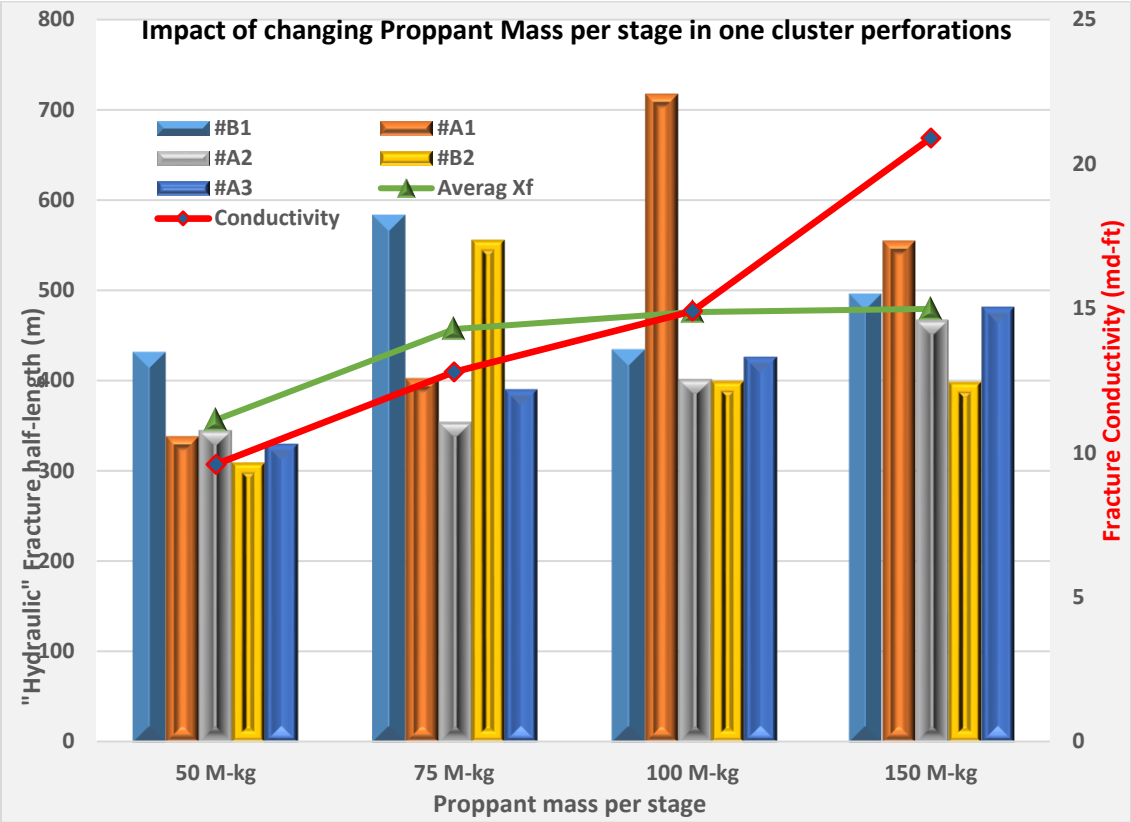

Figure 6-6: Impact of increasing proppant mass in a single fracture cluster from 50 ton to 150 ton on fracture half-length and conductivity

The reservoir permeability of the wells used in the study ranged from 0.00015 mD to 0.00018 mD, and the average dimensionless fracture conductivity (F_{CD}) obtained from calibrated fracture modeling was over 40, making the fractures infinite-acting (Dusterhoft et al.). Equation 48 shows the formula for (F_{CD})

$$F_{CD} = \frac{k_f w_f}{k X_f} \quad \text{...(48)}$$

Where

k_f = fracture permeability (md)

w_f = fracture width (cm)

x_f = fracture half-length (m)

k = reservoir permeability (md)

For the two clusters per stage analysis, the result shows that the "hydraulic" and propped fracture half-lengths increased when the proppant mass was increased from 50 M-kg to 150 M-kg per stage. Figure 6-7 shows the result of hydraulic fracture half-length per cluster and average fracture half-length (xf) obtained from each proppant mass pumped for Well B's 16 stages.

Figure 6-7 highlights two important findings; first, the lateral location of the fracture cluster makes it highly sensitive to the local (in-situ) stress profile, and if the perforation clusters are in high stress zone, the outcome is shorter fracture (xf). For instance, stage 6-cluster two (C2) and stage 7-cluster one (C1), were located in high stress zone and very little fracture half-length growth was observed proppant mass was increased from 50 M-kg to 150 M-kg per stage as shown by Figure 6-7. The second findings was that the average fracture half-length (x_f) per cluster for all 16 stages increased from 150 feet to 250 feet when the proppant mass was increased from 50 M-kg to 150 M-kg. The averages (x_f) are shown as straight lines in Figure 6-7.

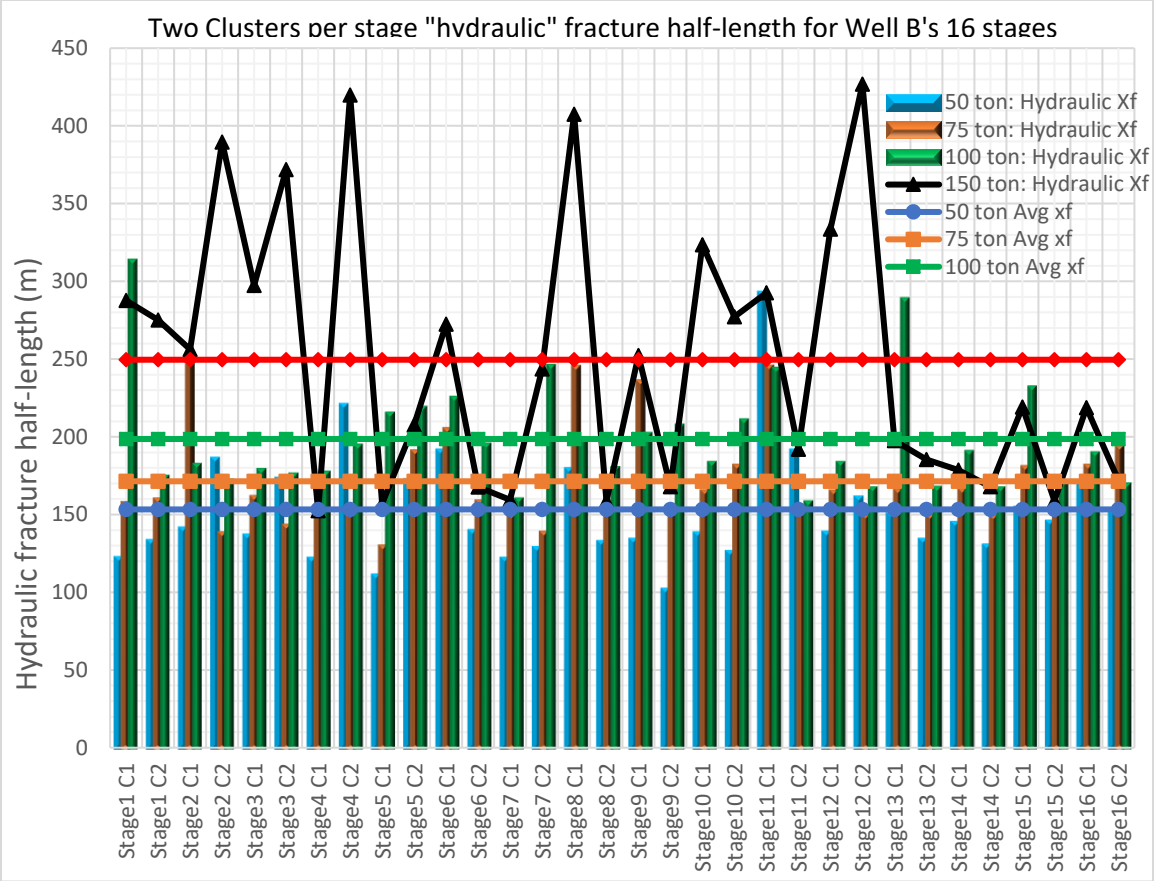

Figure 6-7: Hydraulic fracture half-length per cluster and average (x_f) obtained from each proppant mass pumped for Well B's 16 stages

Similar analysis was done for the three clusters per stage. Figure 6-8 shows the result, and highlights two important findings. The first findings is the impact of fracture cluster interactions, leading to uneven distribution of fracture half-lengths (x_f), especially for the middle cluster in each stage, which was shorter (highlighted by zig-zagging nature of the curve). Secondly, the average fracture half-length per cluster increased when the proppant mass was increased from 50 M-kg to 150 M-kg. However, when the averages were compared for the two clusters per stage versus the three clusters per stage, the half-length decreased. For instance, in the two clusters per stage model, the average cluster half-

length for the 150 M-kg was 250 feet, but decreased to 200 feet in the case of the three clusters per stage as shown by Figure 6-8.

When the number of clusters per was increased from two clusters per stage to three, four or even five clusters per stage, the fracture half-lengths created had uneven distributions. The result of the increased clusters per stage was that some parts of lateral section (near the heel) had shorter fractures while other part of the horizontal well (near the middle) had longer fractures. This could present two problems; first, it lead to production interference of near-by wells or kill the well by fracturing into it. Secondly, well spacing could be come an issues since different parts of the horizontal well had different fracture half-lengths and spacing, making uniform well spacing development difficult.

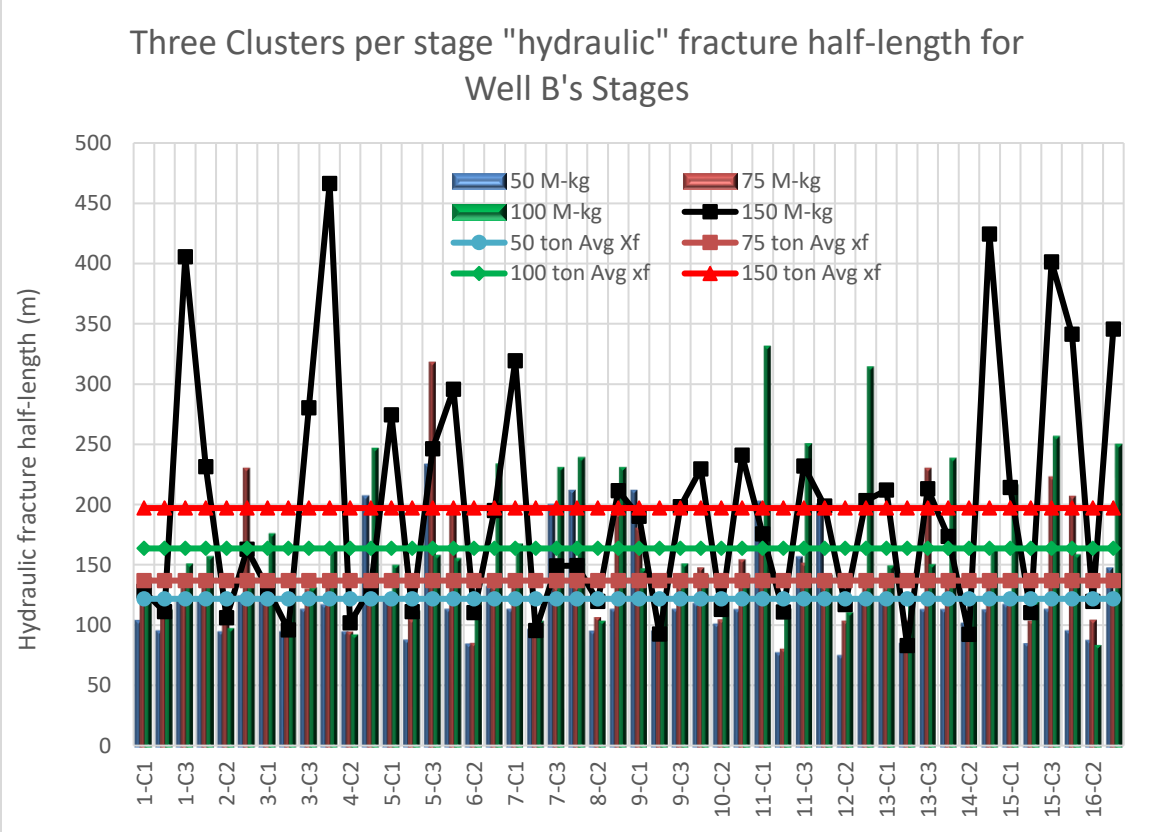

Figure 6-8: Three clusters per stage "hydraulic" (x_f) and average fracture half-length for each proppant mass 50 M-kg to 150 M-kg

Figure 6-9 shows the "hydraulic" fracture half-length obtained from proppant mass and fracture clusters sensitivity analysis. The amount of proppant mass was increased from 50 ton to 150 ton in kilograms, and the number of fracture clusters was increased from one cluster to five clusters per stage. The result shows three important findings; first, the fracture half-length (x_f) is inversely proportional to the number fracture clusters per stage. As the number of fracture clusters per stage was increased from one cluster to five, the fracture half-length created decreased for all proppant mass (from 50 M-kg to 150 M-kg).

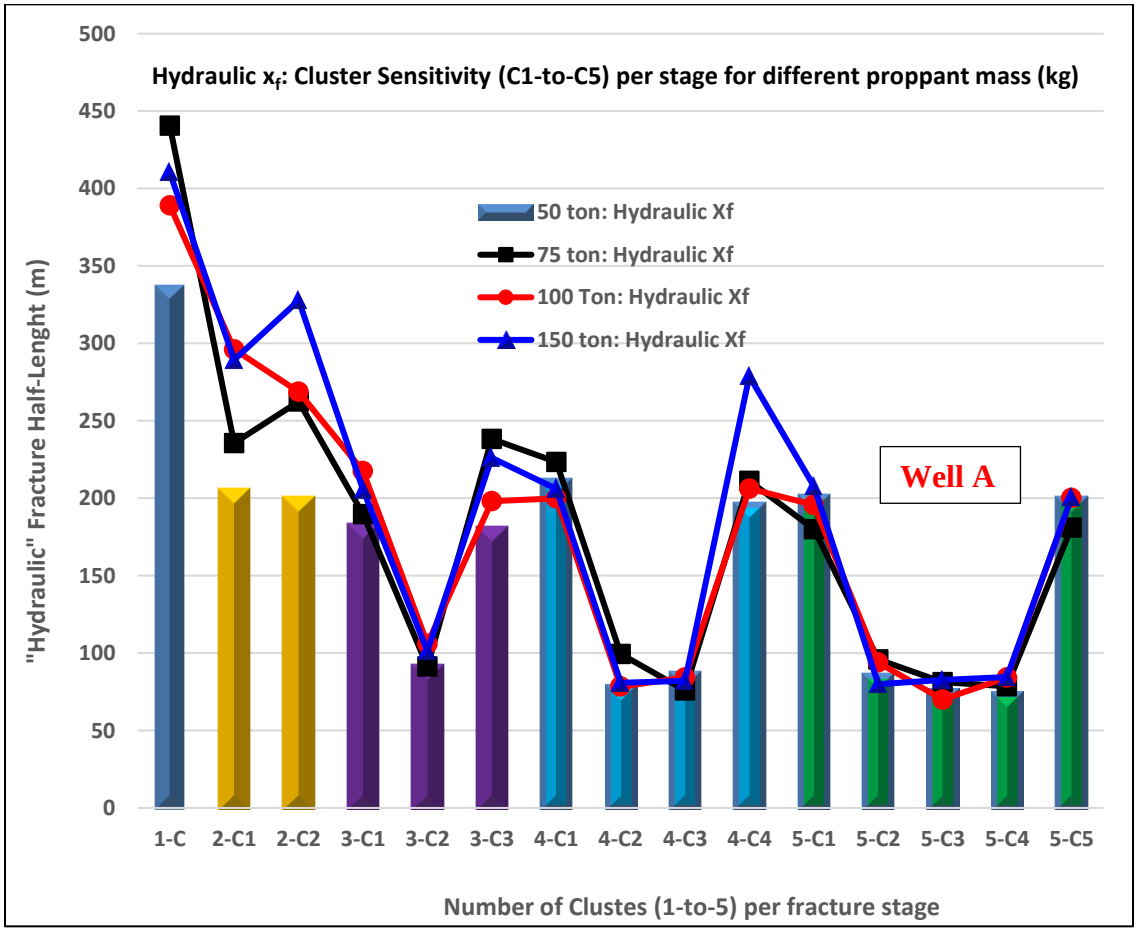

Figure 6-9: "Hydraulic" fracture half-length (xf) obtained from cluster sensitivity (C1-to-C5 per stage for different proppant mass of (50 ton to 150 ton) kg

The results of Figure 6-9 also shows that from two fracture clusters to five, when the amount of proppant mass was increased from 50 ton to 150 ton, there was noticeable increase in "hydraulic" half-length. For instance, for the two fracture clusters per stage, when proppant mass was increased from 50 ton (highlighted in orange color columns) to 150 ton, the fracture half-length increased from 200 m to 300 m per cluster. Thirdly, the stress profile at each fracture cluster perforation determines the length of fracture half-length created and the geometry of the hydraulic fracture.

Similarly, Figure 6-10 shows the "propped" fracture half-length obtained from fracture clusters from (C1-to-C5) per stage and proppant mass (from 50 ton to 150 ton) declined in each step. The short-hand mathematical formulation of the number of steps involved for each sensitivity was $[\boldsymbol{X_{ij}}]$**,** where the number of fracture clusters [i=1,2,3,4,5], and the amount of proppant mass in each step was [j=50,75,100,150].

The results of Figure 6-10 shows similar trends and findings to that of Figure 6-9. Additionally, the result of Figure 6-10 shows that the middle perforation clusters (from C3-to C5) got very little proppant and had disproportionately shorter fracture half-lengths. On the other hand, the first and last perforation clusters received most of the proppant pumped and had longer fracture half-lengths. For instance, in the four clusters per stage configuration, the two middle clusters had, on average, propped fracture half-lengths of about 20m. Secondly, the result also shows that the best performing combination of fracture clusters and proppant mass and fracture spacing measured in terms of propped fracture half-length created per kilogram of proppant mass used was the two clusters per stage configuration. For example, in the two fracture clusters per stage, increasing the amount of

proppant mass from 50 M-kg to 150 M-kg, led to noticeably increase in the propped fracture half-length created.

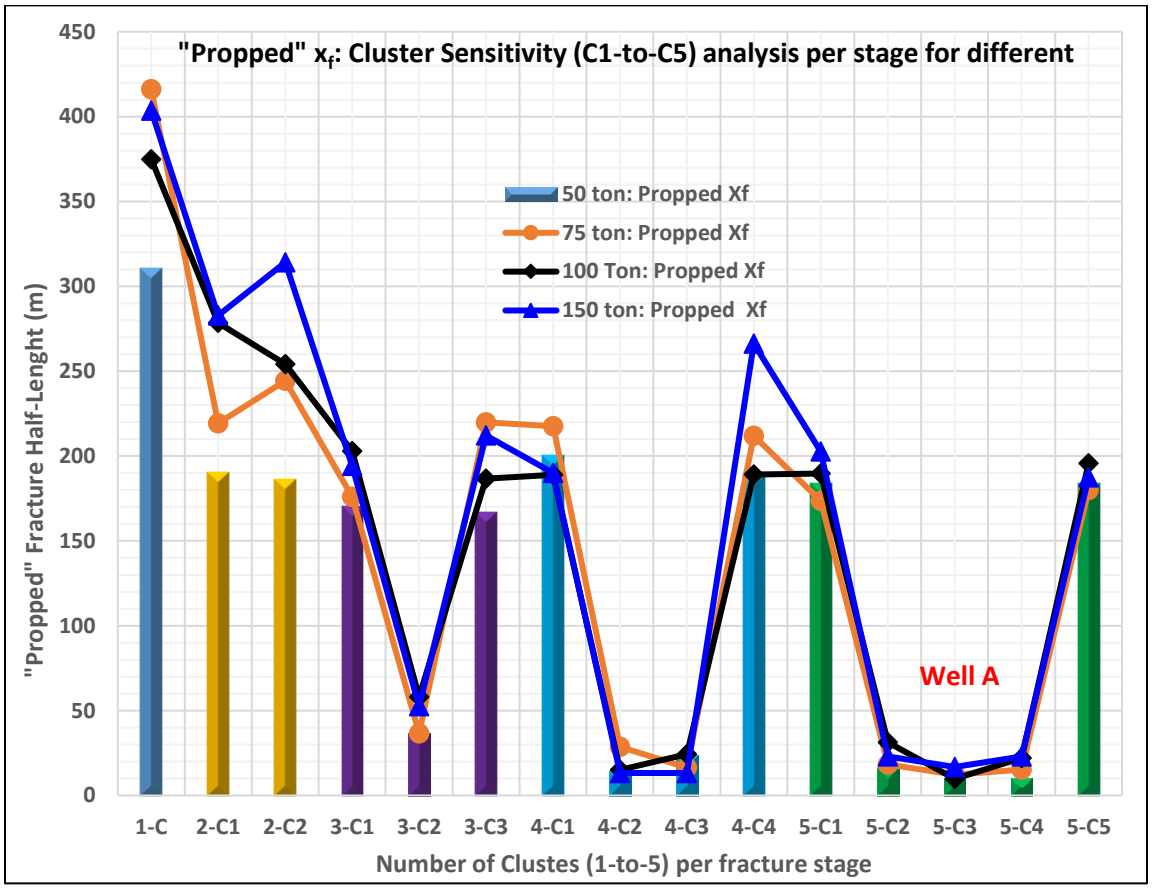

Figure 6-10: "Propped" fracture half-length (xf) obtained from cluster sensitivity (C1-to-C5) per stage for different proppant mass of (50 ton- to- 150 ton) kg

Figure 6-11 shows a radar chart, which is a good way of visualizing multivariate data.The result compares the multiple quantitative sets of parameters in the optimization and sensitivity analysis. The results of Figure 6-11 makes it easier to see the outliers or parameters that have same values. For instance, the middle perforation clusters in the four clusters (4-C3 & 4C4)) and five clusters (5-C3, 5-C4 & 5-C5) configurations were outliers

and had very short fracture half-length. Secondly, the polygon lines in the chart which represent different amount of proppant mass (50 ton to 150 ton) are overlaid on top of each other where no benefit was derived from increased proppant mass. Thirdly, the value of increasing either the number of fracture clusters or amount of proppant mass were found where the polygon lines in the chart get clear separations. For instance, from one cluster (1-C) to two clusters (2-C2 & 2-C2), there was clearly discernible increase in value both for the number of fracture clusters per stage and the amount of proppant used.

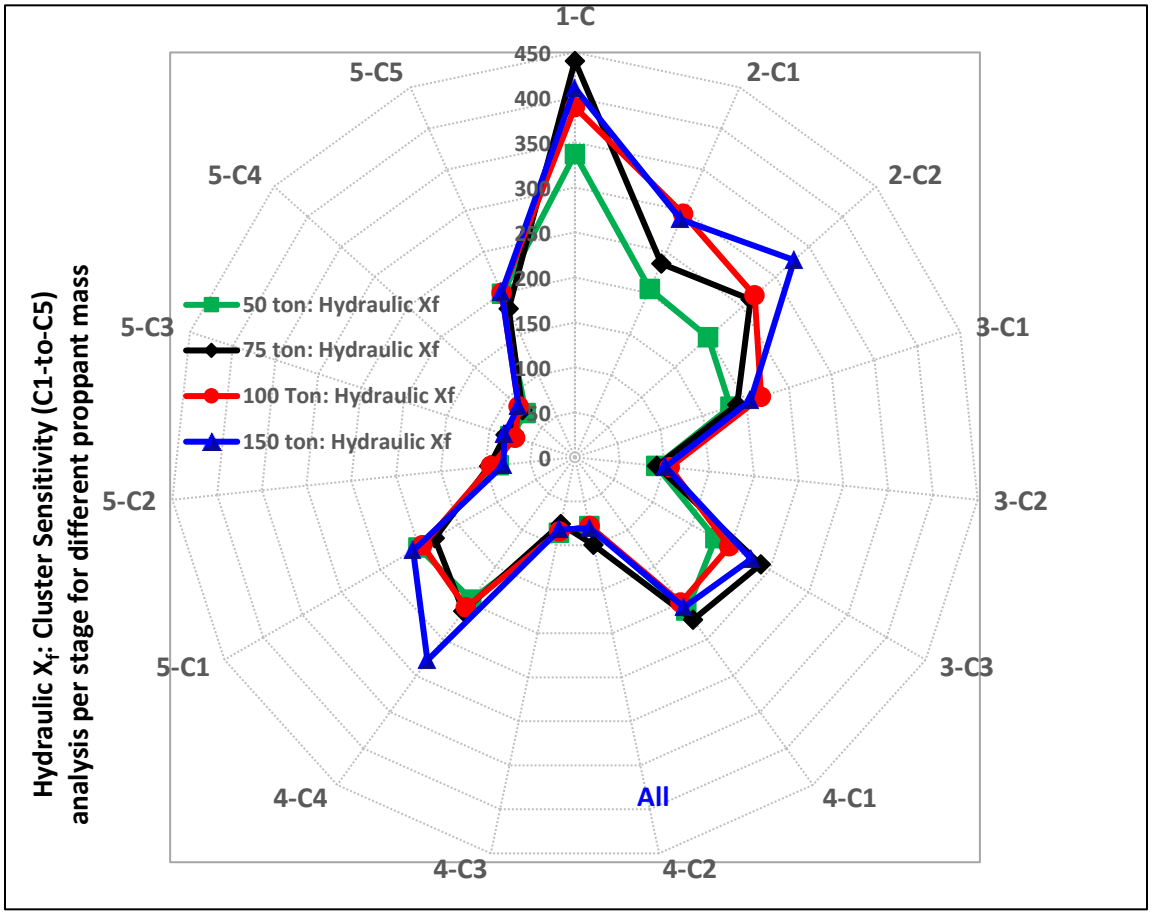

Figure 6-11: "Hydraulic" fracture half-length (xf) viewed 360 degree from the wellbore for number of clusters (C1-to-C5) and different proppant mass (50 ton -to-150 ton) kilograms per stage

Figure 6-12 also shows radar chart for the sensitivity analysis of the five clusters per stage configurations. On average, the five clusters per stage configuration had the shortest fracture half-lengths.

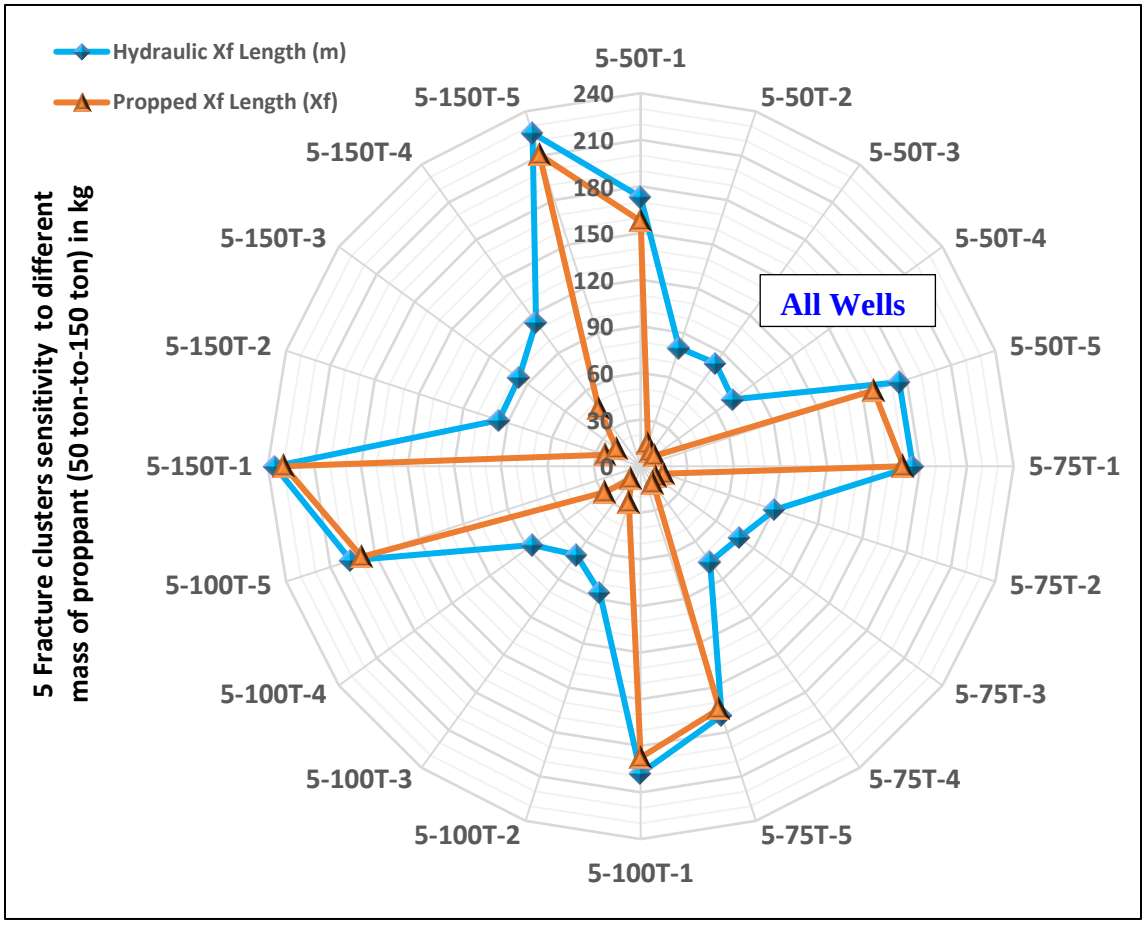

Figure 6-12: Sensitivity analysis for 5 clusters per stage for different proppant mass (50 ton-to-150 ton) kilograms per stage

Figure 6-12 shows the “hydraulic” and “propped” fracture half-lengths created in the 5 clusters per stage when the amount of proppant mass was increased from 50-to-150 ton. The results shows that the “hydraulic” fracture half-length increased when the amount

of proppant was increased, but the propped fracture half-length didn't increase proportionately. For example, the first perforation clusters in the five cluster configuration (5-150T-1) and last (5-150T5) had longer propped x_f, while the middle clusters (5-150T-2, 5-150T-3 & 5-150T-4) had shorter propped x_f, in the 150 ton proppant mass.

If "hydraulic" fracture half-length was used as an optimization metrics, then the five clusters per stage configuration would give optimal design (where hydraulic fracture half-length = un-propped fracture half-length (x_f) plus propped fracture half-length (x_f). For instance, in tight sand gas reservoirs or shale gas reservoirs, "Hydraulic" fracture half-length (x_f) might be good optimization metrics. Previous studies have shown that gas can flow in very small cracks, and (Britt and Schoeffler 2009) found that gas can flow through un-propped cracks at effective confining stresses.

The results from the fracture cluster sensitivity (2, 3, 4, and 5 clusters per stage), proppant mass sensitivity (50 kg, 75 kg, 100 kg, and 150 kg per stage) and fracture spacing sensitivity (20 m, 25 m, 33 m, 49 m and 98 m per stage) yielded two important optimization metrics. First, the fracture optimization objective was to gradually increase the amount of proppant used per stage from the toe to the heel of lateral as shown in Figure 4-5. In the optimized stimulation model design, proppant was gradually increased from (50 M-kg to 150 M-kg) per stages as fracture treatment moved the toe of the lateral to the heel. Additionally, the friction pressure losses declined (meaning more horsepower availability) and the amount of proppant mass per fracture stage was substantially increased for stages near the heel of the lateral.

Figure 6-13 shows post-fracture treatment pressure analysis as a function of fracture stage location, amount of proppant mass per stage used versus a model with an optimized

proppant mass selection that takes advantage of the available horsepower (because of the decrease in friction pressure loss near the heel of the horizontal well).

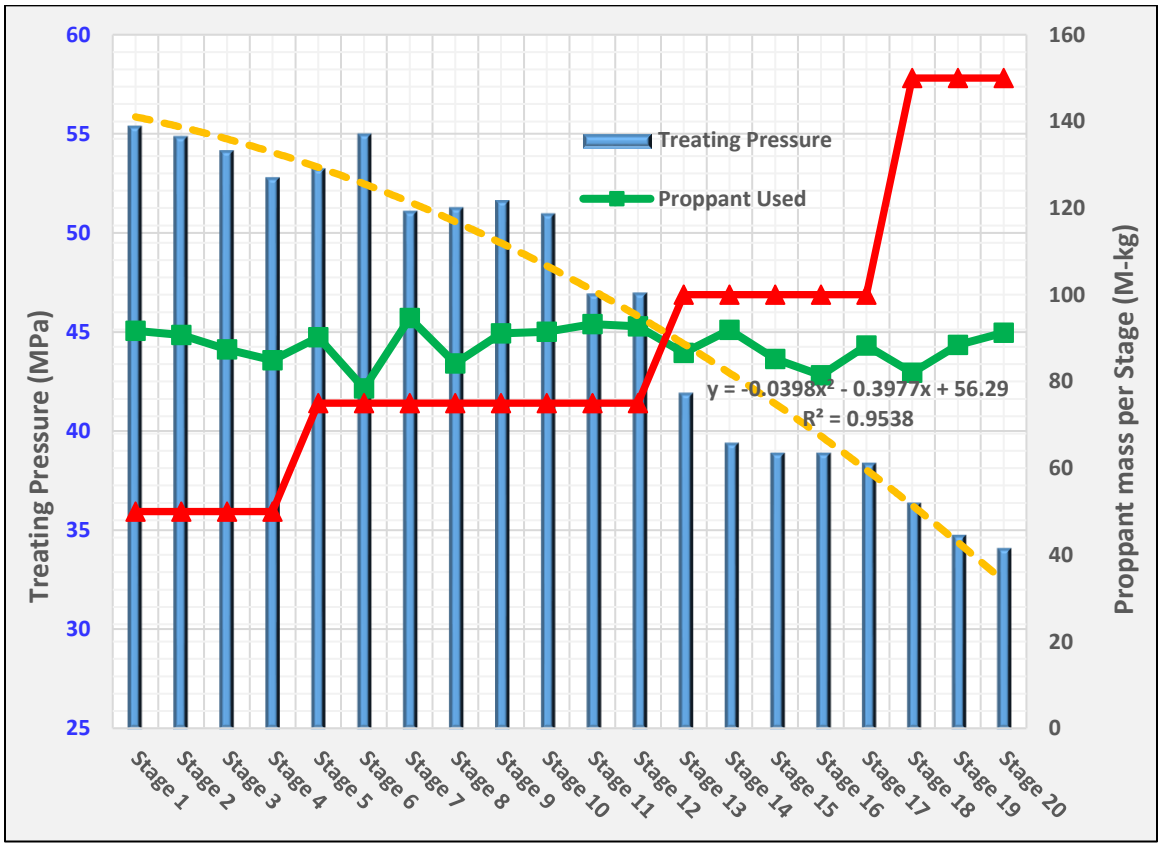

Figure 6-13: Well A post-fracture treatment pressure analysis and optimized proppant selection model

Table 6-1 shows the three types of stimulation designs used in the study. The first model was current well A design (which was how Well A was hydraulically stimulated). The second model was “optimized fracture design-2” (which added two clusters per stage from stage 13-to-20), and the third model was “optimized fracture design-3” (which added two clusters per stage for (stages 13-to-17), and three clusters per stage (for stages 18-to-20)). Secondly, all three stimulation designs used the same amount of proppant type and

mass (about 1,750 ton in total) as shown in Table 6-1. Thirdly, the pump rate, treatment volume and treatment pressures were all obtained from the post-fracture analysis. Only the volume of fracturing fluid was adjusted to account for the changes in the amount of proppant mass (from 50-to-150 ton) per stage.

Table 6-1: Comparison of the three stimulation models (optimized vs well design)

Welll A Stimulation Design now			Optimized Frac Design-2 Clusters added				Optimized Frac Design-2,3 clusters added			
Stage Number	Stage Spacing (m)	Proppant Mass per stage (ton kg)	Stage Number	Fracture Clusters	Stage Spacing (m)	Proppant Mass per stage (ton kg)	Stage Number	Fracture Clusters	Stage Spacing (m)	Proppant Mass per stage (ton kg)
Stage 01	85	92	Stage 01	01-C1	85	50	Stage 01	01-C1	85	50
Stage 02	85	91	Stage 02	02-C1	85	50	Stage 02	02-C1	85	50
Stage 03	85	87	Stage 03	03-C1	85	50	Stage 03	03-C1	85	50
Stage 04	85	85	Stage 04	04-C1	85	50	Stage 04	04-C1	85	50
Stage 05	85	90	Stage 05	05-C1	85	75	Stage 05	05-C1	85	75
Stage 06	85	78	Stage 06	06-C1	85	75	Stage 06	06-C1	85	75
Stage 07	85	95	Stage 07	07-C1	85	75	Stage 07	07-C1	85	75
Stage 08	85	84	Stage 08	08-C1	85	75	Stage 08	08-C1	85	75
Stage 09	85	91	Stage 09	09-C1	85	75	Stage 09	09-C1	85	75
Stage 10	85	92	Stage 10	10-C1	85	75	Stage 10	10-C1	85	75
Stage 11	98	93	Stage 11	11-C1	98	75	Stage 11	11-C1	98	75
Stage 12	72	93	Stage 12	12-C1	72	75	Stage 12	12-C1	72	75
Stage 13	85	87	Stage 13	13C1	43	100	Stage 13	13C1	43	100
Stage 14	97	92		13C2	43			13C2	43	
Stage 15	98	85	Stage 14	14C1	49	100	Stage 14	14C1	49	100
Stage 16	99	81		14C2	49			14C2	49	
Stage 17	98	88	Stage 15	15C1	49	100	Stage 15	15C1	49	100
Stage 18	98	82		15C2	49			15C2	49	
Stage 19	98	88	Stage 16	16C1	49	100	Stage 16	16C1	49	100
Stage 20	98	91		16C2	49			16C2	49	
			Stage 17	17C1	49	100	Stage 17	17C1	49	100
				17C2	49			17C2	49	
			Stage 18	18C1	49	150	Stage 18	18C1	33	150
				18C2	49			18C2	33	
			Stage 19	19C1	49	150	Stage 19	19C1	33	150
				19C2	49			19C2	33	
			Stage 20	20C1	49	150		19C3	33	
				20C2	49		Stage 20	20C1	33	150
								20C2	33	
								20C3	33	
1			2				3			
Total Proppant		1,766				1,750				1,750

Figure 6-14 shows two planar reservoir simulation models; optimized fracture model-3 (labelled as #3 in Table 6-1), and current model for well A (labelled as #1 in Table 6-1). Comparison of the two planar reservoir models show two important

optimization metrics; first, the current well A design had 20 fracture stages while the "optimized design model-3" had 30 fracture stages (see Table 6-1 for each design's layout). Secondly, the fracture stages near the heel of the horizontal well had shorter fracture half-lengths (x_f), smaller fracture spacing (33m & 49m) and used higher amount of proppant mass per stage for the case of the "optimized design model-3".

Thirdly, for the case of the "optimized design model-3", the uneven nature of the created fracture half-lengths might become an issue for field development and well spacing. For instance, the fractures are shorter near the heel, longer in the middle and short at the toe of the horizontal well. To remedy this kind of problem, the second optimized design model (labelled as #2 in Table 6-1), was built and the stimulation model greatly improved the fracture half-length distributions while vastly increasing well performance (see the results of Figure 6-15 and Figure 6-16).

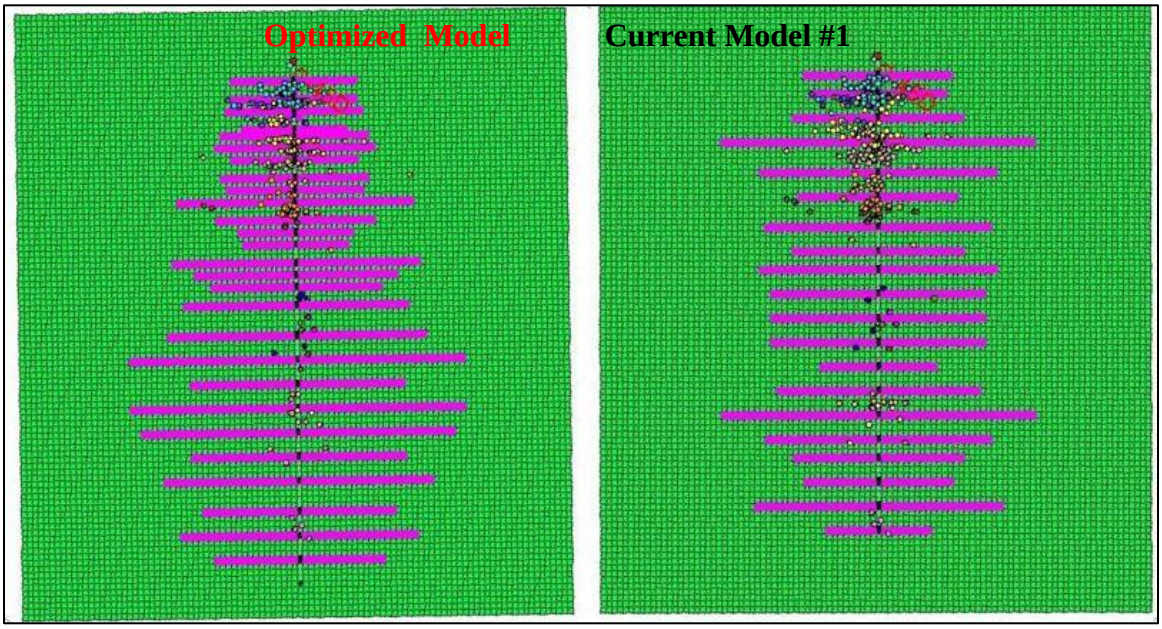

Figure 6-14: Comparison of stimulation models- optimized model #3 versus current model (#1)

The performance of the three stimulation design models were compared using compositional reservoir simulation models that were created for the study of integrated reservoir modeling. For more details on the procedures and steps used to construct the "integrated reservoir models" can be found in a paper published by the authors (Kassim et al. 2016a).

Three well performance metrics often used in the oil and gas industry are cumulative production, discounted recovery (DR) and present value (PV). In comparing the performance of the three stimulation design models, cumulative well production and discounted recovery (DR) were used in this study. The Internal rate of return (IRR) or the interest rate used in the study was 10% per annum.

Discounted recovery (DR), which is cumulative recovery discounted at an annual interest rate, was used to compare the economic performance of each planar reservoir simulation created from the three stimulation design models (two optimized designs vs current fracture design).

$$DR = \sum_{i=1}^{n} \frac{N_i}{(1+r)^i} \qquad \text{...(49)}$$

Where;

$DR = \text{Discounted recovery in (bbls or Mscf)}$

$N_i = \text{Cumulative production (bbls or Mscf) in time, i}$

$r = \text{interest rate (\%), and n} = \text{number of years}$

The present value (PV) is the expected future cash-flow coming from the oil and gas production discounted at an annual rate, and can be calculated by multiplying DR (discounted recovery) by the price of oil or gas as shown below by equation 50.

$$PV = (P_O) * \sum_{i=1}^{n} \frac{N_i}{(1+r)^i} \quad \text{...(50)}$$

Where

P_O = price of oil (in any currency).

Figure 6-15 shows cumulative gas production and discounted recovery (DR) for the three models. The results show that the best performing model (blue) was the "optimized frac design-2 clusters added"), in terms of cumulative gas production and discounted recovery (gold color). The second best performing model was the "optimized design model-3" (pink color) in terms of discounted recovery (DR) metrics, but had slightly lower cumulative gas production than current well A (in black color). All three models were history matched to well production data (shown as the red curve near the origin).

Secondly, the optimization and sensitivity analysis showed that single cluster per stage stimulation design models can be greatly improved by adding more clusters per stage near the heel of the lateral section. The modification of the last eight stages of the original design to two clusters per stage vastly improved well performance as shown by Figure 6-15.

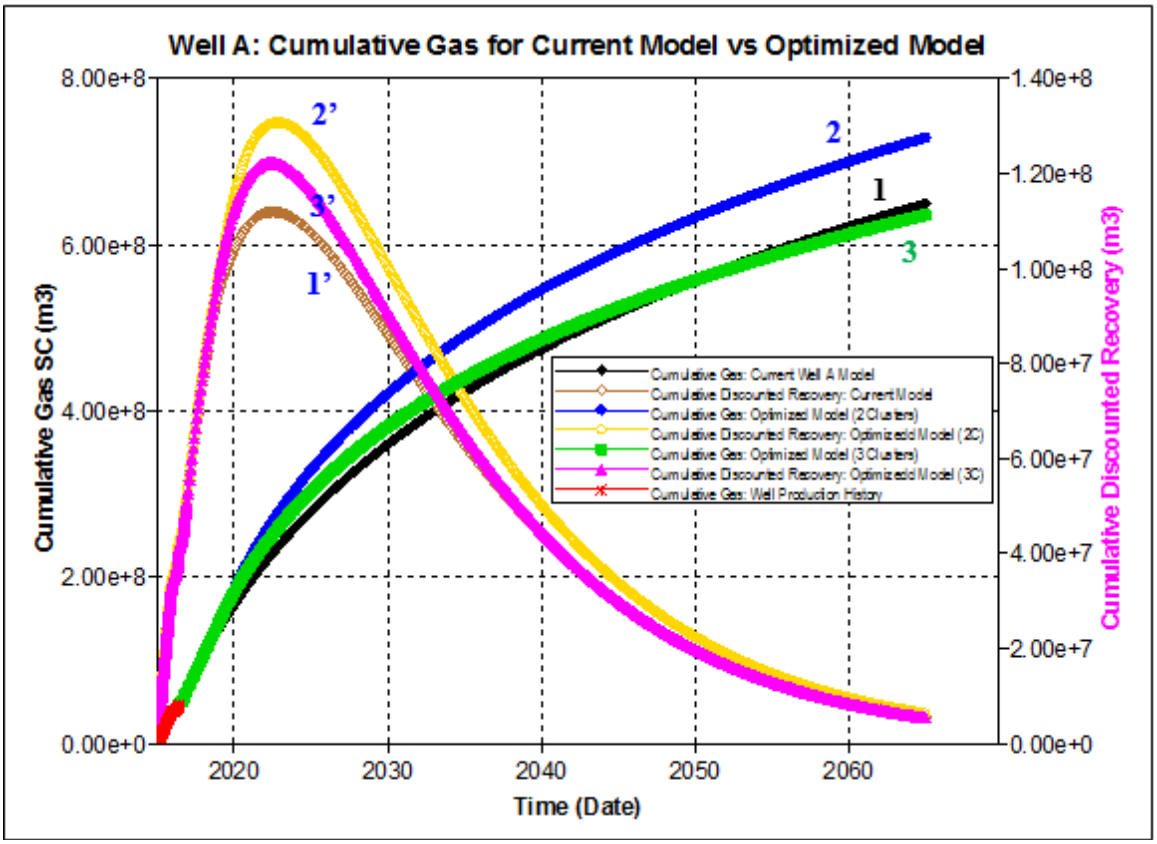

Figure 6-15: Comparison of results from the reservoir simulation for EUR and DR for current model vs two Optimized models

The debate going on in the oil and gas industry is whether increasing the number of clusters per stage improves the well performance, and what are the best metrics for measuring well performance? Initial well production (IP) or well recovery (EUR). Figure 6-16 shows well deliverability (sometimes called absolute open flow (AOF)) results for the three-stimulation design models (Current well A design versus two optimized stimulation designs shown in Table 6-1 as [1],[2] & [3]). The well deliverability test was modeled by constraining the well flow with only bottom-hole pressure (BHP), which was set to 250 psi.

The result of Figure 6-16 shows two important findings; first, adding more fracture clusters per stage in well stimulation can lead to higher initial well production and may increase EUR if designed properly. For instance, the two optimized stimulations models that had multiple clusters per stage performed better than well A model in terms of cumulative gas SC (standard condition), discounted recovery (DR) and well deliverability. Secondly, the optimized stimulation design-3, which had a mixture of 2 and 3 clusters per stage had the highest initial production (IP), but lower cumulative gas production than the optimized stimulation design-2, which had fewer multiple clusters per stage. Thirdly, Figure 6-16 shows that when all the three models were normally operated (just like oilfield operation, and not in AOF mode) and history matched, the model with highest cluster per stage (optimized stimulation design-3) had the lowest cumulative gas production. In short, well performance metrics based on initial well production (IP) may not the best indicator or might even lead to lost reserve.

The results from Figure 6-15 and Figure 6-16 show that optimization metrics should not be based on a single production performance indicator such as initial production (IP) or EUR (estimated ultimate recovery), which might have a lot of uncertainty. Rather multiple key performance indicators or assigning weights to performance indicators that historical matched field or well production data should be used. Secondly, balancing cost versus incremental production is the key to stimulation design optimizations. More fracture clusters per stage means more stimulation cost, and eventually the law of diminishing returns would be encountered.

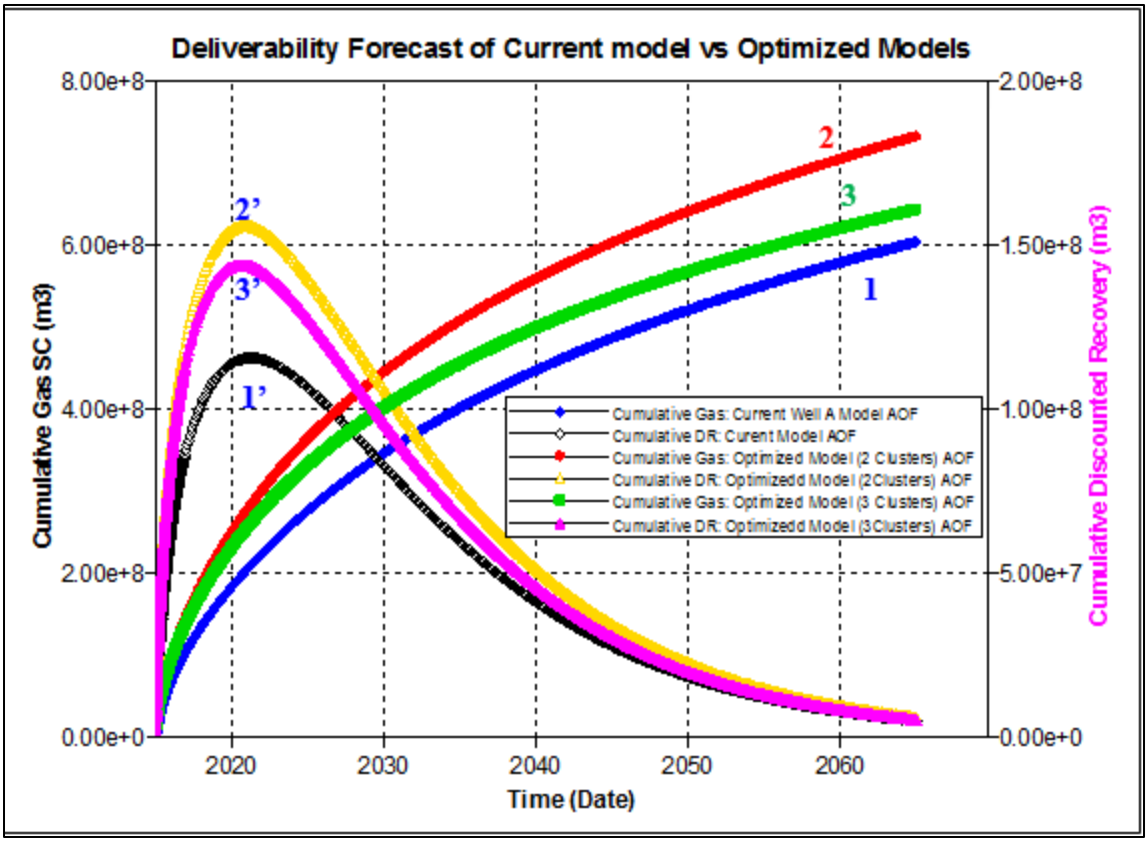

Figure 6-16: Comparison of Deliverability forecast for Well A versus Optimized models. All models were constrained with 250 psi flowing pressure only

6.2.2. Results from New Fracture Optimization Trends. The new optimization trends are "bigger" fracture sands per stage and more fracture stages in horizontal wells, which means longer laterals or more clusters per stage. In this study, two sets of parameters, "big frac" sand treatments and shorter fracture spacing, were used to investigate the impact of each optimization parameters on key stimulation performance indicators.

Multivariate analysis of the optimization parameters such as the set of clusters per stage [i = 3, 4, 5, 6, 7, 8], and proppant mass [j = 200, 300, 400] M-kg were done using the following equations;

$$C_{Avg[i]} = \frac{\frac{1}{n}\sum_{i=1}^{n} C_{[i,j]}}{M_j} \quad ...(51)$$

$$H_{Avg[i]} = \frac{\frac{1}{n}\sum_{i=1}^{n} H_{[i,j]}}{M_j} \quad ...(52)$$

$$P_{Avg[i]} = \frac{\frac{1}{n}\sum_{i=1}^{n} x_{[i,j]}}{M_j} \quad ...(53)$$

Where;

$C_{Avg[i]}$ = Average normalized fracture conductivity for fracture clusters per stage [I = 3, 4, 5, 6, 7, 8] per proppant mass [j = 200, 300, 400] M-kg

$C_{[i,j]}$ = Conductivity of fracture clusters per stage [I = 3, 4, 5, 6, 7, 8] per proppant mass [j = 200, 300, 400] M-kg

M_j = proppant mass (M-kg) per fracture cluster stage [j = 200, 300, 400]

$H_{Avg[i]}$ = Average normalized "hydraulic" fracture half-length for fracture clusters per stage [I = 3, 4, 5, 6, 7, 8] per proppant mass [j = 200, 300, 400] M-kg

$H_{[i,j]}$ = "hydraulic" fracture half of each clusters [I = 3, 4, 5, 6, 7, 8] per proppant mass [j = 200, 300, 400] M-kg

$P_{Avg[i]}$ = Average normalized "propped" fracture half-length for fracture clusters per stage [I = 3, 4, 5, 6, 7, 8] per proppant mass [j = 200, 300, 400] M-kg

$P_{[i,j]}$ = "Propped" fracture half of each clusters [I = 3, 4, 5, 6, 7, 8] per proppant mass [j = 200, 300, 400] M-kg

The other trend in hydraulic fracture optimization is cost control in all phases of the completion operations. As a result, "slick-water" has become the dominant fracturing fluid

of choice because it is cheaper and better environmentally than other fracturing fluids. Rebol (2016) presented a paper which shared how they salvaged a horizontal well that encountered drilling problems where they were unable to execute liner cement job. Ultimately, they selected coil-tubing system, and completed the well with 50 stages, fracture spacing of 25 meters-to-30 meters and used slick-water as fracturing fluid. This example highlights the new trends in stimulation optimizations of more fracture stages, shorter fracture spacing and use of slick-water.

Figure 6-17 shows results of eight clusters per fracture stage with different amount of proppant mass (200, 300, and 400) M-kg. The fracture cluster spacing was 12.5 meters, and used slick-water as treatment fluid. Figure 6-17 also shows the "hydraulic" and propped fracture half-lengths for fracture cluster. The results highlight three important points; first, since slick-water (even with friction reducers) is poor transporter of frac sands and often leads to pre-mature screen-outs; the result shows that it was not ideal fracturing treatment fluid for "big frac sand" jobs.

The stimulation models had a lot of screen-outs when the proppant mass was increased from 200 M-kg to 400 M-kg, and the screen-out limited fracture half-length growth. However, there were some fracture stage clusters that saw some improvement in fracture length growth. Secondly, the results shows that, on average, the middle clusters' "hydraulic" fracture half-lengths increased when the proppant was increased from 200 M-kg to 400 M-kg. Thirdly, the result of Figure 6-17 shows that some of the middle clusters were propped with sand when the proppant mass was doubled from 200 M-kg to 400 M-kg. For instance, the cluster C5 (fifth cluster) propped length increased from about 10 meters to 128 meters.

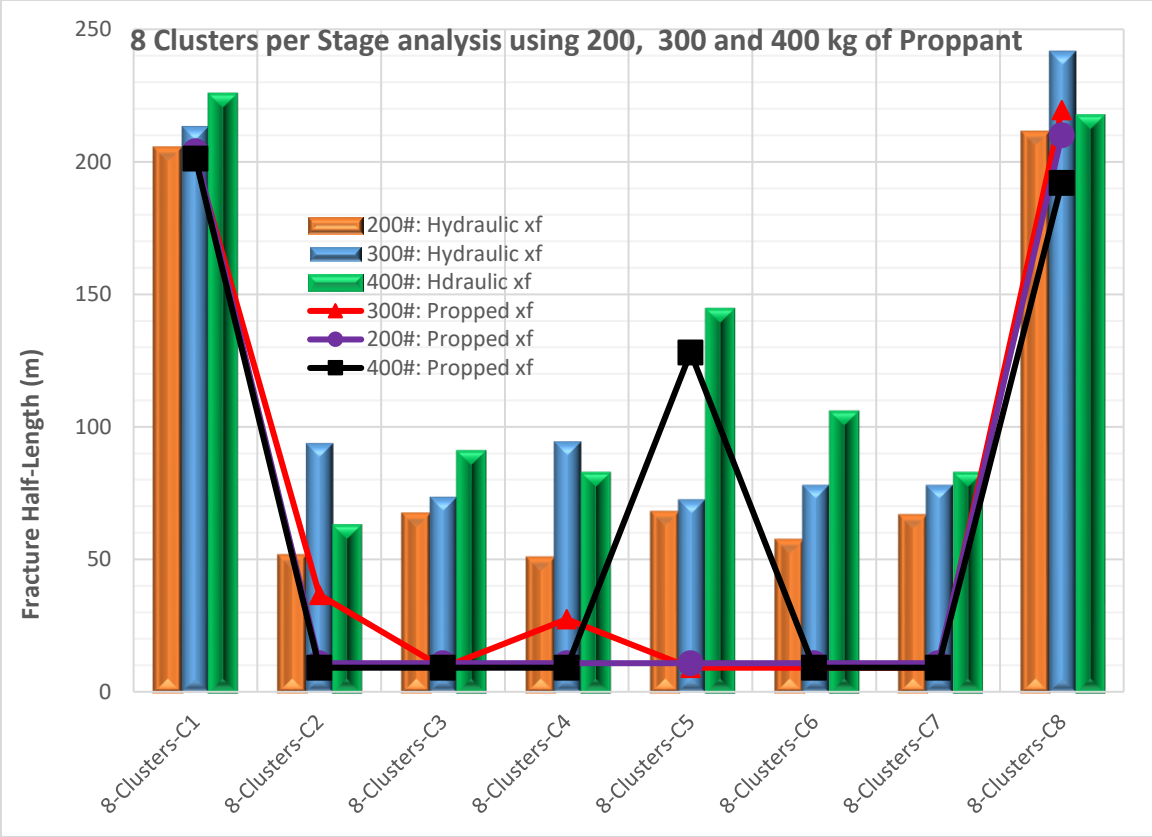

Figure 6-17: Results of eight fracture clusters per stage with different amount of proppant mass (200, 300 and 400) M-kg

The fracture clusters per stage modeled were from three clusters per stage to eight clusters per stage, but only the results of the seven and eight clusters would present here because the findings showed similar trends and patters in most the cases. Figure 6-18 shows the result for the seven clusters per stage and proppant mass from 200 M-kg to 400 M-kg.

The result of the seven clusters per stages shows the un-even distribution of fracture half-lengths in the clusters where clusters C1 was long and C7 was the longest, but the rest of the middle clusters were very short. This would make oilfield development and well spacing difficult to plan. Do operators plan for 250 meters or 500 meters well spacing, and what about well interference during stimulation treatment?

Another metric that is often used for optimization in hydraulic fracturing is the kilograms of proppant mass used per meter of the lateral section (kg/m or lb/ft). In Figure 6-18 the fracture cluster spacing was 14.3 meters or seven fracture clusters in one hundred meter interval. When the proppant mass used was increased from 2,000 kg/m to 4,000 kg/m (1,344 lb./ft. to 2,688 lb./ft.), there was no significant increase in fracture half-length (both hydraulic and propped) as in Figure 6-18.

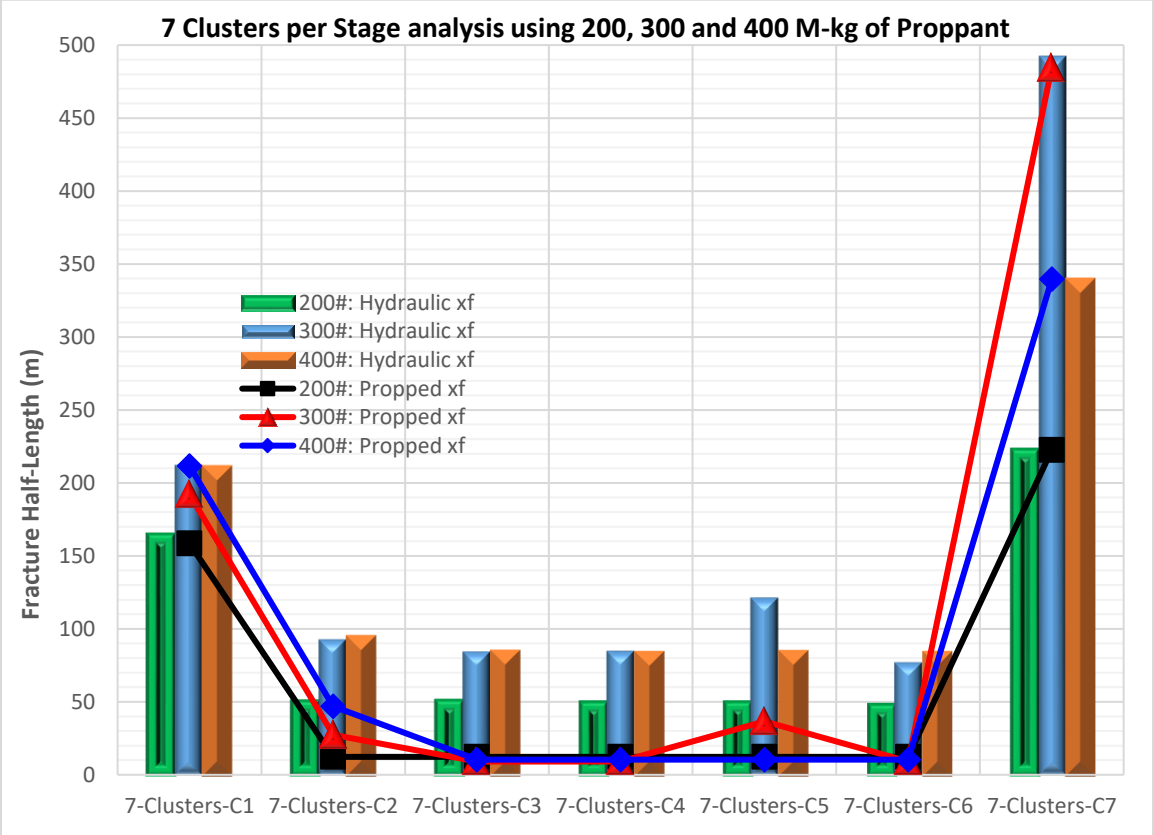

Figure 6-18 Results of seven fracture clusters per stage with different amount of proppant mass (200, 300 and 400) M-kg

The result shows that treating all the seven fracture clusters in the one hundred interval without isolation or means to divert treatment fluids to the middle clusters, would yield un-evenly distributed shorter fractures. However, putting more completion and zonal isolation equipment in the wellbore would substantially increase cost.

One of the biggest challenges of quantifying the effects of any stimulation optimization is the uncertainty of which parameters lead the improvements in the results, often measured in terms of well productivity or EUR. In this study, to measure the effects of the "big frac sands" and shorter fracture spacing, the results were normalized to the values obtained in the 200 M-kg fracture treatments case. Figure 6-19 shows normalized average "hydraulic" fracture half-lengths for different sets of clusters and proppant mass. The results answer two important questions; first, what fracture half-length improvements were observed compared to the 200 M-kg proppant mass for each fracture clusters per stage? Secondly, did the use of more proppant mass led to improved fracture conductivity per fracture clusters?

The results of Figure 6-19 shows that the "hydraulic" fracture half-length increased when proppant mass was increased from 200 M-kg to 400 M-kg, but only for the three clusters per stage to the five-clusters per stage. From 6 clusters per stage to eight clusters per stage, there was no clear colorations between proppant mass increases and improvements in "hydraulic" half-length per fracture clusters. Secondly, Figure 6-19 shows that there was clearly observable improvement in fracture conductivity for each clusters per stage when proppant mass was increased from 200 M-kg to 400 M-kg.

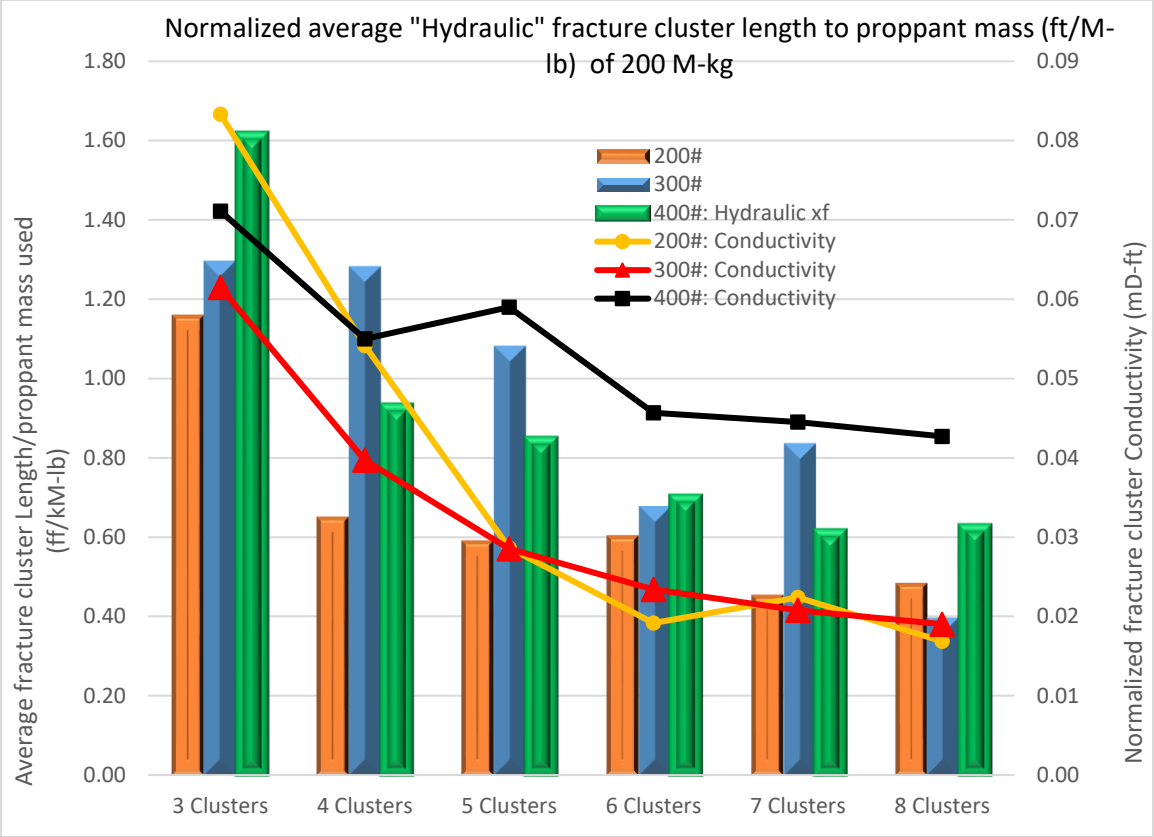

Figure 6-19: Normalized average "hydraulic" fracture clusters length to proppant mass of 200 M-kg

The summary of findings highlighted by Figure 6-19 suggest that putting more fracture clusters per stage and increasing proppant mass per stage would clearly lead to improved fracture conductivity, but would not always lead to increased fracture half-length per cluster.

Figure 6-20 shows normalized propped fracture half-length for different sets of fracture clusters and proppant mass. The results were normalized to the values obtained for the 200 M-kg treatments for each fracture clusters per stage. The major findings highlighted the results of Figure 6-20 was the propped fracture half-length increased when proppant mass was increased from 200 M-kg to 400 M-kg, but not linearly. Secondly, in

each fracture clusters per stage (from 3-to-8), the base case (200 M-kg) treatment values were the lowest. For instance, in the three clusters per stage, the base case had the lowest fracture half-lengths.

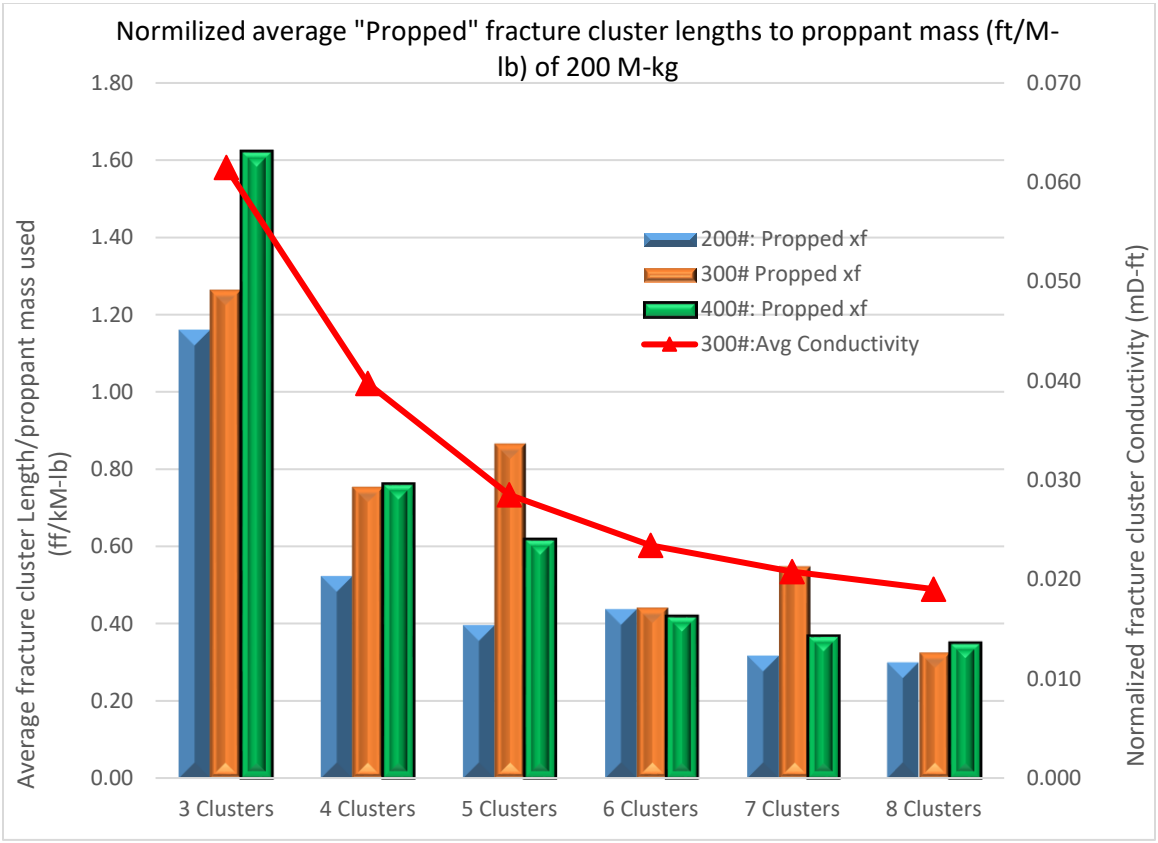

Figure 6-20: Normalized average propped fracture clusters length to proppant mass of 200 M-kg.

The thirdly major findings was that the fracture conductivity was inversely correlated to the number of clusters per stage in all the cases modeled. Similarly, the fracture half-length was inversely related to the number of clusters per stage, but the correlations was not as good as that of the fracture conductivity.

6.3. INTEGRATED RESERVOIR SIMULATION MODELS RESULTS

Three types of integrated reservoir simulation models were built; planar model (Figure 4-22), discrete model based on the micro-seismic mapping only (Figure 4-16), and hybrid model constructed from the integration of planar model and curvature data obtained from 3D seismic (Figure 4-24). Secondly, sensitivity analysis of different reservoir (ϕ, k) and fracture ($k_f w_f$, x_f) parameters that greatly affect the reservoir simulation models were investigated. Robust sensitivity analysis, history matching and model optimization was carried out.. After few parametric simulations to test which parameters have the greatest impact, 10 parameters were selected for sensitivity analysis and the results were compared to target (production history) values. Tornado chart were used to visualize which parameters had the biggest impact on well production.

The "best practices" for reservoir simulation and modeling are to first history match the global parameters that have the biggest impact on well performance. Secondly, to reduce error to an acceptable level (_+10%), well-by-well history matching is recommended especially if the static or dynamic reservoir simulation models would be used for optimization and forecasting. In this study both "best practices" were incorporated into the modeling, and the wells were history matched to pressure and cumulative production well-by-well.

Al-Jenaibi et al. (2011) presented a paper titled "Best Practice for Static & Dynamic Modeling and Simulation History Match Case – Model QA/QC Criteria for Reliable Predictive Mode" where the authors showed a workflow for modeling and history matching. The predictive quality and reliability of the model depends on the sensitivity

analysis parameters that were investigated and whether representative petrophysical properties and fracture dimensions were captured in the reservoir model.

6.3.1. Reservoir Model Sensitivity and Uncertainty Analysis -Results. The history matching part of the reservoir simulation took a lot of time, and required robust computing power. The “best practices” for reservoir simulation and modeling are to first history match the global parameters that have the biggest impact on well performance. Secondly, to reduce error to an acceptable level (_+10%), well-by-well history matching is recommended, especially if the static or dynamic reservoir simulation models would be used for optimization and forecasting. In this study, the wells were history matched to pressure and cumulative production for each well.

Figure 6-21 shows the workflow used for the reservoir simulations’ sensitivity analysis, history matching, optimization and uncertainty assessment. Two “best practices” that were built and strictly followed throughout the reservoir simulation improvements were; first, each step was built on the finding of the previous step, and expanded or limited the scope of the simulations. Secondly, if any of the major parameters in the reservoir simulation were updated or changed, then the whole process was repeated. Hence, there were multiple iteration and refinement of both the input parameters and the objective functions (OF).

The objective function (OF) in the workflow was defined as the input data from production history that the model needed to perfectly match based on set of parameters. For instance, in the history-matching task, the objection functions (OFs) were cumulative gas, cumulative oil, cumulative water and wellhead tubing and casing pressures.

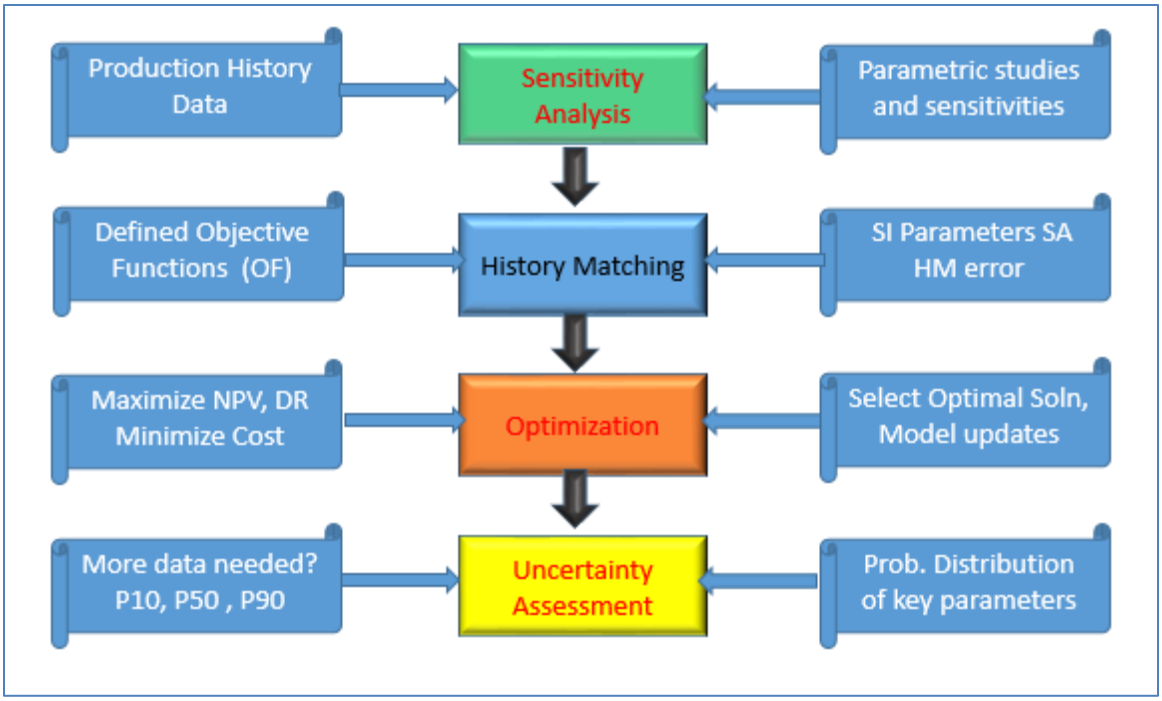

Figure 6-21: Steps and process used for the reservoir simulation's sensitivity analysis, history matching, optimization and uncertainty assessment

The sensitivity analysis (SA) was started with 20 parameters that were selected based on the understanding that the uncertainty can be modeled by independent uncertain parameters. After few simulation runs, the number of independent uncertain parameters were reduced using statistical significance test (i.e. t-test, f-test). However, some of the sensitivity analysis and history matching results would not be shared in this dissertation because of proprietary and intellectual rights concern raised by the company that provided us the data.

Table 6-2 shows an example of statistical results obtained from sensitivity and history matching modeling, which gives four important statistics about the reservoir model. First, the statistical result provided "model fitness" parameters such as "R-Squared" and "R-Squared prediction." In the results shown in Table 6-2, the R-Squared was 98.8%,

which suggest the model's regression equation fitted on the actual data was very good fit. Secondly, the result provides analysis of variance, which gives sum of errors and degree of freedom. The third section of the statistical analysis provides the most critical information about the effect of each parameter on the objective functions (OF), and whether the parameter is significant to the OF based on 95% CI (confidence interval). In Table 6-2, there were 10 parameters in the sensitivity analysis and history matching modeling, and nine parameters were statistically significant as shown by the t-test (Prob> |t|). If the t-test (Prob> |t|) is less than 0.05 (5%), then the parameter was significant.

The last section of Table 6-2 provides linear effect of each parameter on the objective functions (OF), and whether the parameter is positively or negatively correlated to the OF. For instance, the objective function (OF) in the example given by Table 6-2 was for cumulative gas sensitivity analysis. One of the surprising findings from the sensitivity analysis and history matching was the effect of the oil component, "Component C5-to-C7", on cumulative gas. As Table 6-2 shows, the mole fraction of the oil-yielding components, "C5-to-C7", was negatively correlated to the cumulative gas.

Plotting the parameters versus the coefficients given in the last section (coefficients in terms of actual parameters) of Table 6-2, would yield a bar chart similar to Figure 4-26 (given in section 4.3.3). The result shows that the three parameters that had the biggest impact on the objective function (OF = CumGas) were permeability, porosity and the mole fraction of components C5-to-C7. In addition, Table 6-2 shows that non-linear effects on the interaction of parameters such porosity * porosity was very significant. Polynomial regression models such as quadratic models are used for modeling second-degree parameter interaction effects. For instance, the fracture half-length and reservoir pressure

interactions showed that the two parameters were not important (from the quadratic modeling).

Table 6-2: Statistics results from the sensitivity analysis and history matching

Model Classification: Reduced SimpleQuadratic (alpha=0.1)					
Summary of Fit	**Results**				
R-Square	0.988078				
R-Square Adjusted	0.972963				
R-Square Prediction	0.958247		**Objective Function Name: CumGas**		
Mean of Response	9.68E+07				
Standard Error	1.67E+04				
Analysis of Variance					
Source	**Degrees of Freedom**	**Sum of Squares**	**Mean Square**	**F Ratio**	**Prob > F**
Model	10	1.70E+16	1.70E+15	137.746	<0.00001
Error	28	3.46E+14	1.24E+13		
Total	38	1.74E+16			
Effect Screening Using Normalized Parameters (-1, +1) (Sample test !)					
Term	**Coefficient**	**Standard Error**	**t Ratio**	**Prob > |t|**	**VIF**
Intercept	1.07E+08	1.38E+06	77.1537	<0.00001	0
Component C5-to-C7(0.05, 0.15)	906525	915118	0.99061	0.33036	1.14
Component C2-to-C4 (0.05, 0.11)	-2.26E+06	943197	-2.39611	0.02349	1.18
Fractue Length(250, 500)	8.41E+06	959319	8.76702	<0.00001	1.19
Porosity(0.04, 0.07)	5.02E+06	1.21E+06	4.14436	0.00029	1.63
Reservoir Pressure (15000, 29000)	1.42E+07	1.13E+06	12.5047	<0.00001	1.5
PermeabilityI(5E-05, 0.0005)	2.07E+07	956807	21.6055	<0.00001	1.28
Fracture Length*FractureLength	-3.72E+06	1.55E+06	-2.40621	0.02297	1.2
Porosity*Porosity	3.56E+06	1.71E+06	2.0776	0.04703	1.08
Res Press* Res Pressure	-1.60E+07	1.96E+06	-8.14711	<0.00001	1.2
PermeabilityI*PermeabilityI	-1.05E+07	1.82E+06	-5.79044	<0.00001	1.48
Coefficients in Terms of Actual	**Parameters**				
Term	Coefficient				
Intercept	-1.91E+08				
Component C2-to-C7	1.81E+07				
Component C5-to-C7	-1.00E+08				
Fractue Length	353713				
Porosity	-1.99E+09				
Reservoir Pressure	16360.4				
PermeabilityI	5.23E+11				
Fracture Length*Fracture Length	-337.795				
Porosity*Porosity	2.28E+10				
Res Press* Res Pressure	-0.325883				
PermeabilityI*PermeabilityI	-1.05E+15				

Figure 6-22 shows model quality check for the objective function (OF), and displays how close the simulated data matched the actual data. The line (x = y) or the 45 degree line represents a perfect match, and any data points that lie on the line are perfectly predicted by the model. The two lines on each side of the 45 degree line are the lower and upper bound of 95% confidence interval. Any points within the confidence interval are considered significant, and very good match. Figure 6-22 shows reservoir model history matching for well A's cumulative gas, and the result shows it was very good match.

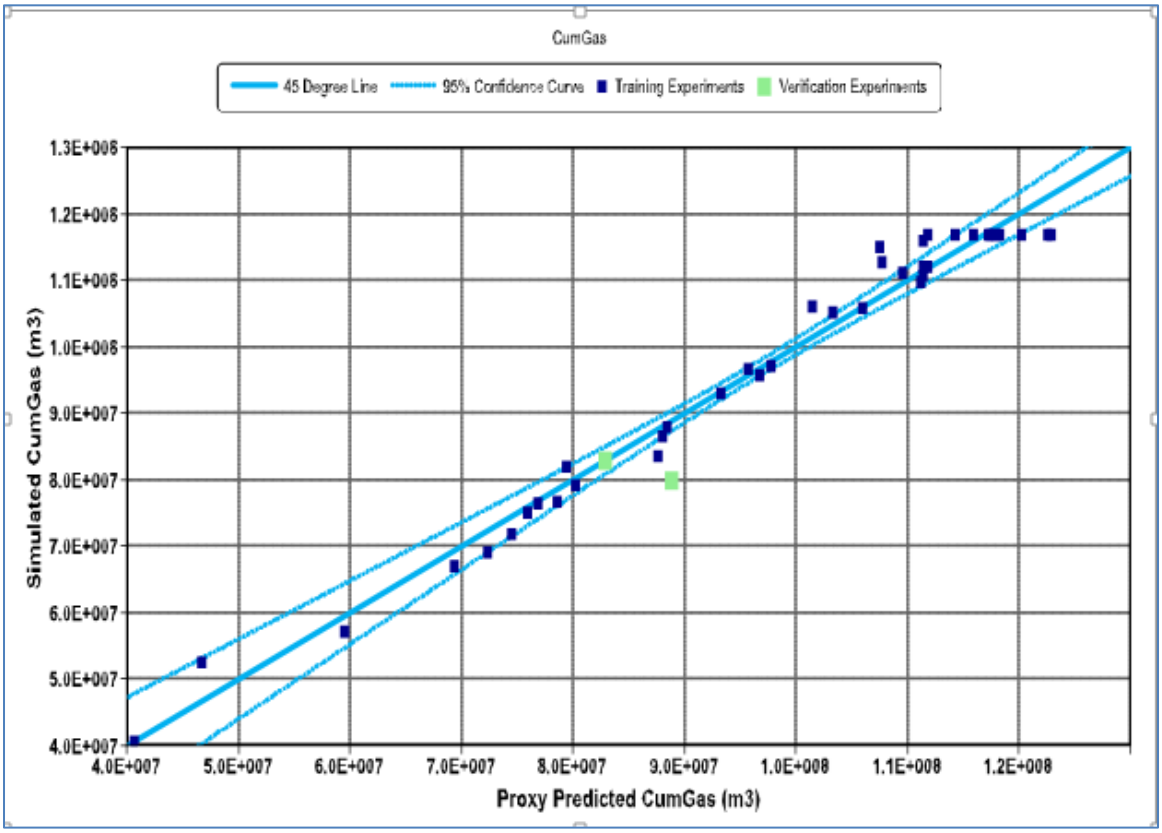

Figure 6-22: Model quality check (QC) between the simulated data and actual production data

Figure 6-23 shows the results of history matched cumulative gas production for well A. The result shows that the simulated data closely matched the actual well cumulative gas production. Secondly, the history matching error was less than 10%, which is within the range of acceptable error (it best practice to keep error within $\pm 10\%$).

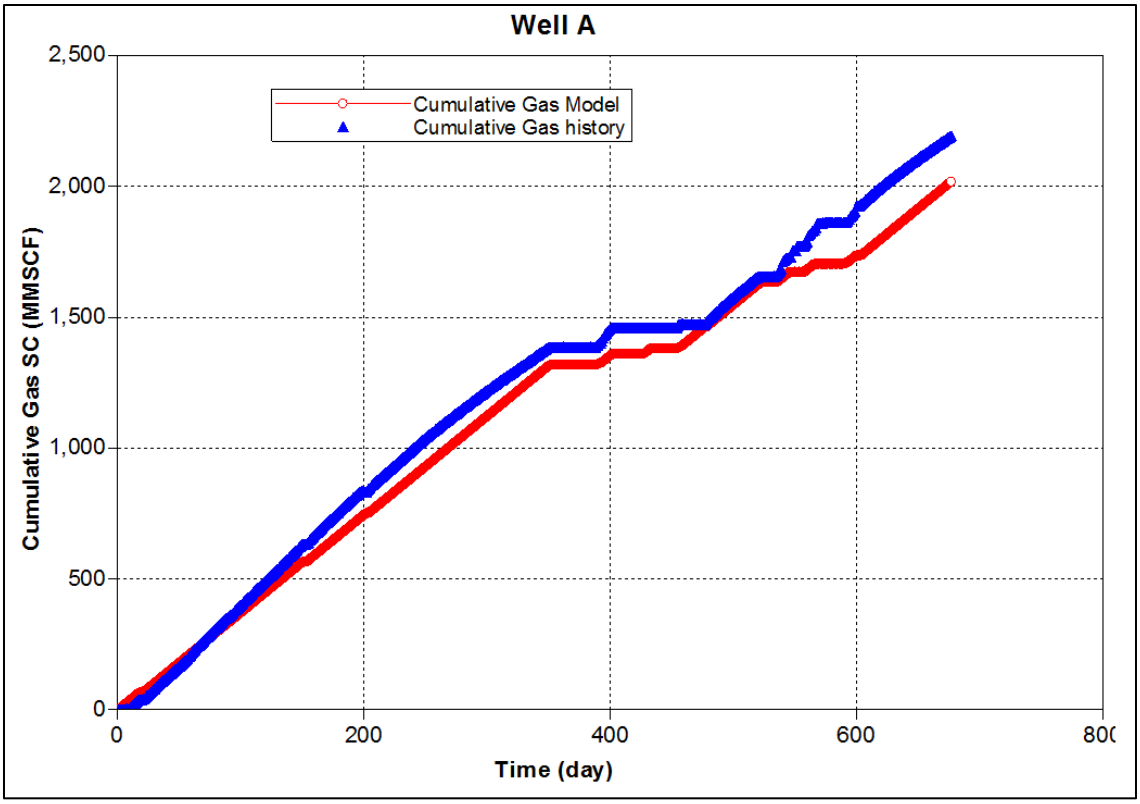

Figure 6-23: Results of reservoir simulation history matching (Well A: Cumulative gas)

Figure 6-24 shows the history matching results for the wellhead pressure of Well A, and the result was a perfect match. It was surprising that the changes in reservoir simulation model matched perfectly that of field pressure history data even though the well was sometimes cyclically shut-in. In reservoir simulations, it is very difficult to history

match wells that are cyclically shut-in or have production interruptions because multiple external parameters can interfere such as nearby wells or stimulation treatment in a different pattern. Some of the external parameters can have transient effect, which the model might not be capture instantaneously.

The predictive quality and reliability of the model depends on the sensitivity analysis parameters that were modeled and whether representative petrophysical properties and fracture dimensions were captured in the reservoir model.

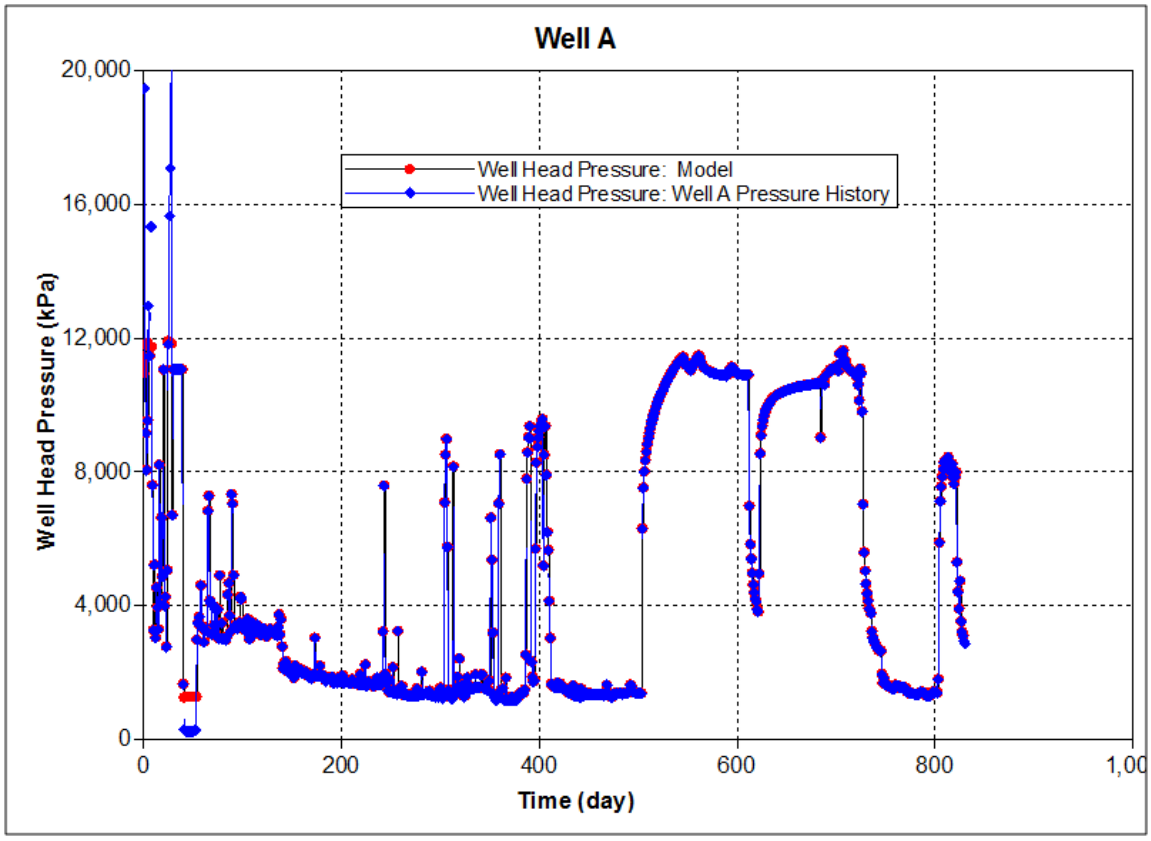

Figure 6-24: Results of reservoir simulation history matching for Well B pressure (showing cyclical shut-ins)

6.3.2. Planar Fracture Models Results. The planar reservoir simulation model (similar to Figure 4-22) was history matched to well production data. The assumptions in the planar model was that there were no natural fissures and that the induced fractures are bi-wing. Secondly, fracture dimensions from the calibrated fracture model were imported into the reservoir model and used for the construction of the planar reservoir simulation model.

In reservoir simulation, the "best practices" are to follow systematic process of quantifying the sensitivity of the objective function (OF) to each parameters, and then refining the number of parameters by eliminating the insignificant variable using statistical test (i.e. interval confidence, t-test). Secondly, develop methods to measure the effect of parameter changes on the objective function (OF) using tools such as polynomial regression models (i.e. linear, quadratic).

Thirdly, select normalization scale method to measure and reduce error (on OF such as production history), especially in the case of history matching error. Assign weights to each of the objective function (OF) based on the understanding and reliability of the data. Fourth, select the set of values from each parameter that give the "optimal solution" model. Percentage error (ε %), which is the difference between simulated data and measured data, is an indicator of the quality of the model. Fifth, the model optimizations requires testing what operating conditions would provide the best outcome. For instance, testing well deliverability or impact of changing wellhead pressure/bottom-hole pressure on well productivity, EUR (estimated ultimate recovery) and well economics such as NPV (net-present value) and ROI (return on investment). The process would provide different scenarios for different operation conditions, allowing oilfield operators to quantify the

uncertainty involved in any decision selected. In this study, all the "best practices" mentioned above were incorporated into the reservoir simulations models used in the dissertation.

In history matching, the global parameters that have the biggest impact on well performance were given bigger weights. Secondly, to reduce error to an acceptable level like($\pm 10\%$), well-by-well history matching is recommended. This is especially significant if the static or dynamic reservoir simulation models would be used for optimization and forecasting. In this study, both "best practices" were incorporated into the modeling, and the wells were history matched to pressure and cumulative production well-by-well.

Figure 6-25 shows the planar reservoir model, which was one of the three reservoir simulation models created to study effect of fracture complexity or lack of, on well performance. The figure also shows hydraulic fracture stages and well trajectory overlaid with micro-seismic events for each stage.

The results from the 3D planar reservoir shows three important findings; first, the planar model shows that the hydraulic fracture stages were confined to the Upper Montney Formation, and there was no fracture height growth (which was also confirmed by the micro-seismic mapping- see Figure 4-16). Secondly, the planar model showed that the fracture stages at the toe of the horizontal well had "representative" fracture dimension and every stage had fracture propagation, especially fracture half-length. This finding contradicted the fracture dimensions obtained from the micro-seismic survey, which showed no fracture dimensions for the stages at the toe (probably caused by location uncertainty or signal to noise ration issues). Thirdly, the planar reservoir model did not model fracture complexity or the effects of secondary fractures on well performance.

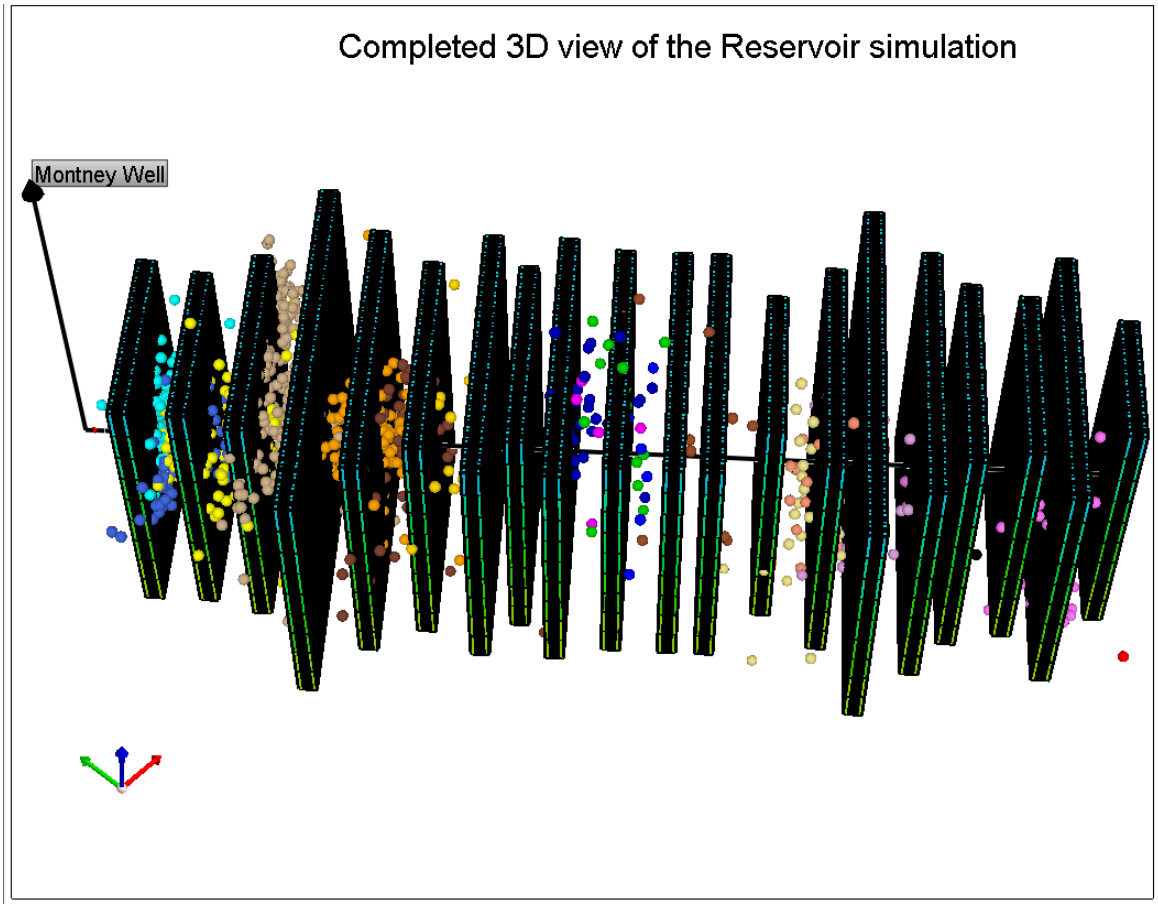

Figure 6-25: 3D view of the Reservoir simulation model showing fracture stages, micro-seismic survey and well trajectory

6.3.3. Hybrid Model (Integration of Planar Model and Curvature Data from 3D Seismic). The micro-seismic mapping data showed the presence of complex fractures in some of the hydraulically fractured stages in Montney Formation. For instance, figures 6 and 7 show that fracture stage 16 in wells A and B indicated the existence of complex fractures in some of the stages. Curvature data from 3D seismic can be used to qualitatively estimate fracture density, spacing and orientation. (Klein et al. 2008) presented a paper titled "3D Curvature attributes: a new approach for seismic interpretation" where he stated that curvature attributes respond to bends and breaks in the seismic reflector and are not

affected by changes in amplitude caused by variations in the fluid and lithology. There are different methods of computing curvature data such divergence formulation (Donias et al. 1998) and fractional derivatives (Chopra and Marfurt 2007) which is given as

$$F_\alpha\left(\frac{\partial \mu}{\partial x}\right) = -i(k_x)^\alpha F(\mu) \quad \text{...(54)}$$

Where

F = Fourier transform, and α = fractional real number (ranges between 1 and 0)

μ = an inline or crossline component of reflector dip

k_x = curvature volume at spatial location x.

Figure 6-26 (a) shows curvature data map from 3D seismic showing location of natural fracture (highlighted in red circle). The darker gray area in the curvature map indicate presence of natural fissures. The figure also shows micro-seismic survey (showing location of hydraulic fracture stages and direction) and relative interaction of induced fractures and natural fissures. Figure 6-26 (b) shows the hybrid reservoir simulation model that was built by integrating planar fracture model and curvature data from 3D seismic. The natural fissure networks (DFN) had permeability of 0.001 mD, and interacted with some of the fracture stages as shown in Figure 6-26 (b). The sensitivity of the hybrid reservoir model to the natural fissure networks (DFN) permeability was investigated. The permeability ranges studied were from 0.0001 mD to 0.001 mD, and the results showed that though well performance increased with higher permeability of the DFN, the hybrid model still tracked the planar model in terms of well productivity and EUR. However, after

10 years of production, the hybrid DFN model started performing lower than the planar model as shown by Figure 6-30.

One of the questions that came up in the research was “do natural fractures have higher permeability than the reservoir matrix permeability?” The answer is “it depends on a lot of factors” because if the natural fractures are filled with the same rock mineralogy as the reservoir matrix, then the heterogeneous deformities that created the fractures might have changed the mineralogy of the fracture faces. Previous research from outcrops have revealed the presence of cemented fractures (Engelder et al. 2009).

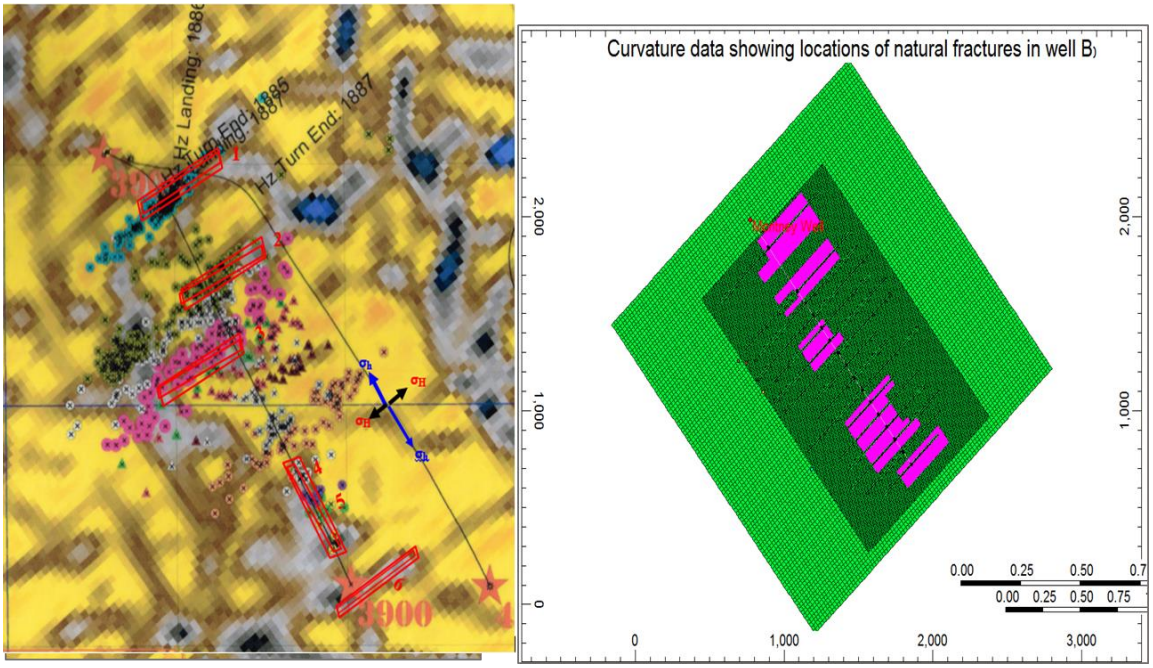

Figure 6-26: Curvature data map (location of natural fracture) and (b) reservoir model showing added natural fissures to the planar model

Cementation (filling of pore space by clay/cement during the diagenetic period) in rock layers reduces reservoir quality such as porosity and permeability (Jonas and Mcbride, 1977), and natural fractures often are filled with clays/cementation. In this study, secondary

fracture conductivity of 0.0001 mD-ft. was used initally to test the effect of fracture complexity on well performance. However, in subsequent simulation runs, the range of conductivity studied was from 0.001 mD-ft to 0.0001 mD-ft. The resulted showed that when the secondary fracture conductivity was increased, the well performance also improved, but still trailed that of the planar reservoir model.

6.3.4. Stimulated Reservoir Volume (SRV) Model Built from Micro-seismic Survey. The discrete fractured reservoir model was constructed using the micro-seismic mapping data, and fracture dimensions were captured through the micro-seismic magnitude and moment. However, only micro-seismic events that were in continuous grid-blocks were included in the model. Figure 6-27 shows the distribution of the recorded micro-seismic events for each hydraulic fracture in 3D geological reservoir model. The figure shows that the micro-seismic events were sparsely populated in the middle section of the horizontal well, and were non-existent at the toe of the lateral.

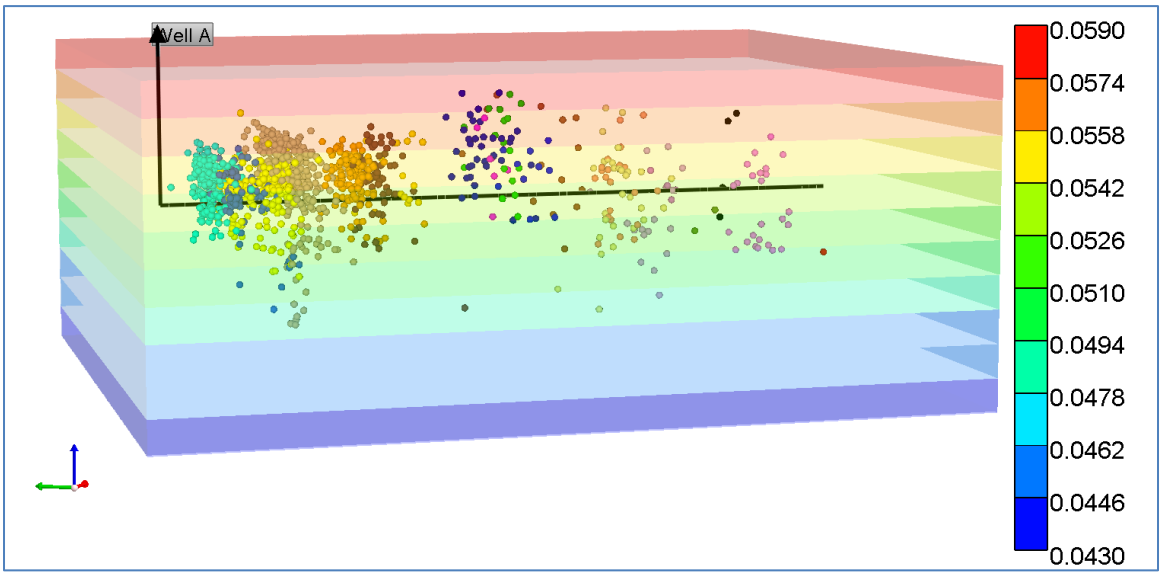

Figure 6-27:3D Reservoir simulation model showing micro-seismic mapping for each hydraulic fracture stage of Well A

Figure 6-28 shows the discrete fracture networks (DFN) and stimulated reservoir volume (SRV) built from the micro-seismic mapping data that were continuous within the grid-blocks of the reservoir model. The use of micro-seismic data was limited for quality control purpose, so that outlier micro-seismic survey "data points" were not included in the construction of the model.

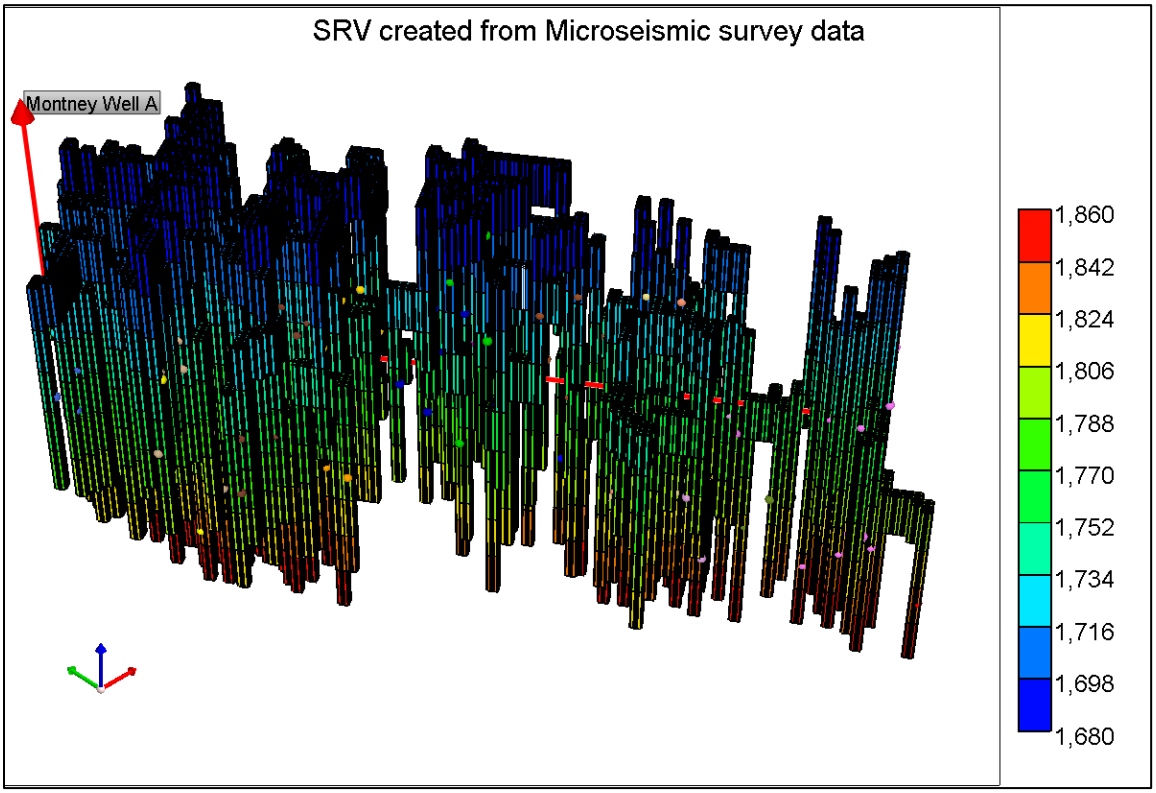

Figure 6-28: Stimulated reservoir volume (SRV) build from micro-seismic mapping (that were built from continuous grid-blocks) of the reservoir model

The result showed that the stimulated reservoir volume (SRV) computed in Figure 6-28 was smaller than that of the planar fracture model (shown in Figure 6-25). This shows that micro-seismic survey may not capture the fracture mechanisms that created the

fracture network (Cipolla and Wallace 2014). Secondly, well productivity and recovery was also smaller in the discrete fractured model compared to the planar model when only connected and continuous grid-blocks of stimulated reservoir volume (SRV) were used. However, if all the micro-seismic events were assumed to be connected and continuous, the model would capture large swath of stimulated reservoir volume and may not be representative of the actual hydraulically stimulated area or volume.

6.4. COMPARISON OF INTEGRATED RESERVOIR SIMULATION RESULTS FROM THE THREE MODELS.

There were three integrated completions and reservoir models (a planar model, and two DFN models (hybrid and SRV from the micro-seismic data) that were built for each reservoir type studied. Figure 6-29 is one of the reservoir simulation models built for the planar and hybrid DFN models. Similarly, Figure 6-29 shows pressure drawdown profile after 30 years of production, and highlights two important findings. First, there was no pressure drawdown outside the stimulated reservoir area, which means no depletion and production came from outside the stimulated area. Secondly, the results shows the impact of shorter fracture half-lengths, which depleted very small area and contributed less to the well production. Additionally, the result shows that in low and ultra-low permeability reservoirs, a lot of reserves are left behind even after years of production. Figure 6-29 shows that outside the hydraulic fractures, there was uneven depletion and the sand-face reservoir pressure was about 10,000 KPa in most of the stimulated area. These findings highlight the need for developing enhanced oil/gas recovery technology for the unconventional resources, which has dismal recovery factors, often in the single digits (less than 10%), and leaves behind a lof of the oil and gas reserves in the ground.

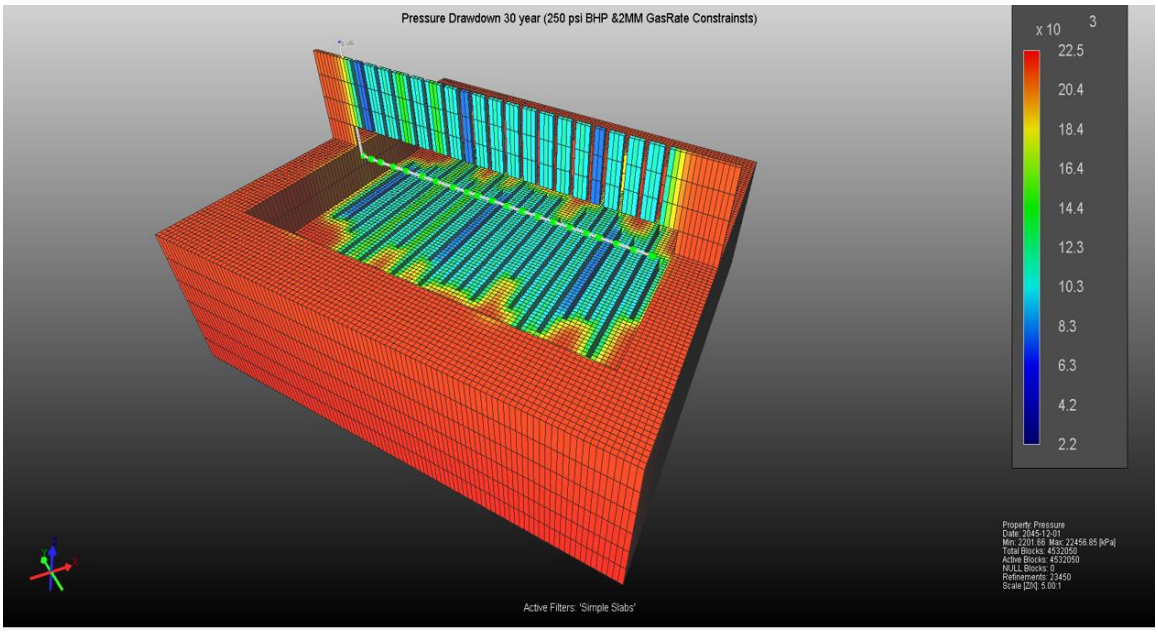

Figure 6-29: Reservoir simulation model showing pressure drawdown profile after 30 years of production for the planar and hybrid DFN reservoir models

Figure 6-30 shows comparison of cumulative gas production for the three integrated reservoir simulation models; planar model (shown by Figure 6-25), hybrid DFN model (shown by Figure 6-26), and SRV model built from MS (shown by Figure 6-28). The results show two important findings; first, for the first 10 years of production, all the three reservoir models forecasted similar trends and had similar cumulative gas production values. Additionally, for the first 15 years, the hybrid DFN model and the SRV (built from MS) had similar production forecasts as shown by Figure 6-30. Secondly, the planar model outperformed the other two models (hybrid DFN model and SRV model built from the micro-seismic) in terms of well productivity and EUR (estimated ultimate recovery). On the other hand, the SRV model built from the micro-seismic survey had the lowest well productivity and EUR among the three integrated reservoir simulation models.

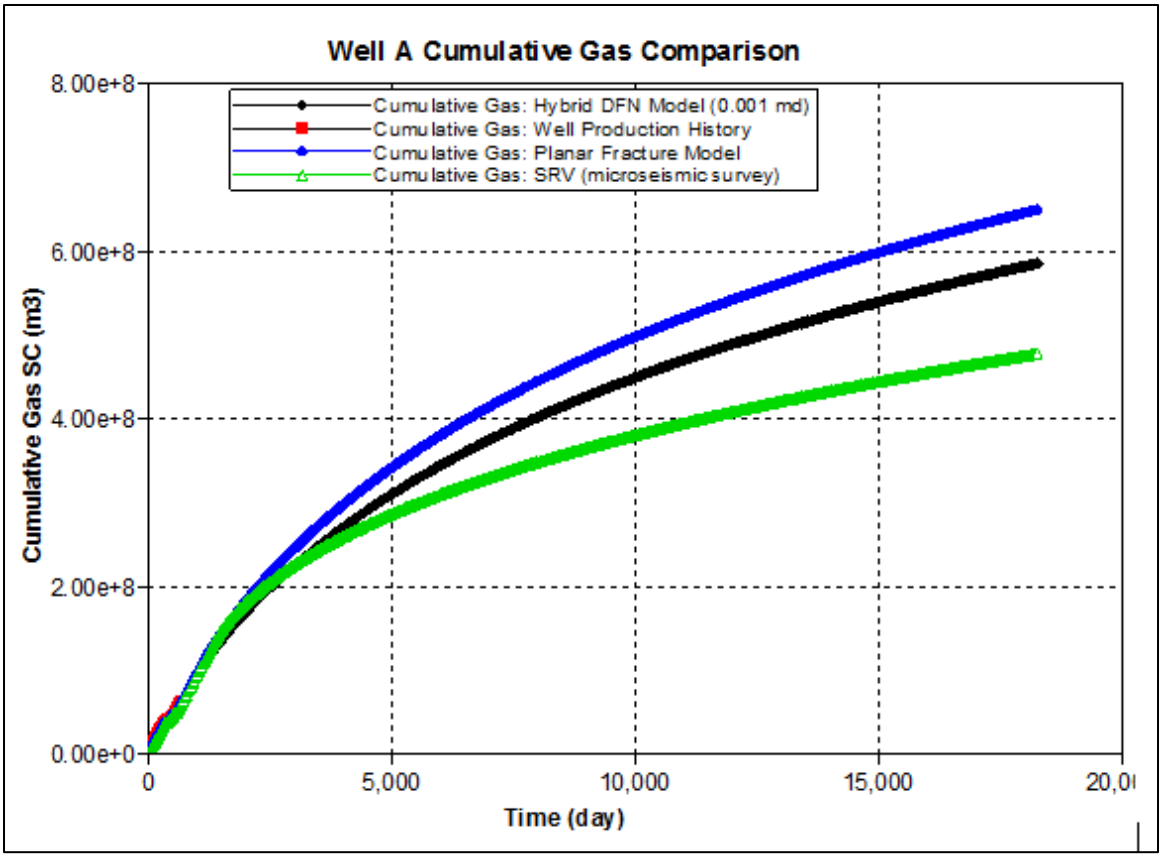

Figure 6-30: Results from the reservoir simulation models (planar and Hybrid models) for cumulative gas

The hybrid DFN model (which was constructed by adding curvature data from 3D seismic to the planar model to account for the existence of discrete fissures networks (DFN) in the reservoir) had the second best performance in terms of well productivity and EUR. The permeability of the discrete fissure networks was assumed to be 0.001 mD (in the reservoir model), which is slightly higher than the reservoir permeability of 0.00018 mD. Secondly, the discrete fissure networks (DFN) location and density were guided by the curvature data from 3D seismic, and natural fractures existed only in some fracture stages of the well as shown by. Additionally, stress dependent permeability was incorporated into the reservoir simulation models and might have impacted the hybrid model

disproportionately since it has both induced hydraulic fractures and discrete fracture networks (DFN).

The other major findings of the study was that in all the wells used in the study, and other wells (i.e. Lower Montney Formation wells) where there was micro-seismic data and curvature data available, the results showed that there was a range of 5-to-10 hydraulic fracture stages that interacted with natural fissures in each of those wells. For instance, Well A, which had 20 stages and was in the Upper Montney Formation, had eight fracture stages that interacted with natural fissures. Additionally, well B, which had 16 stages and was in the Upper Montney Formation had six fracture stages interact with secondary fissures. Well B was better producer even though there were problems during the stimulation treatment, and only 16 out of the 20 hydraulic fracture stages planned were eventually completed.

Figure 6-31 shows comparison of cumulative oil production for the three integrated reservoir simulation models, and the results of the models were different from that of Figure 6-30 (cumulative gas production plot). First, though the planar model eventually outperformed the other two models in terms of well productivity and EUR, the outcome was not definitive in the early years of production. In fact, for the first 30 years, the SRV model built from micro-seismic survey had the highest cumulative oil production as shown by Figure 6-31. Secondly, the hybrid DFN model (shown by Figure 6-26) had the lowest cumulative oil production among the three integrated reservoir simulation models.

The construction of the SRV model from micro-seismic survey had two major uncertainties; first, quantifying the number of micro-seismic events that should be included in the stimulated reservoir volume (SRV) calculation, was a big challenge. It require a

criteria-based method for qualitatively selecting representative micro-seismic mapping data that accurately captured stimulated area. Secondly, whether or not to include discontinuous micro-seismic events in each fracture stages for the determination of fracture dimensions and geometry. These two major uncertainties made it difficult to really compare the result of the SRV model (built from MS) to the other two integrated reservoir simulations models. In the final analysis, only outlier micro-seismic events were omitted in the construction of the SRV model, and in most fracture stages, the micro-seismic survey fracture half-length was used in the model.

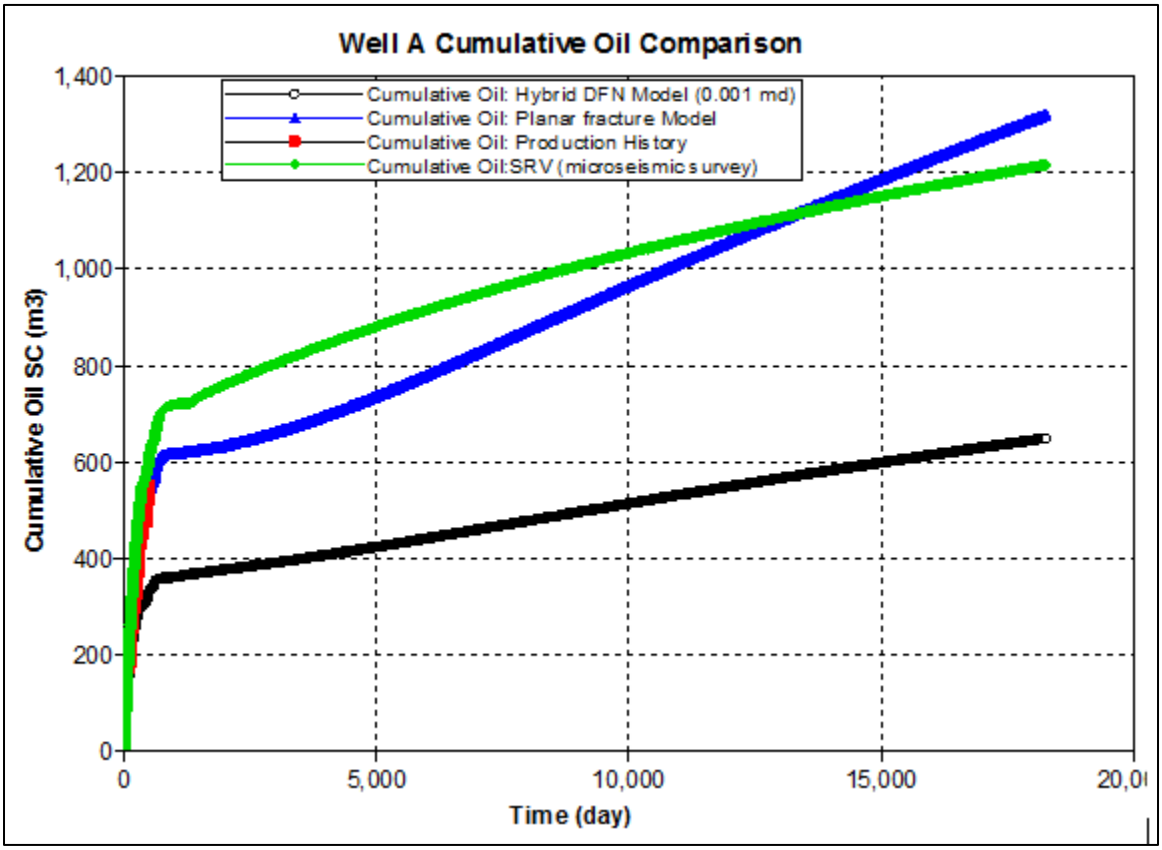

Figure 6-31: Results from the reservoir simulation models (planar and Hybrid models) for cumulative oil

6.5. NUMERICAL RESERVOIR SIMULATIONS VERSUS RATE-TRANSIENT ANALYSIS (RTA) RESULTS

Hydraulically fractured horizontal wells in unconventional resources exhibit transient flow behavior. On a log-log plot, transient flow, for both rate and pressure analysis, can be identified by having one-half (1/2) slope. In the case of DFIT (diagnostic fracture injection test) analysis, if the well is shut-in until the fracture closes, the after-closure analysis (ACA) and its log-log plot can provide other flow regime identifications such as radial flow (i.e. slope of one) and spherical flow (with slop of 3/2).

Production data analysis using rate transient analysis (RTA) in unconventional reservoirs has gained wide application because RTA is less technical, easier and requires lass input data compared to reservoir simulations. Secondly, RTA uses solutions that were developed previously for well testing (i.e. type-curves, decline curve analysis). However, even though RTA calculates two of the most important parameters in production data analysis (k_{SRV} and x_f), there is a lot uncertainty in the well productivity and EUR obtained from RTA. The problem with RTA is the non-uniqueness of the solution obtained from it.

The uncertainty of any parameters obtained from RTA models are magnified if the well displays long-term transient flow, which are common ultra-low permeability reservoirs such as shale gas reservoirs. However, RTA models provide reliable and valuable information from wells exhibiting boundary dominated flow (Anderson and Liang 2011).

Figure 6-32 shows production data for well A (gas and condensate rates) and pressures (tubing and casing). This was one of the production data used for the RTA modeling to extra information such as stimulated reservoir permeability (k_{SRV}) and average fracture half-length (x_f). Well A's production data reveals two important points, which

would late shade light on the results obtained from the RTA modeling. First, Figure 6-32 shows that the gas rate and tubing pressure remained constant throughout (as shown by the dashed black-line), which suggested choked well. Secondly, the condensate rate was very volatile, and the liquid yield (MMcf/bbl.) rapidly decreased close to zero.

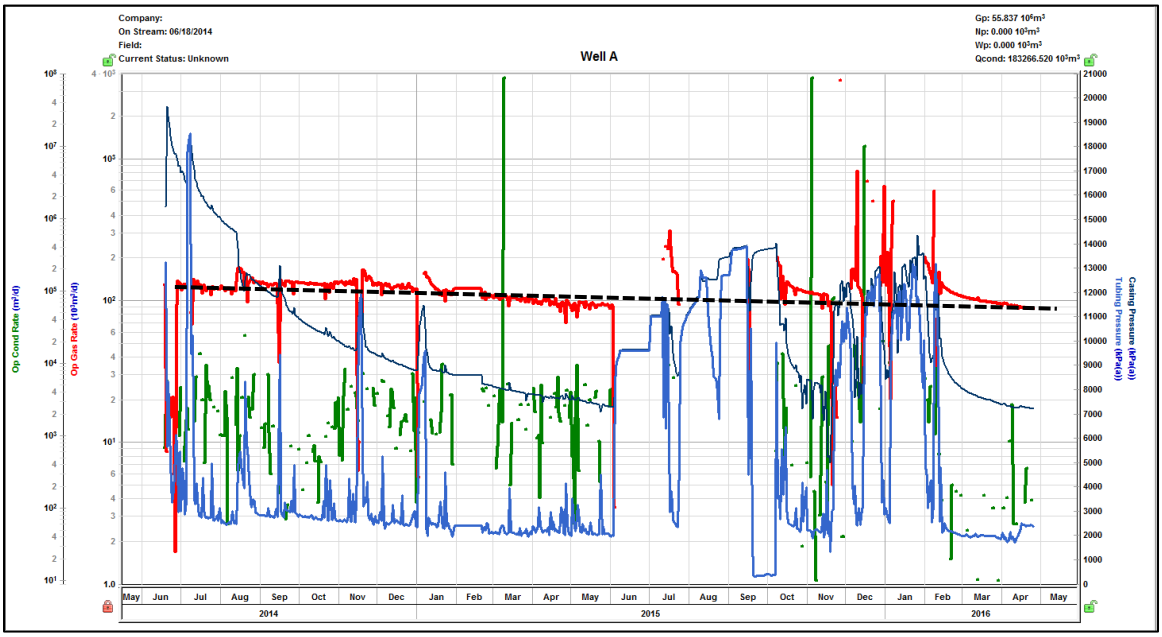

Figure 6-32: Well A production data (gas and condensate rates) and pressure (tubing and casing)

The RTA modeling used equations 46 and 47, and Figure 6-33 shows normalized pressure versus square root time. The log-log plot of $\left({P_i - P_{wf}}/{q}\ vs\ \sqrt{t_{sup}}\right)$ is usually called the "square root time plot", and the slope (m) was used to calculated the stimulated reservoir permeability (k_{SRV}) and average fracture half-length (x_f). The square root plot requires input of the reservoir permeability in order to estimate the average fracture half-

length and vice versa. Hence, RTA gives non-unique solution for both parameters. Figure 6-33 shows the RTA analysis for well A, and when the reservoir permeability obtained from the reservoir simulations models (CMG) were fed into the RTA model, it calculated average fracture half-length of 76 meters (shown in blue circle). The fracture half-length (x_f) from the RTA was a lot smaller than the 300 meters obtained from the reservoir simulation model. Secondly, the RTA analysis of well A production data showed that the well did not reach the end-to linear flow time (t_{EL}). This analysis was confirmed when the production data showed it does not fit the boundary dominated curve shown in Figure 6-33. There were some noise in the production data because of cyclical shut-in, but most of the data fitted very well on the linear flow. The dashed red line is the P50 estimate of the linear flow end time (t_{EL}).

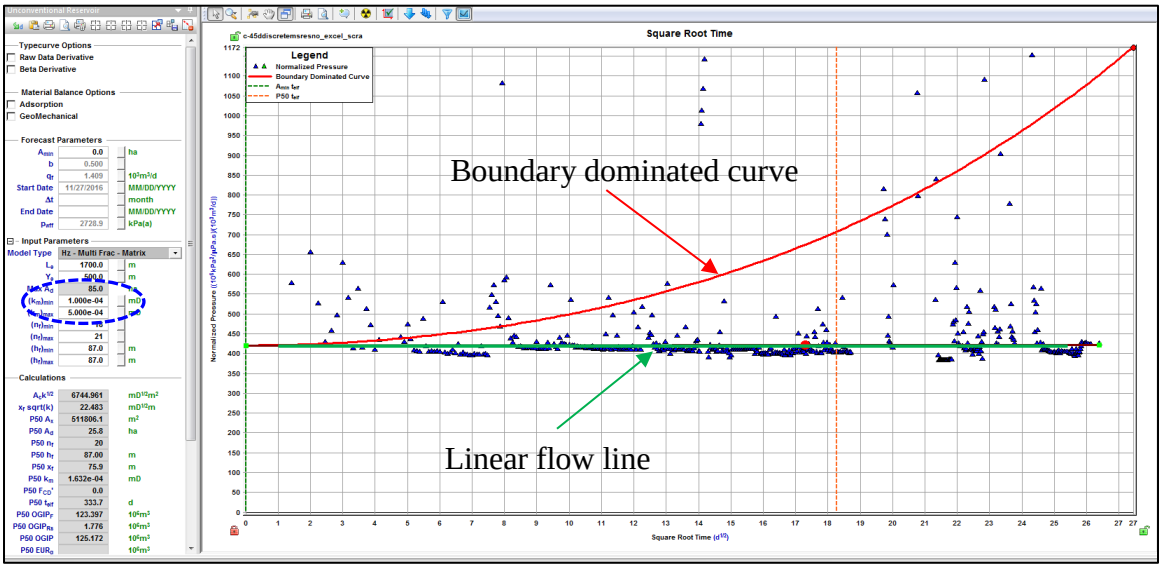

Figure 6-33: Square root time plot showing linear flow line and boundary dominated curve

Figure 6-33 shows allowable A_x versus allowable A_d, which is used to define the estimated range for stimulated reservoir volume (SRV). Figure 6-33 shows four parameters calculated from the square root plot, which are A_x (exposed area of the fractures), A_d (drainage area of the reservoir), P50 fracture half-length, and reservoir permeability. The reservoir permeability (k = 0.0001632 mD) shown in Figure 6-33 was similar to the reservoir permeability (k = 0.00016 mD) obtained in the reservoir simulation models. However, fracture half-lenghth (x_f) was 300 meters in the reservoir simulation model.

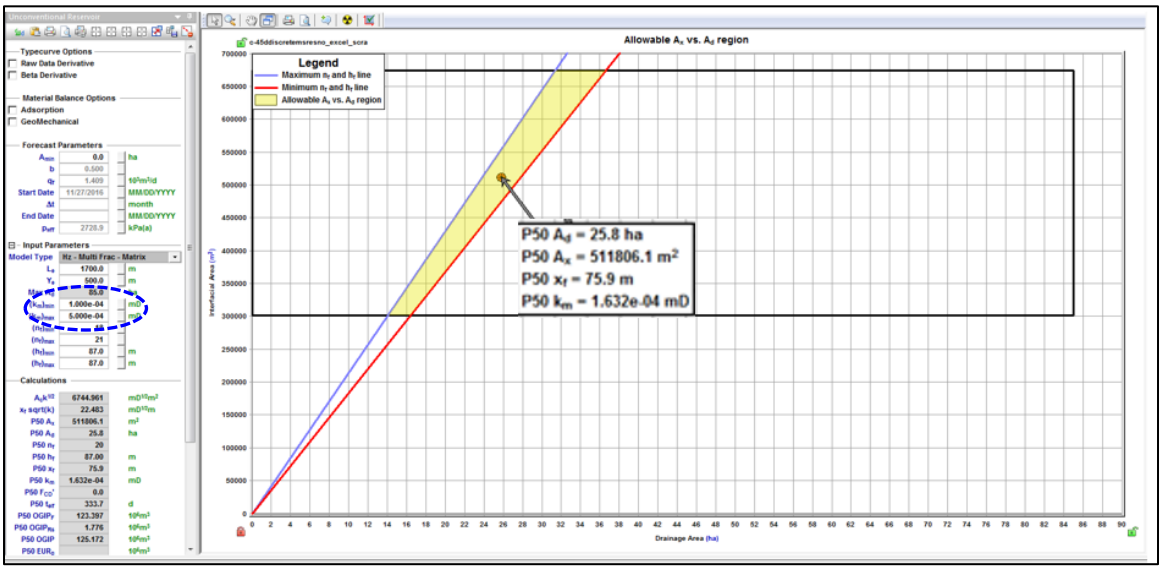

Figure 6-34: Plot of Allowable A_x versus A_d to calculate SRV (stimulated reservoir volume)

To investigate the non-uniqueness solutions of the RTA modeling, the range of reservoir permeability input into the model were adjusted to (k =0.00001 mD to k = 0.0005 mD). In the RTA results shown in Figure 6-33, the range of reservoir permeability were (k =0.0001 mD to k = 0.0005 mD). Figure 6-35 shows another square root time plot of RTA

demonstrating the RTA's non-uniqueness solutions. The result in Figure 6-35 shows the RTA model determined that well A did not reach the end-to linear flow time (t_{EL}). Hence, there was no P50 estimate of the time to the end of linear flow (t_{EL}). There was no dashed red line on the square-root time plot in Figure 6-35, indicating the location of (t_{EL}). Figure 6-35 also displays the boundary-dominated curve, which still does not fit the data, and the liner flow line. For the RTA analysis to be valid, the production data must clearly show the time to the end of linear flow (t_{EL}).

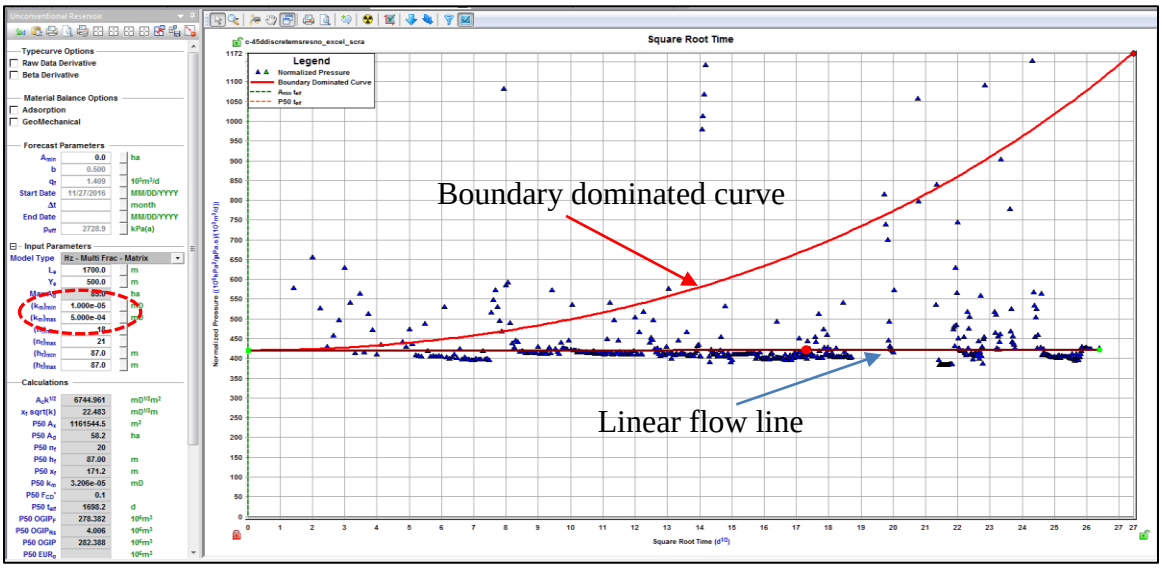

Figure 6-35: Second square root time plot showing non-uniqueness of RTA solutions

Figure 6-36 the Second plot of Allowable (A_x) versus (A_d) to calculate SRV (stimulated reservoir volume), highlighting the non-uniqueness of RTA solutions. The previously obtained four parameters from the RTA model, which were A_x (exposed area of the fractures), A_d (drainage area of the reservoir), P50 fracture half-length, and reservoir

permeability have changed in the second RTA model results. For instance, P50 for A_d was 25.8 hectares (ha) versus A_d = 58.2 (ha) in the second RTA model. Similarly, P50 for A_x was 511806.1 m^2 versus A_x = 1161544.5 m2, while x_f was 75.9 meters versus x_f = 171.2 meters, and the reservoir permeability was (k = 0.000163 mD) versus k = 0.00003206 mD in the second model.

While rate transient analysis (RTA) provides some useful information, it can also mislead or under-estimate well productivity and EUR (estimated ultimate recovery). When the results from RTA were compared to the results from the reservoir simulation model, this study showed that RTA has non-uniqueness of solutions problems, under-estimates fracture half-length, reservoir permeability and overall well productivity. Previous study conducted by (Moinfar et al. 2016) stated that "RTA under-predicted EUR by 6% to 17% when two years of production history was available", and when very short production data, 3 months to 2 years, "the under-estimation increased to 60%."

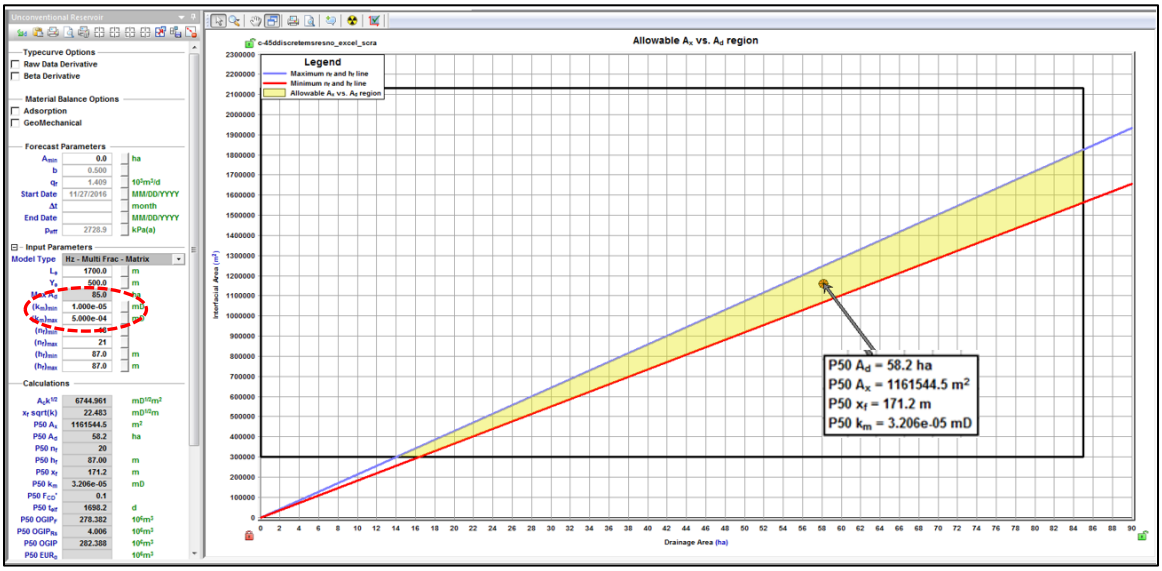

Figure 6-36: Second plot of Allowable Ax versus Ad to calculate SRV (stimulated reservoir volume) showing non-uniqueness of RTA solutions

7. CONCLUSIONS AND RECOMMENDATIONS

The summary, conclusions and recommendations for each part of the research are given separately since the study was divided into two major parts.

7.1. CONCLUSIONS

The research work conducted in this dissertation investigated factors that affect hydraulic fracture complexity and performance in unconventional resources, and methodologies for optimizing stimulation models.

Part 1:

The first part of the research investigated the performance of transversely fractured versus longitudinally fractured horizontal wells in multiphase flow environment. Some of the factors that were investigated are; the effects of relative permeability, non-Darcy flow, adsorption gas, stress dependent permeability on induced fractures, and fracture conductivity changes from the tip to the wellbore. Secondly, three different reservoir simulation models were built to handle each of the three reservoir fluid types studied.

The study used black oil reservoir simulators to study two-phase flow mechanisms such as gas-water (dry gas reservoirs) and under-saturated oil reservoirs (oil-gas-water), and compositional reservoir simulator to model three-phase flow (oil-gas-water). Thirdly, in-depth fluid sampling and equation of state (EoS) modeling were conducted for the black-oil and condensate fluids. The fluid components were lumped into pseudo-components based on the relative closeness of the physical and chemical properties of each components. The lumped pseud-components were fine-tuned with second equation-of-state to make sure

the 2-phase envelope has not shifted and to conserve phase behaviors such as saturation pressure and fluid viscosity after lumping scheme.

Key features of the first part of this study were;

- Methodologies for modeling shale gas and shale oil wells with stress dependent permeability, adsorption gas and non-Darcy flow effect, using black oil models and compositional reservoir simulators.
- Reservoir permeability based cut-off criterion that can be used as guide when selecting whether to drill transversely fractured vs longitudinally fractured horizontal wells.
- Integrating the reservoir objectives and geo-mechanical limitations into horizontal well completions and stimulation strategies.
- Incorporate the effect of reservoir fluid type and fluid properties such as oil composition and density (API) into the decision analysis when comparing transverse horizontal wells to longitudinal horizontal wells.
- Stimulation optimization strategies focused on well recovery, productivity and EUR as function of hydraulic fracture spacing (or number of fracture stages) and reservoir permeability

The following conclusion can be drawn from the Multiphase Flow Performance Comparison of Multiple Fractured Transverse Horizontal Wells versus longitudinal Wells in Tight and Unconventional Reservoirs with Stress Dependent Permeability, which was the first part of this dissertation.

1. The critical permeability at which longitudinally fractured horizontal wells outperform transversely fractured horizontal wells in dry gas reservoir is 0.9 mD for open-hole completion. At higher permeability, transverse fractured horizontal wells experienced non-Darcy flow, which can cause choking effect due to convergent flow near the wellbore.
2. For oil reservoirs that have fluid properties similar to that of Permian basin oil (~API of 38), and can be modeled with black oil reservoir simulators without significant errors, the critical permeability at which longitudinally fractured horizontal wells outperform transversely fractured horizontal wells is 2.0 mD
3. For volatile oil or gas condensate reservoirs (~API 48), the critical permeability varies and depends on the objective target and analysis method used. If the objective is liquids recovery (oil), then the critical permeability is 0.13 mD. However, incorporating well economics and total fluid production (gas and oil in terms of BOE), which the authors recommend, the critical permeability would be 1.8 mD.
4. Critical permeability can be used as a guide for well planning and development, especially if geomechanics and reservoir fluid properties are incorporated into the decision criteria.
5. Well recovery, productivity and EUR are function of permeability and hydraulic fracture spacing (or number fractures) in horizontal wells
6. In low permeability reservoirs, less than 0.5 md for gas reservoirs and 1.0 md for black oil-type reservoirs, longitudinal fractures may not be the best option.

However, there is a transition permeability range, where both transversely fractured horizontal wells and longitudinally fractured well perform equally.

7. Critical permeability also depends on reservoir fluid type (gas, gas condensate or black oil fluids), and the lower the viscosity of the fluid (or mobility ratio), the lower the critical permeability at which longitudinal horizontal wells outperform transversely fractured horizontal wells
8. Stress dependent permeability has no effect on induced hydraulic fracture conductivity in gas and gas condensate reservoirs in low effective stress environment, but has small effect on black oil type reservoirs. Hence, effect of stress dependent permeability depends on reservoir fluid type (properties), rock mechanics and confining effective stress.

Part 2:

The second part of the research developed "a hybrid" integrated completions and reservoir simulation model to investigate the effect of fracture complexity on well performance. The hybrid integrated model was constructed by using all available data such as curvature data from 3D seismic, micro-seismic, geo-mechanical data, well logs, fracability index, mini-frac test, step-rate test, DFIT analysis, core data,post-fracture treatment data, PVT data, production data and well deviations.

Secondly, the study was conducted in a two-step process; first, the calibrated hydraulic fracture model was built using all the available data, particularly the micro-seismic data, which was quality controlled. The second step was the construction of the compositional reservoir model using available data, especially the curvature data from 3D

seismic, which was used to predict the location, density and direction of secondary fissures within the well drainage area.

The result from this study shows that the hybrid integrated completion and reservoir model can be used for selecting optimum lateral placement to target sweet spots that have secondary fissures and good fracability index to maximize production rates, improve hydrocarbon recovery and enhance well economics. Additionally, this dissertation presented a new hybrid model for determining representative stimulated reservoir volume (SRV), which incorporated discrete fracture network modeling to captures the effects of secondary fissures. The hybrid integrated completions and reservoir model was optimized, and then used for production history matching and forecasting.

Key features of the second part of the study are;

- A new methodology for building calibrated fracture model using micro-seismic survey even if the micro-seismic data is of low quality as a result of location bias or signal-noise ratio issues
- A new method for optimizing fracture designs using cluster sensitivity analysis with varying proppant mass per fracture stage that can be used for scenarios analysis.
- A methodology for optimizing fracture design models by adjusting fracture treatment volumes and proppant mass per stage based on well stage location and available net treatment pressure.
- Extending the stimulated reservoir volume (SRV) to include secondary fissure contributions to the overall well production and recovery.

- Use of a discrete fracture network with stress dependent fracture permeability in the compositional reservoir simulator to capture the effects of geomechanical changes during depletion.
- A comparison of well productivity and EUR derived from a planar fracture model versus discrete fracture network based reservoir models.

The following conclusions can be drawn from the second part of the dissertation;

1. Hydraulic fracture treatments in the Montney Formation can create natural fractures in some of the fracture stages and, on average, there were 5-to-10 hydraulic fractures stages that interacted with natural fissures, in each horizontal well. Type of fracture treatment fluids used in the treatment effects fracture complexity, and water-frac treatments, generally lead to the creation and/or dilation of natural fissures.
2. Lower quality micro-seismic data (with location uncertainty and signal to-noise ratio issues) can be used to build calibrated fracture models. The study showed that the calibrated fracture model can be used to remodel and estimate fracture dimensions for all stages in the well.
3. The fracture height growth is confined in the Upper Montney Formation, and both the micro-seismic mapping and calibrated fracture model showed no height growth issues, in most of the hydraulic fracture stages.
4. The leak-off coefficient for Upper Montney wells were found to be within the range of [0.0003-to 0.00045 ft/min$^{1/2}$], which means high fracture fluid efficiency and less fluid loss during the stimulation treatment.

5. The diagnostic fracture injection test (DFIT) of the Upper Montney wells showed pressure dependent leak-off, which indicates presence of natural fissures.
6. PVT analysis and adjustment of pseudo-components during sensitivity analysis and history matching are critical to the integrated reservoir modeling. Molar fraction of different pseudo-components have different impact on cumulative oil and gas.
7. Sensitivity analysis and history matching showed that fracture half-length (x_f) and initial reservoir pressure (Pi) had the biggest effect on well production.
8. The sensitivity analysis also showed that permeability anisotropy had limited effect of well production since reservoir matrix permeability was very low (0.00018 mD).
9. The integrated planar model was easier to construct, required less computer power, and accurately history matched well production. It also required fewer parameter adjustments during sensitivity analysis and optimizations
10. The planar reservoir model, which had no fracture complexity, outperformed both the hybrid DFN model and the SRV model (built from the micro-seismic data), in terms of well productivity and EUR. Hence, fracture complexity in unconventional resources might have less benefit than previously thought.

Conclusions from the hydraulic fracture optimization are:

1. The length of fracture half-length created in multi-cluster fracture treatment is inversely related to the number of cluster perforations per stage, assuming all other stimulation design variables remain the same/constant.
2. Increasing the amount of proppant mass per stage in multi-cluster fracture

stimulation designs would also lead to an increase in the length of "hydraulic" fracture half-length. In this study, one-to-five clusters per stage were thoroughly modeled, but 1-to-8 clusters were studied.

3. The middle perforation clusters in multi-cluster stimulation designs (3 clusters to 8) had, on average, shorter fracture half-lengths and received very little proppant.
4. The first and last perforation clusters in multi-cluster stimulation designs had, on average, longer fracture half-length and received most of the proppant pumped.
5. In the case of one fracture cluster per stage, increasing the amount of proppant mass from 100 ton to 150 M-kg led to no visible increase in fracture half-length
6. In the case of one fracture cluster per stage, increasing the amount of proppant from 50 M-kg to 100 M-kg led to significant increase in the fracture half-length created
7. In the case of five fracture clusters per stage, increasing the amount of proppant from 50 M-kg to 150 M-kg led to increase in the length of the "hydraulic" fracture half-length created
8. Mixing the number of fracture clusters per stage such as using four clusters per stage at the heel and two clusters per stage everywhere else would lead to the creation of fractures with uneven distribution of length; i.e. shorter at the heel and longer in other parts of the horizontal well.
9. Two fracture clusters per stage yielded the highest propped fracture half-length (x_f) per kilogram of proppant used.

10. Adding more fracture clusters per stage near the heel of the horizontal well (in an optimized stimulation design) improved well performance and increased initial well production.
11. Well performance metrics based on initial well production (IP) can be attained by increasing the number of fracture clusters per stage. However, IP based well performance metrics might lead to lost well recovery, and "the law of diminishing returns" may apply

7.2. FUTURE WORK

Because of the limitations of time and manpower, every researcher leaves behind several future research works. Though this dissertation investigated wide array of parameters that affected the unconventional resources, here are suggested future works;

1. Extend the condensate reservoir simulation models by adding adsorption and desorption gas since in shale gas reservoirs the total gas in place (GIP) is made-up of gas adsorbed on the surface of the kerogen, and gas stored in the primary and secondary porosity. Include laboratory test such as core tests (saturation, permeability and porosity), total organic carbon (TOC), and lab derived Langmuir isotherm (LI) parameters.
2. Extend the hydraulic fracture optimization parameters by investigating the impact of fluid types, and proppant sizes and types on results. Use of small sized proppants such as 50/70 with slick-water for the whole stimulation job is now common in the industry (Ely et al. 2014).

3. Extend the range of secondary fracture conductivity to 10 mD-ft. to investigate the effect of having infinite-acting natural fractures. What happens when the secondary fractures behave like induced hydraulic fractures, especially during the transient flow period?

APPENDIX A

PERFORMANCE COMPARISON OF TRANSVERSELY FRACTURED VERSUS LONGITUDINALLY FRACTURED HORIZONTAL WELLS

The following plots are from the dry gas reservoir simulations (gas-water)

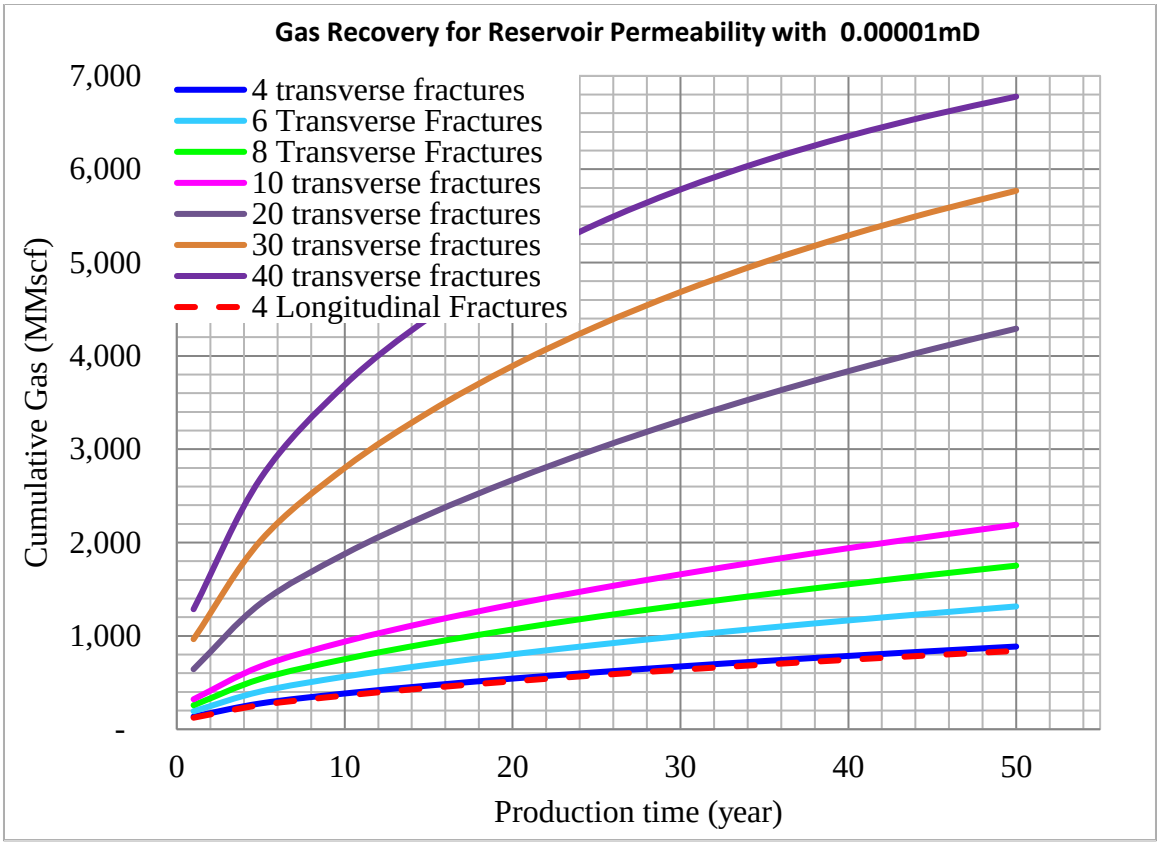

Figure A-1: Cumulative oil production for transversely fractured well with reservoir permeability of 0.00001 mD in dry gas model

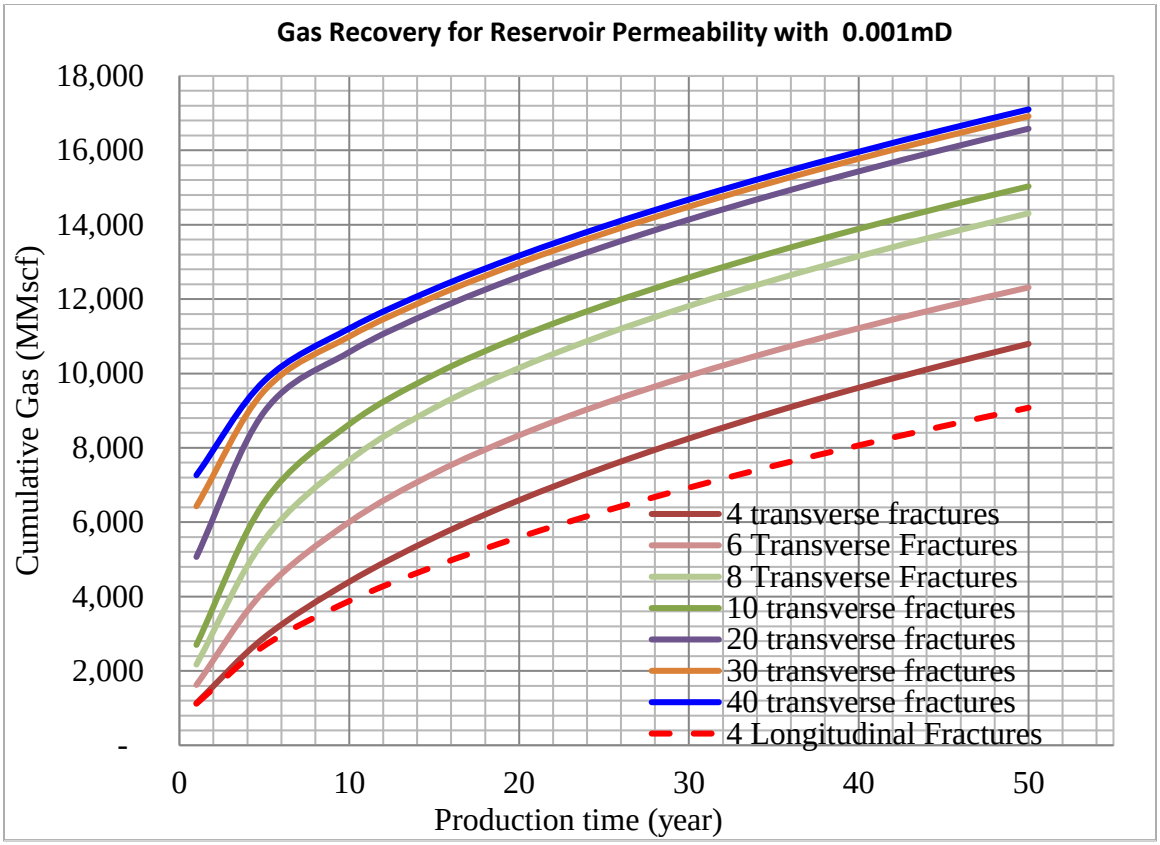

Figure A-2: Cumulative oil production for transversely fractured well with reservoir permeability of 0.001 mD in dry gas model

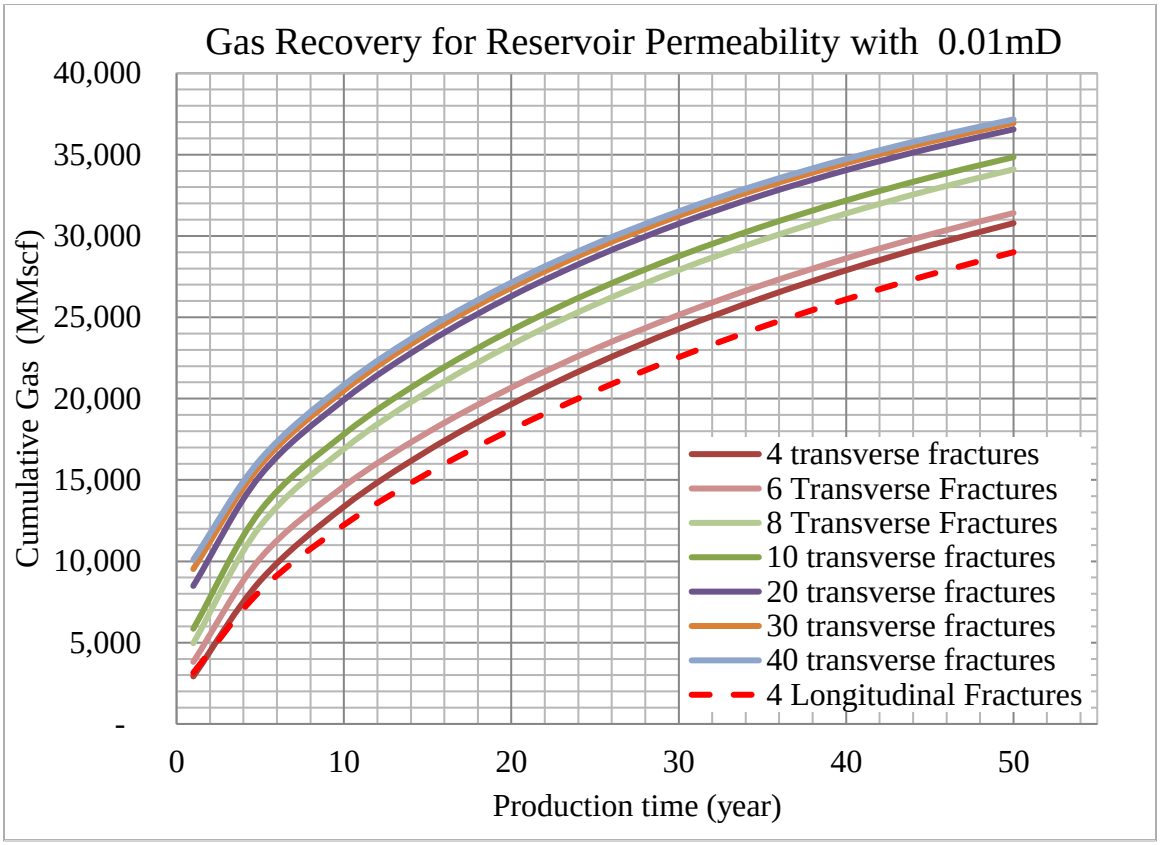

Figure A-3: Cumulative oil production for transversely fractured well with reservoir permeability of 0.01 mD in dry gas model

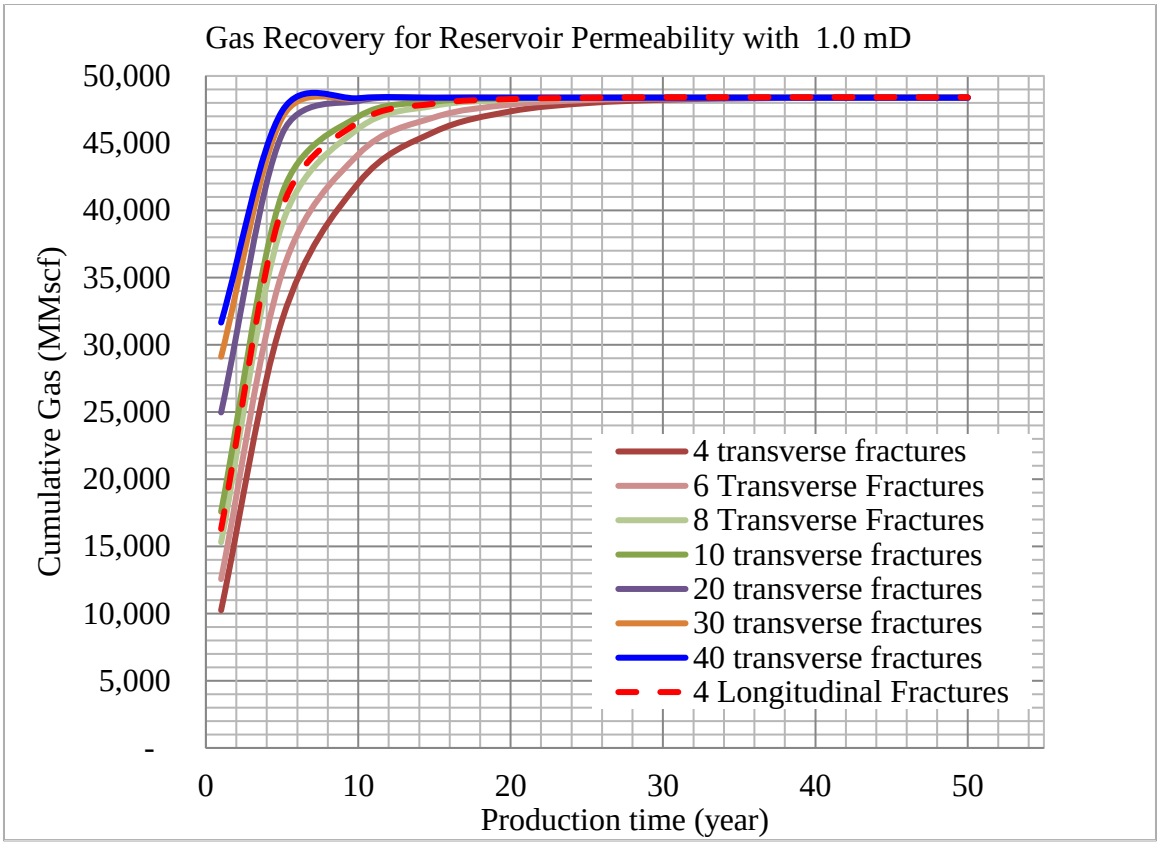

Figure A-4: Cumulative oil production for transversely fractured well with reservoir permeability of 1.0 mD in dry gas model

The following plots are from the black oil reservoir simulations (oil-gas and-water)

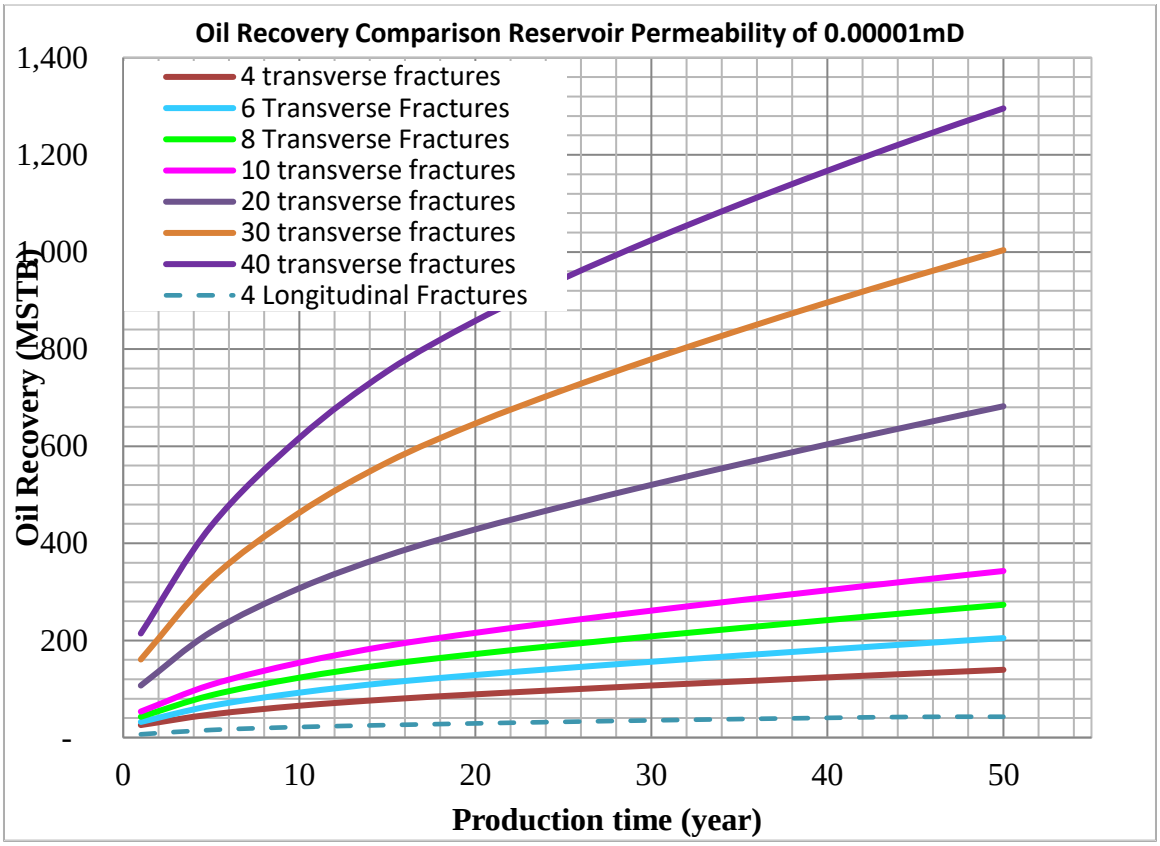

Figure A-5: Cumulative oil production for transversely fractured well with reservoir permeability of 0.00001 mD in black oil model

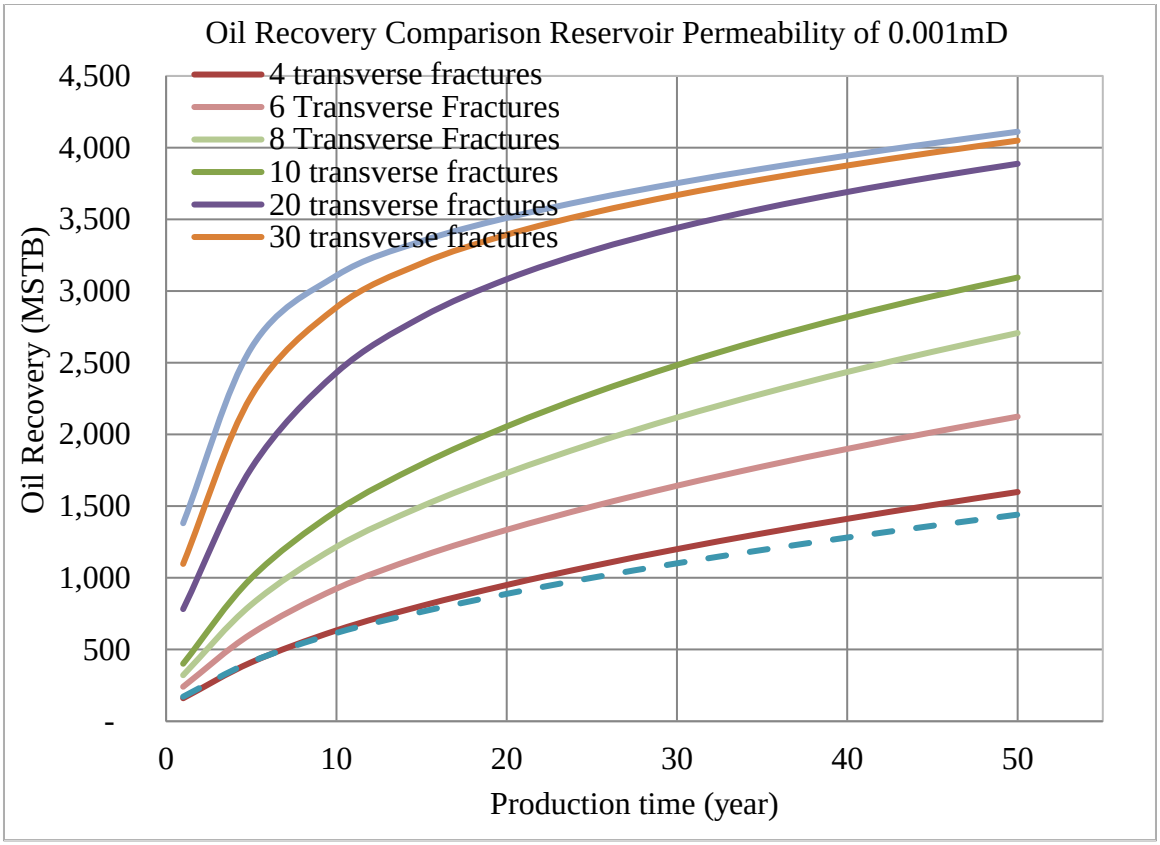

Figure A-6: Cumulative oil production for transversely fractured well with reservoir permeability of 0.001 mD in black oil model

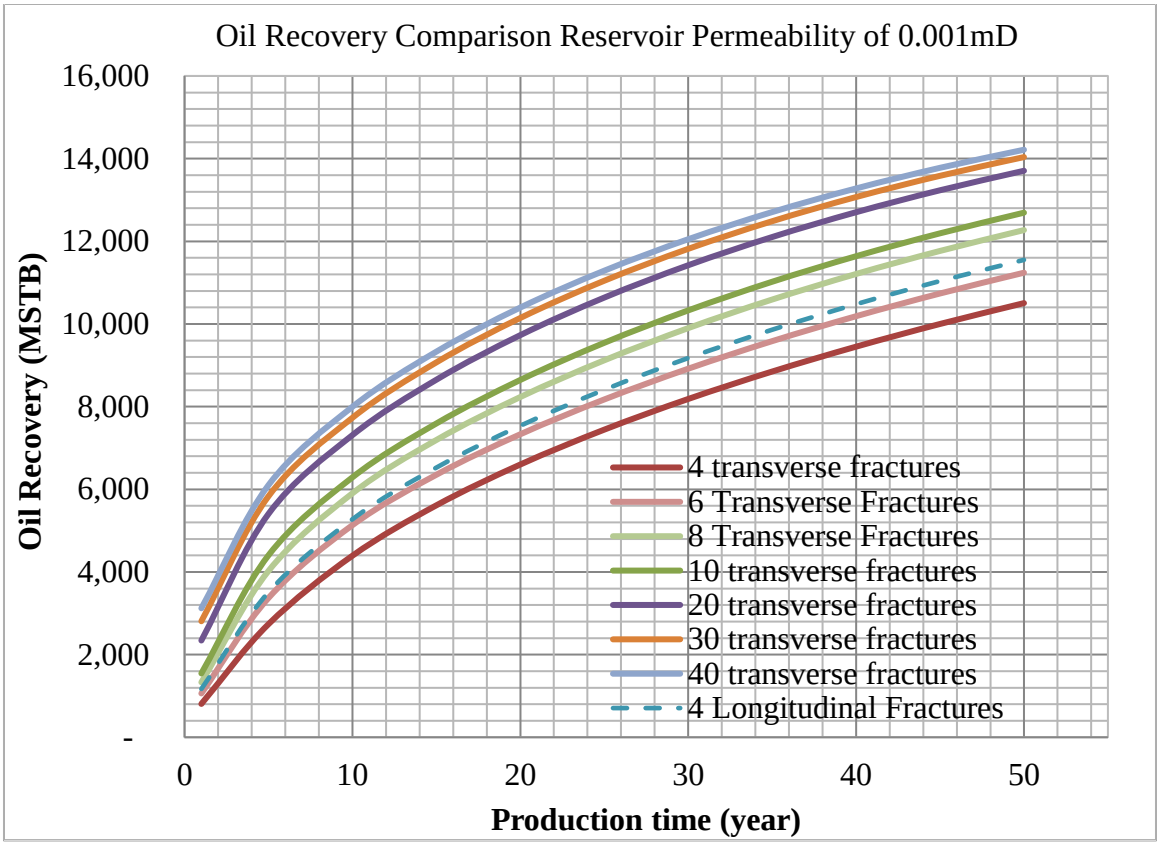

Figure A-7: Cumulative oil production for transversely fractured well with reservoir permeability of 0.1 mD in black oil model

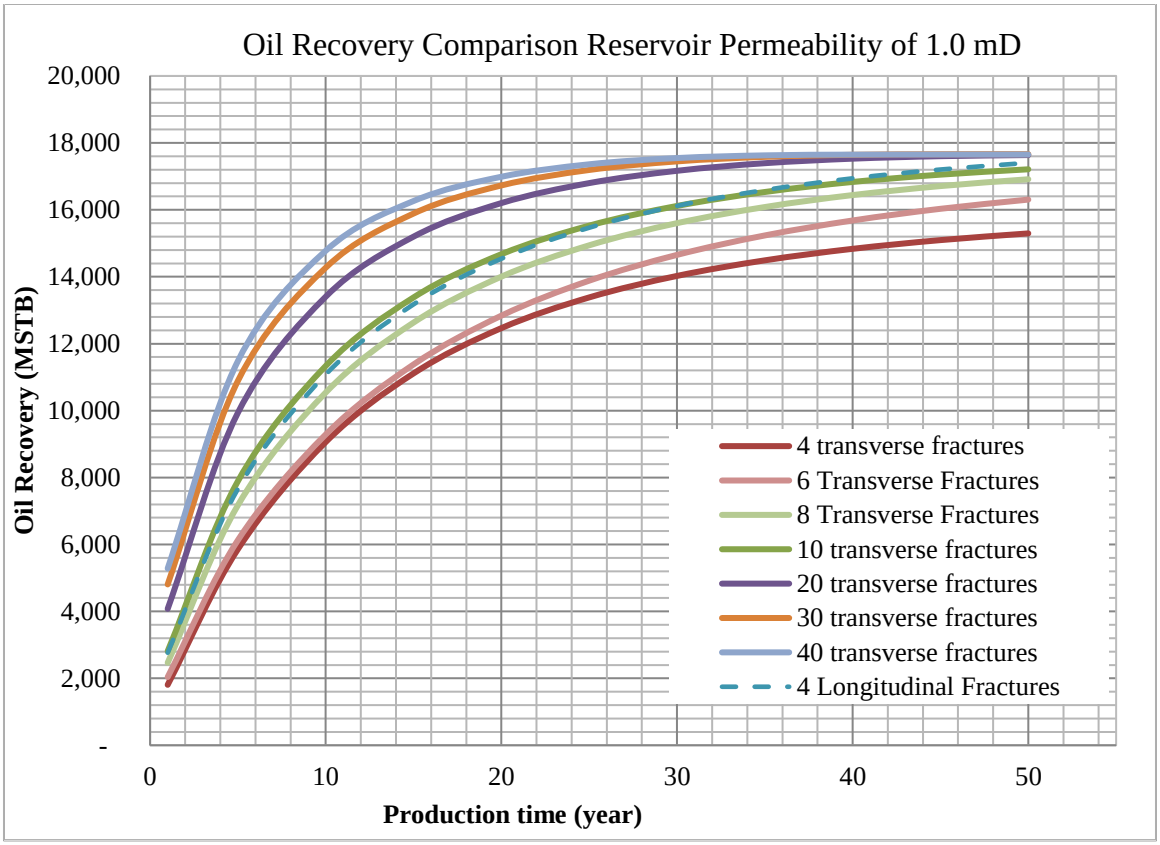

Figure A-8: Cumulative oil production for transversely fractured well with reservoir permeability of 1.0 mD in black oil model

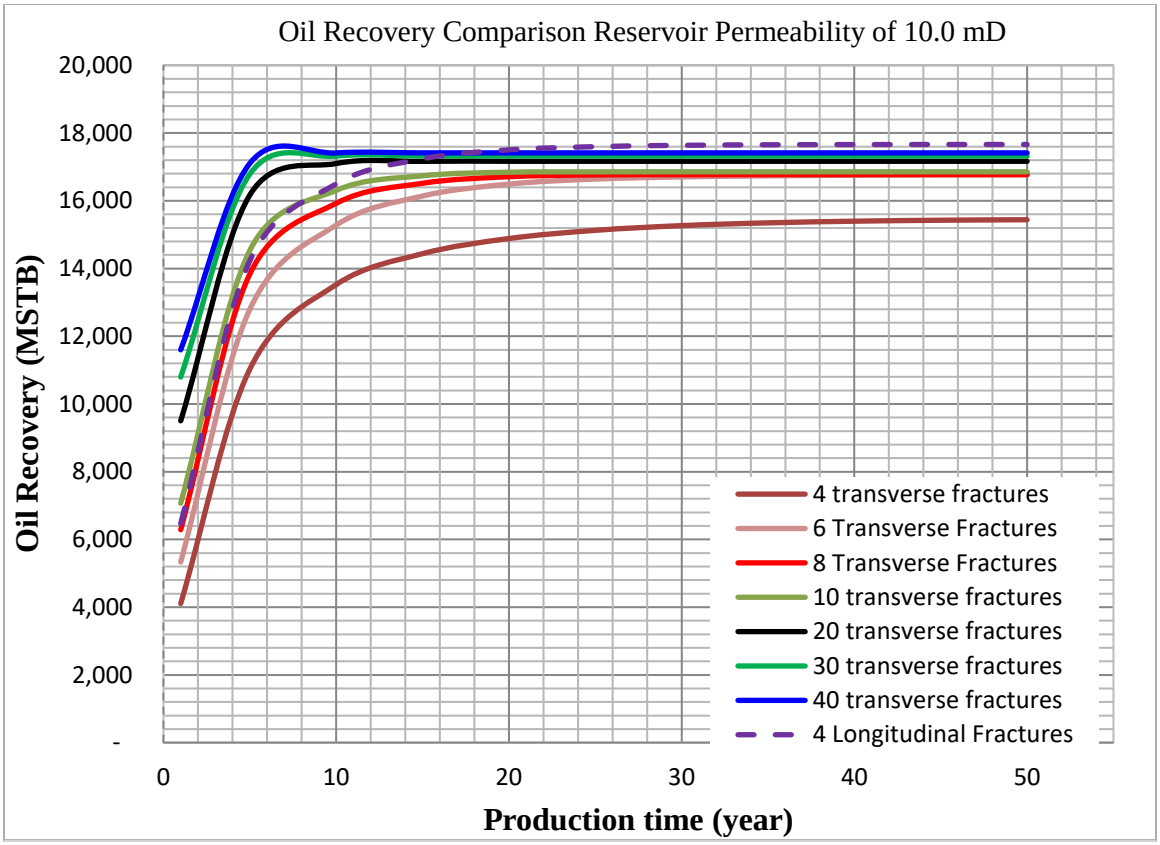

Figure A-9: Cumulative oil production for transversely fractured well with reservoir permeability of 10.0 mD in black oil model

Table A-1: Cumulative gas production from the dry gas reservoir simulation model

Case Number	K (md)	1st year Recovery (MMscf)	5 years Recovery (MMscf)	10 years Recovery (MMscf)	15years Recovery (MMscf)	20 years Recovery (MMscf)	25 years Recovery (MMscf)	30 years Recovery (MMscf)	35 years Recovery (MMscf)	40 years Recovery (MMscf)	45 years Recovery (MMscf)	EUR 50 years (MMscf)
Case 0	0.000001	58	104	139	166	189	209	227	244	259	273	287
case 1	0.00001	136	277	383	468	543	611	673	731	785	837	886
case 2	0.0001	372	860	1,260	1,575	1,847	2,091	2,315	2,524	2,721	2,909	3,088
case 3	0.001	1,133	2,901	4,397	5,585	6,590	7,467	8,250	8,961	9,616	10,225	10,796
case 4	0.01	2,922	8,802	13,359	16,797	19,655	22,119	24,279	26,190	27,891	29,415	30,787
case 5	0.1	5,171	18,584	29,010	35,337	39,353	41,994	43,787	45,041	45,932	46,574	47,042
case 6	1	10,248	31,830	42,023	45,846	47,367	47,980	48,228	48,328	48,368	48,385	48,391
case 7	10	30,666	47,164	48,338	48,395	48,402	48,403	48,403	48,404	48,404	48,405	48,405
					6 Fractures							
Case 0	0.000001	76	145	198	239	273	303	331	356	379	400	420
case 1	0.00001	193	405	564	691	803	904	998	1,085	1,166	1,243	1,316
case 2	0.0001	542	1,272	1,867	2,330	2,724	3,074	3,392	3,685	3,958	4,213	4,454
case 3	0.001	1,623	4,159	6,003	7,311	8,336	9,192	9,938	10,606	11,216	11,782	12,313
case 4	0.01	3,816	10,184	14,607	17,920	20,680	23,059	25,144	26,986	28,624	30,090	31,407
case 5	0.1	6,108	20,546	30,837	36,773	40,431	42,801	44,396	45,497	46,273	46,830	47,234
case 6	1	12,565	35,357	44,161	46,926	47,872	48,205	48,324	48,366	48,381	48,387	48,388
case 7	10	34,651	47,880	48,374	48,397	48,411	48,422	48,426	48,427	48,428	48,428	48,428
					10 Fractures							
Case 0	0.000001	126	242	330	397	454	504	549	590	627	663	696
case 1	0.00001	321	674	938	1,150	1,336	1,505	1,660	1,805	1,940	2,069	2,191
case 2	0.0001	902	2,120	3,116	3,883	4,518	5,057	5,525	5,936	6,303	6,632	6,931
case 3	0.001	2,700	6,541	8,634	9,966	10,982	11,832	12,582	13,261	13,889	14,476	15,031
case 4	0.01	5,855	13,106	17,810	21,321	24,205	26,649	28,753	30,581	32,182	33,593	34,844
case 5	0.1	8,837	26,068	36,170	41,153	43,893	45,508	46,506	47,141	47,555	47,828	48,010
case 6	1	17,578	41,222	46,975	48,091	48,325	48,375	48,385	48,385	48,385	48,385	48,385
case 7	10	39,762	48,310	48,379	48,383	48,386	48,396	48,400	48,401	48,401	48,401	48,401
					20 Fractures							
Case 0	0.000001	253	483	660	795	910	1,010	1,101	1,183	1,260	1,332	1,399
case 1	0.00001	643	1,349	1,878	2,301	2,671	3,003	3,305	3,581	3,836	4,073	4,292
case 2	0.0001	1,802	4,150	5,730	6,683	7,339	7,829	8,218	8,540	8,816	9,059	9,278
case 3	0.001	5,065	8,973	10,573	11,685	12,603	13,409	14,138	14,809	15,434	16,023	16,581
case 4	0.01	8,487	15,277	19,929	23,435	26,298	28,702	30,752	32,514	34,043	35,379	36,554
case 5	0.1	12,966	30,988	39,834	43,718	45,690	46,779	47,410	47,787	48,016	48,157	48,244
case 6	1	24,964	45,671	48,138	48,364	48,385	48,385	48,385	48,385	48,385	48,385	48,385
case 7	10	44,436	48,381	48,381	48,383	48,399	48,414	48,417	48,418	48,419	48,419	48,419
					30 Fractures							
Case 0	0.000001	379	726	991	1,194	1,366	1,517	1,653	1,777	1,891	1,998	2,097
case 1	0.00001	965	2,021	2,799	3,395	3,892	4,317	4,684	5,006	5,290	5,543	5,769
case 2	0.0001	2,688	5,597	7,043	7,792	8,278	8,639	8,930	9,177	9,395	9,593	9,775
case 3	0.001	6,428	9,538	10,992	12,065	12,968	13,764	14,486	15,152	15,773	16,359	16,915
case 4	0.01	9,527	15,895	20,501	23,983	26,824	29,205	31,230	32,969	34,474	35,787	36,940
case 5	0.1	14,982	32,751	40,964	44,444	46,170	47,101	47,627	47,934	48,116	48,225	48,290
case 6	1	29,109	46,876	48,298	48,383	48,384	48,384	48,384	48,384	48,384	48,384	48,384
case 7	10	46,152	48,383	48,383	48,405	48,423	48,436	48,442	48,443	48,444	48,444	48,444
					40 Fractures							
Case 0	0.000001	506	967	1,322	1,592	1,821	2,022	2,204	2,368	2,520	2,661	2,792
case 1	0.00001	1,286	2,690	3,689	4,405	4,963	5,413	5,783	6,092	6,355	6,581	6,779
case 2	0.0001	3,545	6,598	7,761	8,322	8,692	8,979	9,222	9,438	9,636	9,819	9,992
case 3	0.001	7,263	9,804	11,208	12,269	13,165	13,957	14,676	15,340	15,961	16,546	17,101
case 4	0.01	10,096	16,250	20,833	24,304	27,133	29,500	31,512	33,236	34,728	36,027	37,167
case 5	0.1	16,222	33,721	41,571	44,831	46,422	47,267	47,738	48,008	48,165	48,257	48,312
case 6	1	31,651	47,382	48,345	48,384	48,384	48,384	48,384	48,384	48,384	48,384	48,384
case 7	10	46,929	48,383	48,383	48,424	48,433	48,437	48,443	48,446	48,447	48,447	48,447
					4 Lontitudinal							
Case 0	0.000001	105	258	355	425	481	530	572	609	643	673	700
case 1	0.00001	124	259	361	442	514	578	637	693	744	793	839
case 2	0.0001	353	818	1,193	1,482	1,725	1,940	2,134	2,313	2,479	2,635	2,783
case 3	0.001	1,118	2,677	3,880	4,807	5,594	6,293	6,928	7,515	8,065	8,584	9,078
case 4	0.01	3,145	8,188	12,232	15,404	18,098	20,456	22,549	24,420	26,103	27,623	29,003
case 5	0.1	7,275	22,526	32,637	38,170	41,481	43,584	44,979	45,938	46,612	47,092	47,438
case 6	1	16,299	40,154	46,552	47,945	48,280	48,375	48,416	48,416	48,416	48,416	48,416
case 7	10	36,310	48,194	48,378	48,379	48,396	48,412	48,416	48,416	48,417	48,417	48,417

Table A-2: Gas rate from the dry gas reservoir simulation model

Case Number	K (md)	1st year Gas Rate (MSCF/D)	5th year Gas Rate (MSCF/D)	10th year Gas Rate (MSCF/D)	15th year Gas Rate (MSCF/D)	20th year Gas Rate (MSCF/D)	25th year Gas Rate (MSCF/D)	30th year Gas Rate (MSCF/D)	35th year Gas Rate (MSCF/D)	40th year Gas Rate (MSCF/D)	45th year Gas Rate (MSCF/D)	50th year Gas Rate (MSCF/D)
Case 0	0.000001	53	24	17	14	12	10	9	9	8	8	7
case 1	0.00001	165	70	51	43	39	36	33	31	29	27	26
case 2	0.0001	506	262	190	159	140	128	118	111	105	101	96
case 3	0.001	1,876	957	719	595	512	452	408	373	345	323	304
case 4	0.01	6,065	3,061	2,112	1,702	1,448	1,261	1,111	987	882	791	713
case 5	0.1	12,321	7,394	4,384	2,729	1,767	1,181	816	576	413	299	219
case 6	1	24,380	9,132	3,261	1,280	515	208	84	34	14	6	2
case 7	10	43,343	2,143	99	8	1	1	0	0	0	0	0
				6 fractures								
Case 0	0.000001	80	36	25	20	18	16	15	13	12	12	11
case 1	0.00001	246	105	76	65	58	53	49	46	43	41	39
case 2	0.0001	762	391	281	232	202	182	167	155	144	136	128
case 3	0.001	2,777	1,277	833	625	509	435	385	349	321	300	282
case 4	0.01	7,615	3,029	2,034	1,642	1,399	1,218	1,072	951	848	761	685
case 5	0.1	14,092	7,544	4,192	2,515	1,594	1,056	721	504	359	259	189
case 6	1	28,551	8,582	2,528	846	296	105	37	13	5	2	0
case 7	10	41,371	1,115	23	12	7	4	1	0	0	0	0
				10 fractures								
Case 0	0.000001	134	59	41	34	28	26	23	22	20	18	18
case 1	0.00001	412	176	127	108	97	89	81	77	72	68	66
case 2	0.0001	1,271	653	470	380	319	274	239	212	190	172	156
case 3	0.001	4,666	1,619	877	623	504	435	389	357	332	312	296
case 4	0.01	10,106	3,222	2,163	1,729	1,450	1,239	1,072	936	823	727	646
case 5	0.1	18,871	8,083	3,745	1,977	1,133	687	432	279	183	122	81
case 6	1	36,584	6,768	1,236	255	54	12	0	0	0	0	0
case 7	10	35,540	250	0	0	6	4	1	0	0	0	0
				20 fractures								
Case 0	0.000001	267	117	84	68	60	53	46	43	40	37	37
case 1	0.00001	823	350	252	214	190	172	158	146	136	126	117
case 2	0.0001	2,548	1,167	650	424	306	238	192	161	141	126	114
case 3	0.001	7,064	1,235	697	545	468	418	382	354	333	313	298
case 4	0.01	10,272	3,119	2,161	1,724	1,433	1,213	1,039	898	782	686	604
case 5	0.1	22,611	7,598	3,047	1,470	787	447	264	160	98	60	38
case 6	1	43,318	3,772	327	32	0	0	0	0	0	0	0
				30 fractures								
Case 0	0.000001	401	179	127	101	89	78	73	63	59	58	54
case 1	0.00001	1,232	521	361	297	250	216	188	167	147	132	118
case 2	0.0001	3,670	1,203	535	321	227	175	145	126	114	104	97
case 3	0.001	6,514	1,032	659	534	462	413	379	352	330	312	297
case 4	0.01	9,042	3,071	2,146	1,712	1,420	1,200	1,026	885	769	673	593
case 5	0.1	23,140	7,209	2,766	1,299	680	378	218	128	76	46	28
case 6	1	43,495	2,475	141	9	0	0	0	0	0	0	0
case 7	10	17,671	0	0	0	9	5	2	0	0	0	0
				40 fractures								
Case 0	0.000001	535	239	169	134	119	104	97	84	78	77	71
case 1	0.00001	1,646	685	448	344	274	225	187	158	132	114	103
case 2	0.0001	4,581	1,046	408	242	175	144	125	113	104	98	92
case 3	0.001	5,419	956	649	528	460	412	378	351	330	311	297
case 4	0.01	8,081	3,047	2,138	1,705	1,413	1,193	1,018	877	762	666	586
case 5	0.1	23,054	6,975	2,610	1,206	622	340	193	112	65	39	23
case 6	1	42,735	1,821	77	0	0	0	0	0	0	0	0

Table A-3: Recovery factor from the dry gas reservoir simulation model

Case Number	K (md)	1st year Recovery Factor	5 years Recovery Factor	10 years Recovery Factor	15 years Recovery Factor	20 years Recovery Factor	25 years Recovery Factor	30 years Recovery Factor	35 years Recovery Factor	40 years Recovery Factor	45 years Recovery Factor	EUR 50 years factor
Case 0	0.000001	0.1%	0.2%	0.2%	0.3%	0.3%	0.3%	0.4%	0.4%	0.4%	0.5%	0.5%
case 1	0.00001	0.2%	0.5%	0.6%	0.8%	0.9%	1.0%	1.1%	1.2%	1.3%	1.4%	1.5%
case 2	0.0001	0.6%	1.4%	2.1%	2.6%	3.1%	3.5%	3.8%	4.2%	4.5%	4.8%	5.1%
case 3	0.001	1.9%	4.8%	7.3%	9.2%	10.9%	12.4%	13.7%	14.8%	15.9%	16.9%	17.9%
case 4	0.01	4.8%	14.6%	22.1%	27.8%	32.5%	36.6%	40.2%	43.3%	46.2%	48.7%	50.9%
case 5	0.1	8.6%	30.8%	48.0%	58.5%	65.1%	69.5%	72.5%	74.5%	76.0%	77.1%	77.8%
case 6	1	17.0%	52.7%	69.5%	75.9%	78.4%	79.4%	79.8%	80.0%	80.0%	80.1%	80.1%
case 7	10	50.7%	78.0%	80.0%	80.1%	80.1%	80.1%	80.1%	80.1%	80.1%	80.1%	80.1%
					6 Fractures							
Case 0	0.000001	0.1%	0.2%	0.3%	0.4%	0.5%	0.5%	0.5%	0.6%	0.6%	0.7%	0.7%
case 1	0.00001	0.3%	0.7%	0.9%	1.1%	1.3%	1.5%	1.7%	1.8%	1.9%	2.1%	2.2%
case 2	0.0001	0.9%	2.1%	3.1%	3.9%	4.5%	5.1%	5.6%	6.1%	6.5%	7.0%	7.4%
case 3	0.001	2.7%	6.9%	9.9%	12.1%	13.8%	15.2%	16.4%	17.6%	18.6%	19.5%	20.4%
case 4	0.01	6.3%	16.9%	24.2%	29.7%	34.2%	38.2%	41.6%	44.7%	47.4%	49.8%	52.0%
case 5	0.1	10.1%	34.0%	51.0%	60.9%	66.9%	70.8%	73.5%	75.3%	76.6%	77.5%	78.2%
case 6	1	20.8%	58.5%	73.1%	77.7%	79.2%	79.8%	80.0%	80.0%	80.1%	80.1%	80.1%
case 7	10	57.3%	79.2%	80.1%	80.1%	80.1%	80.1%	80.1%	80.1%	80.1%	80.1%	80.1%
					10 Fractures							
Case 0	0.000001	0.2%	0.4%	0.5%	0.7%	0.8%	0.8%	0.9%	1.0%	1.0%	1.1%	1.2%
case 1	0.00001	0.5%	1.1%	1.6%	1.9%	2.2%	2.5%	2.7%	3.0%	3.2%	3.4%	3.6%
case 2	0.0001	1.5%	3.5%	5.2%	6.4%	7.5%	8.4%	9.1%	9.8%	10.4%	11.0%	11.5%
case 3	0.001	4.5%	10.8%	14.3%	16.5%	18.2%	19.6%	20.8%	21.9%	23.0%	24.0%	24.9%
case 4	0.01	9.7%	21.7%	29.5%	35.3%	40.1%	44.1%	47.6%	50.6%	53.3%	55.6%	57.7%
case 5	0.1	14.6%	43.1%	59.9%	68.1%	72.6%	75.3%	77.0%	78.0%	78.7%	79.2%	79.5%
case 6	1	29.1%	68.2%	77.7%	79.6%	80.0%	80.1%	80.1%	80.1%	80.1%	80.1%	80.1%
case 7	10	65.8%	79.9%	80.1%	80.1%	80.1%	80.1%	80.1%	80.1%	80.1%	80.1%	80.1%
					20 Fractures							
Case 0	0.000001	0.4%	0.8%	1.1%	1.3%	1.5%	1.7%	1.8%	2.0%	2.1%	2.2%	2.3%
case 1	0.00001	1.1%	2.2%	3.1%	3.8%	4.4%	5.0%	5.5%	5.9%	6.3%	6.7%	7.1%
case 2	0.0001	3.0%	6.9%	9.5%	11.1%	12.1%	13.0%	13.6%	14.1%	14.6%	15.0%	15.4%
case 3	0.001	8.4%	14.8%	17.5%	19.3%	20.9%	22.2%	23.4%	24.5%	25.5%	26.5%	27.4%
case 4	0.01	14.0%	25.3%	33.0%	38.8%	43.5%	47.5%	50.9%	53.8%	56.3%	58.5%	60.5%
case 5	0.1	21.5%	51.3%	65.9%	72.3%	75.6%	77.4%	78.5%	79.1%	79.5%	79.7%	79.8%
case 6	1	41.3%	75.6%	79.7%	80.0%	80.1%	80.1%	80.1%	80.1%	80.1%	80.1%	80.1%
case 7	10	73.5%	80.1%	80.1%	80.1%	80.1%	80.1%	80.1%	80.1%	80.1%	80.1%	80.1%
					30 Fractures							
Case 0	0.000001	0.6%	1.2%	1.6%	2.0%	2.3%	2.5%	2.7%	2.9%	3.1%	3.3%	3.5%
case 1	0.00001	1.6%	3.3%	4.6%	5.6%	6.4%	7.1%	7.8%	8.3%	8.8%	9.2%	9.5%
case 2	0.0001	4.4%	9.3%	11.7%	12.9%	13.7%	14.3%	14.8%	15.2%	15.5%	15.9%	16.2%
case 3	0.001	10.6%	15.8%	18.2%	20.0%	21.5%	22.8%	24.0%	25.1%	26.1%	27.1%	28.0%
case 4	0.01	15.8%	26.3%	33.9%	39.7%	44.4%	48.3%	51.7%	54.6%	57.1%	59.2%	61.1%
case 5	0.1	24.8%	54.2%	67.8%	73.6%	76.4%	77.9%	78.8%	79.3%	79.6%	79.8%	79.9%
case 6	1	48.2%	77.6%	79.9%	80.1%	80.1%	80.1%	80.1%	80.1%	80.1%	80.1%	80.1%
case 7	10	76.4%	80.1%	80.1%	80.1%	80.1%	80.2%	80.2%	80.2%	80.2%	80.2%	80.2%
					40 Fractures							
Case 0	0.000001	0.8%	1.6%	2.2%	2.6%	3.0%	3.3%	3.6%	3.9%	4.2%	4.4%	4.6%
case 1	0.00001	2.1%	4.5%	6.1%	7.3%	8.2%	9.0%	9.6%	10.1%	10.5%	10.9%	11.2%
case 2	0.0001	5.9%	10.9%	12.8%	13.8%	14.4%	14.9%	15.3%	15.6%	15.9%	16.2%	16.5%
case 3	0.001	12.0%	16.2%	18.5%	20.3%	21.8%	23.1%	24.3%	25.4%	26.4%	27.4%	28.3%
case 4	0.01	16.7%	26.9%	34.5%	40.2%	44.9%	48.8%	52.1%	55.0%	57.5%	59.6%	61.5%
case 5	0.1	26.8%	55.8%	68.8%	74.2%	76.8%	78.2%	79.0%	79.4%	79.7%	79.9%	80.0%
case 6	1	52.4%	78.4%	80.0%	80.1%	80.1%	80.1%	80.1%	80.1%	80.1%	80.1%	80.1%
case 7	10	77.7%	80.1%	80.1%	80.1%	80.2%	80.2%	80.2%	80.2%	80.2%	80.2%	80.2%
					4 Longitudinal							
Case 0	0.000001	0.3%	0.8%	1.1%	1.3%	1.4%	1.6%	1.7%	1.8%	1.9%	2.0%	2.1%
case 1	0.00001	0.2%	0.4%	0.6%	0.7%	0.8%	1.0%	1.1%	1.1%	1.2%	1.3%	1.4%
case 2	0.0001	0.6%	1.4%	2.0%	2.5%	2.9%	3.2%	3.5%	3.8%	4.1%	4.4%	4.6%
case 3	0.001	1.9%	4.4%	6.4%	8.0%	9.3%	10.4%	11.5%	12.4%	13.3%	14.2%	15.0%
case 4	0.01	5.2%	13.6%	20.2%	25.5%	30.0%	33.9%	37.3%	40.4%	43.2%	45.7%	48.0%
case 5	0.1	12.0%	37.3%	54.0%	63.2%	68.6%	72.1%	74.4%	76.0%	77.1%	77.9%	78.5%
case 6	1	27.0%	66.5%	77.0%	79.3%	79.9%	80.1%	80.1%	80.1%	80.1%	80.1%	80.1%
case 7	10	60.1%	79.8%	80.1%	80.1%	80.1%	80.1%	80.1%	80.1%	80.1%	80.1%	80.1%

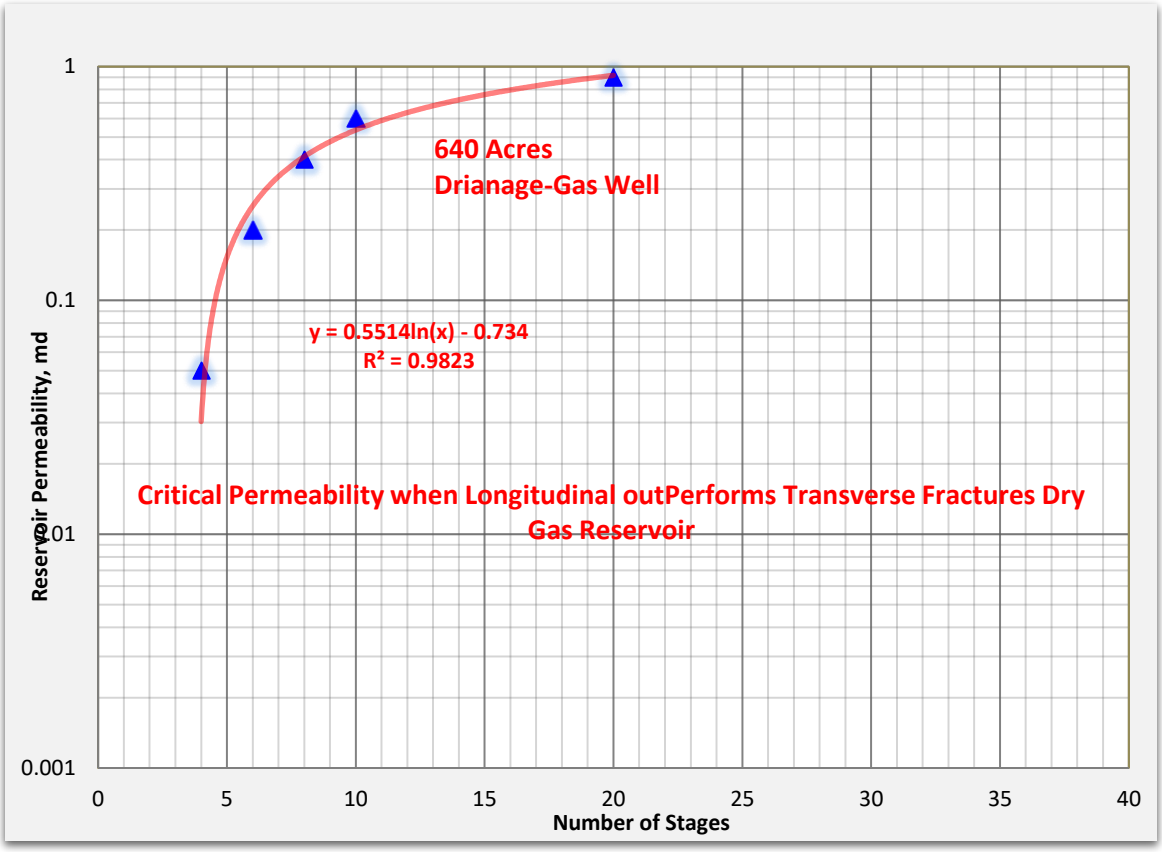

Figure A-10: Critical permeability cut-off for dry gas reservoirs

APPENDIX B

INEGRATED COMPLETIONS AND RESERVOIR MODELING

The formula for the Gaussian distributions are given below:

$$P(x) = \frac{1}{\sigma\sqrt{2\pi}} e^{-(x-\mu)^2/(2\sigma^2)} \quad \ldots \text{(B1)}$$

Where;

$P(x)$ = probability density function

μ = mean

σ = standard deviation

σ^2 = variance

The Skewness and Kurtosis were calculated using the following equations:

Kurtosis:

$$K = \frac{\sum(x_i - \mu)^4}{(n-1) * \sigma^4} \quad \ldots \text{(B2)}$$

Where;

K = kurtosis

n = number of samples in the data, and the other variable were explained previously

Table B-1: Statistical analysis of the Upper Montney porosity distribution

Mean	STEDev	Max Value	Min Value	Skewness	Kurtosis
0.06	0.02	0.26	0.02	4.68	39.09

Porosity	Frequency of value
0.030	7
0.035	8
0.041	15
0.046	20
0.051	39
0.057	30
0.062	26
0.067	41
0.073	23
0.078	12
0.083	17
0.089	5

Table B-2: Statistical analysis of the Upper Montney net-pay distribution

Mean	STDev	Max Value	Min Value	Skewness	Kurtosis
83.04	64.83	535.00	0.00	2.06	7.17

Interval thinckness	Frequency of value
20	73
40	87
60	82
80	91
100	100
120	51
140	26
160	25
180	9
200	12

Table B-3: Fracture dimensions obtained from the MS data for each stage in well A

Stage Number	Fracture (Xf) Length (m)	Fracture (Hf) Length (m)	Number of Events	Comments
1	NA	NA	NA	1 events only on one side
2	155	97	25	
3	131	99	4	
4	NA	NA	NA	2 events only on one side
5	148	28	5	
6	152	114	16	
7	304	130	30	
8	154	115	21	
9	263	147	14	
10	255	72	10	
11	149	116	17	
12	151	92	7	
13	107	101	35	
14	248	157	259	
15	455	147	153	
16	582	161	166	
17	781	164	127	
18	343	131	236	
19	299	105	91	
20	260	91	226	
Averge	274	115	80	

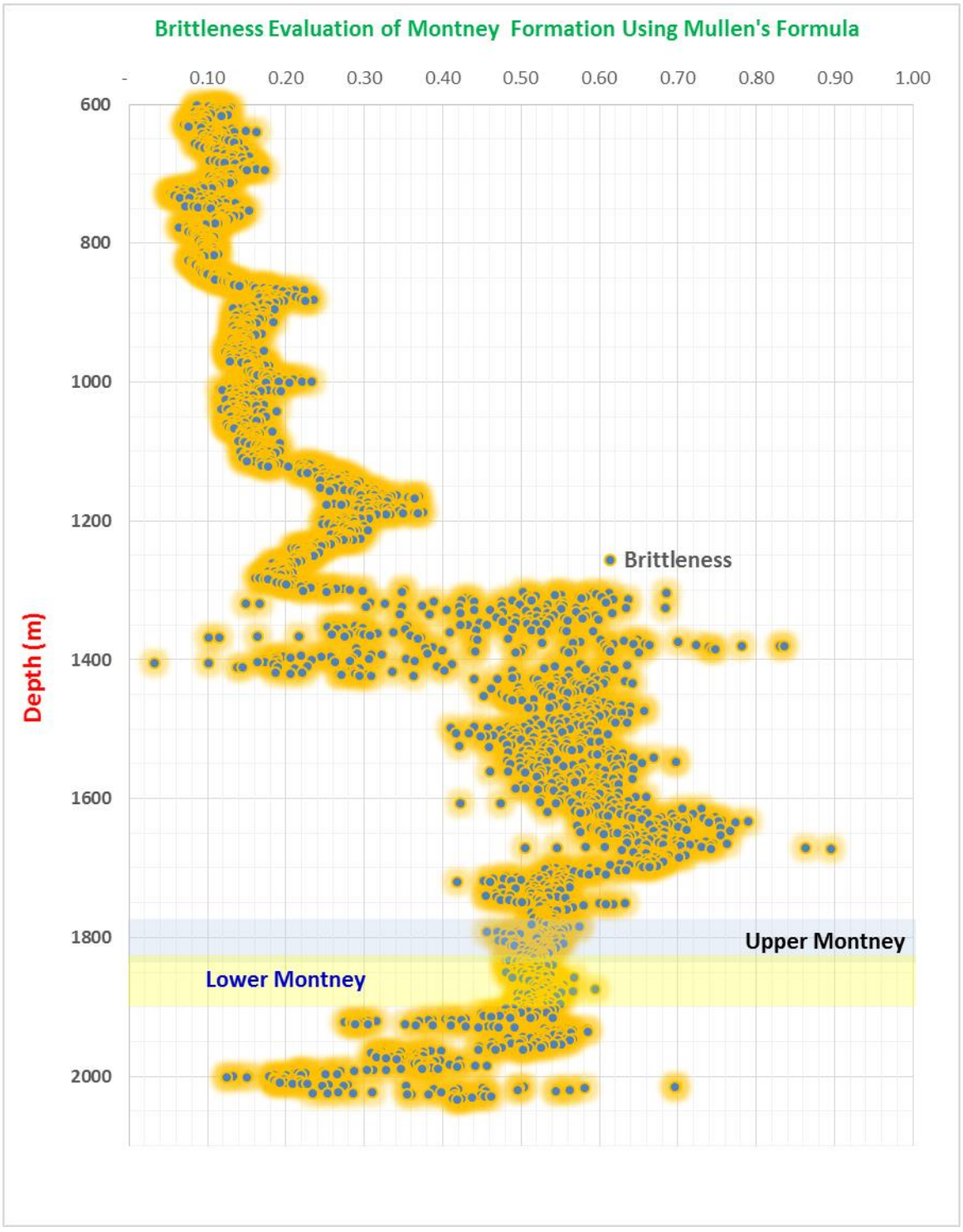

Figure B-1: Fracability Index evaluation using Mullen's formula

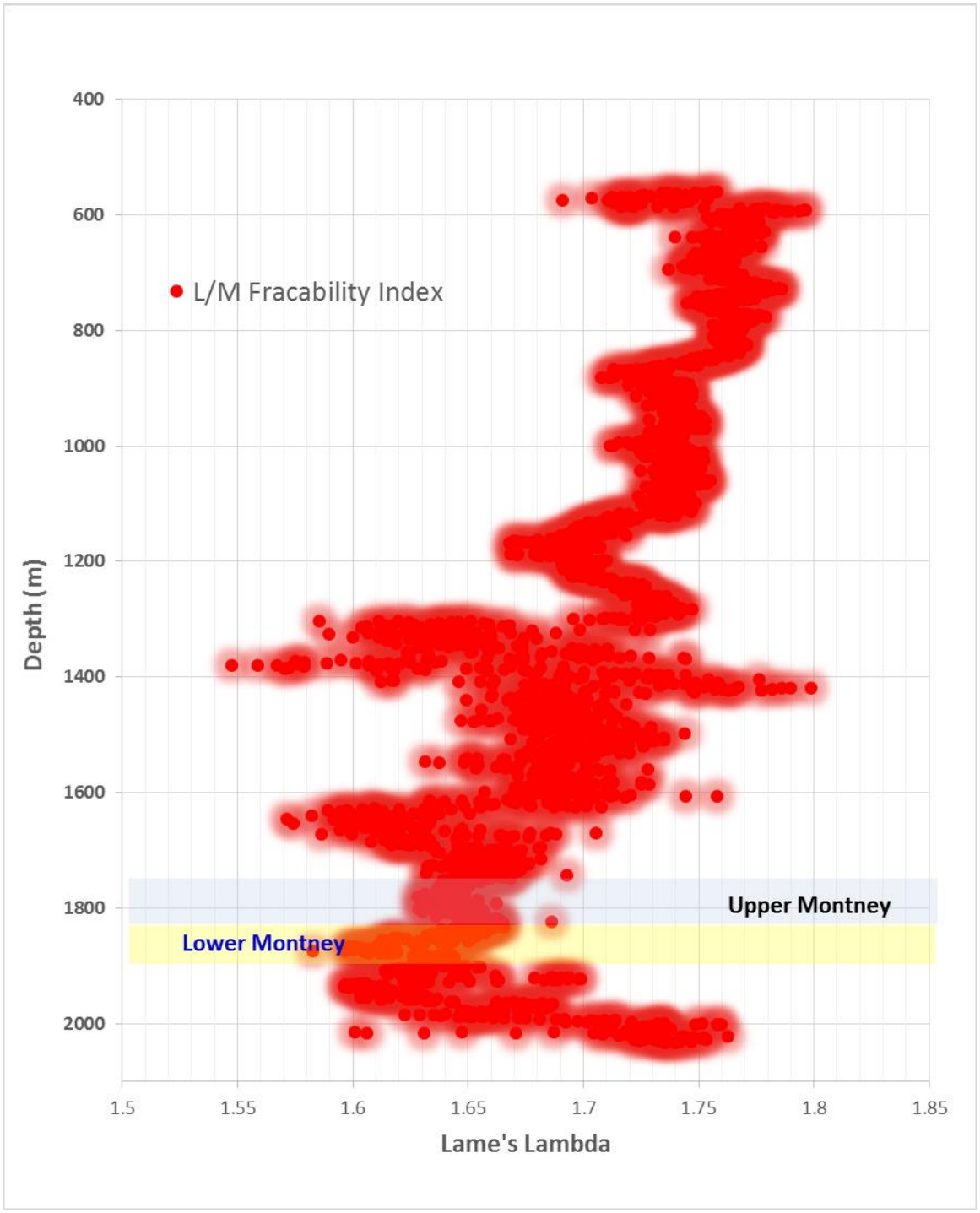

Figure B-2: Fracability Index evaluation using Lame's (λ/μ)

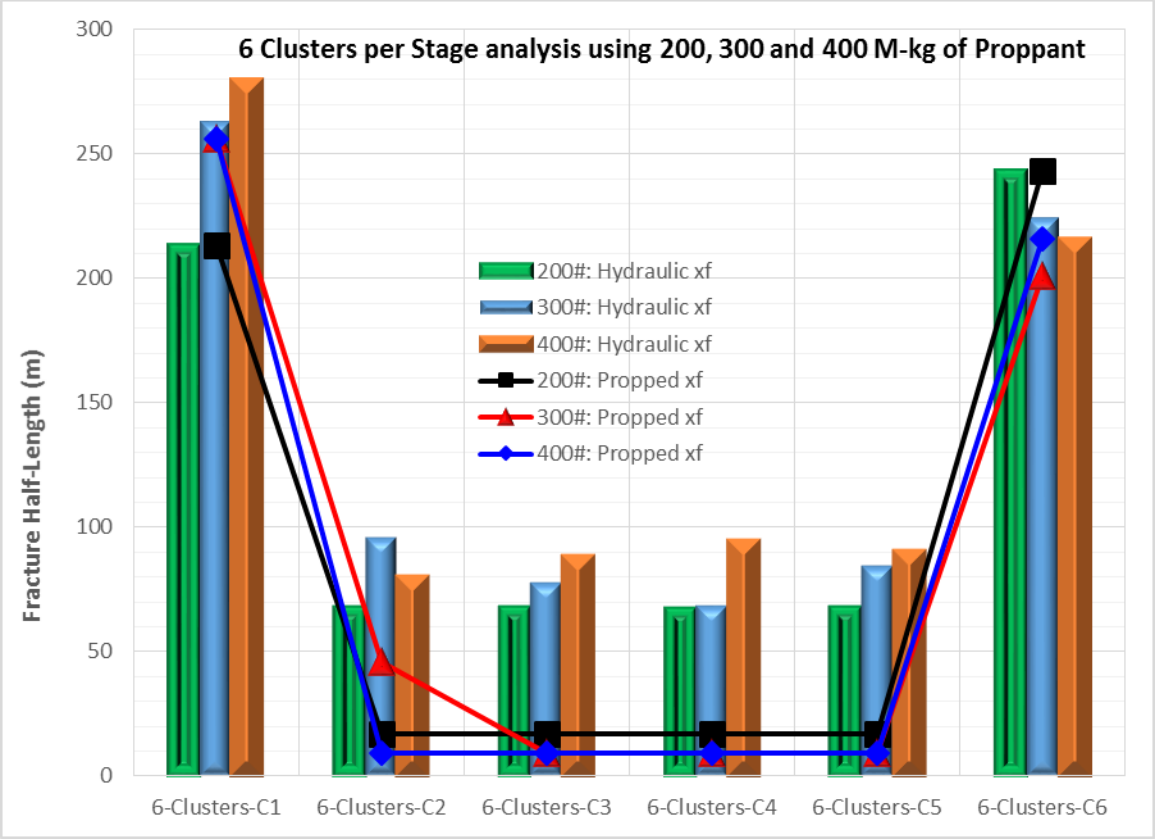

Figure B-3: Six clusters per stage analysis using massive amount proppant mass

APPENDIX C

PUBLICATION FROM THIS DISSERTATION

PUBLISHED PAPERS

Kassim RS, Britt LK, Fracturing NSI, Dunn-Norman S, Yang F (2016a) SPE-181813-MS Multiphase Flow Performance Comparison of Multiple Fractured Transverse Horizontal Wells vs longitudinal Wells in Tight and Unconventional Reservoirs with Stress Dependent Permeability. 1–36. SPE Asia Pacific Hydraulic Fracturing Conference, Beijing, China, 24-26 August

Kassim RS, Britt LK, Dunn-Norman S, Lang B (2016b) SPE-181774-MS "An Integrated Completion and Reservoir Modeling Methodology for Horizontal Shale Wells : A Montney Formation Example". SPE Liquids-Rich Basins Conference - North America, Midland, TX USA, 21 - 22 September

Kassim RS, Britt LK, Fracturing NSI, Dunn-Norman S, Lang B (2017) SPE-185046- "Building Calibrated Hydraulic Fracture Models From Low Quality Micro-seismic Data And Utilizing It For Optimization: Montney Example." SPE Canada Unconventional Resources Conference, Calgary, Alberta, Canada, 15-16 February.

Kassim RS, Britt LK, Fracturing NSI, Dunn-Norman S, Lang B (2017) URTeC- 2677519 "Optimization of Integrated Completion and Reservoir Models for Hydraulically Fractured Horizontal Wells: Montney Case Study." URTeC- Unconventional Resources Technology Conference & Exhibition, Austin, TX USA 24-26 July

PAPER IN REVIEW

Kassim RS, Britt LK, Fracturing NSI, Dunn- S (2016a) SPE-181813-MS Multiphase Flow Performance Comparison of Multiple Fractured Transverse Horizontal Wells vs longitudinal Wells in Tight and Unconventional Reservoirs with Stress Dependent Permeability. SPE Journal (submitted)

BIBLIOGRAPHY

Al-Jenaibi F, Salameh LA, Recham R, et al (2011) Best practice for static & dynamic modeling and simulation “History match case - Model QA/QC criteria for reliable predictive mode.” Soc Pet Eng - SPE Reserv Characterisation Simul Conf Exhib 2011, RCSC 2011 764–776. doi: 10.2118/148279-MS

Anderson DM, Liang P (2011) Quantifying Uncertainty in Rate Transient Analysis for Unconventional Gas Reservoirs. SPE North Am Unconv Gas Conf Exhib 14–16 June. SPE 145088–MS. doi: 10.2118/145088-MS

Anderson OL (2013) Shale Revolution or Evolution : Opportunities and Challenges for Europe.

Armaco JT (2015) SAUDI ARAMCO JOURNAL OF TECHNOLOGY, Winter 2015.

B.R. Meyer M& AI (1989) Three-Dimensional Hydraulic Fracturing Simulation on Personal Computers: Theory and Comparison Studies.

Bowker KA (2007) Development of the Barnett Shale Play , Fort Worth Basin * By Nearly all of the gas and condensate production from the Barnett Shale is in Newark East field . new-well drilling and old-well reworks / refracs (Figure 1). In 2003 the field also produced a.

Branagan PT, Peterson RE, Warpinski NR, Wright TB (1996) Characterization of a Remotely Intersected Set of Hydraulic Intersection Well No. 1-B, GRVDOE Multi-Site Project. SPE Annu Tech Conf 351–361.

Britt LK, Schoeffler J (2009) The Geomechanics Of A Shale Play: What Makes A Shale Prospective! SPE East Reg Meet 23–25. doi: 10.2118/125525-MS

Britt LK, Smith MB (2009a) Horizontal Well Completion, Stimulation Optimization, And Risk Mitigation. SPE East Reg Meet 23–25. doi: 10.2118/125526-MS

Britt LK, Smith MB (2009b) Horizontal Well Completion, Stimulation Optimization, And Risk Mitigation. SPE East Reg Meet 23–25. doi: 10.2118/125526-MS

Brunauer S, Emmett PH, Teller E (1938) Gases i n Multimolecular Layers. J Am Chem Soc 60:309–319. doi: citeulike-article-id:4074706

Bumb AC, McKee CR (1988) Gas-Well Testing in the Presence of Desorption for Coalbed Methane and Devonian Shale. SPE Form Eval 179–185. doi: http://dx.doi.org/10.2118/15227-PA

Cander H (BP E and P (2012) What Are Unconventional Resources? A Simple Definition Using Viscosity and Permeability. AAPG Annu Conv Exhib 80217:1–3.

Carroll J (Bloomberg), Wethe D (Bloomberg) (2017) Chesapeake Energy Declares " Propageddon " With Record Frack - Bloomberg Chesapeake Energy Declares " Propageddon " With Record Frack https://www.bloomberg.com/news/articles/2016-10-20/chesapeake-declares-propageddon-with-record-frack-in-louisiana. 2016–2018.

Chopra S, Marfurt KJ (2007) Volumetric curvature attributes for fault / fracture characterization. 25:19–30.

Chu L, Ye P, Harmawan I, Du L (2015) Characterizing and simulating the non-stationarity and non-linearity in unconventional oil reservoirs: Bakken application. J Unconv Oil Gas Resour 9:40–53. doi: 10.1016/j.juogr.2014.10.002

Cipolla C, Maxwell S, Mack M (2012) Engineering Guide to the Application of Microseismic Interpretations. SPE 152165. SPE Hydraul Fract Conf 6–8. doi: 10.2118/152165-MS

Cipolla C, Wallace J (2014) Stimulated Reservoir Volume: A Misapplied Concept? SPE Hydraul Fract Technol … 4–6.

Cipolla C, Warpinski N, Mayerhofer M, et al (2010) The Relationship Between Fracture Complexity, Reservoir Properties, and Fracture-Treatment Design. SPE Prod Oper 25:1–25. doi: 10.2118/115769-PA

Crosby ZS, Mejia C, Langford C, et al (2016) Optimized Completions Design With Integrated LWD and Well Site Geochemistry for Petrophysical Analysis and Enhanced Well Placement.

Dawson M (Dawson EAL. (2013) Unconventional Resource Development.

Denney D (JPT STE (2013) Integrated Microseismic Monitoring for Field Optimization - Marcellus Shale. 2–6.

Derder O (2013) Characteristics of the Triassic Upper Montney Formation (Unit C),. 1–6.

DOE/FE to E (2016) Long Term Applications Received by DOE / FE to Export Domestically Produced LNG from the Lower-48 States (as of December 20 , 2016) All Changes Since Last Issuance on November 30 , 2016 Are In Red Company Long Term Applications Received by DOE / FE to E.

Donias M, Baylou P, Keskes N (1998) Oriented Patterns: 2-D and 3-D Estimation from Differential Geometry. 236–240.

Dusterhoft CR, Kumar A, Siddiqui S, Spade G Optimizing Fracture Stimulation Design in Unconventional Reservoirs.

Economides, Michael John U of H (2002) Unified Facture Design.

Economides MJ, Yang M, Martin a N (2010) Fracturing Horizontal Transverse , Horizontal Longitudinal and Vertical Wells: Criteria for Decision. Can Unconv Resour Int Pet Conf 1–19.

EIA Report E (2015) Technically Recoverable Shale Oil and Shale Gas Resources :

Ely JW, Fowler SA, Tiner RL, et al (2014) "Slick Water Fracturing and Small Proppant" The future of stimulation or a slippery slope?

Engelder T, Lash GG, Uzcátegui RS (2009) Joint sets that enhance production from Middle and Upper Devonian gas shales of the Appalachian Basin. Am Assoc Pet Geol Bull 93:857–889. doi: 10.1306/03230908032

Evans JP, Forster CB, Goddard J V. (1997) Permeability of fault-related rocks, and implications for hydraulic structure of fault zones. J Struct Geol 19:1393–1404. doi: 10.1016/S0191-8141(97)00057-6

Evans RD, Civan F (1994) Evans and Civan (1994) Non-Darcy Multiphas flow.pdf. 199.

Fast RE, Murer AS, Timmer RS (1994) Description and Analysis of Cored Hydraulic Fractures – Lost Hills Field, Kern County, California. SPE Prod Facil 9:107–114. doi: 10.2118/24853-PA

Fisher MK, Wright CA, Davidson BM, et al (2002) Integrating Fracture Mapping Technologies To Improve Stimulations in the Barnett Shale. SPE Prod Facil 20:85–93. doi: 10.2118/77441-PA

Hallam SD, Last NC (1991) Geometry of hydraulic fractures from modestly deviated wellbores. J Pet Technol 43:742–748. doi: \href{http://dx.doi.org/10.2118/20656-PA}{DOI}

Hulsey BJ, Cornette B, Pratt D, Corporation RE (2010) SPE 138806 Surface Microseismic Mapping Reveals Details of the Marcellus Shale. Scenario 12–14.

investor presentation N (2016) Eclipse-Resources Investor Presentation August 2016 http://www.theoilandgasconference.com/downloads_TOGC_2016/Eclipse-Resources.pdf.

Jonas EC, Mcbride EF (1977) Di agenesis of Sandstone and Shale : Application to Exploration by.

JPT (2012) JOURNAL OF PETROLEUM TECHNOLOGY, July 2012.

JPT (2011) JOURNAL OF PETROLEUM TECHNOLOGY, July 2011.

Juell AO, Whitson CH (2013) Optimized Well Modeling of Liquid-Rich Shale Reservoirs. SPE Annu Tech Conf Exhib. doi: 10.2118/166380-MS

Kassim RS, Britt LK, Dunn-norman S, Lang B (2016a) SPE-181774-MS An Integrated Completion and Reservoir Modeling Methodology for Horizontal Shale Wells : A Montney Formation Example.

Kassim RS, Britt LK, Fracturing NSI, Dunn- S (2016b) SPE-181813-MS Multiphase Flow Performance Comparison of Multiple Fractured Transverse Horizontal Wells vs longitudinal Wells in Tight and Unconventional Reservoirs with Stress Dependent Permeability. 1–36.

Khalid A, Antonin S (1979) Petroleum Reservoir Simulation. 476.

Klein P, Richard L, James H (2008) 3D curvature attributes: A new approach for seismic interpretation. First Break 26:105–111.

Kuuskraa VA, Stevens SH, Moodhe K. (2013) World shale gas and shale oil resource assessment.

Lane HS (1995) Estimating gas desorption parameters from Devonian shale well-test data. Energy Sources 17:313–336. doi: 21272

Liu, Tianyu TAU (2012) Moderate-Permeability Gas Reservoir.

Lopez E a., Naranjo a., Mejia JM, Alzate G a. (2014) Coupled Fluid Flow / Geomechanics Simulator for Modeling Multiphase Flow and Geomechanical Processes .

Maxwell SC, Urbancic TI, Steinsberger N, et al (2002) Microseismic Imaging of Hydraulic Fracture Complexity in the Barnett Shale. SPE Int 1–9. doi: 10.2523/77440-MS

Mayerhofer MJ, Lolon EP, Warpinski NR, et al (2008) What is Stimulated Reservoir Volume (SRV)?

Meyer BR, Bazan LW (2011) A Discrete Fracture Network Model for Hydraulically Induced Fractures : Theory , Parametric and Case Studies. SPE Hydraul Fract Technol Conf 1–36. doi: 10.2118/140514-MS

Moinfar A, Erdle JC, Patel K, Modeling C (2016) Comparison of Numerical vs Analytical Models for EUR Calculation and Optimization in Unconventional Reservoirs.

Nolte KG (1986) Determination of Proppant and Fluid Schedules From Fracturing-Pressure Decline. SPE Prod Eng 1:255–265. doi: 10.2118/13278-PA

Pearson CM, Bond AJ, Eck ME, Schmidt JH (1992) Results of Stress-Oriented and Aligned Perforating in Fracturing Deviated Wells. SPE J Pet Technol 44:10–18. doi: 10.2118/22836-pa

Quirk D, Ziar AS, Well T, Service W (2010) The E ffect of O ut-of- P lane L oading on the F racture of Aluminium 2024. 1–10.

Rassenfoss S (JOURNAL OPT (2013) Making Unconventional Resources Less So. 40–44.

Rebol AE (Corporation AP (2016) SPE-181769-MS Completing a 50-Stage Delaware Basin Well Without Annular Isolation , Using Coiled Tubing Deployed Jet Perforating.

Rickman R, Mullen M, Petre E, et al (2008) A practical use of shale petrophysics for stimulation design optimization: All shale plays are not clones of the Barnett Shale. SPE Annu Tech Conf Expo 1–11. doi: 10.2118/115258-MS

S.D. Seba SOI (1987) SPE 16310 The Only Investment Selection Criterion You Will Ever Need.

Saldungaray P, Palisch TT (2012) SPE 151128 Hydraulic Fracture Optimization in Unconventional Reservoirs. 23–25.

Shi Y, Wang C-Y Pore pressure generation in sedimentary basins-overloading versus aquathermal..pdf.

U.S. Energy Information Administration (2016) Short-term energy outlook.

U.S Energy Information Administration (2016a) Trends in U . S . Oil and Natural Gas Upstream Costs.

U.S Energy Information Administration (2016b) Oil Wells Drilled Horizontally Are Among the Highest-Producing Wells. Energy Collect 2016–2017.

Valko P, Economides MJ (1996) 3 1 149. 1–7.

Warpinski NR, Branagan PT, Peterson RE, et al (1997) Microseismic and deformation imaging of hydraulic fracture growth and geometry in the C sand interval, GRI/DOE M-site project. SPE Annu. Tech. Conf. 87–98.

Warpinski NR, Mayerhofer MJ, Vincent MC, et al (2008) Stimulating Unconventional Reservoirs: Maximizing Network Growth While Optimizing Fracture Conductivity. SPE Unconv Reserv Conf. doi: 10.2118/114173-MS

Warpinski NR, Natl S, Wright TB, et al (1999) Microseismic Monitoring of the B-Sand Hydraulic-Fracture Experiment at the DOE / GRI Multisite Project. SPE Int 242–250. doi: 10.2118/36450-MS

Whiston C, Brulé M (2000) Phase Behavior.

Whitson CH, Sunjerga S (2012) PVT in Liquid-Rich Shale Reservoirs. SPE Annu Tech Conf Exhib 8–10. doi: 10.2118/155499-MS

Wolhart SL, Odegard CE, Warpinski NR, et al (2006) Microseismic fracture mapping optimizes development of low-permeability sands. JPT, J Pet Technol 58:62–64. doi: 10.2118/95637-MS

Woo V, Pope TL, Abou-khalil E, et al (2011) Fracture Stimulation Optimization in Horizontal Cardium Completions. Can Unconv Resour Conf 1–7. doi: 10.2118/146785-MS

Yang F, Britt LK, Fracturing NSI, Dunn-norman S (2015) The Effect of Well Azimuth or Don ' t Let Your Landman Plan Your Well Path !

Yang F, Britt LK, Fracturing NSI, Dunn-norman S (2014) Performance comparison of transverse and longitudinal fractured horizontal wells over varied reservoir permeability. 3–5.

Ye P, Chu L, Harmawan I, et al (2013) SPE 164543 Beyond Linear Analysis in an Unconventional Oil Reservoir. 1:10–12.

Zimmer U (2011) Calculating Stimulated Reservoir Volume (SRV) with Consideration of Uncertainties in Microseismic-Event Locations. Can Unconv Resour Int Pet Conf 1–13.

VITA

Rashid Kassim has worked in the oil and gas industry since 2007. Most recently, he worked as completions and reservoir geomechanics engineer doing-consulting work for NSI Fracturing LLC. He has also worked as production optimizations engineer for Baker Hughes in Oklahoma, and as production engineer for Chevron in California.

Kassim received his bachelor degree in Organic Chemistry, with a minor in Business Management (2005) from the University of Minnesota, and Master of Science in Petroleum Engineering (2007) from the New Mexico Institute of Mining and Technology. He also received Master of Science in Engineering Management and Graduate Certificate in Financial Engineering (2016), and PhD in Petroleum Engineering from Missouri University of Science and Technology in May 2017.

Kassim held several leadership positions in professional associations, including the Society of Petroleum Engineering (SPE) as treasurer (2007), vice-president of the Associated Students of the University of Missouri (2014), and served in board of directors for Non-Profit organizations in California.

His research interests are hydraulic fracturing and optimization, and integrated modeling of horizontal wells, especially in unconventional resources. Other research interests include energy investment, oil price modeling and hedging strategies for oil and gas companies.